DEFORMATION ANALYSIS METHODS FOR DRILLED SHAFT FOUNDATIONS SUBJECTED TO LATERAL AND OVERTURNING MOMENT LOADS

by

Byron Holth Foster

A thesis submitted to the faculty of
The University of Utah
in partial fulfillment of the requirements for the degree of

Master of Science

Department of Civil and Environmental Engineering

The University of Utah

May 2016

The University of Utah Graduate School

STATEMENT OF THESIS APPROVAL

The thesis of **Byron Holth Foster**

has been approved by the following supervisory committee members:

Evert C. Lawton	, Chair	**1/14/2016** Date Approved
Steven F. Bartlett	, Member	**1/14/2016** Date Approved
Chris P. Pantelides	, Member	**1/14/2016** Date Approved

and by **Michael E. Barber**, Chair of the Department of **Civil and Environmental Engineering**

and by David B. Kieda, Dean of the Graduate School

ABSTRACT

Drilled shaft foundations are widely used in many civil engineering applications where deep foundations are required because they are relatively easy to construct and are suitable for resisting lateral, axial, and overturning moment loads. While the analysis of drilled shafts subjected to axial loads is fairly straightforward, it is much more difficult to analyze drilled shafts subjected to lateral and overturning moment loads due to the complex nature of the soil-structure interaction.

It has been suggested that the *p-y* model, which is currently the most commonly used model for performing these types of analyses, considerably overestimates deformation of semi-rigid to rigid drilled shafts subjected to lateral and overturning moment loads. While the *p-y* model has been shown to reasonably predict deformation of flexible steel pipe piles and drilled shafts, it has not been verified for rigid to semi-rigid drilled shafts. The major objectives of this investigation were to identify other methods in current use that might be more appropriate for analyzing this type of drilled shaft and to assess the accuracy of each analysis method by comparing the results from each method to the results of large-scale load tests.

The literature review revealed several analysis methods, which range from simple analytical methods to complex numerical methods. In addition to the *p-y* model, other commonly used analysis methods include the strain wedge model and the four-spring model. All of these models are semi-empirical and rely to some extent on

experimentally-observed data and simplifying assumptions about the soil-structure interaction. The *p-y* model, the strain wedge model, and the four-spring model are implemented in the commercial software packages *LPile*, *DFSAP*, and *MFAD*, respectively. Several large-scale load tests for rigid to semi-rigid drilled shafts were also identified in the literature review. The information from these load tests was used to perform analyses using the *LPile*, *DFSAP*, and *MFAD* program, and the results were compared to the experimentally-observed results.

The results suggest that *MFAD* is the most accurate model for granular soils and that *DFSAP* is the most accurate model for cohesive soils. For the foundations considered in this investigation, there was no apparent correlation between the accuracy of the *DFSAP* or *MFAD* results and the rigidity of the foundation; however, the accuracy of the *LPile* results tended to decrease as the foundation rigidity increased. A parametric study was conducted to investigate how the soil input properties affect the results, and how sensitive the models are to variations in these properties. The parametric study showed that *LPile* and *DFSAP* are most sensitive to input properties of the angle of internal friction (ϕ) and undrained shear strength (s_u) of the soil, while *DFSAP* is most sensitive to the modulus of deformation (E_p) of the soil. A statistical analysis of the combined data from each analysis method resulted in design equations for estimating semi-rigid to rigid drilled shaft deflection using *LPile*, *DFSAP*, or *MFAD* for a target level of reliability.

To my family, for their unwavering love and support.

TABLE OF CONTENTS

LIST OF SYMBOLS AND NOTATION

$A_{s,c}$	=	ultimate soil resistance correction factor
$A_{v,min}$	=	minimum area of transverse reinforcement
a	=	depth to center of rotation of pile
B	=	diameter (or width) of pile or footing
$B_{s,c}$	=	nondimensional coefficient for determining p_m
$\overline{BC}$	=	width of mobilized passive wedge
BEF	=	beam-on-elastic-foundation
b_w	=	diameter of concrete column
C	=	curve fitting coefficient
C_i	=	curve fitting coefficient
C_u	=	coefficient of uniformity
CPT	=	cone penetration test
D	=	depth of pile embedment; pile diameter
D/B	=	ratio of embedded depth to diameter of pile
DMT	=	dilatometer test
D_{50}	=	mean particle size
EI	=	flexural rigidity of pile or footing
E	=	secant modulus of soil from laboratory stress-strain curve

E_{ds} = drained secant modulus

E_P = modulus of deformation

E_s = modulus of subgrade reaction

E_{si} = secant modulus of initial linear portion of *p-y* curve

E_{US} = undrained secant modulus

E_{PMT} = pressuremeter modulus

e = void ratio of soil

f'_c = compressive strength of concrete

f_{yt} = yield strength of transverse reinforcement

f_r = rupture strength of concrete

H = height of passive wedge in front of pile

h = depth of passive wedge

i = sub-layer index

J = nondimensional coefficient for clay *p-y* curves

K_o = coefficient of lateral earth pressure for at-rest conditions

K_a = coefficient of lateral earth pressure for active conditions

k = coefficient of subgrade reaction

k_b = base shear spring

k_h = horizontal coefficient of subgrade reaction

k_{ht} = current tangent value of the horizontal subgrade modulus

k_θ = vertical side shear moment spring

$k_{\theta b}$ = base moment spring

$[k_B]$ = beam stiffness matrix

$[k_h]$ = lateral spring stiffness matrix

$[k_E]$ = stiffness matrix for each pile element

$[k_\theta]$ = vertical side shear moment stiffness matrix

L = pile length

LL = liquid limit

M = internal bending moment of pile

M_{ult} = ultimate moment capacity of pile

N_p = lateral bearing factor

N_k = CPT cone factor

n_h = constant of subgrade reaction

P = soil reaction per unit area

PI = plasticity index

PMT = pressuremeter test

p = soil reaction per unit length

$p(x)$ = soil reaction as a function of axial direction x

p_a = atmospheric pressure

p_c = theoretical ultimate soil resistance

p_{cd} = theoretical ultimate soil resistance from lateral flow of soil around pile

p_{ct} = theoretical ultimate soil resistance from a passive wedge in sand

p_m = soil resistance at point m in Figure 2.12

p_o = applied lateral load at pile head

p_u = ultimate soil resistance per unit length

p_{ult} = theoretical ultimate soil resistance per unit length

Q_{ult} = ultimate shear capacity of pile

Q_v = axial (vertical) force acting on pile or footing

q_c = CPT cone tip resistance

q_u = unconfined compressive strength of soil

r = radius of pile

R = reliability of pile design

S_1 = pile shape adjustment factor

S_2 = pile shape adjustment factor

SL = horizontal stress level within the passive wedge

SL_t = stress level of shear along pile sides

s = center-to-center spacing of transverse reinforcement

s_u = undrained shear strength of cohesive soils

UC = unconfined compression test

UU = unconsolidated undrained triaxial test

Δu = excess porewater pressure

V = internal shear force in the pile

V_i = incremental lateral load applied to pile head

W = distributed load along the length of the pile

$w(x)$ = distributed load along a beam as a function of axial direction x

w_n = natural water content of soil

X_o = depth to zero-deflection point as measured from the top of the pile

x = distance along the length of the pile or footing

x_r = transition depth from wedge-type failure to flow-around failure

y	=	lateral deflection of the pile at point x along the length of the pile
$y(x)$	=	pile deflection profile as a function of axial direction x
y_o	=	pile head deflection
y_{50}	=	deflection at 50% of the ultimate soil resistance, p_u
α	=	angle of passive wedge from the vertical pile face; angle of passive wedge from a line parallel to applied lateral load; pile adhesion factor
β	=	angle of passive wedge from the vertical pile face
β_m	=	mobilized angle of passive wedge from the vertical pile face
γ'	=	submerged (effective) unit weight of soil
δ	=	linearized deflection angle of pile from vertical
$\delta_{probable}$	=	probabilistic pile deflection
$\delta_{predicted}$	=	pile deflection predicted from a particular analysis method
ε	=	horizontal strain within the passive wedge of soil; axial strain
ε_d	=	axial strain corresponding to σ_d
ε_{50}	=	strain at 50% of the maximum stress on a laboratory stress-strain curve
ζ	=	normalization factor
θ	=	slope of the pile
$\theta(x)$	=	pile slope profile as a function of axial direction x
θ_m	=	mobilized angle of passive wedge from horizontal
λ	=	curve fitting parameter
ν	=	Poisson's ratio
ρ_s	=	longitudinal steel reinforcement ratio
ρ_d	=	dry density of soil

$\Delta\sigma_h$	=	change in horizontal stress in passive wedge
$\Delta\sigma_{hf}$	=	change in horizontal stress at failure in passive wedge
σ_1	=	major principal stress
σ_3	=	minor principal stress
σ_d	=	deviatoric stress from triaxial test
σ'_{vo}	=	vertical effective stress
τ	=	shear stress in soil; shear stress along pile sides
τ_{ult}	=	ultimate shear stress along pile sides
ϕ'	=	effective angle of internal friction of soil
ϕ	=	angle of internal friction of soil; curvature of pile
ϕ'_m	=	mobilized effective friction angle; angle of passive wedge from a line parallel to applied lateral load
ϕ_s	=	mobilized friction angle between pile sides and sand

ACKNOWLEDGEMENTS

I would like to give special thanks to the University of Utah and the department of Civil Engineering for providing me with an incredible opportunity to receive a world-class education. I would like to especially thank my advisor, Dr. Evert Lawton, for providing me with the opportunity and resources to work on this research, for his mentorship over the years, and for always making his classes exciting and challenging. I would also like to thank Dr. Steven Bartlett and Dr. Chris Pantelides for their guidance and support in my academic pursuits and their participation on my committee. This research would not have been possible without financial support from PacifiCorp. My sincerest thanks to Pete Singh and Ben Fowler of PacifiCorp for their support and assistance with this project.

1 INTRODUCTION

1.1 Background

A drilled shaft is a type of deep foundation that is widely used in many civil engineering applications. They are constructed by drilling a hole to a specified depth and diameter, placing a rebar reinforcing cage inside the hole, filling the hole with concrete, and allowing sufficient time to elapse for the concrete to develop its prescribed design strength. Drilled shafts are commonly used to support buildings, bridges, transmission line structures, radio towers, oil platforms, windmills, and many other types of structures. They are used in lieu of other types of deep foundations, such as steel pipe piles, because they are fairly easy to construct, they are durable, the materials are readily available, and they do not require special transportation considerations for very large foundations.

Drilled shafts can be used where relatively small deep foundations are required, but oftentimes they are used when foundations with very large lengths and diameters are required, such as for single-pole transmission line structures and windmills. These foundations become very expensive very quickly due to the specialized equipment and personnel required for their construction, the large quantities of concrete and steel reinforcement required, and the additional challenges associated with mobilizing large pieces of equipment to areas that are remote or otherwise not easily accessible. As such, it is desirable to design the drilled shaft to be large enough for the application in which it will be used, including the required factors of safety, but not larger.

It was recently brought to the attention of the author by the director of engineering of a regional power company that several of the drilled shaft foundations that have been designed for their single-pole transmission line structures are considerably larger than one would reasonably expect for the anticipated subsurface and loading conditions. He explained that the allowable deflection and rotation of the top of the shaft typically governs the design, and that a computer program known as *LPile* was being used to conduct the lateral load analysis and foundation design. He also explained that the geotechnical investigation for most projects was probably not rigorous enough to give the design engineer the confidence to minimize the conservatism in the soil properties that are used for design.

Naturally, the following questions arose from the observation that these foundations might be overdesigned: 1) Are the foundations *actually* being overdesigned? 2) Can the anticipated overdesign be attributed to the model, the input parameters (soil properties), or a combination of both? 3) What alternative methods are available for performing such analyses, and how do the results of each method compare with each other? 4) Which method actually provides the most accurate results? These questions were the impetus for this thesis.

A literature review was conducted to gain an understanding of how the *LPile* model is used in practice and how it was formulated. It turns out that *LPile* is a semi-empirical model that employs load transfer functions known as *p-y curves* to represent the stress-strain-strength characteristics of the soil. These *p-y* curves were developed from the results of a small number of large-scale lateral load tests that were performed in different types of soil.

The popularity of *LPile* can likely be attributed, at least in part, to the following:

1) It is easy to use; 2) it is fairly inexpensive; 3) it requires relatively few input parameters; 4) it predicts deflection and rotation at the top of the foundation, which typically controls the design; 5) it reasonably accounts for the nonlinearity of the shaft and the soil; 6) the algorithms employed to obtain solutions are, in part, formulated from the results of large-scale load tests, which gives engineers confidence in the model's ability to provide accurate results; 7) it predicts the shear force and bending moment along the length of the shaft, which allows the engineer to properly design a foundation that has sufficient shear and moment capacity; and 8) it is a very efficient program, which allows the engineer to perform parametric studies quickly and easily.

As mentioned previously, *LPile* is based on the results of large-scale load tests. Therefore, the results of any analysis obtained using this model will reflect the conditions of the experiments from which the *p-y* curves were derived. If the subsurface characteristics, foundation characteristics, and loading characteristics of the foundation being analyzed are similar to the same characteristics of the large-scale load test from which these curves were derived, the results should be reasonably accurate; however, it is difficult to gauge the accuracy of such an analysis if this criterion is not satisfied.

The large-scale load tests that were used to derive the *p-y* curves were performed on steel pipe piles and one drilled shaft with very large length-to-diameter ratios. It was discovered during the literature review that the soil response is considerably influenced by the rigidity of the foundation, which decreases as the length-to-diameter ratio increases. The literature review also revealed that limited research has been conducted to investigate whether it is appropriate to conduct lateral load analyses of semi-rigid drilled shafts using *p-y* curves that were established for flexible foundations. As such, one of the main objectives of this investigation is to gain insight into the accuracy of the *LPile*

model for these types of foundations.

The literature review revealed that several models have been developed for analyzing laterally loaded drilled shafts and piles. Most of these models were developed over the last century, and range in complexity from simple equilibrium models to advanced numerical models. Many of these models were derived to predict the ultimate capacity of a laterally loaded drilled shaft or pile. In most cases, the tolerable deflection or rotation of the top of the foundation is reached before the ultimate capacity, so these models are of limited value in the final design of a laterally loaded drilled shaft. These models will not be discussed in detail in this thesis.

The alternative design methods that are being considered for this thesis must provide, at a minimum, the deflection and rotation at the top of the shaft, as well as the soil resistance along the length of the shaft. The alternative design models that were identified in the literature review that satisfy these criteria include *FB-Multipier* (formerly *FLPier*), Moment Foundation Analysis and Design (*MFAD*), and Deep Foundation System Analysis Package (*DFSAP*). General Finite Element Method (FEM) and Finite Difference Method (FDM) codes such as ABAQUS and FLAC3D, respectively, have also been used to perform analyses of laterally loaded drilled shafts, but they are not being considered in this investigation. The *FB-Multipier* program uses the same *p-y* curves as *LPile* to model the soil-structure interaction (Hoit, Hays, & McVay, 1997), and as such, it will not be included in this investigation. Therefore, the models that will be included in this investigation are *LPile*, *DFSAP*, and *MFAD*.

In order to assess the accuracy of these models for semi-rigid drilled shafts, a large-scale lateral load test must be performed at a site where a rigorous geotechnical investigation has been conducted. Because research funds were not available for

conducting such an experiment, it was decided that the literature review would also be conducted to discover whether similar experiments have been performed and published by other researchers. The information from these experiments can be used to perform analyses using the aforementioned methods, and the results of the analyses can be compared to the observed results. Several large-scale lateral load tests were identified in the published literature, and the information and results from these load tests were used as the basis of comparison between the models being considered in this investigation.

1.2 Objectives of the Research

The purpose of this research is to identify and evaluate several methods that are used to analyze laterally loaded semi-rigid drilled shafts. This will be accomplished by achieving the following objectives:

- Determine which analysis methods are currently being used – primarily by practicing engineers – by conducting a thorough review of the literature;
- Compile a list of large-scale load tests reported in the literature and determine which load tests are suitable for performing a comparison between analytical and observed results;
- Perform an analysis of each suitable large-scale load test using select analysis methods currently used in professional practice and the reported foundation and subsurface information;
- Conduct a parametric study to gain insight into how the input parameters affect the results of the analysis methods considered in this thesis;
- Compare the results of the large-scale load tests with the results of each

analysis method and make recommendations regarding the use of each method for analyzing semi-rigid drilled shafts;

1.3 Organization of the Thesis

This thesis is organized into six chapters. An overview of each chapter is as follows:

- 1 Introduction – Discusses the genesis of the project, the statement of the problem, why the results are important, and a brief review of the relevant literature;
- 2 Literature Review – Presents the findings of the literature review including the relevant analysis methods and the database of large-scale lateral load tests;
- 3 Methodology – Presents relevant information about the large-scale lateral load tests that were used for this investigation, how the models for each large-scale load test were developed, and how the input parameters for each model were estimated;
- 4 Results – Presents the results of each analysis along with the results of the large-scale load tests, and the results of the parametric study;
- 5 Discussion – Discusses the simulations of each large-scale load test and how the simulation results from each analysis method compare with the observed results; discusses the results of the parametric study and how the input parameters affect the results; discusses the results of the statistical analysis of the data and the resulting regression equations;
- 6 Conclusions and Recommendations – Presents the conclusions reached from

the analysis, recommendations based on the conclusions, and recommendations for future research.

1.4 Limitations of the Investigation

It is acknowledged that the comparison of each large-scale load test simulation with the observed data should be based on the moment, displacement, and soil resistance profiles in addition to the deflection and rotation of the top of the foundation; however, there are insufficient data available in the literature to make such a comparison. As such, the basis of comparison for the models used in this thesis is the deflection of the top of the foundation only. Although this is not ideal, deflection and rotation of the top of the foundation control most designs, so comparison of deflections at the top of the foundation is still very useful.

There are numerous ways of conducting a geotechnical field investigation, and likewise, there are numerous ways of estimating soil parameters from the results obtained from the field investigation and concomitant laboratory testing. Rigorous estimation of soil properties from the information available is outside the scope of this research. Soil properties that are reported along with the results of large-scale load tests will generally be used without modification, and a reasonable effort will be made to estimate the required soil properties that are not directly reported using methods that are consistent with the current standard of geotechnical engineering practice.

2 LITERATURE REVIEW

A literature review was conducted to 1) identify alternative analysis methods currently being used that might be more suitable for analyzing laterally loaded rigid to semi-rigid drilled shafts subjected to large lateral or overturning moment loads; 2) gain further insight and understanding of how the *p-y* method and each of the alternative analysis methods were formulated, their basic assumptions, and their limitations; and 3) identify the large-scale lateral load tests of rigid to semi-rigid drilled shafts that are reported in the published literature. The results of the literature review are presented in this section.

2.1 Introduction

The prediction of the interaction between drilled shafts and the surrounding soil and the overall foundation response to lateral loading is among the most complex topics in geotechnical engineering (Janoyan & Whelan, 2004). In order to analyze a laterally loaded drilled shaft, the stress-strain-strength characteristics of the foundation and surrounding soil must be evaluated (Chen & Kulhawy, 1994). In most civil engineering applications, the forces acting upon or caused by the superstructure impart lateral loads, axial loads (uplift and compression), and overturning moments on the head of the foundation. The combination of these loads and the resulting soil resistance that develops is a highly complex three-dimensional problem as shown in Figure 2.1. This three-

dimensional problem is difficult to solve, and it is difficult to realistically represent this three-dimensional soil-structure interaction problem as a two-dimensional problem that is easier to solve (Phoon & Kulhawy, 2005).

Several methods have been developed for analyzing laterally loaded piles and drilled shafts. In general, the purpose of the analysis is to estimate the ultimate capacity of the foundation. The ultimate capacity can be defined in terms of the maximum allowable deflection or rotation of the top of the foundation or an ultimate limit state. The ultimate limit state is reached by failure of the soil, failure of the foundation, or excessive deformation that will cause loss of structural integrity of the superstructure (Salgado, 2008). No standard definition for ultimate capacity exists, but Hirany and Kulhawy (1988) have discussed several of the proposed methods shown in Figure 2.2.

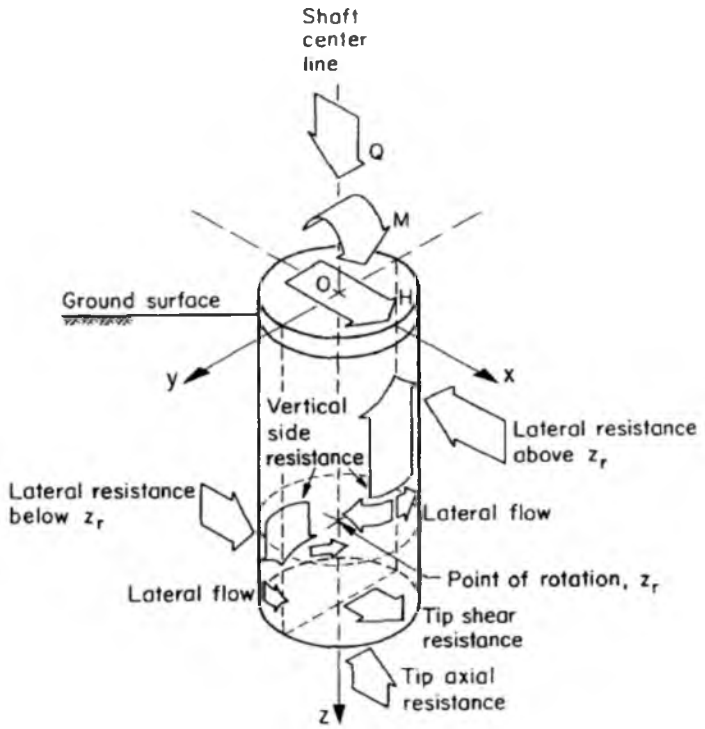

Figure 2.1. Load and soil resistance components of a drilled shaft (Chen & Kulhawy, 1994)

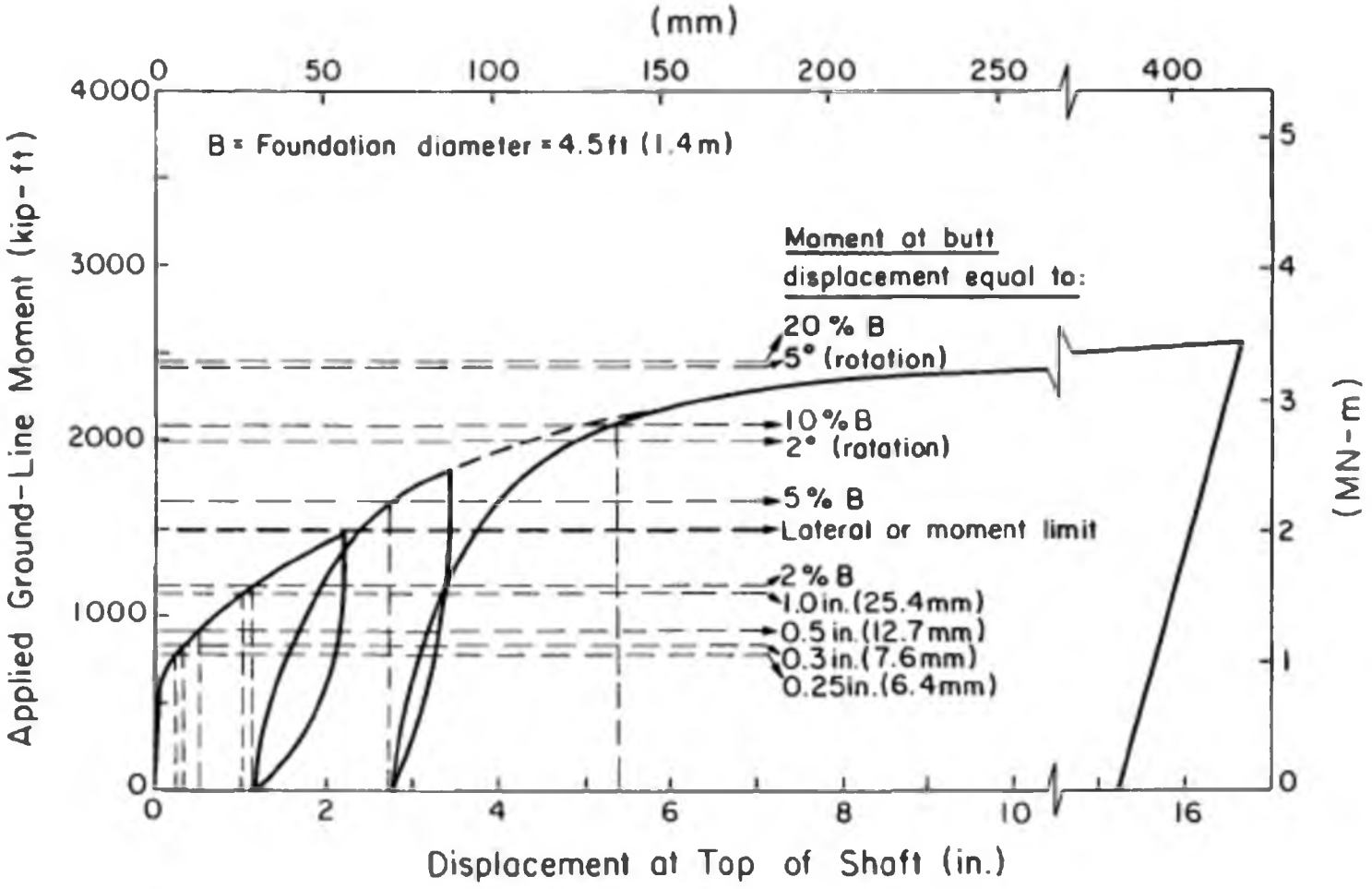

Figure 2.2. Comparison of lateral load interpretation criteria (Hirany & Kulhawy, 1988)

Most of the models that have been developed over the past several decades [(Broms, 1964a), (Broms, 1964b), (Poulos, 1971a), (Poulos, 1971b)] are based on a two-dimensional representation of the forces that act on the foundation. The forces from the soil are estimated from the strength characteristics of the soil, which are typically defined by the undrained shear strength (s_u) for undrained analyses, and angle of internal friction (ϕ) for drained analyses, and an assumed stress distribution along the foundation. The ultimate capacity is calculated by satisfying limit equilibrium for the applied forces and the soil resistance forces.

The limit equilibrium models are still used to some extent in current design practices, and research has shown that these models generally predict the loads required to reach the ultimate limit state of laterally loaded drilled shafts quite well when used properly (Davidson, Cass, Khilji, & McQuade, 1982). Unfortunately, most of these models have limited, if any, capacity to predict the deflection and rotation that occurs at any point along the shaft.

The amount of tolerable deformation in most designs is typically on the order of 5 to 50 mm, which is less than the amount of deformation required to reach the ultimate limit state of most drilled shafts (Salgado, 2008). As such, these limit equilibrium methods are of limited value in most design problems. Furthermore, the basis of comparison between methods for this investigation is the lateral deflection at the top of the foundation, which precludes the use of these methods for this investigation.

The methods that are considered in this investigation provide, at a minimum, the deflection and rotation of the foundation head and the internal bending moment and shearing stress at all points along the foundation. The deflection and rotation is used for the purposes of meeting the specified limit state as previously discussed, and the

maximum internal bending moment and shearing stress are required to perform the structural analysis of the foundation. The analysis methods that will be considered for this investigation must provide values for these parameters, at a minimum.

2.2 Drilled Shaft Behavior

The deflection and rotation that occurs at the top of the drilled shaft is dependent, in part, upon the fixity conditions of the foundation head, the rigidity of the foundation, and the stiffness of the soil [(Kasch, Coyle, Bartoskewitz, & Sarver, 1977), (Chen & Kulhawy, 1994)]. Foundations with a fixed head, such as foundations that are integrated into a pile cap, are outside of the scope of this thesis and will not be discussed.

The flexural rigidity (*EI*) of the drilled shaft increases as the embedded-depth-to-diameter (*D/B*) ratio decreases, and conversely, the *EI* decreases as *D/B* increases. No standard method has been developed to describe the flexural rigidity of drilled shafts, but several criteria have been developed as described by Chen and Kulhawy (1994). In general, shafts with *D/B* ratios greater than 10 are flexible, while shafts with *D/B* ratios less than 10 are semi-rigid. Shafts with *D/B* ratios less than 4 are typically considered to be rigid, but for this thesis they are considered to be semi-rigid.

The typical behavior of a rigid, semi-rigid, and flexible drilled shaft subjected to lateral loading is shown in Figure 2.3. For rigid drilled shafts, it is assumed that bending of the foundation does not occur. Instead, the foundation rotates about a fixed point during lateral or moment loading. The soil resistance is primarily comprised of passive earth pressure on the opposite side of the direction of loading above the point of rotation and on the same side as the direction of loading below the point of rotation. Additionally, shearing resistance develops along the sides of the foundation and along the tip of the

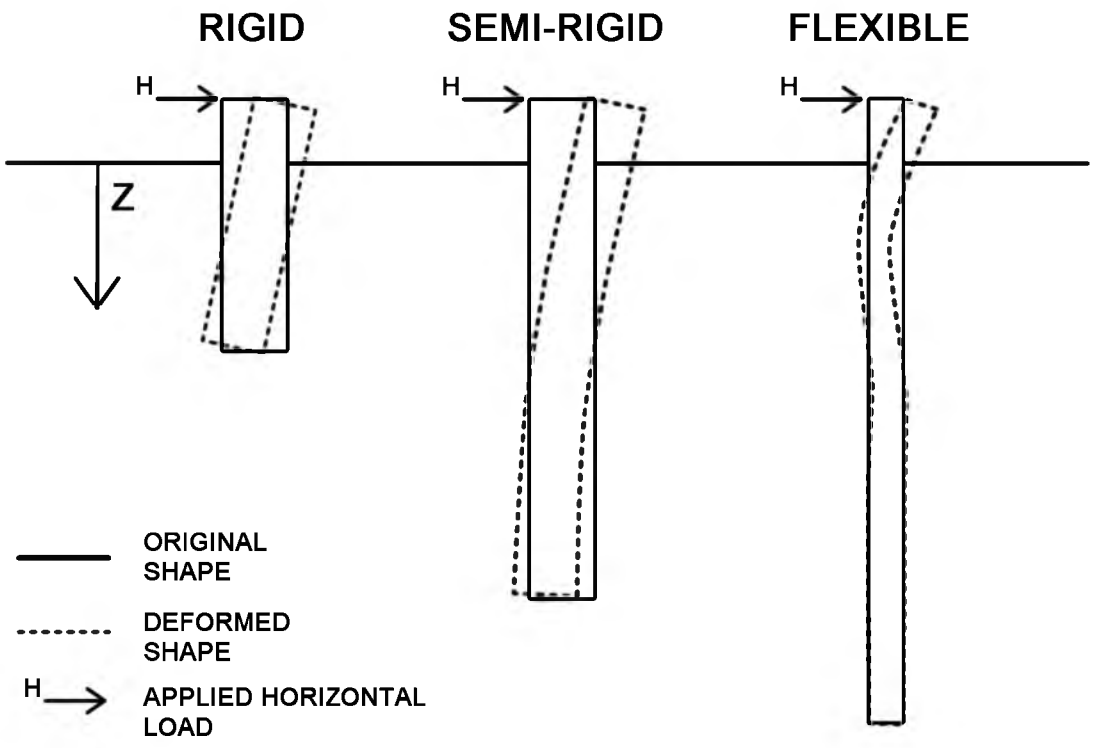

Figure 2.3. Behavior of rigid, semi-rigid, and flexible drilled shafts subjected to lateral loading under free head conditions [After Kulhawy and Chen (1995)]

foundation as shown in Figure 2.1. Research conducted by Smith and Slyh (1986) and Janoyan and Whelan (2004), among others, have suggested that shearing resistance is responsible for most of the soil resistance at small deformation and that passive earth pressure resistance is responsible for most of the soil resistance at large deformations.

Semi-rigid drilled shafts experience flexural bending about a single point. For drilled shafts, the bending is usually extensive enough to cause cracking of the concrete. The soil resistance develops in much the same way as rigid drilled shafts, but there is not as much movement at the base of the foundation.

Flexible drilled shafts exhibit bending behavior that is demonstrably different from rigid and semi-rigid drilled shafts. Flexural bending occurs about multiple points of rotation, and considerably more bending occurs. As with semi-rigid drilled shafts, the amount of bending that occurs typically causes cracking of the concrete. One of the most important differences between semi-rigid and flexible drilled shafts is that the bases of flexible drilled shafts are assumed to be fixed. The soil resistance that develops within the upper portion of the drilled shaft is comprised of passive earth pressure resistance and shearing resistance.

As previously discussed in Section 1.1, the focus of this investigation is primarily on semi-rigid drilled shafts, and the criterion that will be used to characterize a drilled shaft as semi-rigid is that it must have a D/B ratio less than 10.

2.3 Beam on Elastic Foundation (BEF) Analysis

A common design problem that arises in geotechnical engineering is the analysis and design of beam-like structures supported by the subgrade, such as strip footings or grade beams. This analysis can be performed using the Euler-Bernoulli beam equation, which is a special case of the theory of elasticity (Salgado, 2008). The Euler-Bernoulli beam equation is a fourth-order differential equation that was derived to represent the relationship between the deflection and applied load of a simplified, one-dimensional beam (Beer, Johnston, & DeWolf, 2006). An example of this derivation is shown by Beer et al. (2006), and the resulting equation is

$$EI\frac{d^4y}{dx^4} = -\omega(x) \qquad \textbf{(2.1)}$$

where:

EI = flexural rigidity or bending stiffness of the beam

$\omega(x)$ = distributed load as a function of x

The complete solution to Equation (2.1) yields the deflection (y), slope (θ), curvature (ϕ), moment (M), and shear (V) at any point along the beam for a given distributed load $\omega(x)$.

For the case of a beam subjected to arbitrary loading and supported by the subgrade, the distributed load in Equation (2.1) can be replaced by the soil reaction, $p(x)$, which is a function of the contact pressure. The general distribution of contact pressure for a smooth, perfectly rigid footing with width B is shown for both clay and sand in Figure 2.4.

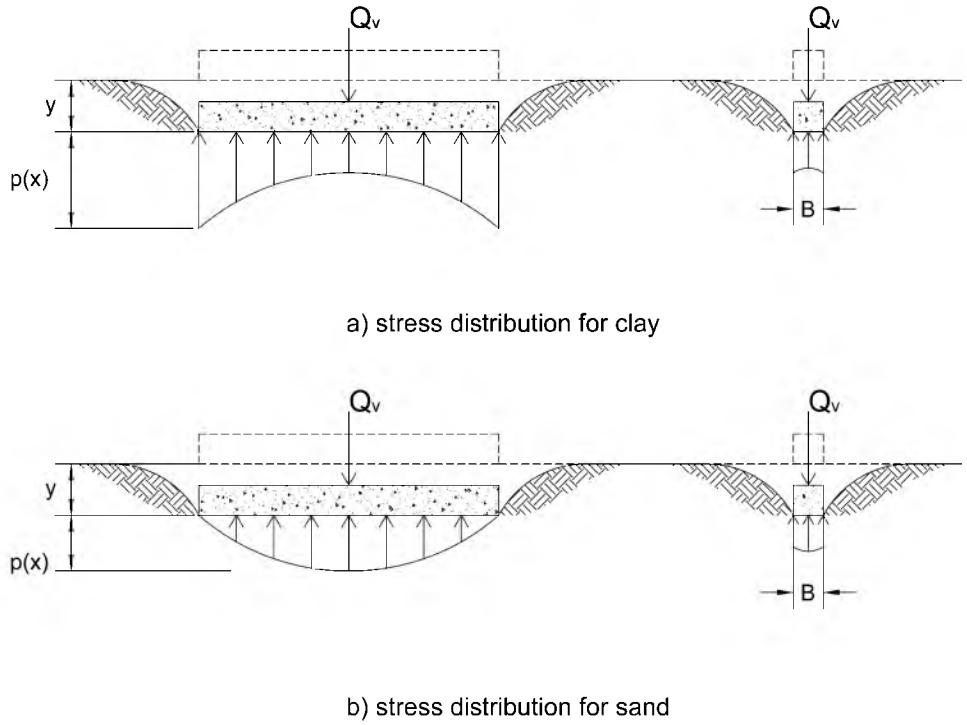

Figure 2.4. Contact pressure beneath footing for a) clay and b) sand [After Terzaghi (1955)]

According to Terzaghi et al. (1996), the relation between the stress-deformation characteristics of the subgrade and the contact pressure on the base of a perfectly smooth and rigid footing is by no means simple. Furthermore, the relation becomes even more complicated if the footing is not rigid. Winkler (1867) hypothesized that the soil reaction at any point along the beam is proportional to the displacement of the beam at the same point as shown in Equation (2.2):

$$P = ky \tag{2.2}$$

where:

y = deflection at a point along the beam

k = coefficient of subgrade reaction

P = soil reaction per unit area

In Equation (2.2), k can be thought of as the constant of proportionality between the soil reaction and beam deflection. If it is assumed that the soil reaction is uniform across the width of the beam, both sides of Equation (2.2) can be multiplied by B and Equation (2.2) can be written as

$$p = kBy = E_s y \tag{2.3}$$

where:

p = soil reaction per unit length

E_s = kB = modulus of subgrade reaction

If the soil reaction (p) from Equation (2.3) is substituted into Equation (2.1) for the distributed load of $\omega(x)$, the resulting equation is the so-called BEF equation, which is

$$EI\frac{d^4y}{dx^4} + E_s y = 0 \qquad \textbf{(2.4)}$$

The soil reaction represented by Equation (2.3) is shown in Figure 2.5(a). Unlike the soil reaction shown in Figure 2.4, the soil reaction in Figure 2.5(a) is not dependent upon soil type or the location of the soil reaction with respect to the location along the beam. This illustrates one of the major assumptions in the Winkler (1867) hypothesis, which is that the soil reaction is dependent only upon the displacement of the soil and is independent of the soil conditions or displacement of adjacent points along the beam. For this reason, the soil reaction along a beam given by Equation (2.3) has often been represented as a series of uncoupled linear springs acting at discrete, evenly spaced points along the beam as shown in Figure 2.5(b). The resulting soil reaction is a series of uniformly distributed loads as shown in Figure 2.5(c).

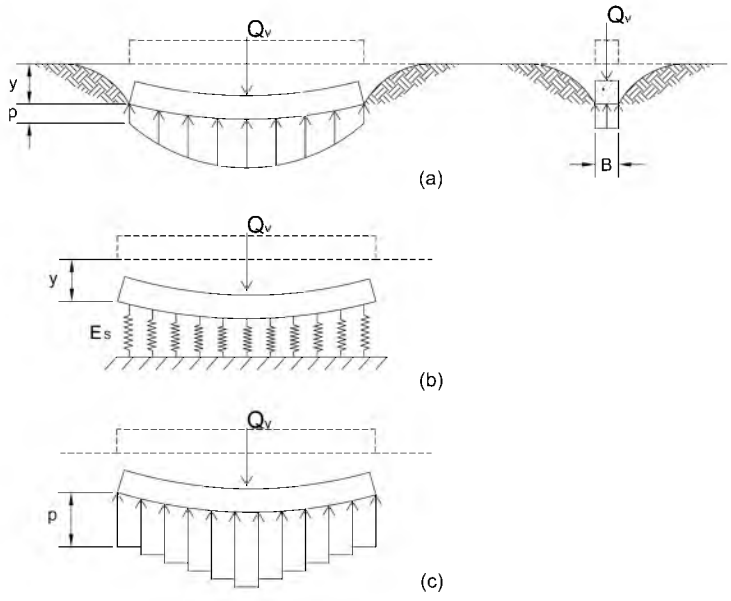

Figure 2.5. Soil reaction along a flexible footing
[After Terzaghi et al. (1996) and Salgado (2008)]

The theory for beams on elastic foundation can be extended to model vertical beam-columns embedded in the subgrade. In this scenario, a pile that is subjected to lateral and axial loads is at least partially embedded in the subgrade, and the soil reaction that develops is a function of pile deflection. An additional term can be added to the BEF equation shown in Equation (2.4) to account for an axially applied load (Q_v). Furthermore, an additional term can be added to account for a distributed lateral load being applied to some portion of the pile. The modified form of the BEF equation that includes these additional terms is presented in Equation (2.5).

$$EI\frac{d^4y}{dx^4} + Q_v\frac{d^2y}{dx^2} + E_s y + W = 0 \qquad \textbf{(2.5)}$$

$$E_s = k_h B = -\frac{p}{y} \qquad \textbf{(2.6)}$$

where:

EI = flexural rigidity or bending stiffness of the pile

x = distance along the length of the pile

y = lateral deflection of the pile at a point x along the axis of the pile

B = diameter or width of the pile

k_h = horizontal coefficient of subgrade reaction

E_s = modulus of subgrade reaction

p = soil reaction per unit length

Q_v = axial (vertical) force acting at a point x along the axis of the pile

W = distributed load acting along the length of the pile

Equation (2.5) is amenable to closed-form solution for simple loading conditions and constant or linearly varying values of EI and E_s as shown by Hetenyi (1946). The complete solution to Equation (2.5) yields profiles for deflection (y), slope (θ), curvature (ϕ), moment (M), shear (V), and soil resistance (p) as shown in Figure 2.6 (curvature not shown). Solutions to Equation (2.5) can be obtained when the boundary conditions for y, θ, M, and V are known at the ground surface (Janoyan, Stewart, & Wallace, 2001), or if they can be reasonably assumed at some other point along the pile, such as at the base of a very long pile. The equations for y, θ, M, *and* V are show in Equations (2.7) through (2.10).

$$\theta = \frac{dy}{dx} \tag{2.7}$$

$$\phi = \frac{d\theta}{dx} = \frac{d^2y}{dx^2} \tag{2.8}$$

$$M = \phi EI = EI\frac{d^2y}{dx^2} \tag{2.9}$$

$$V = \frac{dM}{dx} = EI\frac{d^3y}{dx^3} \tag{2.10}$$

Until about 1956, the BEF equation was typically solved using a constant value of E_s and EI out of mathematical necessity, despite the well-known fact that E_s is not, in fact, constant (McClelland & Focht, 1958). The assumption that EI and E_s are constant yields an elastic solution, which is not realistic for the vast majority of real engineering

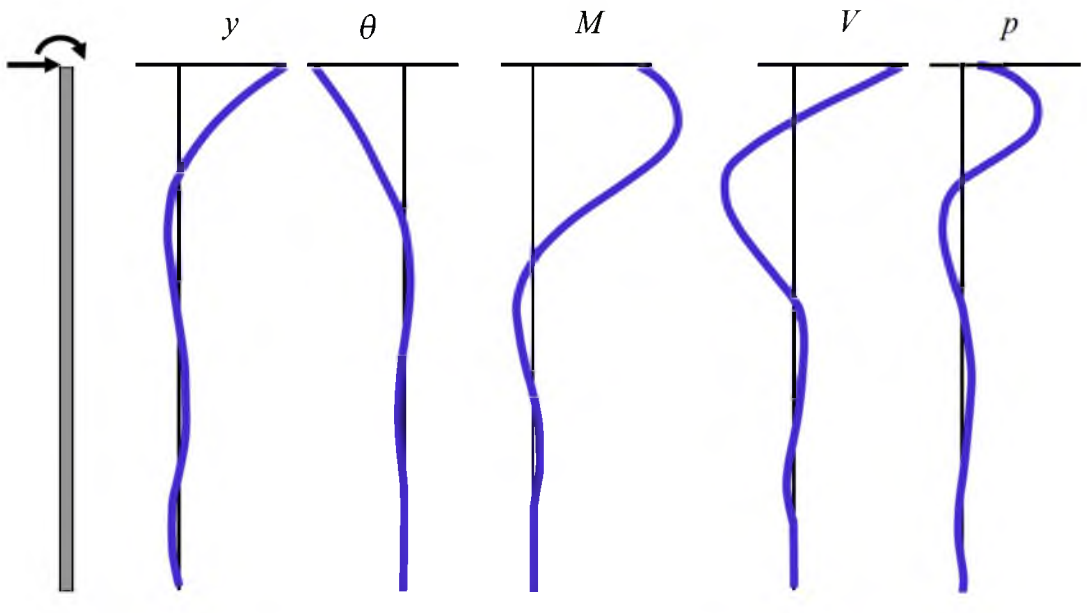

Figure 2.6 Profiles of complete solution of a laterally loaded drilled shaft (Isenhower & Wang, 2010)

problems. A more realistic solution to the BEF equation can be obtained using relationships for EI and E_s that vary as a function of both pile deflection and depth; however, this makes it more difficult, if not impossible, to obtain a closed form solution. For this reason, numerical methods are the preferred technique for obtaining more realistic solutions to the BEF equation.

McClelland and Focht (1958) discussed early attempts at increasing the versatility of the BEF equation by using the finite difference technique to obtain a solution, but that the correctness of the solution ultimately depends on the stress-strain relationship assigned to the soil for the purpose of analysis. Matlock (1970) stated that, with the availability of numerical solutions to the BEF equation, the most important but difficult part of the problem is to express the soil resistance characteristics, which implies difficulty in expressing E_s.

2.3.1 Modulus of Subgrade Reaction, E_s

One of the earliest and most comprehensive discussions on the topic of subgrade reaction was presented in the seminal paper by Terzaghi (1955). Terzaghi (1955) stated that there is an erroneous conception that is widespread among engineers that the numerical value of k, and by extension E_s, depends exclusively on the nature of the subgrade. Terzaghi (1955) suggested that k is not actually a fundamental soil property, but that its value depends on the characteristics of the soil, the area acted upon by the subgrade reaction, and the load applied to the foundation. According to Terzaghi (1955), E_s decreases as the loaded area increases. Furthermore, he suggested that E_s is somewhat independent of depth for stiff clays and increases with depth for soft clays and sands.

While Terzaghi (1955) presented an in-depth discussion of the factors that affect the subgrade modulus, he describes the subgrade reaction as a fictitious pressure that satisfies Equation (2.6) in contrast to the real soil pressure (Terzaghi, Peck, & Mesri, 1996). He showed that the subgrade reaction resulting from a constant subgrade modulus is not the same as the real contact pressure on the foundation. For example, the soil reaction of a smooth, perfectly rigid beam that satisfies Equation (2.6) would be a uniformly distributed load, which is in contrast to the actual contact pressure presented in Figure 2.4. This variance is even more pronounced if the load Q_v shown in Figure 2.4 does not act at the centroid of the footing, and acts, for example, towards the left side of the beam. In this case, the real contact pressure increases towards the left side of the beam and decreases towards the right side to satisfy static equilibrium, but the soil reaction from Equation (2.6) is still a uniformly distributed load as the settlement of a rigid footing is uniform, and thus static equilibrium is not satisfied (Terzaghi, Peck, & Mesri, 1996). Nevertheless, Terzaghi (1955) acknowledged the usefulness of the

subgrade reaction approach within its limitations, particularly for flexible foundations, and presented methods for characterizing k from plate load tests.

Terzaghi (1955) also presented a procedure for conducting a lateral load test of a steel pipe pile and characterizing the subgrade modulus from the results. One of the first attempts to characterize E_s from the results of a large-scale lateral load test using the method presented by Terzaghi (1955) was performed by McClelland and Focht (1958).

McClelland and Focht (1958) obtained experimental data from a large-scale lateral load test of a steel pipe pile embedded in soft marine clay at an offshore site in Texas. The test pile had a diameter and embedded length of 2 ft and 75 ft, respectively, and was instrumented with several strain gauges placed in diametric pairs along the length of the foundation. Curvature profiles were estimated from the strain gauge data for each load increment by taking the difference in strain between diametric pairs and dividing the result by the diameter of the pile. A procedure similar to the one described later in Section 2.4.1 was used to obtain p and y profiles from the curvature data, with the most notable difference being that integration and differentiation of the curvature profiles was performed using graphical methods.

For the range of lateral loads applied to the top of the test pile, McClelland and Focht (1958) plotted p-y data pairs at several depths along the pile. The resulting soil reaction vs. deflection curves, referred to as p-y curves, were used to evaluate E_s at each depth from the relationship shown in Equation (2.6). McClelland and Focht (1958) performed triaxial compression tests on several samples from a range of depths at the test site, and showed that a correlation existed between the p-y curves and the stress-strain curves from the triaxial tests. The p-y curves were converted into so-called field stress-strain curves by converting y into one-dimensional strain, ε, by somewhat arbitrarily

dividing y by the pile radius, r, as shown in Equation (2.11).

$$\varepsilon = \frac{y}{r} = \frac{2y}{B} \tag{2.11}$$

It was then shown that the field stress-strain curve at a given depth could be estimated by multiplying the deviatoric stress from a triaxial compression test performed at confining stress equal to the same depth by 5.5 for all values of strain. This relationship is shown in Equation (2.12).

$$\frac{p}{B} = 5.5\sigma_d \tag{2.12}$$

where σ_d = deviatoric stress from the triaxial compression test. It should be noted that the deviatoric stress at failure is equal to $2c$ for purely cohesive soils, and therefore, the ultimate soil resistance at any depth is equal to $11c$ when $\sigma_d = 2c$ in Equation (2.12). Equation (2.11) and (2.12) can be rearranged to determine E_s from the secant modulus of the triaxial test as

$$E_s = \frac{p}{y} = 11E \tag{2.13}$$

Because E from a triaxial compression test is nonlinear, the estimated value of E_s from Equation (2.13) must also be nonlinear. Thus, using the numerical procedure outlined by McClelland and Focht (1958), nonlinear solutions could be obtained for the laterally loaded pile problem using estimations of E_s from laboratory testing.

Although the work performed by McClelland and Focht (1958) was largely

praised as being a much-needed step forward in characterization of the subgrade modulus and performing nonlinear analysis of laterally loaded piles, it was met with considerable skepticism and criticism as seen in the discussion of the paper.

Ripperger (1958) posited the question of whether such a soil modulus actually exists, and if so, if its value can be uniquely defined for a specific soil. He concluded that it is true that a secant modulus can be obtained mathematically in the sense that the soil reaction at any point along a pile can be divided by the corresponding deflection, but that E_s cannot be unique for a soil because it depends not only on the elastic characteristics of the soil, but on many other factors that are not easily characterized. Ripperger (1958) further stated that, in light of all of the factors that contribute to the relationship between subgrade reaction and deflection, it does not seem likely that E_s, even if uniquely defined, could be related to E by a simple numerical factor. Reese (1958) suggested that only the ultimate soil resistance could be approximated using a rational method, and that ultimate soil resistance could be modeled as either a flow-around failure or a mobilized passive wedge in front of the pile near the ground surface. Reese (1958) showed that the ultimate soil resistance could be has high as $12c$ for flow around failure and as low as $2c$ for passive wedge failure, and suggested that the ultimate soil resistance of $11c$ found by McClelland and Focht (1958) was therefore reasonable at depths where flow-around failure occurs, but that it is probably too high near the ground surface where passive wedge-type failure occurs.

McClelland and Focht (1958) acknowledged in the discussion that this numerical factor of 5.5 in Equation (2.12), and thus 11 in Equation (2.13), is not unique to the soil type, and that it will most certainly change for a different soil type and pile configuration; however, they suggest that the only way to truly evaluate E_s for any soil-pile interaction

is through a load test of that pile, and that using the proposed correlation for obtaining E_s from laboratory testing is a reasonable way of approximating E_s without having to conduct and actual full-scale load test. Furthermore, they state that the theoretical values of ultimate soil resistance of *12c* and *11.42c* estimated by Reese (1958) and Meyerhof (1951), respectively, at least somewhat substantiate their proposed value of *11c*. It should also be noted that Skempton (1951) performed a similar comparison between laboratory test data and observed soil reaction-settlement data from field tests of various types of structures, and concluded that a reasonable value of the ultimate soil resistance of soft clay is *9c*. This provides further evidence that the value of *11c* proposed by McClelland and Focht (1958) is reasonable.

Considerable research has been conducted since McClelland and Focht first attempted to correlate E_s with the results of laboratory testing. Most of this research has been performed with the same objective, which is to correlate E_s with in-situ or lab testing data, while attempting to account for the factors thought to influence E_s. McClelland and Focht (1958) concluded that E_s generally depends on depth, deflection, pile diameter, pile stiffness, pile length, soil type, and load magnitude. Welch and Reese (1972) suggest that E_s is also a function of shear strength, moisture content, stress history, and the effective stress state of the surrounding soil. Ashour and Norris (2000) have shown theoretically how E_s depends on cross-sectional shape, and fixity of the pile head. Clearly, there is strong theoretical and experimental evidence to suggest that E_s is a not a fundamental soil property, and that its value is entirely dependent upon the specific characteristics of a given soil-structure interaction.

Despite the obvious limitations of subgrade reaction theory and the challenges associated with characterizing E_s for a particular soil-structure interaction problem,

subgrade modulus theory and the BEF equation provide a convenient mathematical framework for performing a nonlinear analysis of a laterally loaded pile (McClelland & Focht, 1958). The concept of solving the BEF equation using numerical methods and a nonlinear representation of E_s and EI is still appealing to this day. Brown et al. (1994) state that this approach has been widely accepted because of its simplicity and ability to capture the essential aspects of pile behavior, including nonlinear soil resistance, gapping around the pile, and variable soil and pile properties. According to Norris (1986), the BEF solution technique for laterally loaded piles is often preferable to elastic continuum or finite element methods because the formulation is simple, it can readily handle both layered and nonlinear soil response, parameter input is well-documented in the literature, and the method has been found to predict response that compares favorably with field behavior over a large range of deflection.

The literature review that was conducted for this investigation, in addition to the author's consultation with several practicing engineers in the field of deep foundation design, revealed that virtually all of the methods that are currently used to perform these types of analyses are still based on this approach. There are examples of other methods of analysis being used, such as the finite element method and finite difference method, but these methods appear to only be used in special circumstances, and are far from routine. The details of the three methods being considered in this analysis and how they approach solving the BEF equation with nonlinear representation of E_s and EI will be discussed in Section 2.4 through 2.6.

2.3.2 Nonlinear Solution Techniques

Closed-form solutions to the BEF equation for a pile at least partially embedded in the subgrade, as shown in Equation (2.4), have been presented by Hetenyi (1946); however, these closed-form solutions are tedious, and require unrealistic assumptions about E_s and EI that preclude their use from routine analyses. More realistic solutions can be obtained using numerical methods, such as the finite difference method (1970). These details of these techniques are outside the scope of this investigation; however, the general solution scheme proposed by McClelland and Focht (1958) will be discussed within this section because the solution scheme used by *LPile* and *DFSAP* is very similar.

McClelland and Focht (1958) describe a procedure for obtaining nonlinear solutions for the BEF equation using *p-y* curves as follows: A pile deflection curve is assumed for a given loading condition. The strain is calculated at several points along the deflection curve above the point of zero deflection using Equation (2.11), and corresponding soil reaction is computed from a triaxial compression test performed at the same depth and Equation (2.12). An E_s profile is estimated by computing E_s for each p and y data pair using Equation (2.13). A simplification of the E_s vs. depth profile is made, and the BEF equation in difference form is solved using this simplified relationship. The E_s profile is computed from the p and y profiles obtained from the BEF solution and compared to the simplified E_s profile. This procedure is iterated until convergence is achieved.

2.4 LPile and the *p-y* Method

The so-called *p-y* method is an extension of the work performed by McClelland and Focht (1958) described in Section 2.3, and is described as such for the *p-y* curves that

are used to obtain nonlinear solutions to the BEF equation. Recall from Section 2.3 that a *p-y* curve for a particular point along a laterally loaded pile represents the subgrade reaction per unit length, p, and the corresponding pile deflection, y, at that point for a range of applied loads. Because *p-y* curves represent a force-displacement relationship, they can be used to mathematically represent the behavior of a nonlinear spring. A series of these springs can be used to model the subgrade reaction as shown in Figure 2.7.

The subgrade modulus, E_s, is the secant modulus of a *p-y* curve, and its value can be estimated at any point along the *p-y* curve using Equation (2.6). Thus, if the *p-y* curves are known for several points along the foundation, E_s can be characterized in terms of p and y and numerical methods can be used to obtain nonlinear solutions to the BEF equation for a pile at least partially embedded in the subgrade shown in Equation (2.5).

Modern computers have made it fairly straightforward to solve the BEF equation using numerical methods (1970); however, there is still considerable difficulty in estimating the "correct" *p-y* curves for any particular pile embedded in the subgrade. Because *p-y* curves are simply an expression of subgrade reaction theory discussed in Section 2.3.1, they are subject to the same challenges associated with characterizing E_s. As such, it is not currently possible to determine the "correct" *p-y* curves for a particular soil-pile interaction based on the fundamental physics of the problem. Furthermore, it is not possible to directly measure *p-y* curves in a large-scale load test due to the complexity of the soil response to loading, as shown in Figure 2.1, and the inadequacy of sensor technology to directly measure all of the components that contribute to the total soil reaction (Janoyan & Whelan, 2004).

It follows from the discussion in Section 2.3 that *p-y* curves are unique to every

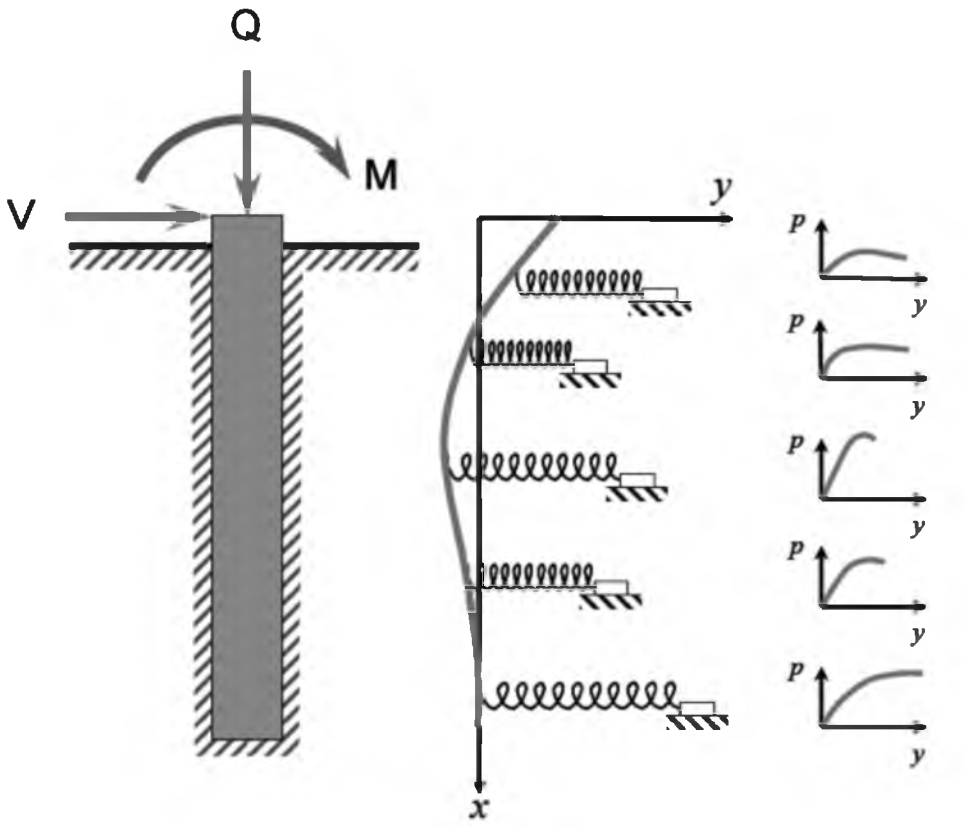

Figure 2.7 Model of subgrade reaction for a laterally loaded pile using independent springs and associated nonlinear *p-y* curves (Isenhower & Wang, 2010)

soil-structure interaction, and therefore, the only way to estimate the "correct" *p-y* curves for a particular pile or drilled shaft is by back-calculating the *p-y* curves from a large-scale load test using techniques described in Section 2.4.1. The cost to conduct such a load test is prohibitively high for most projects (Kulhawy, et al., 1983). As such, it is desirable to be able to estimate the *p-y* curves using some other technique. McClelland and Focht (1958) showed that it is possible to back-calculate *p-y* curves at any particular depth from the results of a large-scale load test of a steel pipe pile, and subsequently proposed a method to estimate *p-y* curves from the results of laboratory triaxial tests. Despite early criticism of the viability of correlating the subgrade reaction with

laboratory test results, as discussed in Section 2.3, considerable research has since been performed to establish methods for estimating *p-y* curves from in-situ tests and laboratory tests to obviate the need for conducting full-scale load tests.

Methods that are commonly used to back-calculate *p-y* curves from large-scale load tests are presented in Section 2.4.1, which is followed by a discussion of how back-calculated *p-y* curves from several large-scale load tests were used to formulate semi-empirical relationships between *p-y* curves and soil properties that are readily available from laboratory or in-situ testing in Section 2.4.2. In-situ tests, such as the pressuremeter test (PMT) and dilatometer test (DMT), can be used to establish soil properties for estimating *p-y* curves using semi-empirical methods, but they have also been used to estimate *p-y* curves directly [(Anderson, Townsend, & Grajales, 2003), (Briaud, Smith, & Tucker, 1985), (Briaud, Smith, & Meyer, 1983), (Robertson, Davies, & Campanella, 1989)]. These methods will be discussed in greater detail in Section 2.4.3.

2.4.1 Estimation of *p-y* Curves from Large-Scale Load Tests

The *p-y* curve for a particular foundation at a given depth can be back calculated from the results of a well-instrumented large-scale lateral load test. The instrumentation of a large-scale lateral load test typically includes inclinometers, strain gauges, displacement transducers, and load cells (Reese, Cox, & Koop, 1975). The inclinometer measurements can be obtained by individual inclinometers placed along the pile within a guide casing, or by placing an inclinometer casing along the length of the pile and using a single instrument to take measurements along the casing for each loading increment [(Brown, Hidden, & Zhang, 1994), (Geokon, Inc., 2012)]. The strain gauges are placed in diametric pairs along the line of loading and at several depths along the length of the

pile. The displacement and applied load are measured at the pile head using displacement transducers and a load cell, respectively.

The basic procedure for computing *p-y* curves from inclinometer data is outlined by Brown et al. (1994). The slope profile along the pile is calculated directly from the inclinometer data. This slope profile is integrated once using the known deflection of the pile head as a boundary condition to obtain the deflection profile along the pile as shown in Equation (2.14). The slope profile is differentiated three times and multiplied by *EI* to obtain the soil resistance profile along the pile as shown in Equation (2.15).

$$y(x) = \int \theta(x)\, dx \tag{2.14}$$

$$p(x) = EI \frac{d^3}{dx^3} y(x) \tag{2.15}$$

where:

x = distance along the length of the pile

EI = flexural rigidity of the shaft

$y(x)$ = deflection of the shaft as a function of x

$p(x)$ = soil reaction per unit length as a function of x

$\theta(x)$ = slope of the shaft as a function of x

The basic procedure for computing *p-y* curves from strain gauge data is outlined by Yang and Liang (2006). The curvature (ϕ) is calculated at each pair of strain gauges as the difference between the measured strains divided by the distance between the strain gauges. The fifth-order polynomial shown in Equation (2.16) is then used to fit the

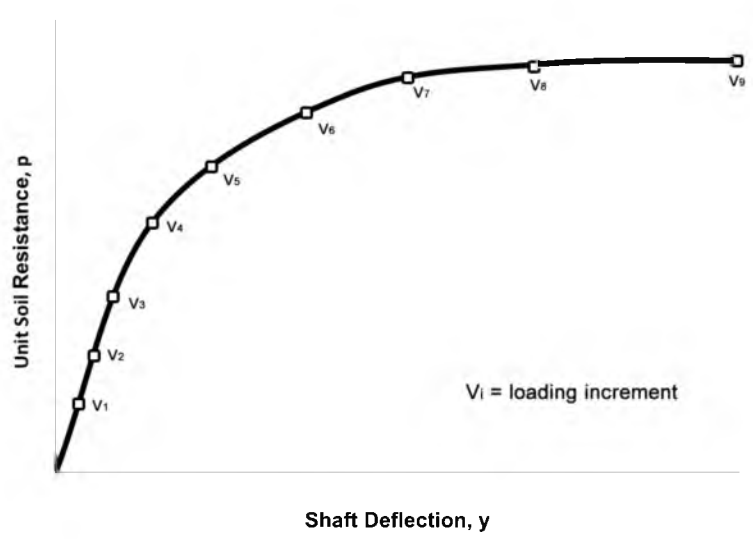

Figure 2.8 Typical *p-y* curve obtained from back analysis of inclinometer or strain gauge data for each incremental load

discrete curvature data points to obtain the curvature profile of the pile, $\phi(x)$. Deflection as a function of depth, $y(x)$, is obtained by double integration of the curvature profile as shown in Equation (2.17) using the known slope and deflection at the pile head as boundary conditions. The moment profile is obtained by multiplying the discrete values of ϕ by EI as shown in Equation (2.18). A third-order piecewise polynomial is then fitted to each 5 successive values of ϕ using the least-squares method as shown in Equation (2.19). Each piecewise polynomial is twice differentiated with respect to x as shown in Equation (2.20) to obtain the soil resistance profile, $p(x)$. As with the procedure for inclinometer data, the procedure is repeated for each loading increment, V_i, to obtain the *p-y* curve for a specified depth as shown in Figure 2.8.

$$\phi(x) = C_1 + C_2x + C_3x^{2.5} + C_4x^3 + C_5x^4 + C_6x^5 \qquad \textbf{(2.16)}$$

$$y(x) = \int \left(\int \phi(x) dx \right) dx \tag{2.17}$$

$$M = \phi EI \tag{2.18}$$

$$M(x)_i = C_1 + C_2 x + C_3 x^2 + C_4 x^3 \tag{2.19}$$

$$p(x)_i = \frac{d^2}{dx^2} M(x)_i \tag{2.20}$$

where:

x = distance along the length of the shaft

M = internal bending moment of the shaft

EI = flexural rigidity of the shaft

$\phi(x)$ = curvature of shaft as a function of x

$y(x)$ = deflection of the shaft as a function of x

$M(x)_i$ = Internal bending moment as a function of x for 5 successive data curvature data points

C_i = unknown curve fitting coefficients

$p(x)_i$ = soil resistance as a function of x for 5 successive curvature data points

Brown et al. (1994) state that the use of inclinometers is advantageous because they are much less expensive and much less susceptible to damage than strain gauges; however, the soil resistance data are prone to reduction error because the slope distribution must be differentiated three times in order to obtain p. They further state that

it is perfectly acceptable to compute the deflection profile from inclinometer data, but that the soil resistance profile will likely have too much error to be useful. Other researchers such as Lin and Liao (2006) have devised more sophisticated methods for obtaining p from inclinometer data that have been shown to have much less error.

Strain gauges are generally considered to give the most accurate estimation of curvature; however, Matlock (1958) showed that even a 1% difference in moment values can result in estimated values of p that are nearly 200% greater due to the error associated with double-differentiation. As such, Matlock (1958) suggested that careful consideration be given to strain gauge spacing and that the pile itself be calibrated against known moment profiles before being installed and tested. A large-scale lateral load test was performed by Janoyan et al. (Janoyan, Stewart, & Wallace, 2001) on a drilled shaft that was instrumented with inclinometers, strain gauges, and other instruments in order to quantify the variability of p. Their results showed that there was considerable variability in p when estimated using data from different instrumentation, and that redundant sources of instrumentation should always be used when possible.

2.4.2 Estimation of *p-y* Curves Using Semi-Empirical Methods

There are several methods that can be used to develop the p-y curves required to perform an analysis of a laterally loaded pile or drilled shaft. The semi-empirical methods were developed to allow the designer to establish p-y curves without having to back-calculate p-y curves from a full-scale lateral load test as described in in Section 2.4.1. Semi-empirical methods are most commonly used in current practice because they are easy to use, require only a few input properties from the soil in which the foundation will be constructed, and give designers an added degree of confidence in the results

because they were partially developed from the results of large-scale load tests (Brown, Morrison, & Reese, 1988).

As discussed in Section 2.3, McClelland and Focht (1958) developed the first semi-empirical method for estimating *p-y* curves from the results of a large-scale lateral load test of a steel pipe pile. They back-calculated *p-y* curves from the range of applied loads using a procedure similar to the one described later in Section 2.4.1, with the most notable difference being that integration and differentiation of the curvature profiles was performed using graphical methods. These back-calculated *p-y* curves were correlated with stress-strain curves from triaxial testing, and the resulting equations for p, y, and E_s from triaxial stress-strain curves are

$$p = 5.5B\sigma_d \tag{2.21}$$

$$y = 0.5B\varepsilon_d \tag{2.22}$$

$$E_s = \frac{p}{y} = 11E \tag{2.23}$$

where:

p = soil resistance per unit length

B = diameter (width) of shaft

y = deflection of the shaft corresponding to p

σ_d = deviator stress from a triaxial compression test

ε_d = axial strain corresponding to σ_d

E_s = modulus of subgrade reaction

E = secant modulus of soil from triaxial compression test

Several semi-empirical methods have been developed in the decades since McClelland and Focht (1958) first proposed their methodology for estimating *p-y* curves from laboratory test data. As discussed in Section 2.3, E_s is not a fundamental soil property, but is a unique property of each individual soil-structure interaction. As such, methods for developing *p-y* curves must necessarily take into consideration the properties of the soil *and* the properties of the foundation. The semi-empirical methods that are currently available in programs such as *LPile* and *FB-Multipier* were generally developed within the theoretical framework of soil mechanics and experimental observation, and most were developed in conjunction with large-scale load tests of steel pipe piles or drilled shafts. The relationships for *p* and *y* were parameterized to account for variables thought to affect the *p-y* curves, and these relationships were modified until there was sufficient agreement between the observed and predicted results.

The semi-empirical methods are generally described by the type of soil or rock for which they are intended to be used, as well as any distinguishable characteristics of the particular method. For example, the four methods that are available for clay are described as *soft clay* (Matlock, 1970), *stiff clay with free water* (Reese, Cox, & Koop, 1975), *stiff clay without free water* [(Welch & Reese, 1972), (Reese & Welch, 1975)], and *modular stiff clay without free water* (Isenhower & Wang, 2010). The semi-empirical *p-y* curves that are currently available in *LPile* 13 are as follows:

- Soft Clay (Matlock, 1970)
- Stiff Clay with Free Water (Reese, Cox, & Koop, 1975)

- Stiff Clay without Free Water [(Welch & Reese, 1972), (Reese & Welch, 1975)]
- Modular Stiff Clay without Free Water (Isenhower & Wang, 2010)
- Sand (Reese, Cox, & Koop, 1974)
- API Sand (O'Neill & Murchison, 1983)
- Liquefied Sand (Rollins, Hales, & Ashford, 2005)
- Weak Rock (Reese L. C., 1997)
- Strong Rock (Vuggy Limestone) (Reese & Nyman, 1978)
- Piedmont Residual
- Silt (cemented c-phi)
- Loess
- Elastic Subgrade

The data available in the literature for large-scale lateral load tests conducted on semi-rigid drilled shafts are limited. As such, the semi-empirical methods for soft clay, stiff clay without free water, and sand are the only methods that will be included in this investigation. The formulation of the API Sand *p-y* curve (1983) is similar to the formulation of the Reese et al. (1975) *p-y* curve and in the author's experience, the difference in results tends to be small. The Reese et al. (1975) *p-y* curve was chosen for use in this investigation. The development of these semi-empirical methods and the procedures used to estimate *p-y* curves using these methods are discussed within Section 2.4.2.1 through 2.4.2.3.

2.4.2.1 Soft Clay (Matlock, 1970)

Matlock (1970) conducted a large-scale lateral load test of a steel pipe pile that was 12.75 inches in diameter and 42 feet long. The pile had a *D/B* ratio of 39.5, which suggests the pile behaved as a very flexible pile. The pile was instrumented with 35 pairs of electric strain gauges, with spacing ranging from 6 inches in the upper section to 4 feet in the lower section. The pile was calibrated before being installed to provide extremely accurate determinations of internal bending moment.

The pile was driven into soft clay with average s_u of approximately 800 psf at Lake Austin, Texas. A total of two lateral load tests were conducted, with the first being a static load test and the second being a cyclic load test. The load was applied to the pile at the ground surface under free-head conditions with the use of a hydraulic ram. After the load tests were completed, the pile was recovered and re-driven near Sabine Pass, Texas. The soil at Sabine Pass consisted of soft clay with average s_u of approximately 300 psf. The soil was somewhat overconsolidated due to desiccation, and fissures and cracks were present in the soil structure. The testing procedures were similar to those at Lake Austin, but two static and two cyclic load tests were performed - one each for free-head conditions, and one each for fixed-head conditions. Free water was present above the ground surface at both testing locations.

The *p-y* curves from all of the load tests were back calculated using a procedure similar the strain gauge procedure described previously in Section 2.4.1. Values for p and y were obtained for each loading increment from the strain gauge data using numerical differentiation and integration, respectively. Matlock (1970) stated that he was quite confident in the profiles of p and y because of the calibration of the pile and instrumentation that was performed prior to the pile being installed and tested.

Based on Matlock's observations during the load tests, he developed generalized shapes of *p-y* curves for both static and cyclic loading. The *p-y* curve for static loading is shown in Figure 2.9. Cyclic loading is outside the scope of this investigation, and as such, the *p-y* curves for cyclic loading are not discussed.

One of the major objectives of Matlock's research was to develop parametric equations for these *p-y* curves that were functions of parameters that can be obtained from laboratory or field tests. The following paragraphs describe how the equations for these curves were formulated.

Several researchers, including McClelland and Focht (1958), Reese (1958), Hansen (1961), and Broms (1964b), among others, have spent considerable effort

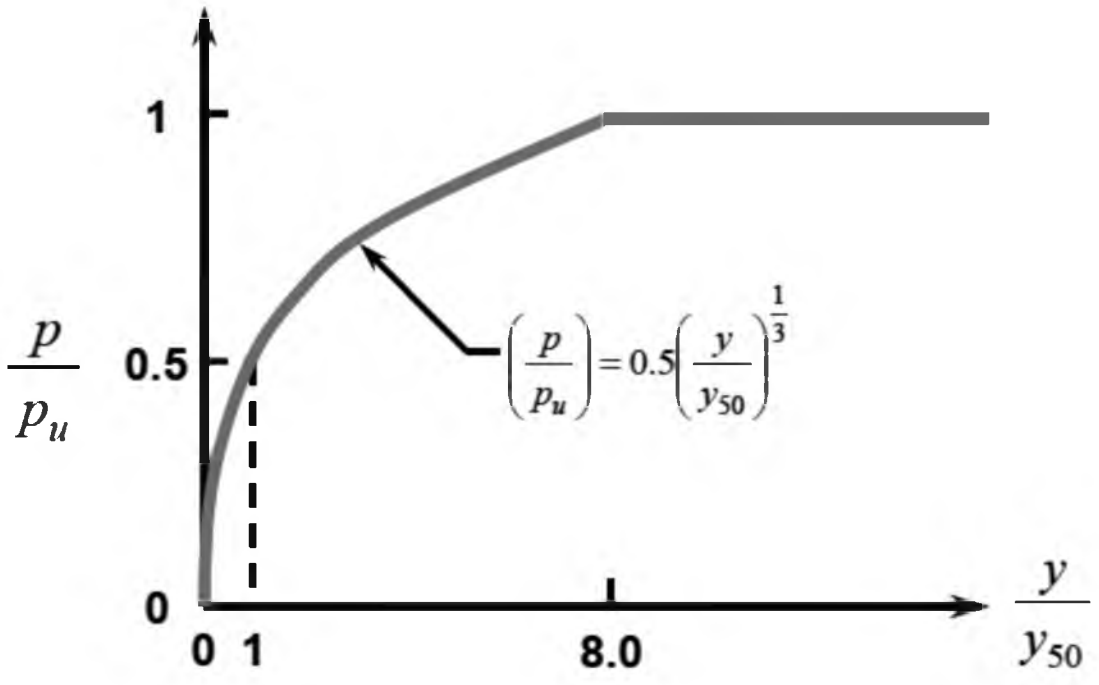

Figure 2.9 General shape of *p-y* curve for static loading in soft clay (Isenhower & Wang, 2010)

studying the ultimate strength of cohesive soils. Based on the general consensus of these researchers, Matlock estimated the ultimate soil resistance per unit length (p_u), which is the horizontal straight-line portion of the *p-y* curves shown in Figure 2.9, using Equation (2.24).

$$p_u = N_p B s_u \tag{2.24}$$

where:

p_u = ultimate soil resistance per unit length

N_p = lateral bearing factor

B = pile diameter

s_u = undrained shear strength of the soil

Several values have historically been used for the lateral bearing factor, N_p, but Matlock opted to use a value of 9 as proposed by Broms (1964b) and Skempton (1951). Note that Equation (2.24) is equivalent to Equation (2.21) where $\sigma_d = 2s_u$.

Reese (1958) suggested that Equation (2.24) is valid for flow-around type of failure shown in Figure 2.10(a), but that a passive wedge-type failure shown in the free body diagram of Figure 2.10(b) occurs near the ground surface. If the shearing resistance between the pile and the soil is assumed to be zero, and the angle of the passive wedge is assumed to be 45 degrees for undrained conditions at failure, Reese showed that

$$N_p = \left[2 + \frac{\gamma'_{avg}}{s_u} x + 2.83 \frac{x}{B}\right] \tag{2.25}$$

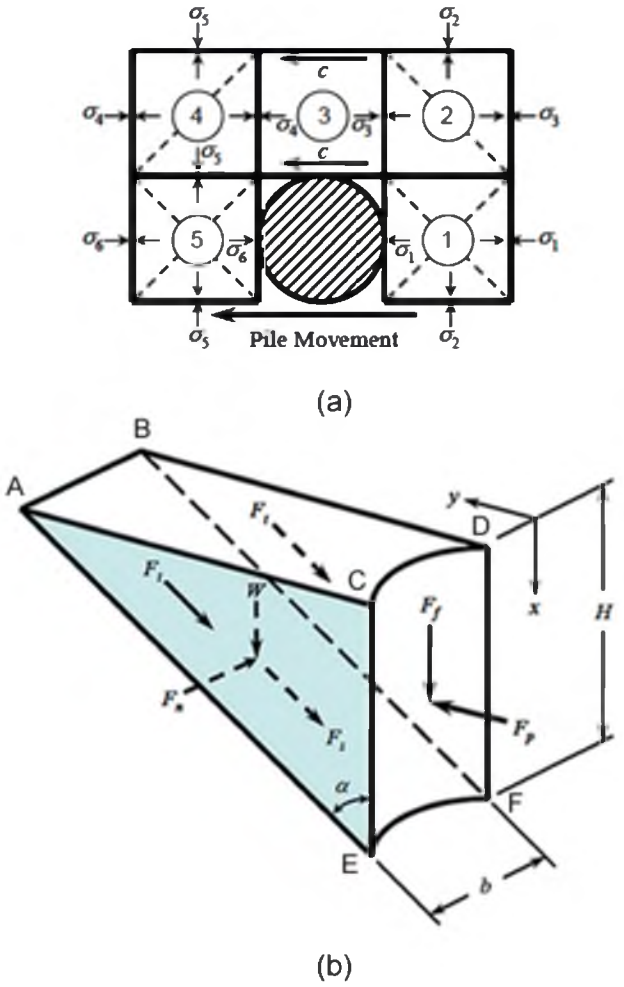

Figure 2.10. Ultimate soil resistance for (a) flow-around failure, and (b) passive wedge-type failure for cohesive soil [After (Reese L. C., 1958)]

where:

γ'_{avg} = average effective unit weight from ground surface to *p-y* curve

s_u = undrained shear strength of the soil

x = distance along the length of the shaft to the *p-y* curve

B = pile diameter

It should be noted that Equation (2.25) was derived from the passive wedge shown in Figure 2.10(b) by differentiating the sum of the horizontal forces.

Matlock accepted that N_p is affected by the presence of the ground surface, as proposed by Reese (1958), and that the close proximity to the ground surface tends to reduce the value of N_p; however, he modified Equation (2.25) by increasing the first term from 2 to 3 and by replacing the third term of 2.83 with a nondimensional coefficient, J, as shown in Equation (2.26).

$$N_p = \left[3 + \frac{\gamma'_{avg}}{s_u} x + J\frac{x}{B}\right] \tag{2.26}$$

Matlock (1970) stated that the first term in Equation (2.26) ranges from 2 to 4 for a flat plate and a square pile, respectively, where the increased value of 4 accounts for the side shear that develops along the sides of the square pile. Although not stated explicitly, in can be inferred from Matlock's chosen value of 3 for this term that he thought that cylindrical pile behavior was somewhere between a flat plate and a square pile.

Reese (1958) suggested that an appropriate value for J can be as high as 2.83, as shown in Equation (2.25). Matlock used a value of 0.5 for J to obtain good agreement between the predicted and observed results of the Sabine Pass tests; however, he had to use a value of 0.25 to obtain good agreement between the predicted and observed results in the stiffer clay at Lake Austin.

The depth at which failure transitions from wedge-type failure to flow-around failure, x_r, can be estimated from Equation (2.26) by selecting a value for J, setting N_p equal to 9, and solving for x. The p-y curves above this depth are estimated from Equation (2.24), while the p-y curves below this depth are estimated from Equation (2.26).

As previously discussed, Terzaghi (1955) stated that the coefficient of subgrade

reaction was only valid up to approximately half of the ultimate soil resistance. Based on the work of Skempton (1951), Matlock assumed the deflection of the pile at one half of the ultimate soil resistance (y_{50}) could be related to the strain at one half of the maximum stress on a laboratory stress-strain curve (ε_{50}) using the equation shown in Equation (2.27).

$$y_{50} = 2.5\varepsilon_{50}B \tag{2.27}$$

where:

y_{50} = deflection at one half of the ultimate soil resistance, p_u

ε_{50} = strain at one half of the maximum stress on a laboratory stress-strain curve

Finally, from Equations (2.24) and (2.27), the equation for p less than p_u, as shown in Figure 2.9, is

$$p = 0.5p_u\left(\frac{y}{y_{50}}\right)^{1/3} \tag{2.28}$$

It can be seen in Figure 2.9 that the value of p is assumed to be the constant value of p_u beyond $y = 8y_{50}$.

The coefficient of 2.5 in Equation (2.27) was suggested by Skempton (1951) for uniformly loaded footings with a length-to-diameter ratio of 10. He suggests values between 1.7 and 2.5 for length-to-diameter ratios less than 10. McClelland and Focht (1956) have suggested values as small as 0.5 should be used. Bhushan et al. (1979) conducted several large-scale load tests on semi-rigid and rigid drilled shafts in stiff clay, and they found that *p-y* curves computed with a value of 2.0 instead of 0.5 for *J*, 2.0

instead of 2.5 in Equation (2.27), and 1/2 instead of 1/3 in Equation (2.28) were in much better agreement with the experimental results. It should be emphasized that these tests were conducted in stiff clay, but the importance that these parameters can have substantial variability, which can significantly affect the results, cannot be understated. Furthermore, these parameters cannot be changed in *LPile*, and as such, it is expected that unrealistic results can occur when analyzing drilled shafts with D/B ratios less than 10.

As previously discussed in this section, Matlock reduced J from the theoretical maximum value of 2.83 proposed by Reese (1958) to 0.5 and 0.25 to obtain good agreement between the observed and predicted results for the Sabine Pass and Lake Austin load tests, respectively. Although Matlock states that J should be thought of as a rational but essentially empirical constant, it is worth noting that the suggested value of 2.83 by Reese (1958) does have important physical significance. The horizontal component of the shearing resistance along plane *ABEF* of the passive wedge shown in in Figure 2.10(b) is $2cH \sec(\alpha)$ where $J = 2 \sec(\alpha)$. When the passive wedge is fully mobilized, $\alpha = 45$ degrees for undrained conditions and $J = 2\sec(45°) = 2.83$. Because J is a function of α, a reduction of its value suggests that α would also have to be reduced; however, this would result in nonvanishing trigonometric terms in the first two terms of Equation (2.26), and would therefore result in a different formulation for N_p. Furthermore, the state of stress on the passive wedge can only be defined at failure using Mohr-Coulomb theory, and as such, there is difficulty in theoretically justifying the use of a different value of α and a passive wedge that has not yet reached failure.

The reduction of the theoretical value of J helped Matlock achieve better agreement between observed and predicted p-y curves; however, the implication of

modifying J without consideration of the rest of the terms in Equation (2.26) is that J truly is reduced to an empirical adjustment factor, as Matlock suggested. It should be understood that the values of 0.5 and 0.25 that were used in this method are a significant deviation from theory. By inspection of Equation (2.26), the reduction of J from 2.83 to some lesser value will result in a deeper transition point from wedge-type failure to flow-around failure. For this experiment, x_r is increased by a factor of approximately 4 and 7 for $J = 0.5$ and 0.25, respectively. This results in lower ultimate soil resistance over a greater depth from the ground surface because N_p is less than the limiting value of 9 within the passive wedge.

It is not clear why Matlock chose to modify J instead of applying a correction factor to the entire equation for N_p; however, it can be inferred that a reduction in the soil reaction over a greater depth than the depth of the passive wedge was required to obtain satisfactory agreement between observed and predicted results. Furthermore, it is not clear whether this deviation from theory highlights a limitation of the theory itself or whether it was unique to this load test. There are insufficient large-scale load test data available to determine whether J of 0.5 is an appropriate correction factor to correct for a potential limitation of the theory, or whether it is simply a curve-fitting parameter for the specific load tests conducted by Matlock. As previously discussed, Bhushan et al. (1979) conducted several large-scale load tests on semi-rigid and rigid drilled shafts in stiff clay, and found that p-y curves estimated with a value of 2.0 for J were in much better agreement with the back-calculated p-y curves. Therefore, there is some evidence to suggest that a single value of J is not appropriate for all soil-pile configurations.

It can be seen in this section that Matlock formulated the relationships for p and y within the theoretical framework established by Reese (1958) and Skempton (1951),

respectively. These equations are similar in form to the equations proposed by McClelland and Focht (1958), with the major difference being in the estimation of the shape of the *p-y* curves from laboratory stress-strain curves and the ultimate soil resistance. McClelland and Focht (1958) estimated the shape and ultimate soil resistance of the *p-y* curves by scaling a stress-strain curve from a triaxial test performed at equivalent confining stress by a constant factor of 5.5. Matlock predicted the shape of the *p-y* curves from ε_{50}, which is a single value on the laboratory stress-strain curve, and observation of the shapes of back-calculated *p-y* curves from a large-scale load test. Matlock's estimation of the ultimate soil resistance was nearly identical to the ultimate soil resistance predicted by McClelland and Focht (1958); however, he reduced the soil resistance near the ground surface to account for the passive wedge formation proposed by Reese (1958). Based on the results of the large-scale load test, Matlock further reduced the soil resistance and increased the depth over which the soil resistance should be reduced by reducing *J* in Equation (2.26) to the point where good agreement between observed and predicted results was achieved. While the approach taken by Matlock is supposedly an improvement upon the work of McClelland and Focht (1958), the method is truly semi-empirical in nature, and there are tradeoffs that have been made that increase reliance on one specific large-scale load test, and therefore reduce the reliance on theory and laboratory test data.

2.4.2.2 Stiff Clay without Free Water (Welch & Reese, 1972)

The empirical curves for stiff clays were derived for two conditions: *with free water present* and *without free water present*. In this case, the presence of free water is defined as water being present above the ground surface or a considerable chance that

water will fill the gap that develops behind the foundation during lateral loading (Isenhower & Wang, 2010). Different curves were developed for stiff clays with free water because soils in this condition experience a loss of shear strength during cyclic loading due to soil particles being expelled from around the shaft as water is squeezed out of the gap between the soil and the foundation. None of the large-scale load tests that were used in this investigation were conducted in stiff clay with free water, and as such, only stiff clay without free water will be discussed in this section.

A large-scale lateral load test was conducted by Welch and Reese (1972) on a drilled shaft that had a diameter of 30 inches and an embedded depth of 42 feet. The D/B ratio for this shaft was approximately 16.8, which suggests the behavior of the shaft can be categorized as flexible. A reinforcement cage was constructed from twenty 14-S deformed bars and 1/2-inch diameter transverse spiral reinforcing. The diameter of the cage was 24 inches and the spacing of the reinforcing spiral was 6 inches. A steel pipe with an outside diameter of 10 3/4 inches and a thickness of 1/4 inch was placed in the center of the drilled shaft for attachment of the strain gauges. A total of 31 pairs of strain gauges were placed on the steel pipe with an arbitrary spacing of 15 inches for the upper section of the shaft and 30 inches for the lower section of the shaft.

The drilled shaft was installed near Houston, Texas, in stiff, overconsolidated clay with a groundwater depth of 18 feet. The undrained shear strength of the clay was estimated by conducting several triaxial tests on samples trimmed from 4-inch diameter thin wall tube samples. The triaxial compression tests were conducted by consolidating samples to the effective in-situ overburden stress and then shearing them in undrained conditions. The samples were tested with orientation both perpendicular to the ground surface and parallel to the ground surface to simulate lateral compression of the soil that

occurs during lateral loading of a drilled shaft. No significant differences were observed in the triaxial tests results due to sample orientation, but there was a wide variation in s_u due to the slickensided structure of the clay. There was no discernable pattern of strength variation with depth, and the average value of s_u was reported as 2,200 psf. The average value of ε_{50} was reported as 0.005.

Both static and cyclic lateral loads were applied to the foundation, with the load being applied at approximately 2 feet above ground level. The *p-y* curves at various depths were back calculated using a similar procedure to the one described in Section 2.4.1. The moment profile was established from the strain gauge data using Equation (2.18) and values of *EI* that were determined by directly measuring the bending stiffness of the shaft. The bending stiffness of the shaft was estimated after the completion of all of the tests by excavating the soil around the shaft to a depth of 20 ft and applying a series of lateral loads to the top of the foundation. By calculating the moment from the applied lateral load and measuring the curvature in the shaft at the bottom of the excavation, the bending stiffness can be estimated directly from Equation (2.18). A seventh-order polynomial was fitted to the moment profile data, and differentiation and numerical integration yielded *p* and *y* profiles, respectively, for each loading increment.

Welch and Reese (1972) estimated *p-y* curves for the static loading case from the laboratory test data using the same equations used by Matlock (1970), which are shown in Equations (2.24) through (2.28). After comparing the predicted results with the results obtained from the large-scale load test, they modified these equations to obtain better agreement between the observed and predicted results as discussed in the following paragraphs.

The exponent 1/3 in Equation (2.28) was changed from 1/3 to 1/4 as shown in Equation (2.29).

$$p = 0.5p_u\left(\frac{y}{y_{50}}\right)^{1/4} \quad \textbf{(2.29)}$$

The value of 1/4 was selected because it resulted in a better fit of the data when p/p_u was plotted against y/y_{50} in logarithmic space. It should be noted, however, that the ultimate strength of the soil was not reached during the test because the shaft was not strong enough to resist the bending induced stress. As such, the researchers assumed a value for p_u by doubling the value of p at y_{50}. The deflection required to reach the ultimate soil resistance for soft clays is $y = 8y_{50}$ as shown in Figure 2.9, but this deflection was increased by a factor of two to $y = 16y_{50}$ as shown in Figure 2.11. This implies that stiff soils require more displacement than soft soils to reach their ultimate strength.

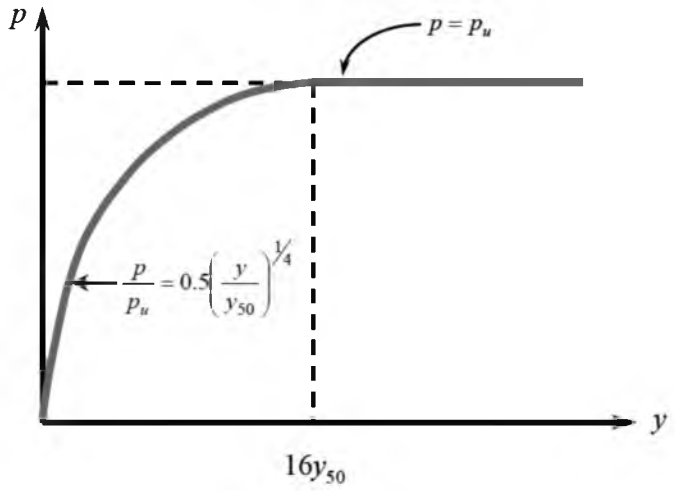

Figure 2.11 General shape of *p-y* curve for static loading in stiff clay without free water (Isenhower & Wang, 2010)

It should also be noted that the default and unchangeable value for J is 0.5 in *LPile*, despite the fact that Matlock (1970) suggested that J was less than 0.5 for medium stiff soils, and Bhushan et al. (1979) showed that J could be as high as 2.0 for stiff soils. The *p-y* curves are estimated at a particular depth for static loading from Equation (2.29), where p_u and y_{50} are calculated from Equations (2.24) and (2.27), respectively.

According to Isenhower and Wang (2010), several tests were reported in the Southeastern United States that exhibited much less initial stiffness than was estimated using the *p-y* curves for stiff clays. It was suggested that k should be incorporated to explicitly account for the stiffness of the soil. As such, the *p-y* curves for stiff clay were modified to allow a value of k to be specified for the soil layer under consideration. The *p-y* curve is calculated as before using Equation (2.29), but the initial portion is also calculated using Equation (2.30):

$$p = (kx)y \tag{2.30}$$

The lesser value of p computed from both equations is used in the final formulation of the *p-y* curves.

As previously discussed in Section 2.4.2.1, the "constant" parameters used in the equations that were developed to predict p and y for stiff clays are not really constant, but they can assume a wide range of values. A potential limitation of LPile is that these parameters cannot be changed for conditions where different values might be more appropriate.

2.4.2.3 Sand (Cox, Reese, & Grubbs, 1974)

A large-scale lateral load test was conducted by Cox et al. (1974) at Mustang Island near Corpus Christi, Texas. Two 24 in. diameter steel pipe piles were driven open-ended into the sand at the test site to a depth of approximately 70 ft and inundated to simulate offshore conditions. The *D/B* ratio for these piles was approximately 35, which suggests the behavior of the piles can be categorized as flexible. Each pile was instrumented with strain gauges to measure the curvature during application of the lateral load. Rotation and deflection were measured at the top of the foundation, in addition to the magnitude of the applied load.

The soil at the site was described as varying from clean fine sand to silty fine sand with high relative density. Laboratory tests were performed on "undisturbed" samples, and the effective angle of internal friction (ϕ') and submerged (effective) unit weight (γ') for the entire subsurface profile was reported as 39 degrees and 66 pcf, respectively.

The piles were tested under both static and cyclic loads, which were applied in increasing increments. A set of *p-y* curves was computed by Reese et al. (1974) from the curvature profile of each loading increment for both static and cyclic loading using Equations (2.17), (2.18) and (2.20). The general shape of the set of *p-y* curves from this method are shown in Figure 2.12.

Theoretical *p-y* curves for sand are represented by three linear segments and one parabolic segment, as shown in Figure 2.12. The initial segment for $y \leq y_k$ is approximately linear, and was established from observations made by Terzaghi (1955) that the soil modulus for granular soils increases in proportion to confinement, which increases with depth as shown in Equation (2.31).

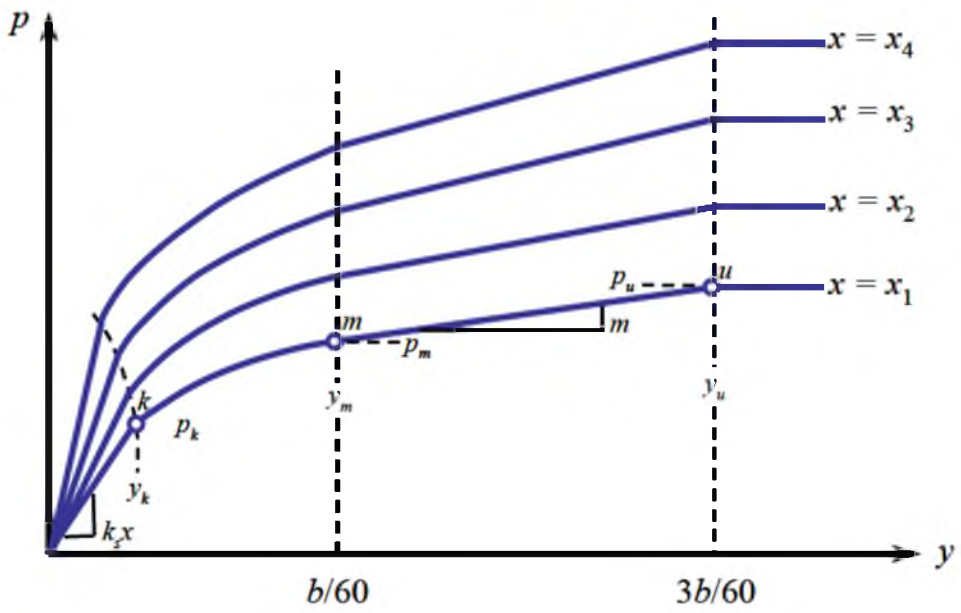

Figure 2.12. General shape of a set of *p-y* curves for static and cyclic loading in sand (Isenhower & Wang, 2010)

$$E_{si} = n_h x \tag{2.31}$$

where:

E_{si} = soil modulus of initial linear portion of *p-y* curve

n_h = constant of subgrade reaction

x = depth below ground surface

It should be noted that the constant of subgrade reaction, n_h, is equal to k_s in Figure 2.12.

Terzaghi (1955) suggested numerical values for the constant of subgrade reaction based on the relative density of the soil and the effective unit weight. The results of the large-scale load tests suggested that these values are much too conservative. The values of the initial soil modulus of the *p-y* curves that were computed from the results of the

large-scale load test were 2.5 and 3.9 times higher than the highest values suggested by Terzaghi (1955) for the static and cyclic load tests, respectively. As such, Reese et al. (1974) suggested using values that are approximately 2.5 times higher than those proposed by Terzaghi (1955). These higher values are the default values used by *LPile* in the absence of user input values and are shown in Table 2.1. The constant of subgrade reaction is related to the horizontal coefficient of subgrade reaction as

$$k_h = n_h\left(\frac{x}{B}\right) \tag{2.32}$$

where:

k_h = horizontal coefficient of subgrade reaction

n_h = constant of subgrade reaction

x = depth below ground surface

B = diameter or width of pile

As discussed by Habibagahi and Langer (1984), several methods and correlations have been developed for predicting the horizontal coefficient of subgrade reaction, which generally confirm that the values proposed by Terzaghi (1955) are too conservative. It should be noted, however, that Terzaghi (1955) stated that the coefficient of subgrade reaction is a function of pile width or diameter, and that the values he proposed were for a 1 ft wide strip. It should also be noted that the values proposed by Reese et al. (1974) in Table 2.1 do not take into account the diameter of the foundation. Additionally, Alizadeh and Davisson (1970) have shown from the results of large-scale load tests that the constant of subgrade reaction is not actually constant, but a function of pile deflection for deflections less than approximately 0.5 in.

Table 2.1. Values of k suggested by Reese et al. (1974)

Relative Density	Recommended k (pci)	
	Submerged	Above GWT
Loose	20	25
Medium	60	90
Dense	125	225

The horizontal linear portion of the curve represents the ultimate soil resistance (p_u). Reese et al. (1974) formulated the ultimate resistance of sand using a theory similar to that of clay, as previously discussed in Section 2.4.2.1, whereby the ultimate soil resistance near the ground surface is represented by a passive wedge, and transitions to a flow-around type of failure at some greater depth. A schematic of the flow-around type of failure, which is based on Mohr-Coulomb failure criterion and virtually identical to flow-around failure for clays shown in Figure 2.10(a), is shown in Figure 2.13(a). The corresponding Mohr's circles for the state of stress in each idealized soil element are shown in Figure 2.13(b). Reese et al. (1974) showed that the ultimate soil resistance that develops from lateral flow of soil around the pile (p_{cd}) can be estimated as

$$p_{cd} = B\gamma' H[K_a(\tan^8(\beta) - 1) + K_o \tan(\phi')\tan^4(\beta)] \quad \textbf{(2.33)}$$

where:

p_{cd} = theoretical ultimate soil resistance from lateral flow of soil around pile

H = depth (height) of passive wedge

B = width or diameter of pile

ϕ' = effective angle of internal friction

β = angle of passive wedge from the vertical face of the pile

K_o = at-rest earth pressure coefficient

K_a = active earth pressure coefficient

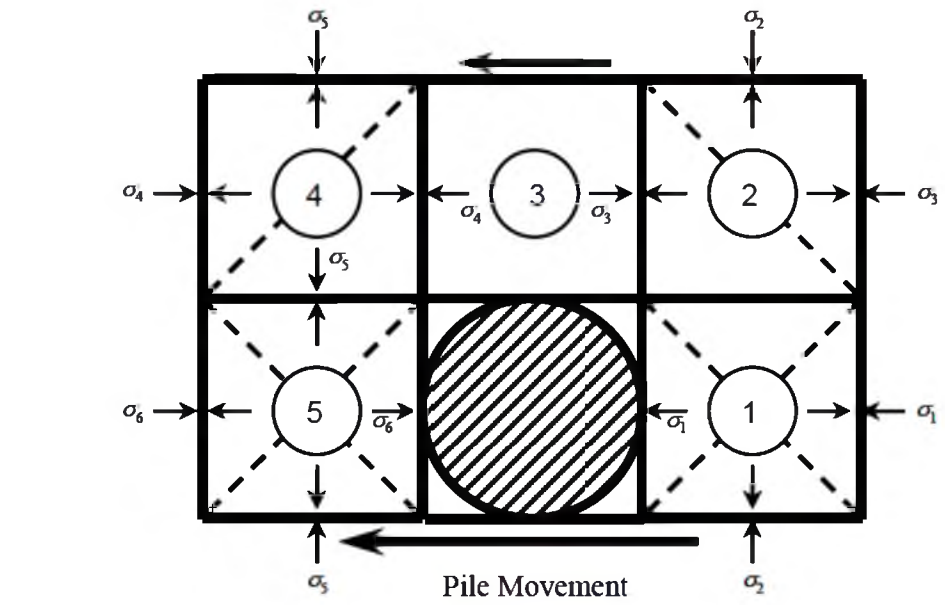

(a)

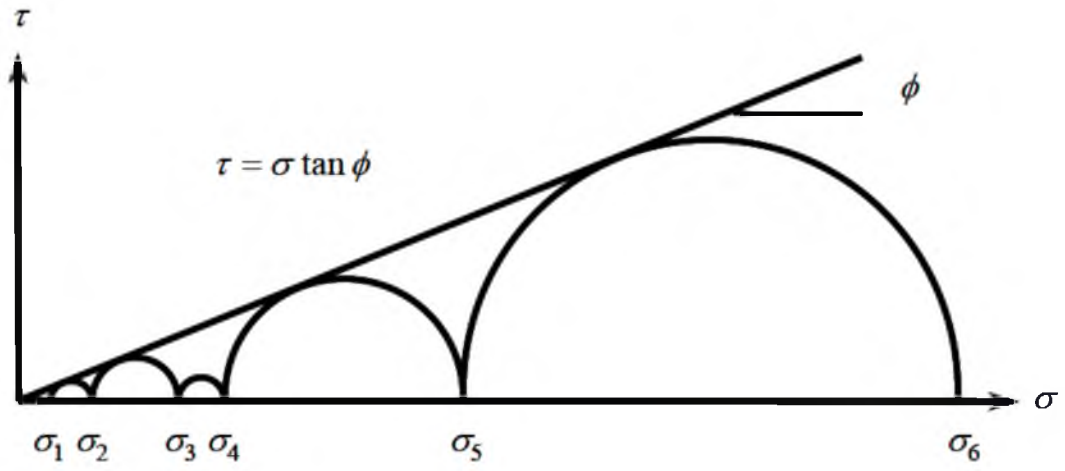

(b)

Figure 2.13. Assumed mode of soil failure by lateral flow around the pile (Reese, Cox, & Koop, 1974)

The passive wedge at failure for sand is shown in Figure 2.14(a). The most notable difference between the passive wedge for sand and the passive wedge for clay, shown in Figure 2.10(b), is the development of a fan in the horizontal direction at an angle of α.

The horizontal soil reaction that develops within the passive wedge can be solved from the geometry of the wedge, assuming Mohr-Coulomb failure is valid for sand (Reese, Cox, & Koop, 1974). By summing the forces that act on the passive wedge and differentiating with respect to x, the soil resistance per unit length within the wedge (p_{ct}) is

$$p_{ct} = \gamma' H \left[\frac{K_o H \tan(\phi')\sin(\beta)}{\tan(\beta-\phi')\cos(\alpha)} + \frac{\tan(\beta)}{\tan(\beta-\phi')}(B + H\tan(\beta)\tan(\alpha)) + K_o H \tan(\beta)(\tan(\phi')\sin(\beta) - \tan(\alpha)) - K_a B\right] \quad \textbf{(2.34)}$$

where:

p_{ct} = theoretical ultimate soil resistance from a passive wedge in sand

H = depth (height) of passive wedge

B = width or diameter of pile

ϕ' = effective angle of internal friction

β = angle of passive wedge from the vertical face of the pile

α = angle of passive wedge from a line parallel to the applied load

K_o = at-rest earth pressure coefficient

K_a = active earth pressure coefficient

The ultimate soil resistance at any point along the pile is the lesser of the two values calculated by Equation (2.33) and (2.34).

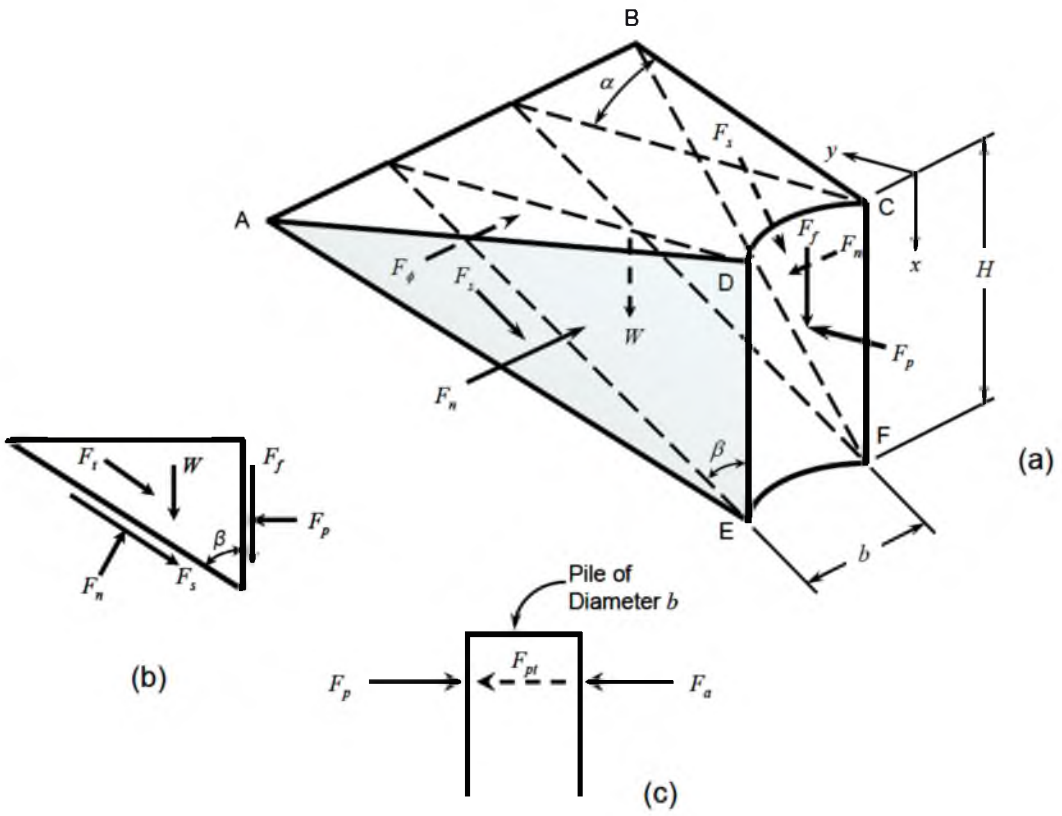

Figure 2.14. Assumed passive wedge type of soil failure (Reese, Cox, & Koop, 1974)

Reese (1962) suggested that α has a maximum value equal to ϕ'; however, Bowman (1958) states that the results of plate load tests in sand show that α is a function of void ratio, and that α is likely to be $\phi'/3$ to $\phi'/2$ for loose sand, and ϕ' for dense sand. The results of the laboratory experiments performed by Reese (1962) on small, laterally loaded tubes in loose sand showed better agreement with analytical results when α was assumed to be ϕ' instead of Bowman's suggested value of $\phi'/2$. Reese et al. (1974) stated that contours of the wedge that formed in front of the test piles in this load test indicated that the value of α was equal to about $\phi'/3$ for static loading and about $3\phi'/4$ for cyclic loading. As such, they state that α can be assumed to be $\phi'/2$, and this is the assumption that is made by *LPile* when estimating *p-y* curves for sand.

The angle β is computed using Rankine's familiar lateral earth pressure theory, which, for lateral earth pressure in the two-dimensional passive case is

$$\beta = 45^o + \frac{\phi'}{2} \tag{2.35}$$

Reese et al. (1974) state that the criteria for using Rankine's theory are not strictly satisfied for the case of a laterally loaded pile; however, they state that some model experiments indicate that Equation (2.35) gives a fairly good approximation of the slope of the failure surface. It should be noted that K_a in Equation (2.34) is also computed using Rankine's theory as

$$K_a = \tan^2\left(45^o - \frac{\phi'}{2}\right) \tag{2.36}$$

There is no recommendation for establishing K_o in the *LPile* manual; however, Reese et al. (1974) suggest using a value of 0.4 for loose sand and 0.5 for dense sand in the absence of precise methods for determining relative density in the field. A value of 0.4 was used for the large-scale load test, and it is assumed that a constant value of 0.4 is used by *LPile*.

According to Reese et al. (1974), the geometric parameters of the passive wedge can assume a wide range of values. They stated that the estimated ultimate soil resistance was in poor agreement with the ultimate soil resistance observed in the load test, even when these parameters were varied over a reasonable range. As such, a simple correction factor ($A_{s,c}$) was introduced to adjust the ultimate soil resistance as

$$p_u = A_{s,c} p_c \tag{2.37}$$

where:

$A_{s,c}$ = ultimate soil resistance correction factor

p_u = ultimate soil resistance

p_c = theoretical ultimate soil resistance

Values of $A_{s,c}$ were computed at several depths from the observed and theoretical ultimate soil resistance, and incorporated into the design aid shown in Figure 2.15. The authors did not state how they determined that the soil resistance at a particular depth was the ultimate resistance; however, the computed values of $A_{s,c}$ were only for the upper 10 ft of soil, or $x/B \leq 5$, which seems reasonable. For depths greater than $5B$, the correction factor approaches a constant value of 0.88 for both static and cyclic loading. This might be satisfactory for flexible foundations where the soil reaches ultimate capacity near the surface, but is probably unsatisfactory for semi-rigid foundations where the displacement of the pile tip might be sufficient to develop ultimate soil capacity.

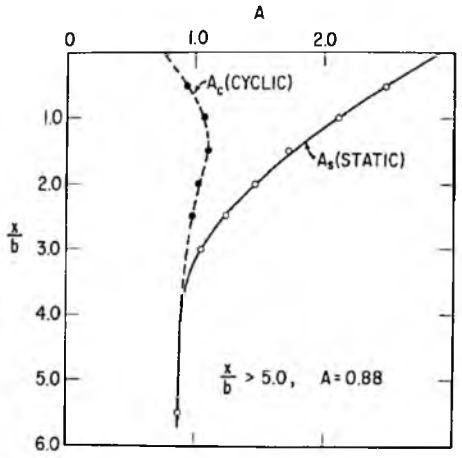

Figure 2.15. Correction factor A for ultimate soil resistance vs. depth for cyclic and static loading (Reese, Cox, & Koop, 1974)

Further inspection of Figure 2.15 shows that $A = 1$ at $x \approx 3.2B$ for static loading. It follows from Equation (2.37) that the ultimate soil resistance for static loading is increased from theory by a factor of $B_{s,c}$ for $x < 3.2B$ and decreased from theory by a factor of $B_{s,c}$ for $x > 3.2B$. This seems to be a more rational approach for adjusting the *p-y* curves to match experimental observations than the approach used for soft clays, which, as discussed in Section 2.4.2.1, was to modify the geometric term J in the passive wedge equation. It should be noted, however, that the values shown in Figure 2.15 are curve-fitting parameters for the load test from which they were derived, and it is not presently known how these factors might change for a different soil and pile configuration.

It can be seen in Figure 2.12 that there is a parabolic section and a linear section of the *p-y* curve between $y = y_k$ and $y = 3B/60$. According to Reese et al. (1974), these two segments of the *p-y* curve were selected empirically to yield a shape consistent with the experimental *p-y* curves. The linear portion of the curve located between points *m* and *u* in Figure 2.12 was established by the points y_m and y_u. The points y_m and y_u were observed in the large-scale load tests at 0.4 and 0.9 in. of pile head deflection, respectively. These deflections were normalized to the pile diameter, which resulted in values of y_m and y_u of $B/60$ and $3B/80$, respectively. The soil resistance at point *m*, p_m, is estimated from the theoretical ultimate soil resistance, p_c, and the nondimensional coefficient $B_{s,c}$ as

$$p_m = B_{s,c} p_c \tag{2.38}$$

where:

$B_{s,c}$ = nondimensional coefficient for determining p_m

p_c = theoretical ultimate soil resistance

p_m = soil resistance at point *m* in Figure 2.12

The coefficient $B_{s,c}$ was computed from the observed data for the upper 10 ft of soil, or $x/B \leq 5$ as shown in Figure 2.16. For depths greater than $5B$, the coefficient $B_{s,c}$ assumes a constant value of 0.5 for static loading and 0.55 for cyclic loading. This might be satisfactory for flexible foundations where the soil reaches ultimate capacity near the surface, but is probably unsatisfactory for semi-rigid foundations where the displacement of the pile tip might be sufficient to develop ultimate soil capacity. Additionally, as for the correction factor $A_{s,c}$, these values are unique to the load test from which they were derived, and it is not presently known how these correction factors might change for other soil-pile configurations.

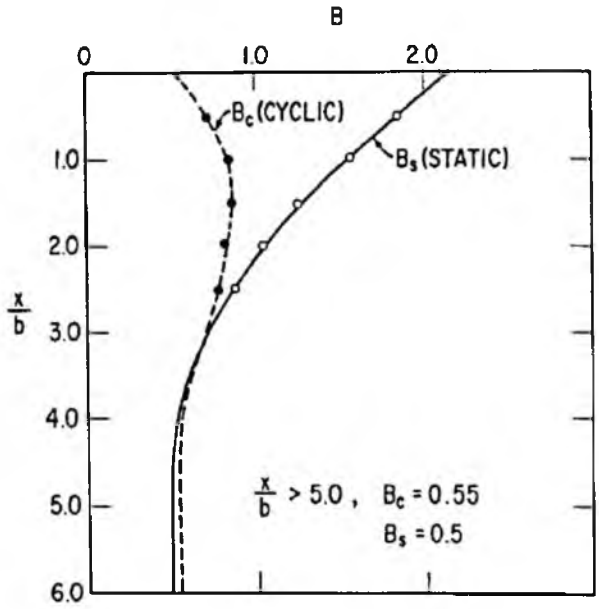

Figure 2.16. Nondimensional coefficient B for calculating soil resistance at point *m* in Figure 2.12 for cyclic and static loading (Reese, Cox, & Koop, 1974)

The parabolic portion of the *p-y* curves shown in Figure 2.12 is determined by fitting a parabola from the origin through point *m* with a slope at *m* equal to the slope of the linear portion between points *m* and *u*. The intersection of the parabolic curve and the initial straight-line portion of the *p-y* curve establishes the point *k* in Figure 2.12.

Reese et al. (1974) have acknowledged that the method presented for establishing *p-y* curves for sands is based heavily on empiricism, and that the method might not be applicable for all foundations or soil conditions. They state, for example, that the presence of clay in a sufficient amount to give some cohesion will cause the soil to behave in an entirely different manner. Furthermore, they specifically admonish the use of caution and judgment when using these curves, and that serious errors can be made by inexperienced analysts.

2.4.3 Estimation of *p-y* curves from In-situ Tests

The in-situ tests that are most often used for computing *p-y* curves are the dilatometer test (DMT) and the pressuremeter test (PMT). The *p-y* curves that are estimated from PMT test and DMT tests have the advantage of being based on lateral deformation properties of the soil (Anderson & Townsend, 1999); however, these tests do not directly capture the effects of the foundation on the *p-y* curves.

According to Robertson et al. (1983), the pressuremeter offers an almost ideal in-situ modeling tool for determining directly the *p-y* curves for a pile. The PMT test is an excellent test for computing *p-y* curves because the test is similar to a laterally loaded pile (Briaud, Smith, & Tucker, 1985). Additionally, the results of the PMT test can be used to derive curves in soils and rock for which no empirical *p-y* curves exist (Little & Briaud, 1988). The DMT test is also an excellent test for computing *p-y* curves because the test

conditions simulate a driven pile, it is inexpensive, and it can be used near the ground surface, where the soil has the most influence on the response of the pile (Robertson, Davies, & Campanella, 1989).

Unfortunately, both PMT and DMT tests are small-strain tests, and only a small amount of the soil is tested. Also, these tests only measure the passive resistance of the soil directly, and do not measure the skin friction, which is a major contributor to the overall soil resistance [(Smith & Slyh, 1986), (Janoyan & Whelan, 2004), (Briaud, Smith, & Meyer, 1983)]. Regardless, the pressuremeter has been shown to provide good results in several case histories as shown by Robertson et al. (1986). The dilatometer has also been shown to provide good results in several case histories as shown by Robertson et al. (1989) and Gabr et al. (1994). Anderson et al. (2003) also compared the results from analyses of laterally loaded piles and drilled shafts using *p-y* curves derived from the DMT and PMT tests. The comparison showed that the results from the dilatometer were in good agreement with the results of the large-scale load tests at small displacements, but that the error increased as the displacement increased. They explained that this makes sense because the membrane on the dilatometer is only pushed 1 mm into the soil during testing. The comparison also showed that the results from the pressuremeter were in good agreement with the results of the large-scale load tests, except for the cases where excess pore water pressure was present.

2.5 DFSAP and the Strain Wedge Model

The strain wedge (SW) model was developed to establish a method for evaluating the modulus of subgrade reaction (E_s) in order to solve the BEF equation for a laterally loaded pile based on the envisioned soil-pile interaction and its dependence on both soil

and pile properties (Ashour, Norris, & Piling, 2002). The SW model was originally formulated by Norris (1986) for sands, and subsequently expanded by Norris and his colleagues to include cohesive soils, "*c*-ϕ" soils, and rock [(Ashour, Norris, & Pilling, 1998), (Ashour et al., 2001)].

Norris (1986) stated that there is some reluctance to extrapolating existing methods for determining BEF parameters to conditions for which there is little or no field evidence. Subsequent publications on the SW model specifically express skepticism for employing the semi-empirical *p*-*y* methods discussed in Section 2.4.2 for analyzing foundations outside of the field-calibrated range. Ashour and Norris (2000) state that these semi-empirical *p*-*y* methods do not account for a change in pile properties such as pile bending stiffness, pile cross-sectional shape, pile-head fixity, and pile-head embedment below the ground surface. Ashour and Norris (2000) reiterate the importance of E_s being dependent upon the soil-pile interaction, but that it would be prohibitively expensive to systematically evaluate all of these effects through load tests. As such, they suggest that the characteristics of the soil-pile interaction that are known to affect E_s can be evaluated through the semi-theoretical means of the SW model.

A survey of the published literature for the SW model revealed that the model uses a very similar solution scheme to the one proposed by McClelland and Focht (1958), and draws heavily from the theoretical basis of the semi-empirical *p*-*y* curve methods discussed in Section 2.4.2. A schematic for the SW representation of the three-dimensional soil-pile interaction and the resulting soil reaction for a laterally loaded pile is shown in Figure 2.17. The equivalent one-dimensional soil-pile reaction is shown in Figure 2.18.

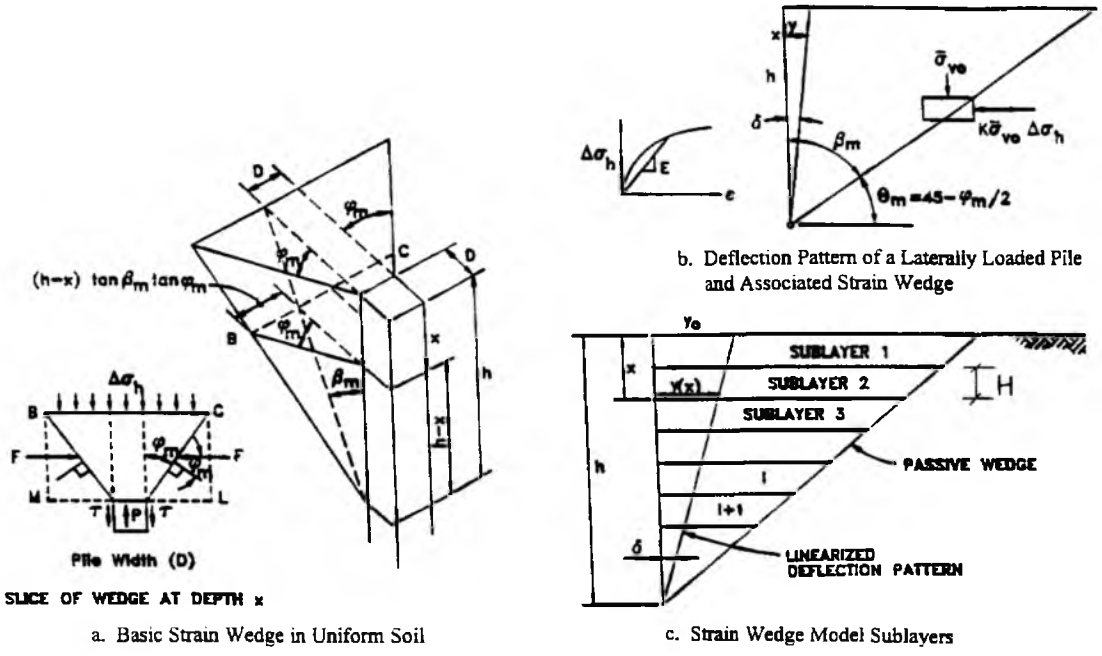

Figure 2.17. Schematic of SW model (Ashour & Norris, 2000)

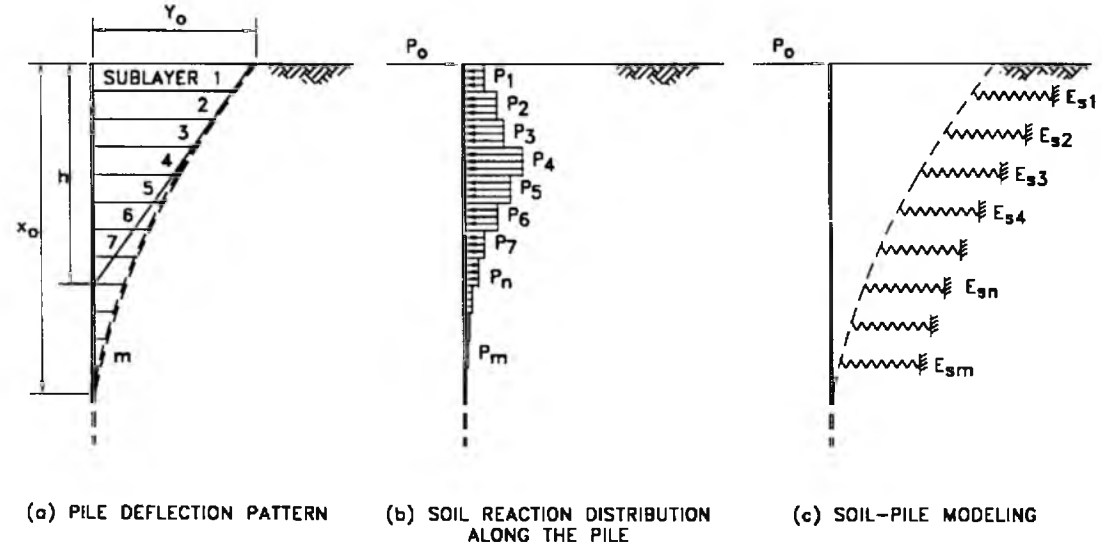

Figure 2.18. One-dimensional distribution of soil-pile reaction along deflected pile (Ashour & Norris, 2000)

It can be seen in Figure 2.17(a) that the soil reaction of a laterally loaded pile in the SW model is a function of the passive soil wedge that forms in front of the pile and the shearing resistance that develops along the length of the pile. It can also be seen in Figure 2.17(a) that the passive wedge is fully defined in terms of the mobilized effective friction angle (ϕ'_m) pile diameter (D) and depth of the passive wedge (h) (Ashour & Norris, 2000). Ashour and Norris (2000) state that h is a function of the pile bending stiffness, diameter, pile head fixity, and pile shape. The width of the mobilized passive wedge, $\overline{BC}$, is calculated as

$$\overline{BC} = 2(h - x)tan(\beta_m)tan(\phi'_m) + D \quad \textbf{(2.39)}$$

where

$$\beta_m = 45 + \frac{\phi'_m}{2} \quad \textbf{(2.40)}$$

It should be noted that the geometry can be defined for each sub-layer, and that the passive wedge for multilayered soils with different strength properties is discontinuous as shown in Figure 2.19. Even though the compound passive wedge is discontinuous across sub-layer boundaries, the strain within the overall passive wedge still remains constant. Furthermore, Ashour et al. (1998) state that the interaction between the sub-layers is accounted for by the continuity of the deflected length of the pile. The passive wedge representation of the soil reaction is virtually identical to the one proposed by Reese (1962), which is shown previously in Figure 2.14. The biggest difference between the way the passive wedge is used in the SW model and the way the passive wedge is used in the semi-empirical *p-y* methods are: 1) the passive wedge shown

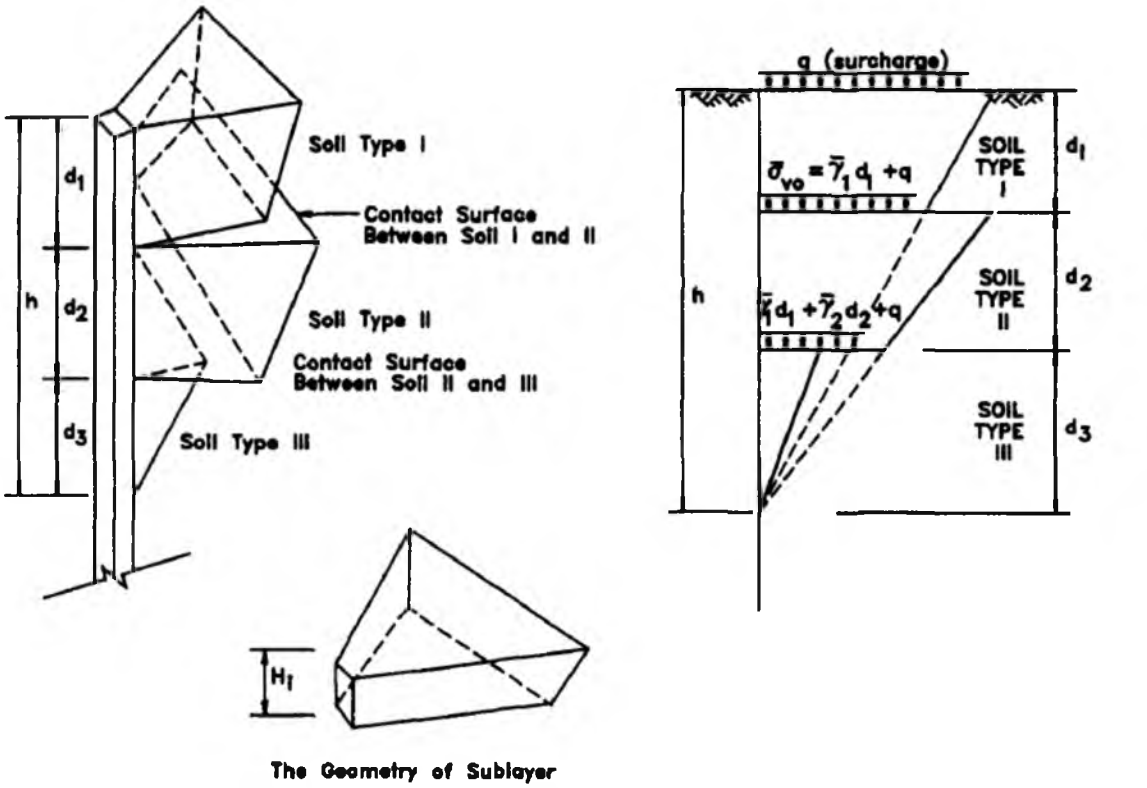

Figure 2.19. Configuration of compound passive wedge for multilayered soil (Ashour, Norris, & Pilling, 1998)

in Figure 2.14 is for sand, whereas the SW model uses this same passive wedge for both sand and clay, which will be discussed later;2) the passive wedge is only used to estimate the ultimate soil resistance in the semi-empirical *p-y* method, and provides no information about the intermediate soil reaction, i.e., it is not directly related to the stress-strain behavior of the soil up to failure, whereas the passive wedge in the SW model is a function of the stress-strain relationship of the soil and directly provides the soil resistance for any increment of pile deflection up to failure; 3) the passive wedge is defined at failure in the semi-empirical *p-y* method, but it is shown to "grow" from zero pile deflection up to failure with increasing pile deflection and resulting soil strain in the SW model. The increasing soil strain in the passive wedge is responsible for the growth

of the passive wedge up to failure, which is shown by the "mobilized" value of terms with subscript *m* in Figure 2.17(a). These terms are defined only at failure for the semi-empirical *p-y* methods, and are thus constant at failure.

The method used by the SW model to estimate E_s is very similar to the method proposed by McClelland and Focht (1958). According to the McClelland and Focht (1958) method discussed in Section 2.3, the first step in evaluating E_s for a laterally loaded pile is to assume the deflected shape of the pile and to estimate the deflection at several discrete points along the pile within the deflected zone. The strain at each point is calculated from the assumed magnitude of displacement, and the laboratory stress for an equivalent strain is estimated from a laboratory stress-strain curve for the same confining stress. The soil reaction p is estimated at each discrete point by multiplying the laboratory stress by a constant value of 5.5, and E_s is calculated at each point using Equation (2.13). This procedure is repeated for several load increments to establish the E_s profile, i.e., the *p-y* curve, for each discrete point along the length of the pile. These E_s profiles are then used to solve the BEF equation.

The specific steps for evaluating E_s using the SW model are somewhat different from the method just described, but the general approach is remarkably similar. Figure 2.17(b) and (c) show that the deflected shape of the upper portion of the pile is assumed to be linear in the SW model; however, it should be noted that this assumption is only made for the assessment of E_s. The final deflected shape is not linear in the upper portion of the pile as shown. The passive wedge in the SW model is discretized into sub-layers, as shown in Figure 2.17(c), and the strain within each sub-layer is estimated from the shear strain. For the assumed linear deflection profile, the shear strain is approximately equal to the angle of pile deflection (δ). Because the shear strain is constant over the

entire depth of the passive wedge, ε is also constant over the entire depth of the passive wedge, hence the name "strain wedge" model (Ashour, Norris, & Pilling, 1998). Like the method proposed by McClelland and Focht (1958), the SW model also relates the change in horizontal stress ($\Delta\sigma_h$) within each sub-layer to ε through the triaxial test.

Because ε is constant within the passive wedge, $\Delta\sigma_h$ is also constant within the passive wedge. The stress-strain relationship between $\Delta\sigma_h$ and ε is related by the secant modulus of the soil (E) from laboratory testing, where

$$E = \frac{\Delta\sigma'_h}{\varepsilon} \tag{2.41}$$

The stress-strain behavior of each sub-layer within the passive wedge is represented by an axial compression triaxial test. In a typical triaxial compression test, the confining stress (σ_3) is held constant, while the axial compressive stress (σ_1) is increased until failure or some other predefined level of strain is reached. In the SW model, $\Delta\sigma_h$ is equal to the deviatoric stress (σ_d) where $\sigma_d = \sigma_1 - \sigma_3$. The confining stress is equal to the overburden stress acting on the sub-layer, and it is assumed that this confining stress does not change as the horizontal stress changes (Ashour, Norris, & Pilling, 1998).

The stress-strain relationship for the sub-layers of the passive wedge in the SW model are represented by a triaxial compression test behavior, but they are not directly related to the actual laboratory stress-strain curves from the pile installation site like they are in the method proposed by McClelland and Focht (1958). In other words, stress-strain curves obtained from triaxial tests performed at confining stress equal to the sub-layer depths are not inputs for the SW model; instead, the stress-strain curves for each

sub-layer are represented by a hyperbolic stress-strain relationship for both sand and clay as shown in Figure 2.20(a). The curves shown in Figure 2.20(a) and (b) are based on the results of laboratory experiments (Ashour, Norris, & Pilling, 1998).

The hyperbolic curve shown in Figure 2.20(a) also represents the so-called stress level (*SL*) within the passive wedge. The *SL* is defined as the change in horizontal stress (or deviatoric stress in the triaxial test) normalized by the change in horizontal stress at failure ($\Delta\sigma_{hf}$) as shown in Equation (2.42). For sands and clays, $\Delta\sigma_{hf}$ is calculated using Equations (2.43) and (2.44), respectively.

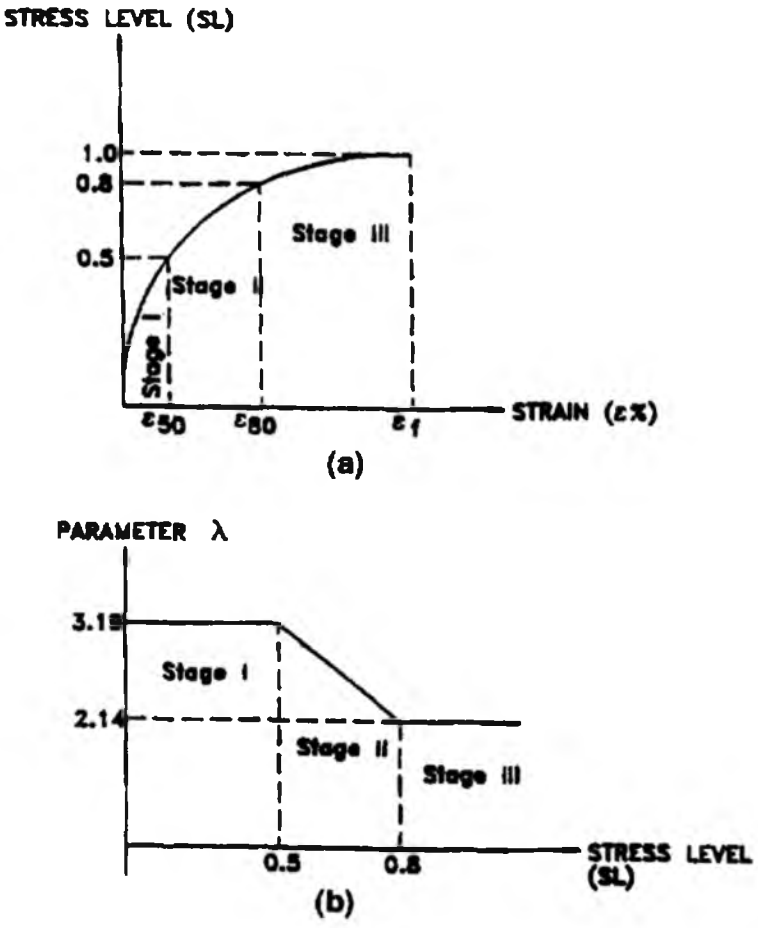

Figure 2.20. Representative hyperbolic stress-strain curve for soil (Ashour, Norris, & Pilling, 1998)

$$SL = \left(\frac{\Delta\sigma_h}{\Delta\sigma_{hf}}\right) = \frac{tan^2(45 + \phi'_m) - 1}{tan^2(45 + \phi') - 1} \quad \textbf{(2.42)}$$

$$\Delta\sigma_{hf} = \sigma'_{vo}\left[tan^2\left(45 + \frac{\phi'}{2}\right) - 1\right] \qquad (sands) \quad \textbf{(2.43)}$$

$$\Delta\sigma_{hf} = 2s_u \qquad (clays) \quad \textbf{(2.44)}$$

where:

SL = stress level of sub-layer

$\Delta\sigma_h$ = horizontal stress change within sub-layer

$\Delta\sigma_{hf}$ = horizontal stress change at failure within sub-layer

ϕ'_m = mobilized effective friction angle of the soil

ϕ' = effective friction angle of granular soils

σ'_{vo} = vertical effective stress acting at the top of the sub-layer

s_u = undrained shear strength of cohesive soils

The curve for SL shown in in Figure 2.20(a) is entirely defined by ε_{50}, ε, and the curve fitting parameter λ shown in Figure 2.20(b). For each sub-layer i, SL_i is calculated from Equation (2.42) or (2.43).

$$SL_i = \frac{\lambda_i \varepsilon}{(\varepsilon_{50})_i} \exp(-3.707 SL_i); \quad SL_i < 0.80 \quad \textbf{(2.45)}$$

$$SL_i = exp\left[\ln(0.2) + \frac{100\varepsilon}{59\varepsilon + 95.4(\varepsilon_{50})_i}\right]; \quad SL_i \geq 0.80 \qquad \textbf{(2.46)}$$

where:

SL_i = stress level of sub-layer *i*

λ_i = curve-fitting parameter for sub-layer *i*

ε = horizontal strain within the passive wedge

$(\varepsilon_{50})_i$ = strain in the soil for sub-layer *i* at 50% of peak strength

It should be noted that ε_{50} is the only input property for *SL* in the SW model. The general shape and curve-fitting parameters of Equation (2.42) and (2.43) are based on experimental results and are said to describe a typical stress-strain curve for both sand and clay (Ashour, Norris, & Pilling, 1998). This assumption seems somewhat simplified, as the general shape of the stress-strain curve shown in Figure 2.20(a) is only representative of normally consolidated soils and soils with large confining stress. As such, this curve does not accurately represent both sands and clays in all conditions.

It should be noted that the SW model is an effective stress model, and that the strain wedge geometry is defined in terms of ϕ'_m for both granular and cohesive soils. The difficulty of an effective stress analysis for undrained loading conditions, as in the case of a laterally loaded pile in cohesive soil, arises from the difficulty of estimating the excess porewater pressure (Δu) that is generated during pile deflection. The excess porewater pressure is estimated in the SW model using the well-known equations developed by Skempton (1954) for estimating the porewater pressure that develops within a soil mass subjected to an applied load. The specific procedures used in the SW model are discussed in further detail in (Ashour, Norris, & Pilling, 1998).

The SW model includes the shearing resistance that develops along the length of the pile in the formulation of the soil reaction. In the semi-empirical *p-y* method, some of the shearing resistance is included by means of the empirical corrections made to the soil resistance equations; however, shearing resistance along the pile is not explicitly included in the soil resistance equations. This is one of the major criticisms of the developers of the SW model because they suggest that it is a major component of the overall soil reaction - particularly for large-diameter piles (Ashour, Norris, & Pilling, 1998). Smith and Slyh (Smith & Slyh, 1986) and Janoyan and Whelan (2004), among others, have shown that most of the soil reaction at small strains results from shearing resistance. This makes sense from a soil mechanics perspective because shear stress mobilizes much more quickly than the normal stresses in the passive zone (Salgado, 2008).

The shear stress component of the soil reaction in the SW model depends on whether the soil is classified as sand or clay. For sands, the shear stress along the pile sides is a function of effective stress and mobilized friction angle between the sand and pile (ϕ_s) (Ashour, Norris, & Pilling, 1998). The shear stress along the pile within sub-layer *i* (τ_i) is calculated as

$$\tau_i = (\sigma'_{vo})_i tan(\phi'_s)_i \quad \textbf{(2.47)}$$

where:

τ_i = shear stress along pile sides within sub-layer *i*

$(\sigma'_{vo,})_i$ = vertical effective stress within sub-layer *I*

$(\phi'_s)_i$ = mobilized effective friction angle at the soil-pile interface within sub-layer *i*

According to Ashour et al. (1998), ϕ'_s develops at twice the rate of ϕ'_m, such that Equation (2.63) becomes

$$\tau_i = 2(\sigma'_{vo})_i tan(\phi'_m)_i \quad \textbf{(2.48)}$$

The value of ϕ'_m, is, of course, limited to the value of ϕ' of the soil, and the ultimate value of shear stress along the pile sides (τ_{ult}) for sands is

$$(\tau_{ult})_i = (\sigma'_{vo})_i tan(\phi')_i \quad \textbf{(2.49)}$$

For clays, the shear stress along the pile sides is a function of s_u, SL, and pile adhesion (α) (Ashour, Norris, & Pilling, 1998). The stress level of shear along the pile sides (SL_t) is different from the SL in the passive wedge (Ashour, Norris, & Pilling, 1998). In the SW model, SL_t is estimated using the Coyle and Reese (1966) "*t-z*" shear stress transfer curves shown in Figure 2.21(a). These curves represent the ratio of the side shear stress of a 1-foot diameter pile embedded in clay to the theoretical shear strength along the interface (αs_u) as a function of pile displacement. Curves A, B, and C in Figure 2.21(a) represent depth ranges of 0 – 3m, 3 – 6m, and > 6m, respectively. Ashour, Norris, and Piling (1998) normalized and simplified these curves by multiplying αs_u by a normalization factor (ζ), which is equal to the peak values of 0.53, 0.85, and 1.0 for curves A, B, and C, respectively. The normalized and simplified curves are shown in Figure 2.21(b). These curves are used to estimate SL_t, for a given magnitude of pile displacement, y.

Once SL_t is estimated from Figure 2.21(b) and the assumed pile deflection within sub-layer i, τ_i for clays can be calculated as

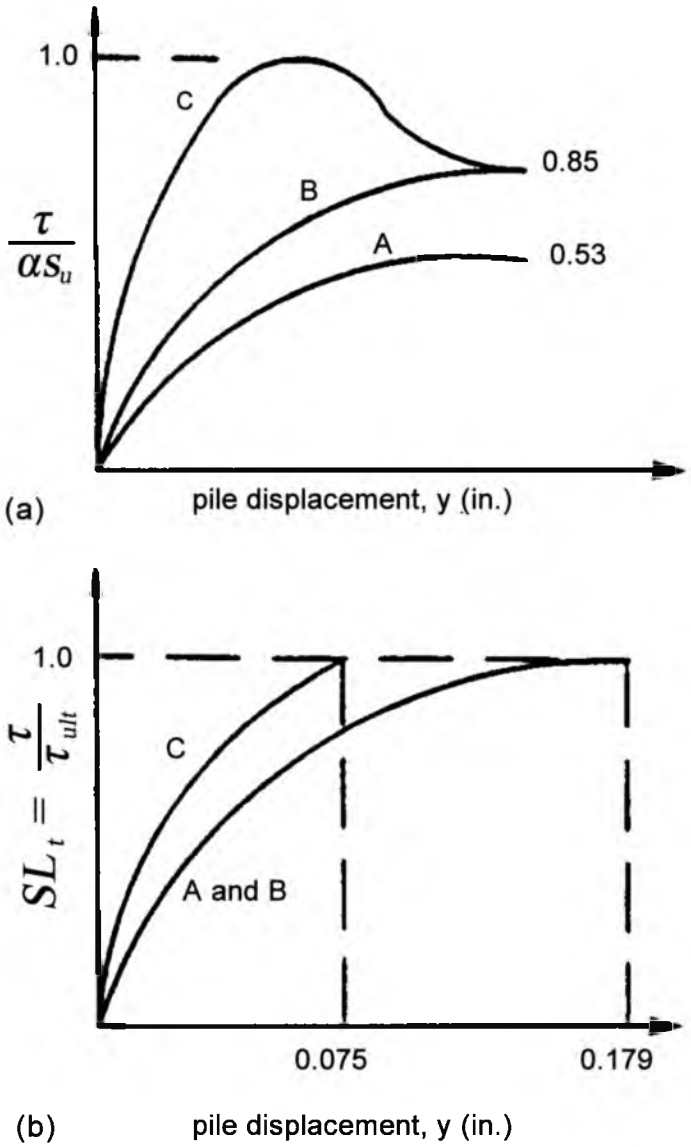

Figure 2.21. Estimation of stress level (SL) along pile sides using (a) Coyle and Reese (1966) shear-transfer curves, and (b) Normalized shear-transfer curves

$$\tau_i = (SL_t)_i(\tau_{ult})_i \tag{2.50}$$

where:

$$(\tau_{ult})_i = \zeta\alpha(s_u)_i \tag{2.51}$$

τ_i = shear stress along pile sides within sub-layer *i*

$(\tau_{ult})_i$ = ultimate shear strength along pile sides within sub-layer *i*

$(SL_t)_i$ = stress level of shear along pile sides within sub-layer *i*

$(s_u)_i$ = undrained shear strength of the soil within sub-layer *i*

ζ = normalization factor

α = pile adhesion factor

The values of pile adhesion factor, α, used in the SW model were recommended by Tomlinson (1957).

The total soil reaction within each sub-layer *i* is calculated for each sub-layer as

$$p_i = (\Delta\sigma'_h)_i \overline{BC_i} S_1 + 2\tau_i D S_2 \quad \textbf{(2.52)}$$

Note that the first and second terms in Equation (2.53) represent the normal and shearing resistance, respectively. It should also be noted that the active earth pressure is not accounted for in Equation (2.52) (Ashour, Norris, & Piling, 2002). The SW model makes some effort in Equation (2.52) to account for the shape of the pile by including the shape adjustment factors S_1 and S_2 proposed by Briaud et al. (1984). S_1 and S_2 are equal to 0.75 and 0.5, respectively, for a circular pile cross section, and 1.0 for a square pile cross section. Alternately, Equation (2.52) can also be written as

$$p_i = A_i D(\Delta\sigma'_h)_i = A_i D E_i \varepsilon \quad \textbf{(2.53)}$$

From Equation (2.52) and the soil strength and geometric properties defined in Equations (2.39) through (2.51), it can be shown that

$$A_i = S_1\left(1 + \frac{(h - x_i)2(tan\beta_m tan\varphi'_m)_i}{D}\right) + \frac{2S_2(\Delta\sigma'_{v0})_i(tan\varphi'_s)_i}{(\Delta\sigma'_h)_i} \quad \textbf{(2.54)}$$

in sand, and

$$A_i = S_1\left(1 + \frac{(h - x_i)2(tan\beta_m tan\varphi'_m)_i}{D}\right) + \frac{S_2(SL_t)_i}{SL_i} \quad \textbf{(2.55)}$$

in clay. It can be seen that Equation (2.53) takes the same form as Equation (2.12) proposed by McClelland and Focht (1958), were A_i = 5.5.

By definition, the ultimate soil resistance, p_u, is reached when SL = 1. In the case where SL = 1 for sands, Equation (2.52) becomes

$$(p_u)_i = \left(\Delta\sigma'_{hf}\right)_i \overline{BC_i} S_1 + 2(\tau_{ult})_i D S_2 \quad \textbf{(2.56)}$$

In the case where SL = 1 for clays, Equation (2.52) becomes

$$(p_u)_i = 10(s_u)_i D S_1 + 2(s_u)_i D S_2 \quad \textbf{(2.57)}$$

It can be seen in Equation (2.56) that p_u for sand is dependent upon $\overline{BC}$, which will continue to grow as the depth of the passive wedge increases with increasing pile deflection. As such, p_u will continue to increase even after SL = 1 (Ashour & Norris, 2000). This differs from p_u for sands in the semi-empirical model discussed in Section 2.4.2.3, which reaches a constant value of the lesser of Equation (2.33) and (2.34).

For circular piles embedded in clay, Equation (2.57) reduces to $p_u = 8.5Ds_u$. For rectangular piles embedded in clay, the coefficient of 8.5 is increased to 12. Recall from

Equation (2.24) and the discussion in Section 2.4.2.1 that Matlock (1970) called this coefficient N_p. According to Matlock (1970), the value of N_p is depth dependent within the passive wedge and ranges from 3 at the ground surface to 9 at the transition to flow-around failure for clays, where it remains constant at greater depths. From Equation (2.57), it appears the value of N_p is constant within each sub-layer in the SW model, and thus p_u is constant.

The pile deflection in the SW model is estimated from the horizontal strain, ε, in the passive wedge and the linearized pile deflection angle (δ) shown in Figure 2.17(b). Using Mohr's circle for strain, Ashour et al. (1998) show that

$$\psi_s = \frac{2}{(1+\nu)\sin(2\theta_m)} \tag{2.58}$$

where

$$\theta_m = 45 - \frac{\varphi'_m}{2} \tag{2.59}$$

Recall that v is Poisson's ratio for the soil within each sub-layer. From geometry, the deflection of each sub-layer is calculated as

$$y_i = H_i \delta_i = H_i \frac{\varepsilon}{\psi_s} \tag{2.60}$$

where:

H_i = vertical thickness of sub-layer i

δ_i = linearized pile deflection angle of sub-layer I

The pile head deflection (y_o) is calculated by summing the pile deflection at each sub-layer within the passive wedge as

$$y_o = \sum_{i=1}^{n} y_i \tag{2.61}$$

for n sub-layers within the passive wedge.

In the SW model, E_s is calculated for each sub-layer i using an incremental form of Equation (2.6) as

$$(E_s)_i = \frac{p_i}{y_i} \tag{2.62}$$

The values of p_i and $(E_s)_i$ from Equations (2.52) and (2.62), respectively, are dependent upon the geometry of the passive wedge that results from the assumed value of ε; therefore, iteration must be used to obtain a convergent solution to the BEF equation shown in Equation (2.4). The general solution scheme for the SW model is described by Ashour et al. (2002), and is summarized according to the author's understanding in the following solution steps:

1) Estimate the soil properties of ϕ', s_u, and ε_{50} for the subsurface profile. Select values of embedment depth and diameter for the drilled shaft, as well as f'_c, longitudinal reinforcement configuration, and transverse steel reinforcement ratio;
2) Select an initial non-zero value of strain, ε, within the passive wedge;
3) Assume a value of h for the chosen value of ε;
4) Calculate SL from (2.45) or (2.46) for each sub-layer;

5) Calculate $\Delta\sigma'_h$ from calculated SL, (2.42), (2.43), and (2.44) for each sub-layer;

6) Calculate E for each sub-layer from the assumed value of ε and the calculated value of $\Delta\sigma'_h$ using (2.41);

7) Calculate ϕ'_m from (2.42) for each sub-layer;

8) Calculate θ_m from (2.59) for each sub-layer;

9) Calculate β_m from (2.40) for each sub-layer;

10) Determine x from pile geometry from assumed h for each sub-layer;

11) Calculate $\overline{BC}$ from (2.39) for each sub-layer;

12) Calculate p for each sub-layer as the lesser of (2.53) and (2.56) or (2.57);

13) Calculate y from (2.60) for each sub-layer;

14) Calculate pile head deflection, y_o, using (2.61);

15) Estimate the E_s profile by calculating E_s for each sub-layer using (2.62);

16) Solve (2.4) (BEF equation) using the E_s profile estimated in the previous step and an arbitrary lateral load, p_o, at the pile head.;

17) Compare the calculated values of y_o and h to the same values resulting from the BEF analysis;

18) Repeat steps 2 through 17 until sufficient convergence is reached for y_o and h. For each iteration, modify p_o as $p_{o,modified} = y_{o,SW}\left(\frac{p_o}{y_o}\right)_{BEF}$;

19) Repeat Steps 2 – 18 for the next incremental value of ε until the desired pile head deflection or lateral load is reached.

2.6 MFAD and the Four-Spring Model

MFAD is a commercially developed program that is based on the software PADLL (Pier Analysis and Design for Lateral Loads), which was originally developed as part of a research project conducted by the Electric Power Research Institute (EPRI) in the early 1980s. This semi-empirical model was developed from the results of 14 large-scale load tests that were conducted throughout the United States as part of the research project (Davidson, Cass, Khilji, & McQuade, 1982). All of the test foundations were considered to be rigid, with *D/B* ratios ranging from 2.5 to 4.2, and the *MFAD* user's manual recommends only using this model for drilled shafts with *D/B* ratios greater than 2 and less than 10. The load tests were conducted in a variety of soil types, with site conditions ranging from purely cohesive to purely granular, and some sites with layered soils and soft rock sockets.

MFAD uses a four-spring load-deflection model and an ultimate capacity model for analysis and design of laterally loaded drilled shafts (EPRI, 2014). Similar to the *p-y* method described in Section 2.4, the four-spring model utilizes springs to represent the soil resistance that develops at discrete points along the pile. As the name somewhat implies, there are four types of springs that are utilized in the four-spring model: a base shear translational spring, a base moment spring, lateral translational springs, and vertical side shear moment springs. One base shear translational spring and one base moment spring are utilized at the bottom of the pile; however, several lateral translational and vertical side shear moment springs are used along the length of the pile as shown in Figure 2.22. A schematic representation of these springs is shown in Figure 2.23. It should be noted that the vertical side shear moment spring is considered a moment spring because the vertical shear force that develops along the length of the pile occurs at the

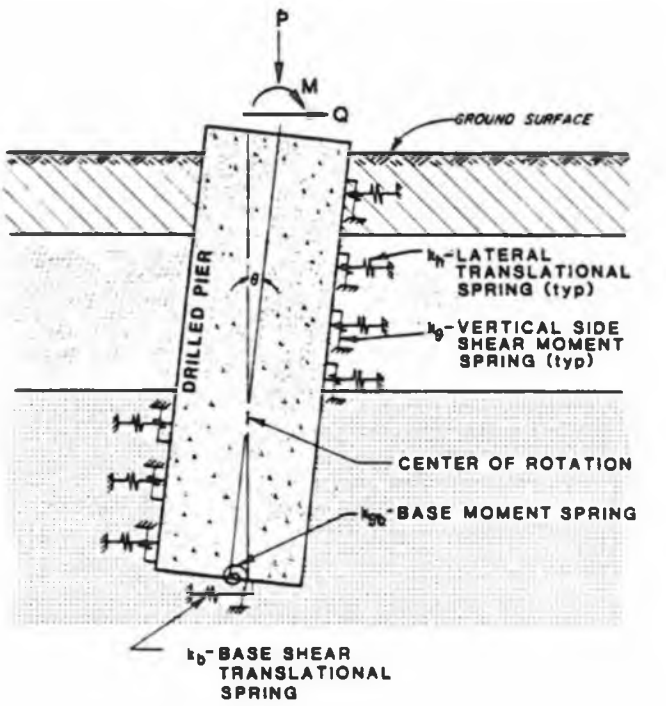

Figure 2.22. Configuration of four-spring model used in MFAD (Davidson, Cass, Khilji, & McQuade, 1982)

radial distance away from the center of the pile.

The lateral translational spring is represented by the curve shown in Figure 2.23(a) which is essentially a *p-y* curve similar to those discussed in Section 2.4. The equation for this curve is shown in Equation (2.63). The equations for the spring constants shown in Figure 2.23(a) through (c) are shown in Equation (2.64) through (2.67).

$$p = 0.6\, p_{ult} \left(\frac{2k_h y}{p_{ult}}\right)^{0.5} \leq p_{ult} \tag{2.63}$$

$$k_h = \left(\frac{5.7E_p}{B}\right)(D/B)^{-0.40} \tag{2.64}$$

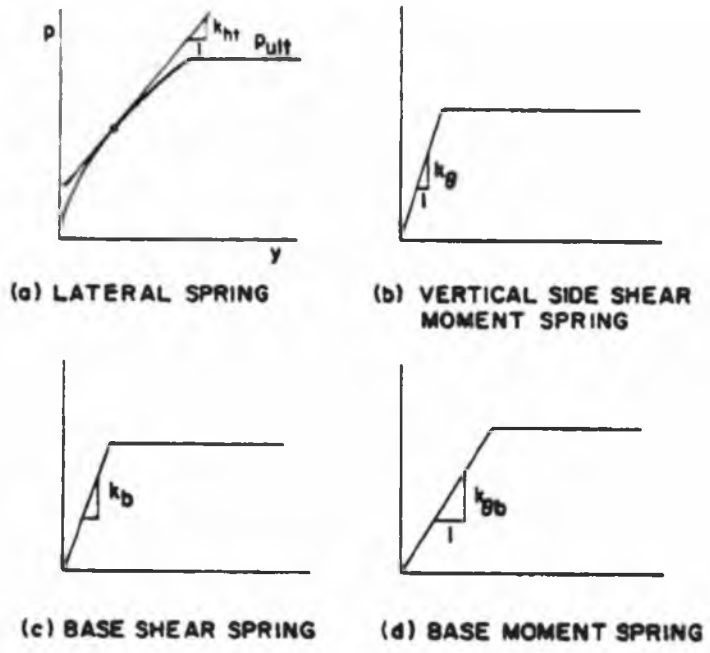

Figure 2.23. Schematic representation of force-deformation characteristics of the nonlinear springs used in MFAD (Davidson, Cass, Khilji, & McQuade, 1982)

$$k_\theta = 0.55E_pB \tag{2.65}$$

$$k_b = \left(\frac{2.1E_p}{B}\right)(D/B)^{-0.15} \tag{2.66}$$

$$k_{\theta b} = 0.24E_pB(D/B)^{0.40} \tag{2.67}$$

where:

p = soil resistance per unit length

p_{ult} = theoretical ultimate soil resistance per unit length

y = deflection of the shaft corresponding to p

B = diameter (width) of shaft

D = embedded depth of shaft

E_p = modulus of deformation as measured by PMT

k_h = horizontal coefficient of subgrade reaction

k_θ = vertical side shear moment spring

k_b = base shear spring

$k_{\theta b}$ = base moment spring

The soil properties required for an *MFAD* analysis are γ, and ϕ or s_u for granular or cohesive soils, respectively. Additionally, as shown in Equations (2.64) through (2.67), *MFAD* uses the deformation modulus (E_P) to represent the stress-strain characteristics of the soil or rock. E_P is also referred to as the pressuremeter modulus (E_{PMT}), and it is used because it accounts for some of the orthotropic effects of lateral loading of the soil surrounding the foundation (Davidson, Cass, Khilji, & McQuade, 1982). According to Kulhawy and Mayne (1990), the deformation modulus is often presumed to be roughly equivalent to E for granular soils and to the undrained secant modulus (E_{US}) for cohesive soils. It should also be noted that one of the major assumptions that is made in the four-spring model is that the foundation is perfectly rigid. As such, the material properties of the foundation are not required, and the nonlinearity associated with concrete cracking and rebar yielding is not accounted for in this model.

As previously discussed, the four-spring model is used to estimate the ultimate capacity and the load-deflection response of the foundation. The ultimate capacity is estimated from limit equilibrium of the applied loads and the springs representing the soil

resistance. The analyst must specify the effective eccentricity, which is defined as the ratio of the applied moment to the applied shear. In practice, this is estimated by *MFAD* from the length of the stickup portion of the pile and loads applied to the top of the stickup. From the forces in the free-body diagram shown in Figure 2.24, three independent equations can be formulated that satisfy static equilibrium; however, there are four unknown variables: the ultimate moment capacity (M_{ult}), the ultimate shear capacity (Q_{ult}), the ultimate lateral force per unit length (p_{ult}), and the depth to the center of rotation of the pile (a). As such, an iterative procedure is used to estimate the fourth unknown variable. This is accomplished by using a trial value of a, solving for the other three unknown variables, and comparing the calculated value of effective eccentricity to the specified value of effective eccentricity. Convergence is said to have been achieved once the difference between the calculated effective eccentricity and the specified effective eccentricity is less than 0.1 percent.

The four-spring model utilizes the stiffness method to obtain deflection and rotation profiles along the foundation. In the stiffness method, the pile is discretized into a finite number of elements, which are connected together by nodes. Each node is assigned a specific number of degrees of freedom to represent translation and rotation. In the four-spring model, each node has two degrees of freedom: one for deflection and one for rotation. For linearly-elastic systems, the number of unknown variables is equal to the number of degrees of freedom. An algebraic equation can be formulated to represent each degree of freedom, and these equations can be solved simultaneously to determine the value of each degree of freedom (in this case, translation or rotation). These values can then be substituted into the system of linear equations to obtain values of shear force and bending moment at each node.

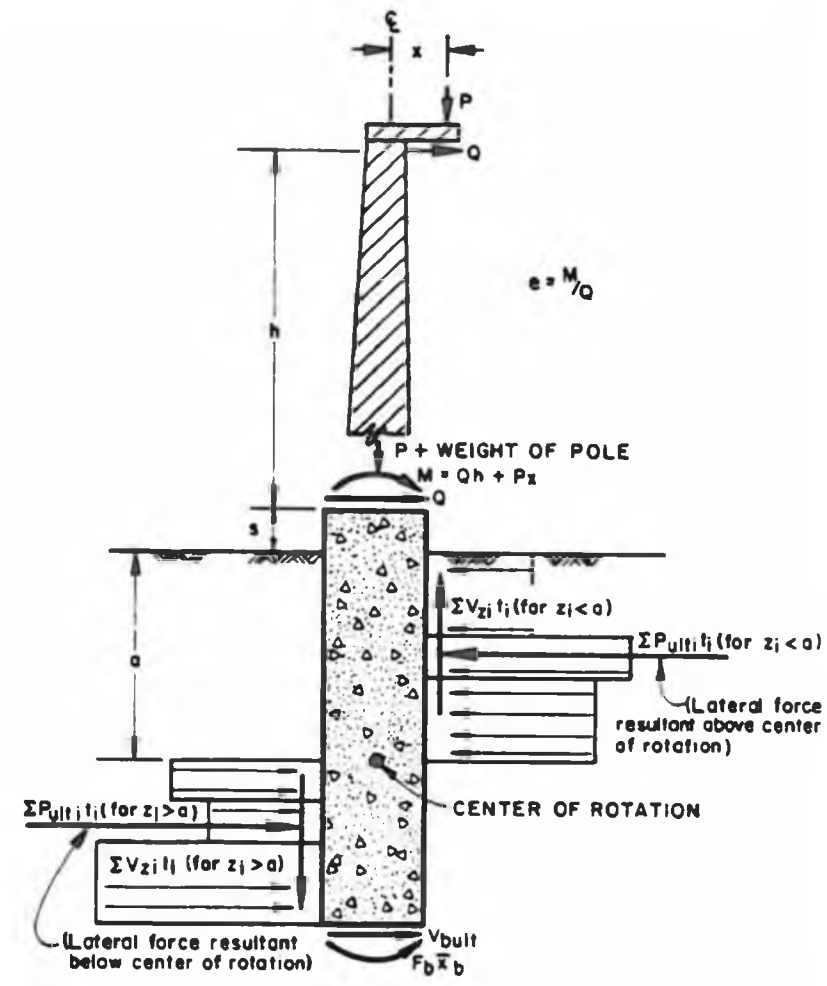

Figure 2.24. Free body diagram of forces acting on a typical pile

The stiffness matrix $[k_E]$ for each element is comprised of three components: the beam stiffness matrix $[k_B]$, the lateral spring stiffness matrix $[k_h]$, and the vertical side shear moment stiffness matrix $[k_\theta]$ as shown in Equation (2.68).

$$[K_E] = [K_B] + [K_h] + [K_\theta] \tag{2.68}$$

The conventional stiffness matrix for a beam subjected to pure bending, i.e., no axial or shear deformation is allowed to occur, is shown in Equation (2.69). The stiffness

matrix for the lateral springs is shown in Equation (2.70). The stiffness matrix for the vertical side shear moment springs is shown in Equation (2.71).

$$[k_B] = \frac{EI}{L^3}\begin{bmatrix} 12 & -6L & -12 & -6L \\ -6L & 4L^2 & 6L & 2L^2 \\ -12 & 6L & 12 & 6L \\ -6L & 2L^2 & 6L & 4L^2 \end{bmatrix} \tag{2.69}$$

$$[k_h] = \frac{k_{ht}LB}{420}\begin{bmatrix} 156 & 22L & 54 & 13L \\ -22L & 4L^2 & -13L & -3L^2 \\ 54 & -13L & 156 & 22L \\ 13L & -3L^2 & 22L & 4L^2 \end{bmatrix} \tag{2.70}$$

$$[k_\theta] = \frac{k_\theta B}{30L}\begin{bmatrix} 36 & -3L & -36 & -3L \\ -3L & 4L^2 & 3L & -L^2 \\ -36 & 3L & 36 & 3L \\ -3L & -L^2 & 3L & 4L^2 \end{bmatrix} \tag{2.71}$$

where:

EI = bending stiffness of the pile

L = pile length

B = diameter of pile

k_{ht} = current tangent value of the horizontal subgrade modulus

k_θ = vertical side shear moment spring

As shown in the stiffness matrices of Equation (2.69) through (2.71), the four-spring model is a nonlinear model, so the solution for the unknown degrees of freedom and subsequent values of shear and bending moment is somewhat more involved. In general, an iterative technique must be used to solve the set of nonlinear simultaneous equations representing the unknown degrees of freedom. The four-spring model uses the

well known modified Newton-Rhapson method by applying an incremental load, solving the system of simultaneous equations for deflection, back-substituting these deflection values into the system of equations to obtain the calculated loads, and comparing the calculated load to the assigned load. If the calculated and assigned loads are within the specified tolerance, convergence is said to have been achieved and the solution is obtained. If convergence has not been achieved, the difference between the calculated force and the assigned force at each node is added or subtracted from the assigned load, and the process is repeated until convergence is achieved.

2.7 Large-Scale Load Tests in the Literature

A thorough survey of the literature was conducted to identify published large-scale tests of laterally loaded drilled shafts that could potentially be used for comparison between observed and predicted results using the methods previously described. The published literature included journal articles, conference proceedings, dissertations, reports, and textbooks. A total of 226 large-scale load tests were discovered during the literature review, and select details are presented for each load test in Table 2.2. The criteria that were used to assess the suitability of each test for use in this investigation are described in Section 3.1.

Table 2.2. Large-scale lateral load tests reported in the literature

Load Test (LT) #	Load Test ID	Year	Test Site	Soil Description	Shaft Diameter, B		Embedded Depth, D		D/B	Load Eccentricity, e		Reference	Use? (Y/N)	If No, why not?
					(m)	(ft)	(m)	(ft)		(m)	(ft)			
1	DS 1-1	1948	NR	Silty clay	0.61	2.00	1.83	6.00	3.00	3.05	10.01	Shilts, Graves, and Driscoll (1948)	N	Not enough information
	DS 1-2				0.61	2.00	1.37	4.49	2.25	3.05	10.01		N	Not enough information
	DS 1-3			Sand and fine sand with gravel	0.61	2.00	1.52	4.99	2.49	3.05	10.01		N	Not enough information
2	DS 2-1	1957	Mt. Gilead, OH	Sandy silt and sandy, silty clay	0.81	2.66	2.50	8.20	3.09	7.44	24.41	Behn (1960)	N	Groundline deflection < 0.5 in.
	DS 2-2				0.81	2.66	3.66	12.00	4.52	7.44	24.41		N	Groundline deflection < 0.5 in.
3	DS 3-1	1957	Mansfield, OH	Organic clay	0.81	2.66	2.41	7.90	2.97	7.35	24.11	Behn (1960)	N	No appropriate soil type in LPile, Groundline deflection < 0.5 in.
	DS 3-2				0.81	2.66	3.66	12.00	4.52	7.38	24.21		N	No appropriate soil type in LPile
4	DS 4-1	1957	Holmesville, OH	Sandy gravel and gravelly sand	0.91	3.00	2.44	8.00	2.67	7.38	24.21	Behn (1960)	N	Groundline deflection < 0.5 in.
	DS 4-2				0.91	3.00	3.75	12.30	4.10	7.38	24.21		N	Groundline deflection < 0.5 in.
5	DS 5-1	1963	42 mi east of Los Angeles, CA	fine-to-coarse grained sand, some gravel and cobbles	1.07	3.50	5.18	17.00	4.86	0.00	0.00	Bhushan, Lee, and Grime (1981)	N	No reinforcement info, belled shaft
	DS 5-2				1.07	3.50	5.18	17.00	4.86	0.00	0.00		N	No reinforcement info, belled shaft
	DS 5-3				1.07	3.50	5.18	17.00	4.86	0.00	0.00		N	No reinforcement info, belled shaft
6	DS 6-1	1970	Naticoke, Ontario, Canada	Fissured clay	0.61	2.00	6.40	21.00	10.49	0.46	1.51	Seychuk (1970)	N	D/B too high
7	DS 7-1	1972	France	Clayey silt	0.95	3.12	4.40	14.44	4.63	2.20	7.22	Baguelin, Goulet, and Jezequel (1972)	N	No English translation of paper available
8	DS 8-1	1972	Ranchi, india	Sandy clay with weathered rock	0.48	1.57	11.00	36.09	22.92	0.00	0.00	Feda (1972)	N	D/B too high
9	DS 9-1	1973	NR	Organic clay over sand	1.30	4.27	13.50	44.29	10.38	2.00	6.56	Franke (1973)	N	D/B too high
	DS 9-2				1.30	4.27	16.50	54.13	12.69	2.00	6.56		N	D/B too high
	DS 9-3				1.30	4.27	19.50	63.98	15.00	2.00	6.56		N	D/B too high
10	DS 10-1	1973	Romania	Clayey silt, sandy clay, silty clay	1.00	3.28	10.00	32.81	10.00	2.25	7.38	Botea, Manoliu, and Abramescu (1973)	N	Not enough soil information
	DS 10-2				1.00	3.28	10.00	32.81	10.00	2.25	7.38		N	Not enough soil information
	DS 10-3			Gravel, sand, silty sand, sandy silt	0.88	2.89	33.00	108.27	37.50	0.80	2.62		N	D/B too high, not enough soil information
	DS 10-4				0.88	2.89	33.00	108.27	37.50	0.80	2.62		N	D/B too high, not enough soil information
	DS 10-5			Gravel with sand, sand, silty sand, clayey silt	0.88	2.89	14.00	45.93	15.91	0.20	0.66		N	D/B too high, not enough soil information
	DS 10-6			Gravel with sand, silty sand, silt, clayey siltand clay	1.27	4.17	38.00	124.67	29.92	0.20	0.66		N	D/B too high, not enough soil information
11	DS 11-1	1973	Ontario, Canada	Loose Silty Sand, Dense fine to medium sand	0.91	3.00	6.10	20.00	6.67	24.38	80.00	Adams and Radhakrishna (1973)	Y	
	DS 11-2				1.52	5.00	6.10	20.00	4.00	3.05	10.00		N	Deflection < 0.5 in.
	DS 11-3			Fine silty sand, dense clayey silt with coarse sand and	0.91	3.00	6.10	20.00	6.67	3.05	10.00		N	No appropriate soil type in LPile
	DS 11-4				1.52	5.00	6.10	20.00	4.00	3.05	10.00		N	No appropriate soil type in LPile
12	DS 12-1	1975	Houston, TX	Stiff clay, silty clay	0.76	2.49	12.80	41.99	16.84	0.00	0.00	Reese and Welch (1975)	N	D/B too high
13	DS 13-1	1976	Southern Florida	Medium dense sand and stiff clay	1.07	3.50	8.99	29.50	8.43	6.55	21.5	Teng and Manuel (1976)	N	Not enough information

Table 2.2. Continued

Load Test (LT) #	Load Test ID	Year	Test Site	Soil Description	Shaft Diameter, B		Embedded Depth, D		D/B	Load Eccentricity, e		Reference	Use? (Y/N)	If No, why not?
					(m)	(ft)	(m)	(ft)		(m)	(ft)			
14	DS 14-1	1976	Pto Tolle, Italy	Loose sand	0.60	1.97	35.00	114.83	58.33	0.60	1.97	Garassino, Jamiolkowski, and Nunes, Costa, and Rausa (1977)	N	D/B too high
	DS 14-2				0.60	1.97	35.00	114.83	58.33	0.60	1.97		N	D/B too high
15	DS 15-1	1977	Rio Niteroi, Brazil	Silt, sand, and clay	1.80	5.91	34.50	113.19	19.17	0.80	2.62		N	D/B too high
	DS 15-2				1.80	5.91	33.70	110.56	18.72	0.80	2.62		N	D/B too high
16	DS 16-1	1977	Pennsylvania	Medium stiff to very stiff clayey silt	1.68	5.50	5.18	17.00	3.09	27.43	90.00	Davidson and Donovan (1977)	N	No appropriate soil type in LPile
	DS 16-2				2.44	8.00	5.18	17.00	2.13	27.43	90.00		N	No appropriate soil type in LPile
17	DS 17-1	1978	Hamilton, Ontario, Canada	Stiff silty clay	1.52	5.00	11.58	38.00	7.60	0.30	1.00	Ismael and Klym (1978)	N	Deflection < 0.5 in.
	DS 17-2				1.52	5.00	5.18	17.00	3.40	0.30	1.00		N	Foundation constructed with 10 ft bell
18	DS 18-1	1979	Southern California	Stiff silty and sandy clay	1.22	4.00	4.57	15.00	3.75	0.23	0.75	Bhushan, Haley, Fong (1979)	N	Constructed with bell at bottom
	DS 18-2				1.22	4.00	4.57	15.00	3.75	0.23	0.75		Y	
19	DS 19-1	1979	Daggett, CA	Dense fine-to-coarse grained sand, silty sand with some gravel	0.61	2.00	5.49	18.00	9.00	0.00	0.00	Bhushan, Lee, and Grime (1981)	Y	
	DS 19-2				0.91	3.00	5.49	18.00	6.00	0.00	0.00		Y	
	DS 19-3				0.91	3.00	5.49	18.00	6.00	0.00	0.00		Y	
	DS 19-4				1.22	4.00	5.49	18.00	4.50	0.00	0.00		N	Deflection < 0.5 in.
20	DS 20-1	1979	Southern California	Stiff sandy lean clay	1.22	4.00	3.81	12.50	3.13	0.23	0.75	Bhushan, Haley, Fong (1979)	N	Constructed with bell at bottom
	DS 20-2				1.22	4.00	3.81	12.50	3.13	0.23	0.75		Y	
	DS 20-3				1.22	4.00	4.72	15.50	3.88	0.23	0.75		N	Constructed with bell at bottom
	DS 20-4				1.22	4.00	4.72	15.50	3.88	0.23	0.75		Y	
	DS 20-5				0.61	2.00	2.74	9.00	4.50	0.23	0.75		Y	
	DS 20-6				0.61	2.00	4.72	15.50	7.75	0.23	0.75		Y	
	DS 20-7				1.22	4.00	5.18	17.00	4.25	0.23	0.75		N	Ground slope 20°
	DS 20-8				1.22	4.00	5.18	17.00	4.25	0.23	0.75		N	Ground slope = 35°
	DS 20-9				1.22	4.00	5.18	17.00	4.25	0.23	0.75		N	Ground slope = 35°
	DS 20-10			Cemented silty sand	1.22	4.00	6.71	22.00	5.50	0.23	0.75		N	Ground slope 55°
21	DS 21-1	1981	Naples, Italy	Sand	0.60	1.97	14.00	45.93	23.33	0.35	1.15	Fenelli and Galateri (1981)	N	D/B too high
	DS 21-2				0.50	1.64	15.00	49.21	30.00	0.50	1.64		N	D/B too high
	DS 21-3				0.50	1.64	15.00	49.21	30.00	0.50	1.64		N	D/B too high
22	DS 22-1	1981	College Station, TX	Stiff clay	0.91	3.00	6.10	20.00	6.67	0.76	2.50	Bierschwale, Coyle, and Bartoskewitz (1981)	Y	
	DS 22-2				0.91	3.00	4.57	15.00	5.00	0.76	2.50		Y	
	DS 22-3				0.76	2.50	4.57	15.00	6.00	0.76	2.50		N	Loading period too long
23	DS 23-1	1981	Brice-Milton, Ontario, Canada	Dense fine to medium sand over loose fine silt	0.91	3.00	6.40	21.00	7.00	0.00	0.00	Ismael and Klym (1981)	Y	
	DS 23-2				0.91	3.00	6.40	21.00	7.00	0.00	0.00		Y	
24	DS 24-1	1981	Steubenville, OH	Silt and sand over bedrock	0.91	3.00	28.22	92.60	30.87	0.00	0.00	Newman, Salver, and Turka (1981)	N	D/B too high, socketed in rock
	DS 24-2				1.52	5.00	38.34	125.80	25.16	0.00	0.00		N	D/B too high, socketed in rock
25	DS 25-1	1982	Richmond, VA	Stiff silty clay and hard clay	1.37	4.50	3.57	11.71	2.61	24.38	79.99	Davidson, Cass, Khilji, and McQuade (1982)	N	Load test data not available
26	DS 26-1	1982	Oklahoma City, OK	Medium stiff to hard silty clay	1.52	5.00	3.81	12.50	2.51	24.38	79.99	Davidson, Cass, Khilji, and McQuade (1982)	N	Load test data not available
27	DS 27-1	1982	Farmersville, OH	Clayey silt, some sand and gravel	1.98	6.50	6.17	20.24	3.12	24.38	79.99	Davidson, Cass, Khilji, and McQuade (1982)	N	Load test data not available
28	DS 28-1	1982	Portland, OR	Stiff clayey silt	1.37	4.50	5.33	17.49	3.89	24.38	79.99	Davidson, Cass, Khilji, and McQuade (1982)	N	Load test data not available

Table 2.2. Continued

Load Test (LT) #	Load Test ID	Year	Test Site	Soil Description	Shaft Diameter, B		Embedded Depth, D		D/B	Load Eccentricity, e		Reference	Use? (Y/N)	If No, why not?
					(m)	(ft)	(m)	(ft)		(m)	(ft)			
29	DS 29-1	1982	Omaha, NB	Clayey silt and silty clay	1.37	4.50	4.57	14.99	3.34	24.38	79.99	Davidson, Cass, Khilji, and McQuade (1982)	N	Load test data not available
30	DS 30-1	1982	Greensburg, PA	Loose to medium silty sand, trace silt	1.52	5.00	6.40	21.00	4.21	24.38	79.99	Davidson, Cass, Khilji, and McQuade (1982)	N	Load test data not available
31	DS 31-1	1982	Heightstown, NJ	Medium to dense silty sand, some clay and gravel	1.52	5.00	4.82	15.81	3.17	24.38	79.99	Davidson, Cass, Khilji, and McQuade (1982)	N	Load test data not available
32	DS 32-1	1982	Baltimore, MD	Clayey silt and silty sand, some gravel	1.52	5.00	4.82	15.81	3.17	24.38	79.99	Davidson, Cass, Khilji, and McQuade (1982)	N	Load test data not available
33	DS 33-1	1982	Kinston, NC	Clayey silty sand, trace gravel	1.37	4.50	4.54	14.90	3.31	24.38	79.99	Davidson, Cass, Khilji, and McQuade (1982)	N	Load test data not available
34	DS 34-1	1982	St. Charles, MI	Loose silt over medium dense sand	1.62	5.30	4.94	16.21	3.05	24.38	79.99	Davidson, Cass, Khilji, and McQuade (1982)	N	Load test data not available
35	DS 35-1	1982	Phoenix, AZ	Loose to dense cemented silty sand	1.47	4.82	4.88	16.01	3.32	24.38	79.99	Davidson, Cass, Khilji, and McQuade (1982)	N	Load test data not available
36	DS 36-1	1982	Garden Grove, CA	Loose and medium silty sand, few clay layers	1.52	5.00	6.19	20.31	4.07	24.38	79.99	Davidson, Cass, Khilji, and McQuade (1982)	N	Load test data not available
37	DS 37-1	1984	San Antonio, TX	Clay and clayey gravel with caliche	0.46	1.50	10.50	34.45	22.83	0.00	0.00	Johnson, Briaud, and Stroman (1984)	N	D/B too high
38	DS 38-1	1984	Daggett, CA	Dense sand and gravelly sand	0.91	3.00	5.42	17.78	5.93	5.43	17.80	Bhushan and Askari (1984)	N	Deflection ≤ 1 mm
	DS 38-2				0.61	2.00	5.18	17.00	8.50	5.43	17.80		N	Deflection ≤ 1 mm
	DS 38-3				1.07	3.50	5.03	16.50	4.71	5.43	17.80		N	Deflection ≤ 1 mm
	DS 38-4				0.91	3.00	5.49	18.00	6.00	5.43	17.80		N	Deflection ≤ 1 mm
	DS 38-5				0.91	3.00	5.49	18.00	6.00	5.43	17.80		N	Deflection ≤ 1 mm
39	DS 39-1	1984	Tampa Bay, FL	Dense sand over clay	1.22	4.00	21.30	69.88	17.46	0.70	2.30	Long and Reese (1984)	N	D/B too high
	DS 39-2				1.22	4.00	21.30	69.88	17.46	0.70	2.30		N	D/B too high
40	DS 40-1	1985	Calgary, Alberta, Canada	Silty fine sand, clayey silt, glacial till	1.50	4.92	15.00	49.21	10.00	0.32	1.05	Clark, McKeown, Lester, and Eibner (1985)	N	No appropriate soil type in LPile
	DS 40-2				1.50	4.92	15.00	49.21	10.00	0.32	1.05		N	No appropriate soil type in LPile
	DS 40-3				0.90	2.95	15.00	49.21	16.67	0.36	1.18		N	D/B too high
	DS 40-4				0.90	2.95	15.00	49.21	16.67	0.36	1.18		N	D/B too high
41	DS 41-1	1985	Houston, TX	Medium stiff to very stiff clay	1.83	6.00	11.43	37.50	6.25	0.28	0.92	Dunnavant and O'Neill (1985)	N	Cyclic test
42	DS 42-1	1985	Alberta, Canada	Clay till	0.67	2.20	7.70	25.26	11.49	0.67	2.20	Harris, Papanicolas, and Rogers (1985)	N	D/B too high
43	DS 43-1	1986	Los Angeles, CA	Sand, silt, and clay	2.44	8.00	18.90	62.00	7.75	1.22	4.00	Naramore and Feng (1990)	N	Poor consturction quality, extensive caving
	DS 43-2				2.44	8.00	18.90	62.00	7.75	1.22	4.00		N	Poor consturction quality, extensive caving
	DS 43-3				1.22	4.00	15.54	51.00	12.75	1.22	4.00		N	Extensive caving, D/B too high
	DS 43-4				1.22	4.00	15.54	51.00	12.75	1.22	4.00		N	Extensive caving, D/B too high
44	DS 44-1	1987	United Kingtom	Dense sandy gravel, dense sand,	1.20	3.94	13.00	42.65	10.83	0.39	1.28	Lyndon, Price, Wardle, and Varey (1989)	N	D/B too high, socketed in rock
	DS 44-2			Highly weathered sandstone	1.50	4.92	13.00	42.65	8.67	0.39	1.28		M	Socketed in rock, no appropriate soil type in LPile

Table 2.2. Continued

Load Test (LT) #	Load Test ID	Year	Test Site	Soil Description	Shaft Diameter, B		Embedded Depth, D		D/B	Load Eccentricity, e		Reference	Use? (Y/N)	If No, why not?
					(m)	(ft)	(m)	(ft)		(m)	(ft)			
45	DS 45-1	1987	Yarmouth, United Kingdom	Soft silt and silty clay	0.76	2.49	24.00	78.74	31.58	0.80	2.62	Price and Wardle (1987)	N	D/B too high
46	DS 46-1	1987	China	Sandy clay	1.04	3.41	11.00	36.09	10.58	0.60	1.97	Lu, Xie, and Zhan (1987)	N	D/B too high
47	DS 47-1	1987	Newmans Bridge, New Zeland	Weak siltstone with overlying layers of alluvial sands and gravel	1.80	5.91	12.10	39.70	6.72	7.83	25.69	Wood and Phillips (1987)	N	Maximum groundline deflection only about 6 mm
	DS 47-2				1.80	5.91	10.60	34.78	5.89	9.33	30.61		N	Maximum groundline deflection only about 6 mm
48	DS 48-1	1988	Germany	Clay	1.20	3.94	40.00	131.23	33.33	0.35	1.15	Amann, Wollenhaupt, and Bahn, (1988)	N	D/B too high
	DS 48-2				1.20	3.94	40.00	131.23	33.33	0.25	0.82		N	D/B too high
49	DS 49-1	1988	Fukuok, Japan	Sand and silt	0.40	1.31	10.00	32.81	25.00	0.20	0.66	Kanai and Yabuuchi (1988)	N	D/B too high
50	DS 50-1	1988	Singapore	Sand, silty sand, and silt	1.00	3.28	26.00	85.30	26.00	1.00	3.28	Goh and Lam (1988)	N	D/B too high
51	DS 51-1	1988	Bedok, Singapore	Soft to stiff silty clay	1.00	3.28	30.50	100.07	30.50	1.00	3.28	Goh and Lam (1988)	N	D/B too high
	DS 51-2				1.00	3.28	18.00	59.06	18.00	1.00	3.28		N	D/B too high
52	DS 52-1	1988	Seto Inland Sea, Japan	Sand, alluvium, and granite	3.00	9.84	70.00	229.66	23.33	0.30	0.98	Fukuoka (1988)	N	D/B too high
	DS 52-2				2.00	6.56	70.00	229.66	35.00	0.30	0.98		N	D/B too high
	DS 52-3				2.00	6.56	40.00	131.23	20.00	0.30	0.98		N	D/B too high
53	DS 53-1	1988	Glenwood Canyon, CO	Sand, gravel, cobbles, and boulders	2.13	7.00	9.75	32.00	4.57	0.50	1.64	Macklin and Chou (1988)	N	No appropriate soil type in LPile, total deflection ≤ 0.2 in.
	DS 53-2				2.13	7.00	10.82	35.50	5.07	0.50	1.64		N	No appropriate soil type in LPile, total deflection ≤ 0.2 in.
54	DS 54-1	1988	Singapore	Clayey silt and silty clay over weathered rock	0.68	2.23	5.00	16.40	7.35	0.50	1.64	Chang and Goh (1988)	N	Socketed in rock
	DS 54-2				0.68	2.23	5.00	16.40	7.35	0.50	1.64		N	Socketed in rock
	DS 54-3				0.68	2.23	5.00	16.40	7.35	0.50	1.64		N	Socketed in rock
	DS 54-4			Clayey silt and silty clay	0.68	2.23	7.10	23.29	10.44	0.35	1.15		N	D/B too high
	DS 54-5				0.68	2.23	7.10	23.29	10.44	0.35	1.15		N	D/B too high
	DS 54-6				0.68	2.23	7.10	23.29	10.44	0.35	1.15		N	D/B too high
55	DS 55-1	1988	Tampa Bay, FL	Loose sand over stiff clay and weathered rock	0.91	3.00	18.20	59.70	19.90	6.37	20.90	Poepsel and Sheahan (1988)	N	D/B too high
	DS 55-2			Loose sand over dense sand	0.91	3.00	19.48	63.90	21.30	6.55	21.50		N	D/B too high
56	DS 56-1	1988	Houston, TX	Loose to dense sand underlain by stiff to very stiff clay	0.91	3.00	29.57	97.00	32.33	0.09	0.30	Little and Briaud (1988)	N	D/B too high
	DS 56-2				1.07	3.50	39.01	128.00	36.57	0.09	0.30		N	D/B too high
	DS 56-3				1.07	3.50	39.01	128.00	36.57	0.21	0.70		N	D/B too high
	DS 56-4				1.07	3.50	39.01	128.00	36.57	0.25	0.83		N	D/B too high
57	DS 57-1	1989	Guadiana, Portugal	Silty sand	0.80	2.62	42.00	137.80	52.50	0.00	0.00	Guedes de Melo and Esteves Ferreira (1989)	N	D/B too high
58	DS 58-1	1989	Maitai River Bridge, New Zealand	Sandy fine to medium gravel	1.80	5.91	12.00	39.37	6.67	8.12	26.64	Wood and Phillips (1989)	N	Load test data not available

Table 2.2. Continued

Load Test (LT) #	Load Test ID	Year	Test Site	Soil Description	Shaft Diameter, B		Embedded Depth, D		D/B	Load Eccentricity, e		Reference	Use? (Y/N)	If No, why not?
					(m)	(ft)	(m)	(ft)		(m)	(ft)			
59	DS 59-1	1989	South Surra, Kuwait	Medium dense cemeted silty sand	0.30	0.98	2.70	8.86	9.00	0.00	0.00	Ismael (1990)	N	Only the average load-deflection curve for all 4 tests was reported
	DS 59-2				0.30	0.98	2.70	8.86	9.00	0.00	0.00		N	Only the average load-deflection curve for all 4 tests was reported
	DS 59-3				0.30	0.98	2.70	8.86	9.00	0.00	0.00		N	Only the average load-deflection curve for all 4 tests was reported
	DS 59-4				0.30	0.98	2.70	8.86	9.00	0.00	0.00		N	Only the average load-deflection curve for all 4 tests was reported
	DS 59-5				0.30	0.98	4.70	15.42	15.67	0.00	0.00		N	D/B too high, part of pile cap
	DS 59-6				0.30	0.98	4.70	15.42	15.67	0.00	0.00		N	D/B too high, part of pile cap
	DS 59-7				0.30	0.98	4.70	15.42	15.67	0.00	0.00		N	D/B too high, part of pile cap
	DS 59-8				0.30	0.98	4.70	15.42	15.67	0.00	0.00		N	D/B too high, part of pile cap
	DS 59-9				0.30	0.98	4.70	15.42	15.67	0.00	0.00		N	D/B too high
	DS 59-10				0.30	0.98	4.70	15.42	15.67	0.00	0.00		N	D/B too high
	DS 59-11				0.30	0.98	4.70	15.42	15.67	0.00	0.00		N	D/B too high
	DS 59-12				0.30	0.98	4.70	15.42	15.67	0.00	0.00		N	D/B too high
60	DS 60-1	1991	Charwell River Bridge, New Zealand	Coarse to fine gravel over sand and silt	1.50	4.92	12.00	39.37	8.00	50.80	166.67	Wood and Phillips (1991)	N	Load test data not available
	DS 60-2				1.50	4.92	11.00	36.09	7.33	52.60	172.57		N	
61	DS 61-1	1991	Thessalonki, Greece	Silty clay with sand	1.00	3.28	36.00	118.11	36.00	0.75	2.46	Hatzigogos, Pitilakis, and Tsotsos, (1991)	N	D/B too high
62	DS 62-1	1991	North Halawa Valley, HI	Clayey silt over weathered basalt	0.76	2.49	20.40	66.93	26.84	0.38	1.25	Parsons Brinckerhoff-Hirota Associates (1991)	N	D/B too high
	DS 62-2				0.76	2.49	21.30	69.88	28.03	0.38	1.25		N	D/B too high
	DS 62-3				0.76	2.49	12.20	40.03	16.05	0.38	1.25		N	D/B too high
	DS 62-4				0.76	2.49	12.20	40.03	16.05	0.38	1.25		N	D/B too high
	DS 62-5				0.76	2.49	21.30	69.88	28.03	0.38	1.25		N	D/B too high
	DS 62-6				0.76	2.49	21.30	69.88	28.03	0.38	1.25		N	D/B too high
63	DS 63-1	1993	Portugal	Sand	1.20	3.94	40.00	131.23	33.33	0.20	0.66	Portugal and Pinto (1993)	N	D/B too high
64	DS 64-1	1993	Amherst, MA	Lacustrine varved clay	0.51	1.67	1.52	4.99	2.98	0.00	0.00	Lutenegger and Miller (1993)	N	Embedment depth too shallow
	DS 64-2				0.51	1.67	2.44	8.01	4.78	0.00	0.00		N	Deflection < 15 mm
	DS 64-3				0.61	2.00	1.52	5.00	2.50	0.00	0.00		N	Embedment depth too shallow
	DS 64-4				0.61	2.00	2.44	8.00	4.00	0.00	0.00		N	Deflection < 15 mm
65	DS 65-1	1994	Canons Park, England	Stiff clay with trace gravel	0.17	0.56	4.50	14.76	26.47	0.20	0.66	Gabr, Lunne, and Powell (1994)	N	D/B too high
66	DS 66-1	1994	Taipei, Taiwan	Silty clay	1.20	3.94	32.70	107.28	27.25	0.30	0.98	Diagnostic Engineering Consultants, Ltd. (1994)	N	D/B too high
67	DS 67-1	1994	Beitou, Taipei, Taiwan	Silty sand and silty gravel	2.00	6.56	65.50	214.90	32.75	0.30	0.98	Diagnostic Engineering Consultants, Ltd. (1994)	N	D/B too high
	DS 67-2				2.00	6.56	64.50	211.61	32.25	0.30	0.98		N	D/B too high
68	DS 68-1	1996	Pascagoula, MS	Clay and sand	2.10	6.89	26.00	85.30	12.38	5.50	18.04	Anderson and Townsend (1999)	N	D/B too high
69	DS 69-1	1997	NR	Silty clay	1.50	4.92	41.80	137.14	27.87	0.20	0.66	Georgiadis, Anagnostopoulos, and Naskos, (1997)	N	D/B too high

Table 2.2. Continued

Load Test (LT) #	Load Test ID	Year	Test Site	Soil Description	Shaft Diameter, B		Embedded Depth, D		D/B	Load Eccentricity, e		Reference	Use? (Y/N)	If No, why not?
					(m)	(ft)	(m)	(ft)		(m)	(ft)			
70	DS 70-1	1997	Auburn University, AL	Clay	0.92	3.00	11.70	38.39	12.79	0.30	0.98	Anderson and Townsend (1999)	N	D/B too high
71	DS 71-1	1998	Neihu, Taipei, Taiwan	Clay and sandy silt	1.20	3.94	38.70	126.97	32.25	0.30	0.98	Diagnostic Engineering Consultants, Ltd. (1998)	N	D/B too high
72	DS 72-1	1999	California	Dense sand	0.41	1.33	5.48	17.98	13.50	0.81	2.66	Chai and Hutchinson (1999)	N	D/B too high
	DS 72-2				0.41	1.33	5.48	17.98	13.50	2.44	7.99		N	D/B too high
	DS 72-3			Loose sand	0.41	1.33	5.48	17.98	13.50	0.81	2.66		N	D/B too high
	DS 72-4				0.41	1.33	5.48	17.98	13.50	2.44	7.99		N	D/B too high
73	DS 73-1	2000	Miami, FL	Sand, silt, and limestone	0.46	1.51	13.70	44.95	29.78	0.00	0.00	Frizzi and Meyer (2000)	N	D/B too high
	DS 73-2				0.46	1.51	13.70	44.95	29.78	0.00	0.00		N	D/B too high
	DS 73-3				0.46	1.51	13.70	44.95	29.78	0.00	0.00		N	D/B too high
	DS 73-4				0.46	1.51	13.70	44.95	29.78	0.00	0.00		N	D/B too high
	DS 73-5				0.46	1.51	29.00	95.14	63.04	0.00	0.00		N	D/B too high
	DS 73-6				0.46	1.51	29.00	95.14	63.04	0.00	0.00		N	D/B too high
74	DS 74-1	2000	NR	Very soft alluvial silt	1.00	3.28	24.00	78.74	24.00	0.50	1.64	Zhang, Kimura, Nakai, and Hoshikawa (2000)	N	D/B too high
75	DS 75-1	2000	Hawthorne, CA	Silty clay, sand and silt	1.98	6.50	14.63	48.00	7.38	12.19	40.00	Janoyan (2001)	Y	
76	DS 76-1	2000	University of Houston, Texas	Stiff overconsolidated clay	0.91	3.00	6.10	20.00	6.67	0.15	0.50	O'Neill, Vipulanandan, and Hassan (2000)	Y	
	DS 76-2				0.46	1.50	6.10	20.00	13.34	0.15	0.50		N	D/B too high
	DS 76-3				0.91	3.00	10.70	35.10	11.71	0.15	0.50		N	D/B too high
	DS 76-4				0.46	1.50	10.70	35.10	23.41	0.15	0.50		N	D/B too high
77	DS 77-1	2000	South Korea	Sandy silt, silty clay, and weathered rock	0.40	1.31	10.50	34.45	26.25	0.20	0.66	Jeon et al. (2000)	N	D/B too high
	DS 77-2				0.40	1.31	11.20	36.75	28.00	0.20	0.66		N	D/B too high
	DS 77-3				0.40	1.31	11.90	39.04	29.75	0.20	0.66		N	D/B too high
78	DS 78-1	2001	San Diego, CA	Clayey to silty sand	0.40	1.31	4.50	14.76	11.25	0.00	0.00	Juirnarongrit and Ashford (2001)	N	D/B too high
	DS 78-2				0.60	1.97	12.00	39.37	20.00	0.00	0.00		N	D/B too high
	DS 78-3				0.90	2.95	12.00	39.37	13.33	0.00	0.00		N	D/B too high
	DS 78-4				1.20	3.94	12.00	39.37	10.00	0.00	0.00		N	D/B too high
79	DS 79-1	2001	Hong Kong	Fill, alluvium, decomposed marble	1.50	4.92	28.00	91.86	18.67	0.75	2.46	Charles, Zhang, and Dora (2001)	N	D/B too high
80	DS 80-1	2001	Taipei, Taiwan	Silty clay with sand	1.00	3.28	37.10	121.72	37.10	0.30	0.98	GECL Engineering Consultants, Ltd. (1997)	N	D/B too high
81	DS 81-1	2001	Taipao, Chiayi, Taiwan	Silty clay, silty sand, and silt	1.50	4.92	35.00	114.83	23.33	0.50	1.64	Huang, Hsueh, O'Neill, Chern, and Chen, (2001)	N	D/B too high
	DS 81-2				1.50	4.92	35.00	114.83	23.33	0.50	1.64	Diagnostic Engineering Consultants, Ltd. (1997)	N	D/B too high

Table 2.2. Continued

Load Test (LT) #	Load Test ID	Year	Test Site	Soil Description	Shaft Diameter, B		Embedded Depth, D		D/B	Load Eccentricity, e		Reference	Use? (Y/N)	If No, why not?
					(m)	(ft)	(m)	(ft)		(m)	(ft)			
82	DS 82-1	2001	North Carolina	Sandy silt and silty clay overlying weathered rock	0.76	2.50	3.40	11.15	4.46	0.30	0.98	Cho et al. (2001)	N	Socketed in rock
	DS 82-2				0.76	2.50	4.30	14.11	5.64	0.30	0.98		N	Socketed in rock
83	DS 83-1	2002	Houston, TX	Stiff clay with sandy silt	0.76	2.49	7.60	24.93	10.00	0.30	0.98	Sarhan, O'Neill, and Hassan (2002)	N	Shafts intentionally constructed with defects
	DS 83-2				0.76	2.49	7.60	24.93	10.00	0.30	0.98		N	Shafts intentionally constructed with defects
	DS 83-3				0.76	2.49	7.60	24.93	10.00	0.30	0.98		N	Shafts intentionally constructed with defects
	DS 83-4				0.76	2.49	7.60	24.93	10.00	0.30	0.98		N	Shafts intentionally constructed with defects
	DS 83-5				0.76	2.49	7.60	24.93	10.00	0.30	0.98		N	Shafts intentionally constructed with defects
	DS 83-6				0.76	2.49	7.60	24.93	10.00	0.30	0.98		N	Shafts intentionally constructed with defects
84	DS 84-1	2002	Dulzura, CA	Decomoposed Granitics - comprised of dense to very	1.02	3.35	3.00	9.84	2.94	0.00	0.00	Bhushan and Scheyhing (2002)	N	Not enough soil information
	DS 84-2				1.27	4.17	3.00	9.84	2.36	0.00	0.00		N	Not enough soil information
85	DS 85-3	2002	La Mesa, CA	Stadium Conglomerate - comprised of cobbles, gravel,	0.81	2.66	6.00	19.68	7.41	0.00	0.00	Bhushan and Scheyhing (2002)	M	No appropriate soil type in LPile
	DS 85-4				0.81	2.66	6.00	19.68	7.41	0.00	0.00		M	No appropriate soil type in LPile
86	DS 86-5	2002	UC San Diego	Friars Formation - friable sandstone comprised of	0.61	2.00	6.00	19.68	9.84	0.00	0.00	Bhushan and Scheyhing (2002)	N	Not enough soil information
	DS 86-6				0.61	2.00	6.00	19.68	9.84	0.00	0.00		N	Not enough soil information
87	DS 87-1	2004	Opelika, AL	Fine sandy silt to silty fine sand	0.91	2.99	11.00	36.09	12.09	0.30	0.98	Mayne (2004)	N	D/B too high
	DS 87-2				0.91	2.99	11.00	36.09	12.09	0.30	0.98		N	D/B too high
	DS 87-3				0.91	2.99	11.00	36.09	12.09	0.30	0.98		N	D/B too high
	DS 87-4				0.91	2.99	11.00	36.09	12.09	0.30	0.98		N	D/B too high
88	DS 88-1	2005	Japan	Silty clay, sandy silt	1.00	3.28	24.00	78.74	24.00	0.75	2.46	Honjo, Zaika, and Pokharel (2005)	N	D/B too high
	DS 88-2				1.00	3.28	20.00	65.62	20.00	0.30	0.98		N	D/B too high
	DS 88-3				0.40	1.31	16.30	53.48	40.75	1.20	3.94		N	D/B too high
	DS 88-4				1.00	3.28	20.00	65.62	20.00	0.50	1.64		N	D/B too high
89	DS 89-1	2005	Japan	Well graded sand, sandy gravel	0.40	1.31	13.30	43.64	33.25	1.20	3.94	Honjo, Zaika, and Pokharel (2005)	N	D/B too high
	DS 89-2				1.00	3.28	19.00	62.34	19.00	1.20	3.94		N	D/B too high
	DS 89-3				0.40	1.31	13.50	44.29	33.75	0.50	1.64		N	D/B too high
90	DS 90-1	2006	Mason, WV	Sand overlying shale	2.59	8.50	20.12	66.00	7.76	9.88	32.40	Yang (2006)	N	Socketed in rock
	DS 90-2				2.59	8.50	17.31	56.80	6.68	16.18	53.10		N	Socketed in rock
91	DS 91-1	2006	Dayton, OH	Rock	1.83	6.00	5.49	18.00	3.00	0.00	0.00	Yang (2006)	N	Socketed in rock
	DS 91-2				1.83	6.00	5.49	18.00	3.00	0.00	0.00		N	Socketed in rock
92	DS 92-1	2007	Jleeb Al-Shuyoukh, Kuwait	Medium dense silty sand overlying dense to very dense sand with silt	0.30	0.98	5.00	16.40	16.67	0.00	0.00	Ismael (2010)	N	D/B too high
	DS 92-2				0.30	0.98	5.00	16.40	16.67	0.00	0.00		N	D/B too high
	DS 92-3				variable	variable	variable	variable	variable	0.00	0.00		N	D/B too high, tapered diameter
	DS 92-4				variable	variable	variable	variable	variable	0.00	0.00		N	D/B too high, tapered diameter
	DS 92-5				variable	variable	variable	variable	variable	0.00	0.00		N	D/B too high, tapered diameter
	DS 92-6				variable	variable	variable	variable	variable	0.00	0.00		N	D/B too high, tapered diameter
	DS 92-7				variable	variable	variable	variable	variable	0.00	0.00		N	D/B too high, tapered diameter
	DS 92-8				variable	variable	variable	variable	variable	0.00	0.00		N	D/B too high, tapered diameter
	DS 92-9				0.50	1.64	5.00	16.40	10.00	0.00	0.00		N	D/B too high
	DS 92-10				0.50	1.64	5.00	16.40	10.00	0.00	0.00		N	D/B too high
93	DS 93-1	2012	Ilan County, Taiwan	Gravel and cobbles with some sand and silt	4.00	13.12	12.00	39.37	3.00	0.55	1.80	Chiou, Ko, Hsu, and Tsai (2012)	N	No appropriate soil type in LPile

3 METHODOLOGY

The methodology section will discuss the large-scale load tests, the general procedures used for establishing the appropriate input parameters for each analysis method, and the approach for conducting the analysis using each method.

3.1 Experimental Criteria

As shown in the database presented in Table 2.2, 214 lateral load tests of large-scale drilled shafts were identified in the literature. The criteria for including these load tests in the database were generally very broad, and additional criteria were established to determine the suitability of including a particular load test in this investigation. It was necessary to establish criteria that allowed a balance to be achieved between only analyzing the highest quality load tests with the most complete and accurate data and analyzing a sufficient number of cases to reach meaningful conclusions. These criteria are discussed within this section.

3.1.1 Foundation Properties

At a minimum, the required foundation properties are the pile length (L), pile diameter (B), embedment depth (D), compressive strength of the concrete (f'_c), and longitudinal steel reinforcement ratio (ρ_s). Ideally, the elastic modulus, reinforcement configuration, and clear concrete cover is also desired; however, these properties were

not reported in enough cases to include them in the experimental criteria.

As previously discussed, the rigidity of the foundation is determined by the *D/B* ratio, and rigid to semi-rigid drilled shafts generally have *D/B* ratios less than 10. As such, only drilled shafts with *D/B* ratios less than 10 are included in this investigation.

3.1.2 Soil Properties

The required soil properties are a function of the soil type and the analysis method being used. The criteria for the soil properties were not formally stated, but in general, the required soil properties for each load test needed to be reported directly, or there needed to be enough information presented to estimate the required soil properties through empirical or analytical relationships. For the cases where the soil properties were reported directly, no effort was made to refine or improve these properties as determining the "best" way to estimate soil properties is outside of the scope of this investigation. Determination of soil properties is discussed further in Section 3.3.

3.1.3 Load-Deflection Curve at Ground Surface

The response of a laterally loaded drilled shaft can be compared to the predicted response for an applied lateral load in several ways. Some of these ways include comparing the lateral deflection at the ground surface, the lateral deflection profile along the shaft, and the bending moment profile along the shaft. It would be ideal to compare the lateral deflection and bending moment profiles along the shaft as these capture the most important components of the soil-structure interaction; however, establishing the lateral deflection and bending moment profiles requires that the foundations be heavily instrumented along the length of the foundation as previously discussed. Unfortunately,

there were very few load tests reported in the literature that incorporated such instrumentation that also met the other criteria discussed within this section. As such, it was decided that the comparison between the observed and predicted foundation response would be made by comparing the lateral deflection at the ground surface for an applied lateral load. Only the large-scale load tests that included these data were used in this investigation.

3.1.4 Flat Ground Surface

Several of the large-scale load tests that were reported in the literature were conducted at sites with sloped ground surfaces. Sloped ground surfaces change the state of stress within the soil during loading, and therefore, the slope introduces a directional variable into the analysis. It was decided that the load tests that were conducted at sites with sloped ground surfaces would not be included in this investigation in order to reduce the number of variables that affect the response of the foundation.

3.1.5 High Quality Construction

For this investigation, high quality drilled shafts are defined as being mostly cylindrical with a constant diameter along the length of the shaft, and having concrete that contains few, if any, air voids or impurities. As previously discussed, drilled shafts are constructed by drilling a hole in the ground, placing a rebar reinforcement cage in the hole, and filling the hole with concrete. In certain types of soils, it can be very difficult to prevent the hole from caving or sloughing. Consequently, the foundation will contain localized sections with a larger diameter, and soil impurities can potentially become trapped within the concrete. Additionally, air voids can occur as a result of using

concrete with very low slump.

The response of a laterally loaded drilled shaft is heavily influenced by the construction quality (R (Sarhan, O'Neill, & Hassan, 2002). Because there is no straightforward way to isolate and account for the effects of poor construction quality, only the large-scale lateral load tests that were performed on high quality drilled shafts, as defined in this section, will be included in this investigation.

3.1.6 Sufficient Lateral Deflection at Shaft Head

Perhaps the most challenging aspect of analyzing a laterally loaded drilled shaft is incorporating the nonlinear stress-strain behavior of the soil and concrete that develops with increasing strain. At very small lateral deflections, and thus very small strains, the soil-structure interaction problem can be modeled reasonably well using linear elastic techniques (Poulos & Davis, 1980). Early attempts to predict the response of laterally loaded drilled shafts showed that the elastic regime is quite small for real foundations, and that linear elastic models significantly under predict lateral deflection for typical working loads (Welch & Reese, 1972). As such, it was decided that only the load tests that had a minimum of 0.5 in. of lateral deflection at the ground surface would be included in this investigation.

3.1.7 Not Socketed into Rock

It is generally preferable to embed foundations into rock where possible because it is typically stronger and stiffer than soil; however, rock introduces several new variables and considerations into the analysis. Although the engineering properties of rock can typically be described by the same parameters used to describe soil, e.g., friction

angle, cohesion intercept, density, and various moduli, other characteristics of the rock are not so easy to account for, such as degree of weathering and fracturing. These characteristics can have a significant influence on the engineering properties of rock. For the purposes of this investigation, foundations that are embedded into rock, i.e., foundations that are installed in a rock socket, were not considered.

3.1.8 Single Free-Head Drilled Shaft

Drilled shafts are commonly used as a single-element foundation, but they can also be combined in groups to form larger and more robust foundations. Drilled shafts are typically combined in groups through use of a pile cap. A pile cap changes the fixity conditions of the top of the drilled shaft, as well as the state of stress that develops within the surrounding soil due to influence effects from the other drilled shafts. For this investigation, only the lateral load tests that were performed on a free-headed single drilled shaft were considered, and drilled shafts that were tested as part of a group or tested with a non-free headed condition were not considered.

3.1.9 Short Testing Period

The time required to perform the lateral load tests reported in the literature was highly variable. Some of the tests were performed by applying a steady lateral load until failure was reached, while others were performed in cycles of loading and unloading over a period of several months. Soils are generally viscoelastic materials, and the engineering properties are dependent upon the rate at which the loads are applied. For this investigation, the time required to perform the load test was not explicitly stated, but in general, the tests that were performed over extended time periods were not considered.

3.1.10 No Bell Construction

Bells are typically constructed to increase the axial capacity of the foundation, but several of the large-scale lateral load tests reported in the literature were performed on foundations that included a bell at the bottom of the foundation. The presence of the bell changes the response characteristics of the foundation and the soil, and it is not possible to model the bell using all of the analysis techniques presented in this investigation. As such, a reasonable comparison cannot be made between the methods for these types of foundations, and as such, foundations with bells at the bottom were not included in this investigation.

3.2 General Modeling Approach for Each Analysis Method

A model was constructed for each large-scale load test that met the experimental criteria using each of the previously discussed analysis methods. In general, the models for each large-scale load test were constructed to be as similar as possible in each analysis method to avoid differences in results that could be attributed to significant differences in modeling techniques. The basic model setup and general assumptions that were made for each analysis method are discussed within this section.

3.2.1 LPile Model Setup

The analyst has the ability to choose whether the foundation is modeled using linear elastic foundation stiffness or nonlinear foundation stiffness. The nonlinear foundation stiffness method can be used by either specifying the moment-curvature relationship for the foundation or by having *LPile* generate the moment-curvature relationship internally. The latter method is used in each model for this investigation,

with the exception of DS 23 as discussed later in Section 3.5.8, and is chosen by selecting "Type 3 – Computation of Moment-Curvature Relations and Nominal Moment Capacity and Pile Response using Nonlinear EI" within the software.

The subsurface profile is constructed by discretizing the continuum into sub-layers with uniform thickness. *LPile* allows the analyst to specify material properties for the top and bottom of the layer, and the program obtains property values for discrete points within the layer by linear interpolation; however, several test cases conducted by the author showed that the difference between specifying separate values for the top and bottom of each layer and using the average of these separate values to represent the entire layer was negligible for the cases considered. It should be noted that it is possible that the differences would not be negligible if the layers are very thick, particularly near the surface, but this phenomenon was not studied in detail in this investigation. In order to avoid establishing multiple subsurface profiles with both linearly varying and constant values, and because the difference between using linearly varying and average values appears to be negligible, it was decided to use one subsurface profile with average values for each sub-layer. The same subsurface profile was used for each analysis method used in this investigation, with the exception that some of the properties were not applicable to all methods.

3.2.2 DFSAP Model Setup

It is fairly straightforward to set up the *DFSAP* models because there are very few options available to the analyst. The analyst must choose the type of foundation, the foundation head fixity condition of free or fixed, and whether the foundation will be modeled using a linear or a nonlinear bending stiffness. For this investigation, all models

were constructed using the nonlinear bending stiffness option. Both longitudinal and transverse reinforcement are entered as reinforcement ratios instead of explicitly defining the number, type, and spacing of the bars; however, the clear concrete cover must still be specified. Additionally, the foundation dimensions, unconfined compressive strength of the concrete, and yield strength of the rebar must be specified.

As with *LPile*, the subsurface is discretized into sub-layers with constant thickness. The current version of *DFSAP* allows the analysis to discretize the subsurface into a maximum of 10 sub-layers, and each layer is identified as *sand*, *clay*, *c-ϕ soil*, or *rock*. Material properties are specified for each soil layer, and the location of the groundwater table, slope of the ground surface, and additional surcharge at the ground surface are entered into the model. It should be noted that the material properties for each sub-layer are constant with depth, with the exception of undrained shear strength. The undrained shear strength for each sub-layer can be specified at the top and bottom of the sub-layer, which creates an undrained shear strength profile that varies linearly with depth between the two specified values. For this investigation, the undrained shear strength is assumed constant within each sub-layer for reasons previously discussed in Section 3.2.1.

For this investigation, each input parameter for each analysis method was estimated manually, even when these values would have been estimated internally by the program if they were not provided. This was done to promote consistency in the soil properties across each analysis method. The only input property that was not computed manually was ε_{50} for granular soils in *DFSAP*. As discussed previously in Section 2.5, *DFSAP* uses ε_{50} for both cohesive and granular soils, whereas *LPile* only uses ε_{50} for cohesive soils. The *DFSAP* literature recommends using values of ε_{50} obtained from

laboratory testing at a confining stress of 0.425 tsf; however, the program will estimate this value if it is not provided. The *DFSAP* software provides a chart for estimating ε_{50} for granular soils as a function of the uniformity coefficient, C_u, and the void ratio, e, of the soil. This chart was originally presented by Norris (1986) and is shown in Figure 3.1. Unfortunately, the author was not able find any documentation in the *DFSAP* literature that states whether this is the chart that is used by *DFSAP* to estimate $\varepsilon 50$ internally, nor does it describe how e or C_u are estimated from the required input properties of γ' and ϕ'. As such, the value of ε_{50} for granular soils was determined internally by *DFSAP* for each model as required.

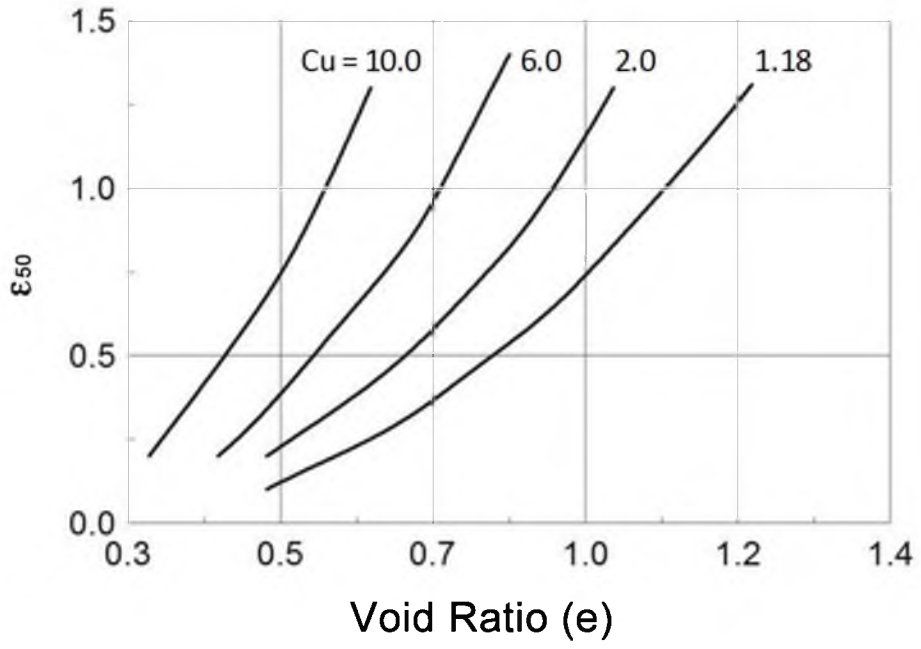

Figure 3.1. Estimation of e_{50} from e and C_u (Norris, 1986)

3.2.3 MFAD Model Setup

The *MFAD* model is the most straightforward of all of the analysis methods used in this investigation because it requires the fewest inputs and has the fewest options available to the analyst. The interface is different from *LPile* and *DFSAP* in that the analyst defines all of the foundations that will be analyzed for a particular project, the representative subsurface profiles that will be used for the project, the load cases that will be applied to each foundation, and the performance criteria in terms of allowable deflection and rotation of the top of the foundation and the allowable non-recoverable deflection and rotation of the top of the foundation. This information is stored in a database and the analyst creates cases of foundation, subsurface profile, loads, and performance criteria. For each particular case, the analyst specifies the depth of embedment, and the program then evaluates the worst-case scenario from the load combinations of foundation capacity, total displacement and rotation of the top of the foundation and non-recoverable displacement and rotation of the top of the foundation. The analyst can then adjust the depth of embedment to optimize the foundation length for that particular case.

For this investigation, a separate load case was created for each load-deflection pair of data reported for the large-scale load test. Since only one load combination was applied for each load case, the program will calculate the total displacement and rotation at the top of the foundation for that particular load combination. This was done for each load combination for each large-scale load test.

The soil profile was created in the same way as *DFSAP* and *LPile* in that the subsurface was discretized into a maximum of 10 sub-layers, the layer type was chosen for each layer, and the material properties were entered for each sub-layer. The depth to

groundwater table was also specified. If the depth to groundwater was not reported in the literature, the depth was entered as some depth below the deepest sub-layer; otherwise, the program assumes the groundwater table is at the ground surface.

The performance criteria was specified as very large values and the actual depth of embedment was specified since the objective was to obtain the total deflection of the top of the foundation for each load case, and not to optimize a foundation design.

3.3 Determination of Soil and Foundation Properties

The required properties that were used in each model were either reported in the literature associated with each load test or were estimated using empirical or analytical relationships. It is understood that the required properties have a major influence on the results of each analysis method and that considerable effort should be made towards determining the most correct soil properties for input into the models. Ideally, the upper bound, lower bound, and best-estimate values would be estimated for each soil property using several techniques and all available laboratory and field test data; however, the thrust of this investigation is focused on comparing the results of different analysis methods, and a lesser emphasis was placed on the absolute accuracy of each method. As such, a reasonable effort was made to determine the best-estimate value for each soil property and to maintain consistency among the stress-strain-strength properties for each analysis method.

The required foundation properties were specified in most of the load tests used for this investigation, as this was a requirement of the experimental design discussed previously. In some instances, the required properties were not specified explicitly, but they could be obtained using equations specified in ACI 318 or by making reasonable

assumptions. Assumed values were only used if it could be shown that the results were not significantly different if a reasonable range of values was used; otherwise, the load test was classified as not meeting the experimental criteria.

3.3.1 Conversion of CPT Tip Resistance (q_c) to SPT N

Several correlations have been developed to estimate soil properties from SPT N values or tip resistance, q_c, from the cone penetration (CPT) test. Therefore, it is convenient to be able to convert from q_c to SPT N, or vice versa, in the absence of data obtained from in-situ testing. Several researchers have developed correlations from numerous data sets over the years, and Kulhawy and Mayne (1990) have conveniently synthesized these data sets into one chart. Additionally, they performed a regression analysis on the data, and developed an equation for SPT N as a function of q_c and the mean particle size, D_{50}. This compiled data set, the curve resulting from the regression analysis, and the equation of the curve are shown in Figure 3.2

It should be noted that there is considerable scatter in the data shown in Figure 3.2, particularly as D_{50} increases. Conversion from one parameter to the other can potentially introduce error and uncertainty into the converted parameter due to the scatter in the correlation. Additional error and uncertainty will be introduced into the analysis if the converted values are used in subsequent correlations to develop model input parameters. As such, conversion from q_c to SPT N, or vice versa, was only performed when it was difficult or impossible to obtain the requisite model input parameters by means of another method.

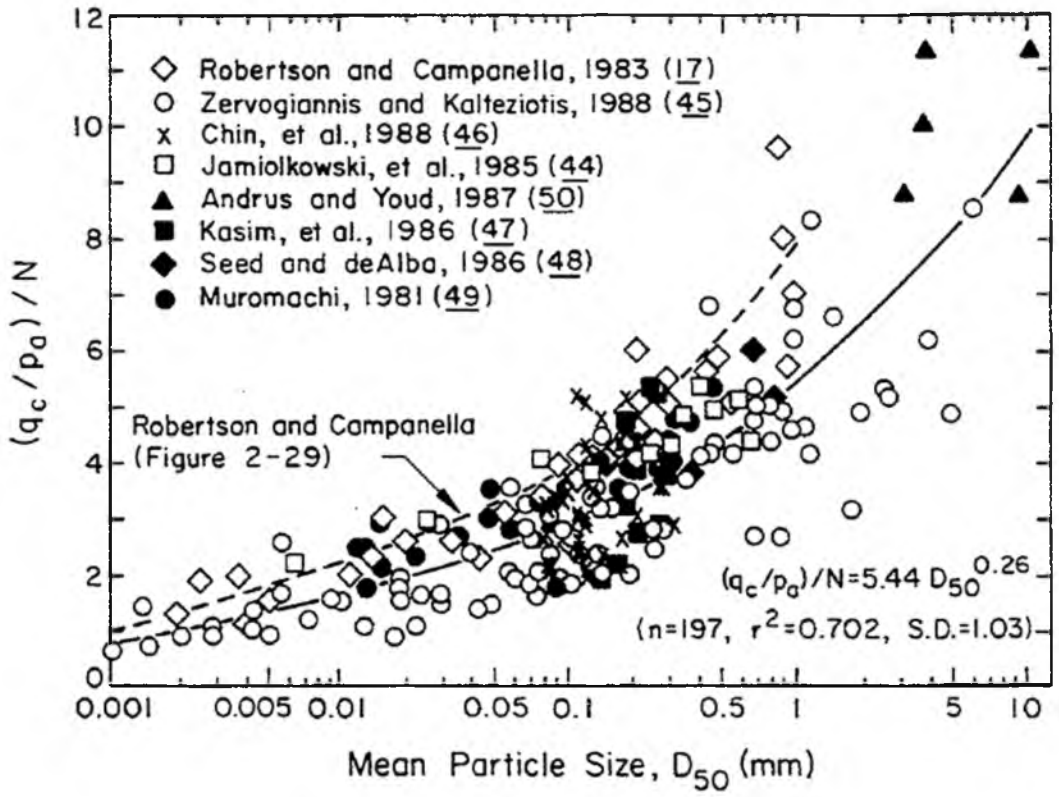

Figure 3.2 Estimation of q_c/N from D_{50} (Kulhawy & Mayne, 1990)

3.3.2 Total Unit Weight, γ

In general, the total unit weight can be estimated from the soil type and description provided in the description of the load test. The total unit weight can be estimated using typical unit weights reported by Kulhawy and Mayne (1990) shown in Table 3.1.

3.3.3 Soil Properties for Cohesionless Soils

The additional soil properties that are required for cohesionless soils include the total angle of internal friction (ϕ) and the horizontal coefficient of subgrade reaction (k). The methods that were used to estimate these properties are discussed within this section.

Table 3.1. Typical unit weight of several types of soil (Kulhawy & Mayne, 1990)

Soil Type	Approximate Particle Size (mm)			Uniformity Coefficient	Void Ratio		Normalized Unit Weight			
							Dry, γ_{dry}/γ_w		Saturated, γ_{sat}/γ_w	
	D_{max}	D_{min}	D_{10}	D_{60}/D_{10}	e_{max}	e_{min}	Min.	Max.	Min.	Max.
Uniform granular soil										
Equal spheres (theoretical)	-	-	-	1.0	0.92	0.35	-	-	-	-
Standard Ottawa sand	0.84	0.59	0.67	1.1	0.80	0.50	1.47	1.76	1.49	2.10
Clean, uniform sand	-	-	-	1.2 to 2.0	1.00	0.40	1.33	1.89	1.35	2.18
Uniform, inorganic silt	0.05	0.005	0.012	1.2 to 2.0	1.10	0.40	1.28	1.89	1.30	2.18
Well-graded granular soil										
Silty sand	2.0	0.005	0.02	5 to 10	0.90	0.30	1.39	2.04	1.41	2.28
Clean, fine to coarse sand	2.0	0.05	0.09	4 to 6	0.95	0.20	1.36	2.21	1.38	2.37
Micaceous sand	-	-	-	-	1.20	0.40	1.22	1.92	1.23	2.21
Silty sand and gravel	100	0.005	0.02	15 to 300	0.85	0.14	1.43	2.34	1.44	2.48
Silty or sandy clay	2.0	0.001	0.003	10 to 30	1.80	0.25	0.96	2.16	1.60	2.36
Gap-graded silty clay w. gravel or larger	250	0.001	-	-	1.00	0.20	1.35	2.24	1.84	2.42
Well-graded gravel, sand, silt, and clay	250	0.001	0.002	25 to 1000	0.70	0.13	1.60	2.37	2.00	2.50
Clay (30 to 50% < 2μ size)	0.05	0.5μ	0.001	-	2.40	0.50	0.80	1.79	1.51	2.13
Colloidal clay (over 50% < 2μ size)	0.01	10Å	-	-	12.00	0.60	0.21	1.70	1.14	2.05
Organic silt	-	-	-	-	3.00	0.55	0.64	1.76	1.39	2.10
Organic clay (30 to 50% < 2μ size)	-	-	-	-	4.40	0.70	0.48	1.60	1.30	2.00

Note: γ_w = 62.4 lb/ft^3 = 1 gm/cm^3 = 0.983 t/m^3 = 9.80 kN/m^3 (at STP conditions).

It should be noted that this is not meant to be an exhaustive discussion on the methods available to estimate these properties, but instead is meant to present the methods that were used to estimate the soil properties for this investigation.

3.3.3.1 Angle of Internal Friction, ϕ

The total angle of internal friction can be estimated from SPT blowcounts (N) using the method proposed by Peck, Hanson, and Thornburn (1974) or Meyerhof (1956). A plot of these two methods is shown in Figure 3.3.

The angle of internal friction is a function of overburden stress (Kulhawy & Mayne, 1990), which is not accounted for in these two methods. An empirical correlation was presented by Schmertmann (1975) to account for the overburden stress, which is shown in Equation (3.1). It should be noted that Kulhawy and Mayne (1990) recommend not using this equation at depths less than 1 to 2 m.

$$\phi = tan^{-1}\left[\left(\frac{N}{12.2 + 20.3\frac{\sigma_{v0}}{p_a}}\right)^{0.34}\right] \quad \textbf{(3.1)}$$

where:

ϕ = total angle of internal friction

N = uncorrected blowcounts from SPT test

σ_{v0} = overburden stress where N was measured

p_a = atmospheric pressure in units of σ_{v0}

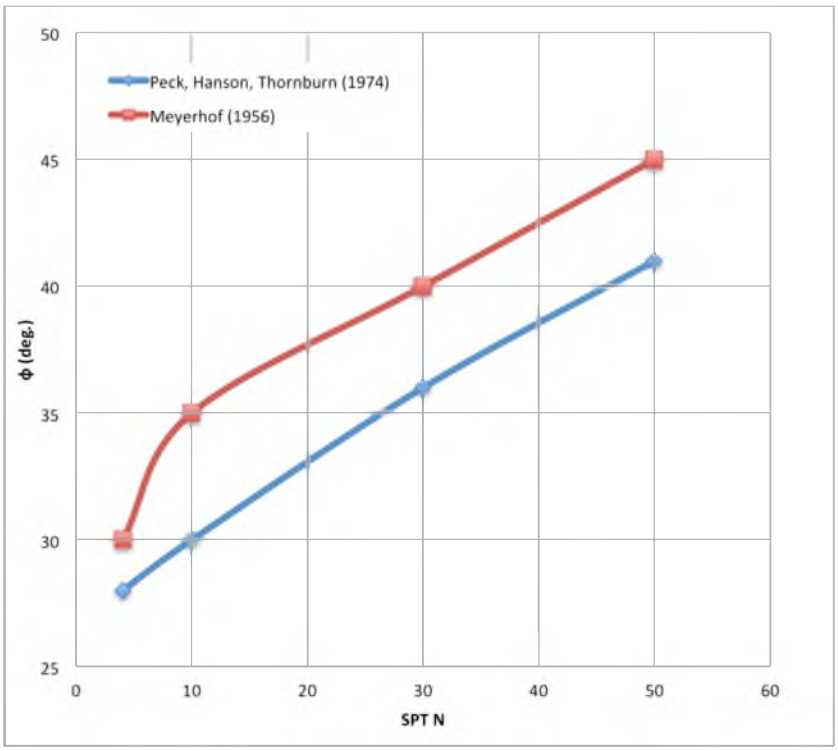

Figure 3.3. Plot of ϕ vs. N

The angle of internal friction, ϕ, can be estimated using the cone tip resistance, q_c, from a CPT sounding. One such method was proposed by Robertson and Campanella (1983), as shown in Figure 3.4. It is also possible to estimate ϕ using the regression performed by Kulhawy and Mayne (1990) shown in Figure 3.5. Additionally, ϕ can be estimated from q_c using the method proposed by Meyerhof (1956) shown in Figure 3.6. Unfortunately, this method does not account for the overburden stress. Just as the overburden stress affects the blowcounts for the SPT test, the overburden stress affects q_c for the CPT test (Kulhawy & Mayne, 1990). As such, the estimated angle of internal friction is dependent upon the overburden stress, and the values obtained using the Meyerhof (1956) method will not be given as much weight in estimating the appropriate design value.

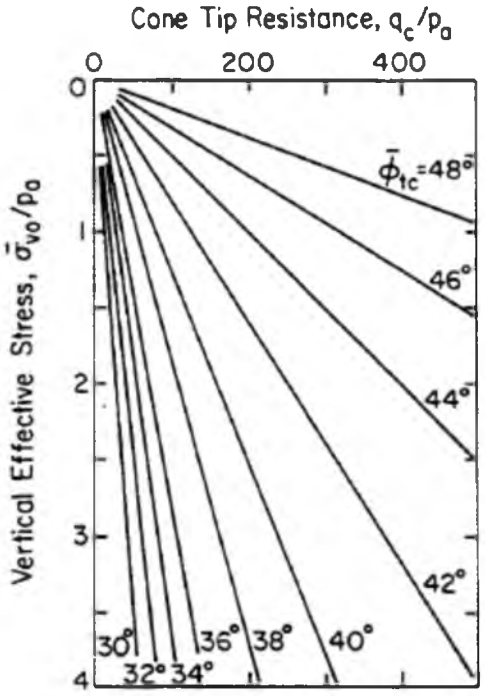

Figure 3.4. Estimation of friction angle from q_c and σ_v (Robertson & Campanella, 1983)

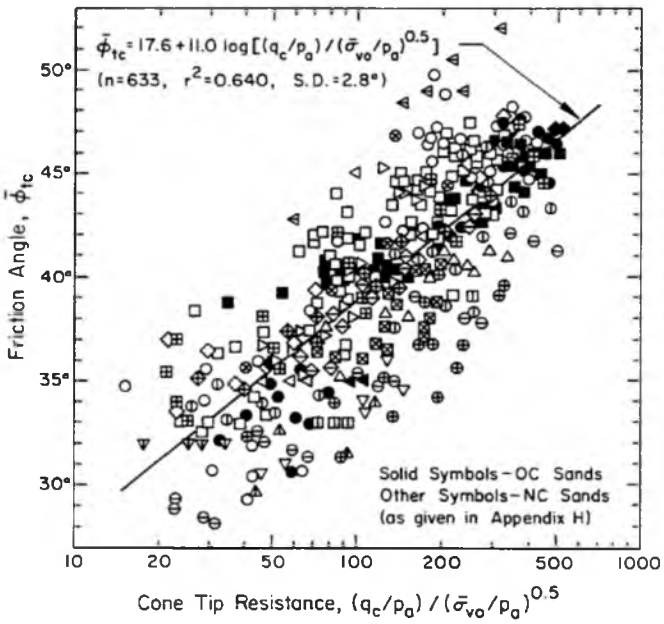

Figure 3.5. Angle of internal friction as a function of normalized q_c (Kulhawy & Mayne, 1990)

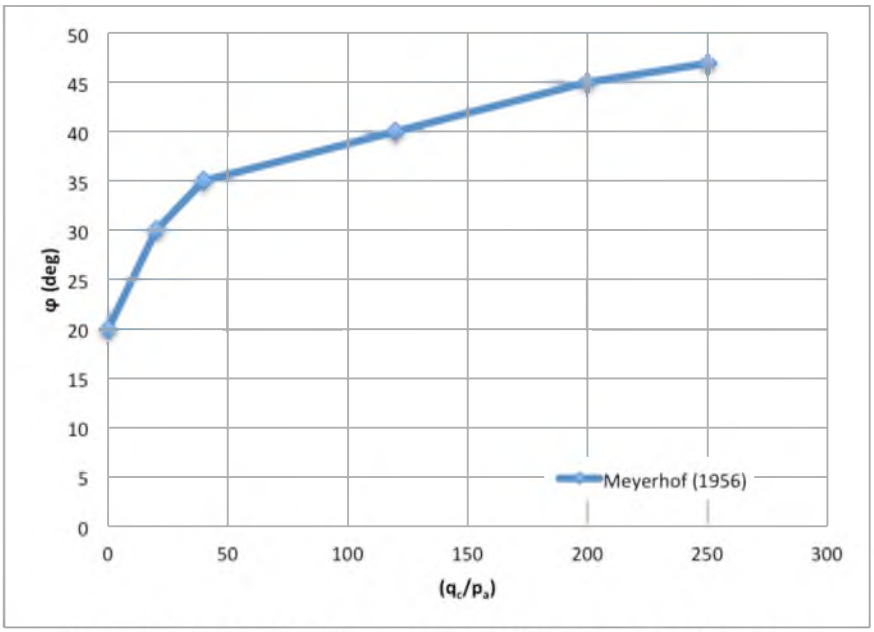

Figure 3.6. Angle of internal friction as a function of q_c (Meyerhof, 1956)

All three of these methods were used to estimate the friction angle when CPT data were provided. SPT blowcounts were provided, with the exception of Equation (3.1) at depths shallower than 6 ft. Engineering judgment was used to estimate the design friction angle by analyzing the results of these methods and any other information that was available that might affect the friction angle.

3.3.3.2 Horizontal Coefficient of Subgrade Reaction, *k*

The horizontal coefficient of subgrade reaction (*k*) is arguably the most difficult parameter to estimate because its value depends on several variables associated with both the soil and the foundation. Several researchers have proposed different methods, but most of these methods involve parameters that were not available in all of the large-scale load tests used for this investigation. As such, a simple method that only considers relative density has been used. This method was first proposed by Terzaghi (1955) but

was later refined by Reese, Cox, and Koop (1974) because the values presented by Terzaghi (1955) were deemed too conservative. The values presented by Reese, Cox, and Koop (1974) were further refined by the American Petroleum Institute (API, 1993), and are shown in Figure 3.7. Note that k in Figure 3.7 is presented as a function of either D_R or ϕ. Estimation of ϕ has already been discussed in Section 0, and D_R can be estimated using Figure 3.8 from Holtz and Gibbs (1979). For this investigation, k for cohesionless soils was estimated using both ϕ and D_R in Figure 3.7.

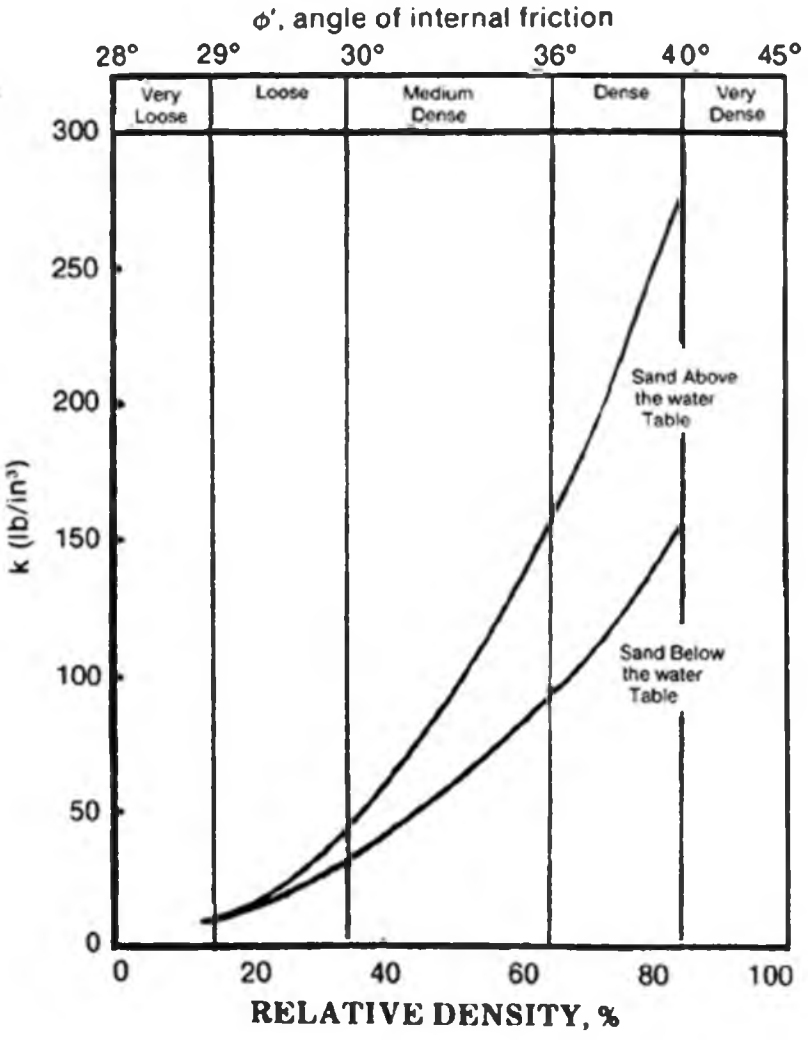

Figure 3.7 Plot of k vs. relative density and ϕ

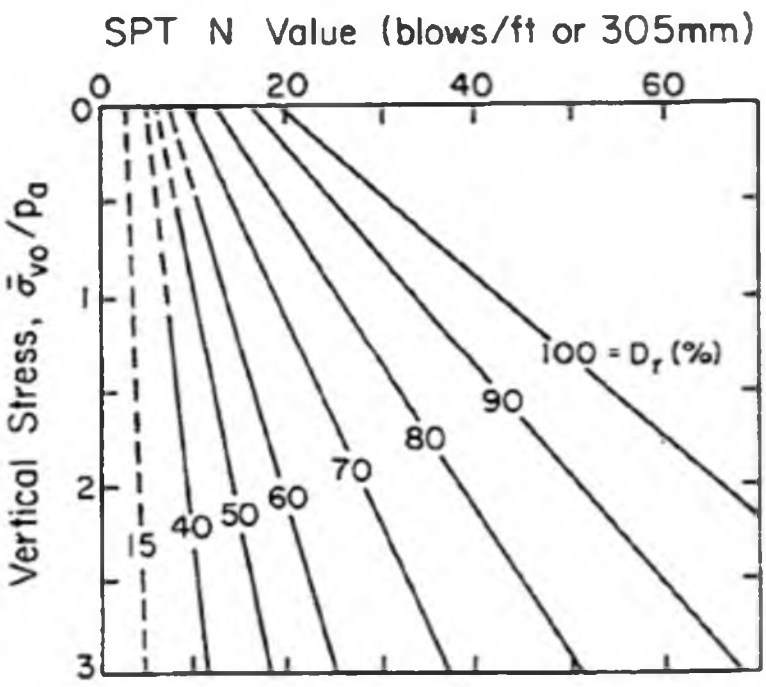

Figure 3.8. Plot of relative density as a function of vertical stress and SPT blowcounts (Holtz & Gibbs, 1979)

3.3.3.3 Modulus of Deformation, E_P

As discussed in Section 2.6, the modulus of deformation in the *MFAD* model is defined as being equivalent to the pressuremeter modulus, E_{PMT} (Davidson, Cass, Khilji, & McQuade, 1982). Davidson (1982) presented a correlation for E_P as a function of SPT N as shown in Figure 3.9. This method was used during development of the *MFAD* model.

Callanan and Kulhawy (1980) presented correlations of E_{ds} as a function of SPT N, as shown in Figure 3.10, which also includes the correlations developed by Schmertmann (1970) shown in Figure 3.9. It can be seen in Figure 3.10 that Schmertmann's correlations are for submerged sands, and that these correlations yield lower values of E_d for all values of SPT N. These lower values can, at least partially, be attributed to the fact that submerged sands are generally less stiff than nonsubmerged

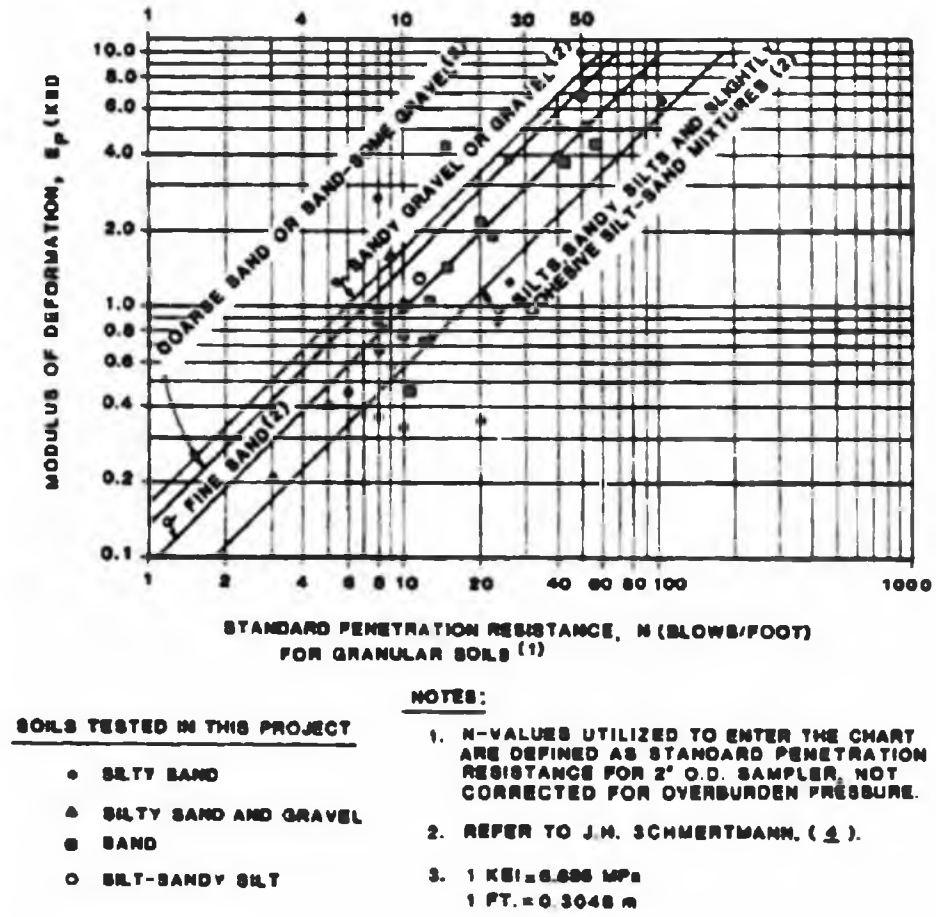

Figure 3.9 Estimation of E_P from SPT N for cohesionless soils (Davidson, Cass, Khilji, & McQuade, 1982)

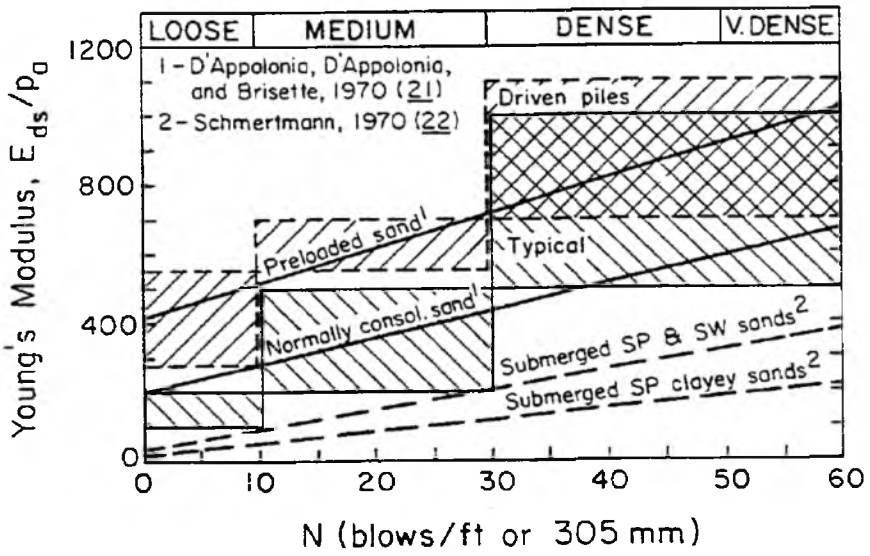

Figure 3.10 Estimation of E_d from SPT N for sands

sands when other contributing factors are equal. It is not clear from the literature whether the other correlations shown in this figure are for submerged or nonsubmerged sands; however, for this investigation, it is assumed that they are for nonsubmerged sands, and values of E_P estimated using Schmertmann's method will be less heavily weighted for nonsubmerged sands.

The modulus of deformation as a function of SPT N was also estimated by Ohya et al. (1982) as shown Figure 3.11. Kulhawy and Mayne (1990) made the observation that there is considerable scatter in the data, and that more than an order of magnitude variation is possible when using this figure to predict E_{PMT} from SPT N values.

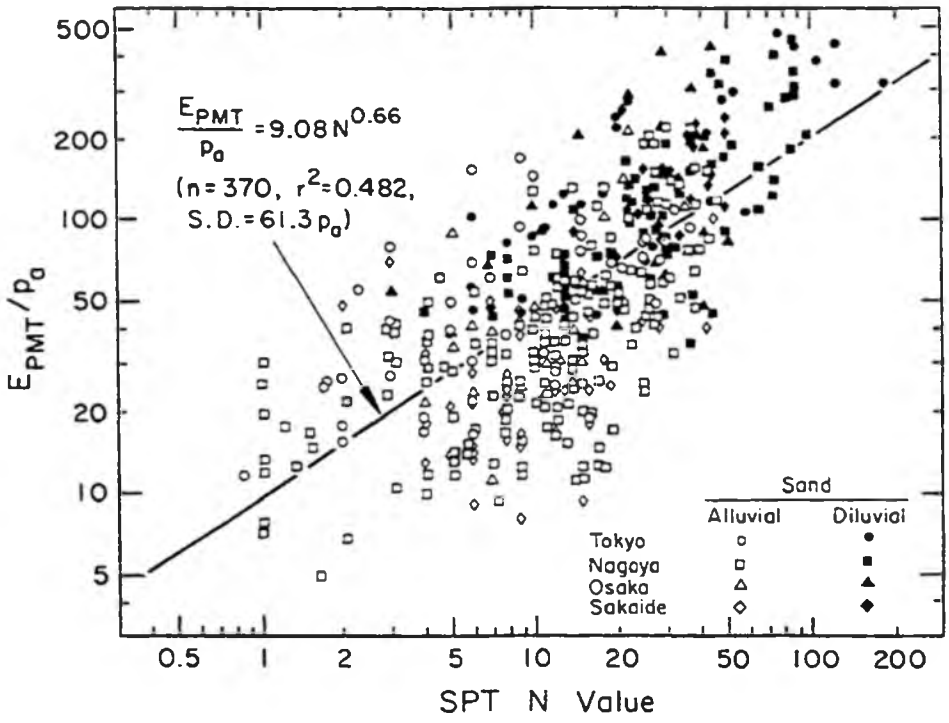

Figure 3.11 Estimation of E_{PMT} from SPT N for granular soils Ohya et al. (1982)

3.3.4 Soil Properties for Cohesive Soils

The required soil properties for cohesive soils include the total unit weight (γ), the undrained shear strength (s_u), the strain at one half of the maximum stress on a laboratory stress-strain curve (ε_{50}), and the horizontal coefficient of subgrade reaction (k).

3.3.4.1 Undrained Shear Strength, s_u

The undrained shear strength is typically computed as half of the deviator stress from an unconfined compression test or from triaxial testing. It can also be estimated from the tip resistance (q_c) of the CPT sounding using the following equation:

$$q_c = N_k s_u + \sigma_{vo} \tag{3.2}$$

where:

q_c = cone tip resistance from CPT sounding

N_k = CPT cone factor

σ_{vo} = vertical overburden stress

s_u = undrained shear strength

The value of N_k is influenced by several factors, such as the overconsolidation ratio (OCR) of the soil, clay fraction, and the actual drainage conditions that exist; however, Salgado (2008) suggests that a range of 10 to 12 is appropriate for most situations. As such, an N_k value of 11 will be used for this investigation.

3.3.4.2 Strain at 50% of Maximum Deviator Stress, ε_{50}

The strain at one half of the maximum stress on a laboratory stress-strain curve, or 50% of the maximum deviator stress, can be estimated from the undrained shear strength values using Figure 3.12. Linear interpolation was used to estimate ε_{50} from intermediate values of s_u/p_a.

3.3.4.3 Horizontal Coefficient of Subgrade Reaction, k

The horizontal coefficient of subgrade reaction, k, can be estimated from the undrained shear strength values shown in Table 3.2. Linear interpolation was used to find k from intermediate values of s_u.

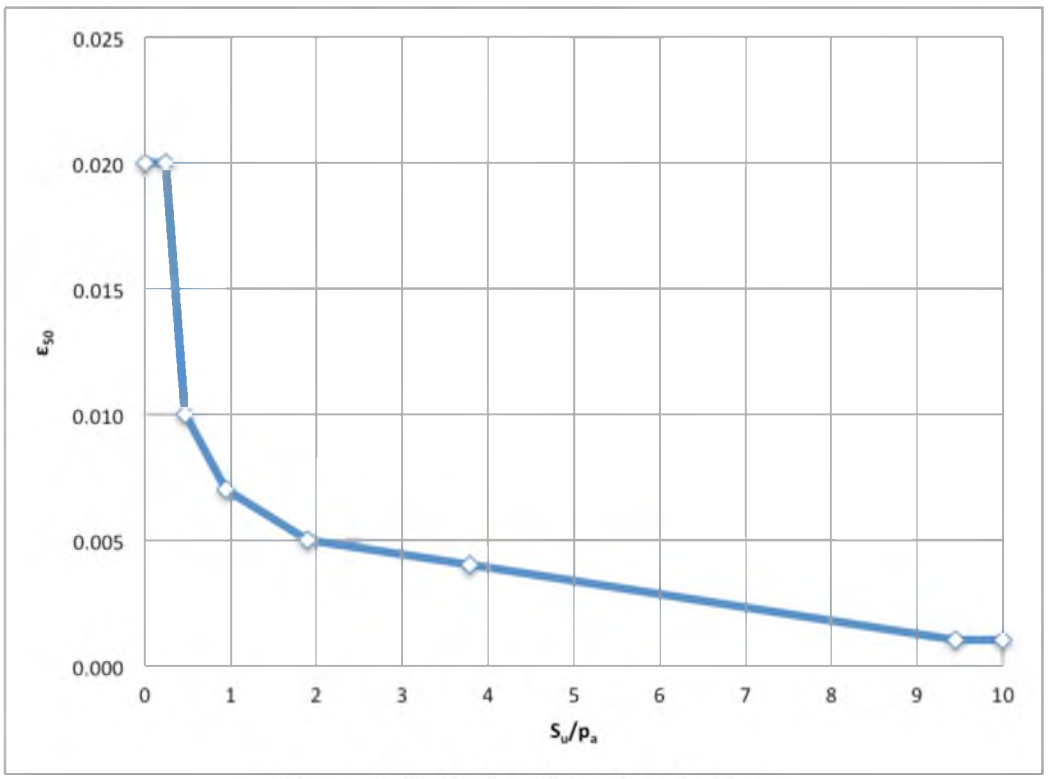

Figure 3.12. Estimation of ε_{50} from s_u (Isenhower & Wang, 2010)

Table 3.2. Estimation of k from s_u (Isenhower & Wang, 2010)

	Average Undrained Shear Strength*		
	50-100 kPa (3-15 psi)	100-200 kPa (15-30 psi)	300-400 kPa (40-60 psi)
k_s (static)	135 MN/m^3 (500 pci)	270 MN/m^3 (1,000 pci)	540 MN/m^3 (2,000 pci)
k_c (cyclic)	55 MN/m^3 (200 pci)	110 MN/m^3 (400 pci)	540 MN/m^3 (2,000 pci)

*The average shear strength should be computed as the average of shear strength of the soil from the ground surface to a depth of 5 pile diameters. It should be defined as one-half the maximum principal stress difference in an unconsolidated-undrained triaxial test.

3.3.4.4 Modulus of Deformation, E_P

As discussed in Section 2.6, the modulus of deformation (E_P) in the *MFAD* model is defined as being equivalent to the pressuremeter modulus, E_{PMT} (Davidson, Cass, Khilji, & McQuade, 1982), which is roughly equivalent to the undrained modulus (E_{US}) for cohesive soils (Kulhawy & Mayne, 1990). Davidson (1982) presented a correlation for E_P as a function of soil consistency, unconfined compressive strength (q_u), and SPT N as shown in Figure 3.13. This method was used during development of the *MFAD* model.

A similar correlation for E_P as a function of SPT N was developed by Ohya et al. (1982), and is shown in Figure 3.14. As with Figure 3.11, Kulhawy and Mayne (1990) made the observation that there is considerable scatter in the data, and that more than an order of magnitude variation is possible when using this figure to predict E_{PMT} from SPT N values.

Poulos and Davis (1980) back-calculated E_{US} from large-scale load tests of drilled shafts and driven piles in compression, and developed the correlation between E_{US} and s_u shown in Figure 3.15.

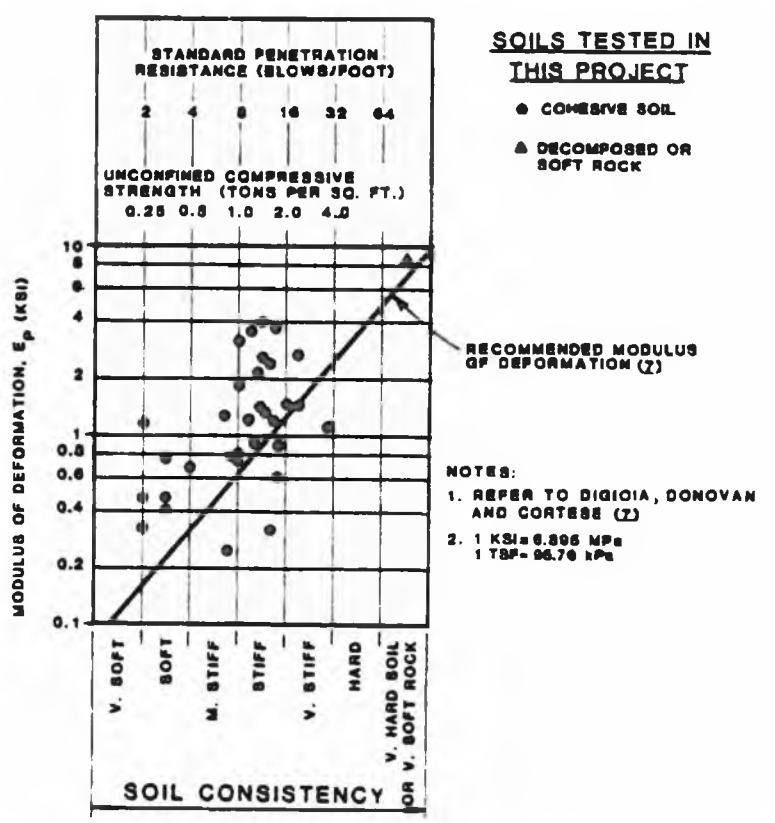

Figure 3.13 E_P as a function of soil consistency, q_u, and SPT N for cohesive soils (Davidson, Cass, Khilji, & McQuade, 1982)

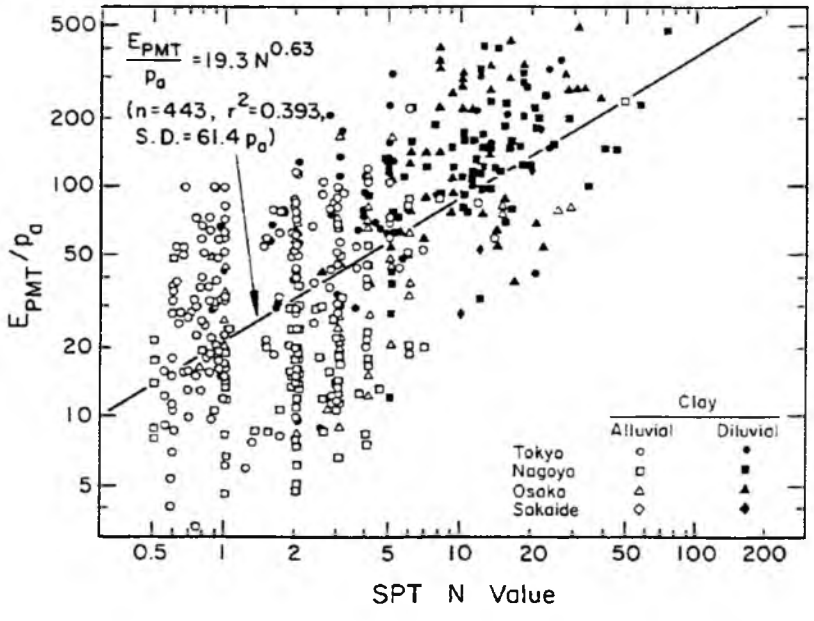

Figure 3.14. Estimation of E_{PMT} from SPT N values Ohya et al. (1982)

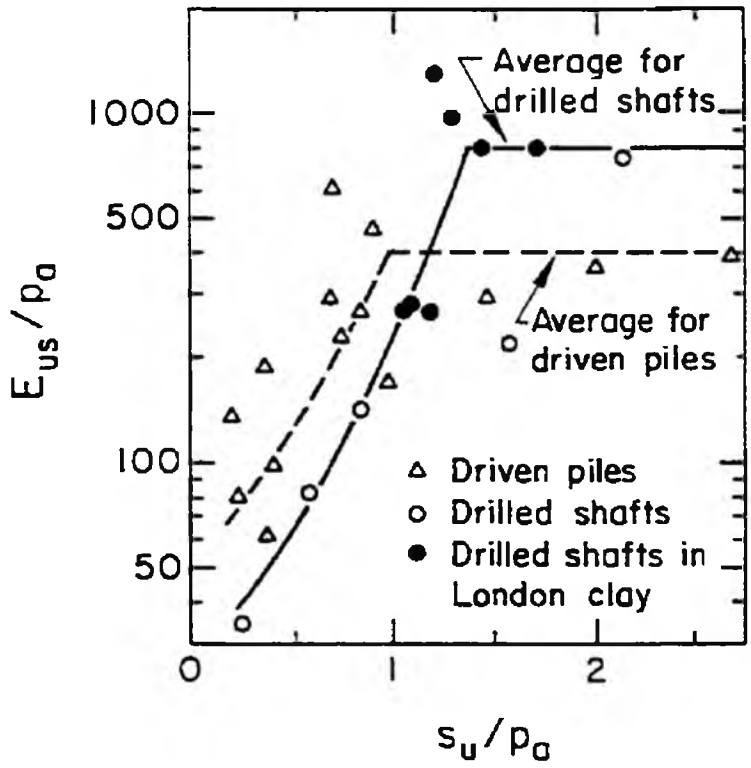

Figure 3.15. Estimation of E_{US} from s_u (Poulos & Davis, 1980)

For this investigation, E_P was estimated from the three methods discussed in this section. For load tests where s_u and ε_{50} are provided, E_P was calculated as s_u/ε_{50} to maintain compatibility among analysis methods.

3.4 Foundation Properties

It was assumed that the minimum amount of transverse steel reinforcement, as prescribed by ACI 318-11, was used in cases where it was not reported. Generally, the transverse steel reinforcement ratio had little influence on the behavior of the foundations, as its primary purpose is to increase the shear strength of the foundation and provide confinement for the concrete. The ACI 318-11 minimum transverse steel

reinforcement for a cylindrical concrete column is calculated as

$$A_{v,min} = max\left(0.75\sqrt{f'_c}\frac{b_w s}{f_{yt}}, \frac{50 b_w s}{f_{yt}}\right) \quad \textbf{(3.3)}$$

where:

$A_{v,min}$ = minimum area of transverse steel

f'_c = compressive strength of concrete

b_w = diameter of concrete column

f_{yt} = yield strength of transverse reinforcement

s = center-to-center spacing of transverse reinforcement

If the transverse reinforcement steel is specified, e.g., a #3 bar, then Equation (3.3) can be solved for s. The transverse steel reinforcement ratio can be calculated based on the area and spacing of the reinforcement.

The modulus of elasticity of the concrete can be estimated from the unconfined compressive strength of the concrete and the following equation from ACI 318-11:

$$E = 57{,}000\sqrt{f'_c} \quad \textbf{(3.4)}$$

where:

E = modulus of elasticity of concrete (psi)

f'_c = unconfined compressive strength of concrete (psi)

The rupture strength of concrete, f_r, can be estimated from ACI 318-11 and the unconfined compressive strength of the concrete as

$$f_r = 7.5\sqrt{f'_c} \tag{3.5}$$

where:

f_r = rupture strength of concrete (psi)

f'_c = unconfined compressive strength of concrete (psi)

3.5 Full-Scale Load Test Details

The details of the large-scale load tests that met the experimental criteria discussed in Section 3.1 are discussed within this section. For the sake of brevity, each load test will simply be referred to as "DS" followed by the test number and the foundation number as shown in Table 2.2.

3.5.1 Load Test 11 in Ontario, Canada

The results of a large-scale lateral load test program were presented by Adams and Radhakrishna (1973). The load tests were conducted at two test sites located in London, Ontario, Canada. The soils at the first site primarily consisted of loose silty sand and dense fine-to-medium grained sand. The soils at the second site primarily consisted of dense silty sand and glacial till, which is described as dense clayey silt with coarse sand and gravel. Two test foundations were constructed at each site with diameters of 2 and 4 ft and embedment depths of 20 ft. The *D/B* ratio for these foundations was 6.7 and 4, respectively. The only foundation from this load test program that met the experimental criteria was DS 11-1, which was constructed at the first site.

3.5.1.1 Soil Profile and Properties

The field investigation that was performed to establish the engineering properties of the soils at the site was not discussed in the paper presented by Adams and Radhakrishna (1973). They did mention that they performed pressuremeter tests at each site in order to obtain design values of the horizontal coefficient of subgrade reaction, but they did not provide any further information about the tests or the testing procedures. A generalized subsurface profile is shown in Figure 3.16, which also shows that standard penetration testing (SPT) was performed at the site.

The information presented in Figure 3.16 was used in conjunction with the methods outlined in Section 3.3.3 to estimate the values of the required soil properties for each analysis method. These values are presented in Table 3.3. It can be seen in Table 3.3 that there are multiple values for some of the soil parameters. The design values, which are shown in Table 3.4, were established from the range of estimated values for each parameter.

It should be noted that the design value of k was increased slightly for each sub-layer despite the fact that these values were given. This was done for two reasons: 1) The reload value of k was provided in Figure 3.16, but it is unlikely that the test was performed at "reload" conditions, and 2) the estimated values of k from D_R and ϕ were generally much higher as shown in Table 3.3. As such, it was decided that the most realistic value of k was somewhere between the "initial" and "reload" values.

The discretization of sub-layers and the design values for each required soil property for *LPile*, *DFSAP*, and *MFAD* are shown in Table 3.5, Table 3.6, and Table 3.7, respectively.

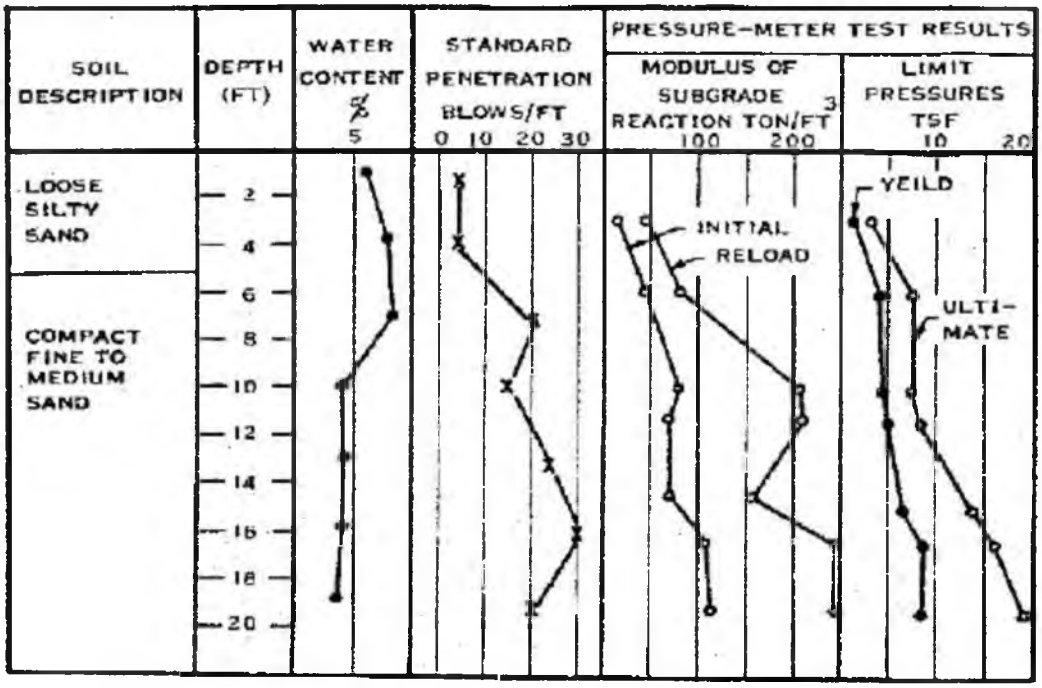

Figure 3.16. Generalized subsurface conditions for Load Test 11

Table 3.3. Estimation of required soil properties for Load Test 11

Layer Depth		N [1]	γ [2]	σ_{v0}/P_a	ϕ [3]	ϕ [4]	ϕ [5]	D_R [6]	k [7]	k [8]	k [1]
Top (ft)	Bottom (ft)		(lb/ft^3)		(deg)	(deg)	(deg)	(%)	(pci)	(pci)	(pci)
0.0	5.0	4	110	0.13	-	28.0	29.8	35	40	45	45
5.0	8.0	18	120	0.37	-	32.5	38.3	82	265	140	55
8.0	12.0	15	120	0.57	40.6	31.6	37.3	71	190	160	65
12.0	16.0	22	120	0.79	42.5	33.7	39.4	80	250	230	90
16.0	18.0	30	120	0.96	44.4	36.0	41.2	86	285	290	130
18.0	21.0	20	120	1.11	39.7	33.1	38.9	71	190	195	130

Notes

(1) From reported test data

(2) From Kulhawy and Mayne (1990)

(3) From Schmertmann (1975)

(4) From Peck, Hanson, and Thornburn (1974)

(5) From Meyerhoff (1956)

(6) From Holtz and Gibbs (1979)

(7) From API (1993) using D_R

(8) From API (1993) using ϕ

Table 3.4. Design value of soil properties for Load Test 11

Layer Depth		γ	γ'	ϕ	k	E_p
Top (ft)	Bottom (ft)	(pcf)	(pcf)	(deg)	(pci)	(ksi)
0.0	5.0	110	110	30.0	45	0.9
5.0	8.0	120	120	35.0	70	2.2
8.0	12.0	120	120	36.0	85	2.0
12.0	16.0	120	120	38.0	125	2.4
16.0	18.0	120	120	41.0	150	3.0
18.0	21.0	120	120	37.0	140	2.1

Table 3.5. LPile sub-layer properties input for DS 11-1

	Layer Depth							
LPile Soil Type	Top (ft)	Bottom (ft)	γ (pcf)	γ' (pcf)	φ (deg)	S_u (psf)	ε_{50}	k (pci)
Sand	0.0	5.0	110	110	30.0	-	-	45
Sand	5.0	8.0	120	120	35.0	-	-	70
Sand	8.0	12.0	120	120	36.0	-	-	85
Sand	12.0	16.0	120	120	38.0	-	-	125
Sand	16.0	18.0	120	120	41.0	-	-	150
Sand	18.0	21.0	120	120	37.0	-	-	140

Table 3.6. DFSAP sub-layer properties input for DS 11-1

DFSAP Soil Type	Layer Thickness (ft)	γ' (pcf)	φ' (deg)	S_u (psf)	ε_{50}
Sand	5.0	110	30.0	-	-
Sand	3.0	120	35.0	-	-
Sand	4.0	120	36.0	-	-
Sand	4.0	120	38.0	-	-
Sand	2.0	120	41.0	-	-
Sand	3.0	120	37.0	-	-

Table 3.7. MFAD sub-layer properties input for DS 11-1

MFAD Layer Type	Depth to Bottom of Layer (ft)	γ (pcf)	φ (deg)	S_u (ksf)	E_p (ksi)
Soil	5.0	110	30.0	-	0.9
Soil	8.0	120	35.0	-	2.2
Soil	12.0	120	36.0	-	2.0
Soil	16.0	120	38.0	-	2.4
Soil	18.0	120	41.0	-	3.0
Soil	21.0	120	37.0	-	2.1

3.5.1.2 Foundation Properties

DS 11-1 had a diameter of 3 ft and an embedment depth of 20 ft, which results in a *D/B* ratio of 6.7. The unconfined compressive strength of the concrete was 5,000 psi. The modulus of elasticity was estimated to be 4.03 x 10^6 psi using Equation (3.4). The configuration of the foundation reinforcement was not specified explicitly; however, it was described as being "heavily reinforced". Several trial runs with both *LPile* and *DFSAP* showed that a minimum reinforcement ratio of 3.5% was required for the shaft to reach the reported maximum displacement. As such, it was assumed that (22) #11 longitudinal bars were placed 3.7 in. on center (o.c.) from the face of the foundation, which results in the target reinforcement ratio of 3.5% and approximately 3 in. of clear concrete cover.

It was not specified whether shear reinforcement, i.e., transverse reinforcement, was used, so it was assumed that the minimum transverse steel reinforcement required by ACI 318-11 was placed over the entire length of the foundation. Assuming #3 bars are used for transverse reinforcement, the spacing was calculated to be 7 in. using Equation

(3.3) and the transverse shear reinforcement ratio is 0.15%. The modulus of elasticity of the reinforcement is assumed to be 29,000 ksi and the yield strength is assumed to be 60,000 ksi. A schematic drawing of the foundation is shown in Figure 3.17. It should be noted that the foundation extended 10 ft above the ground surface, which is not shown in this figure. The foundation input properties for *LPile*, *DFSAP*, and *MFAD* are shown in Table 3.8, Table 3.9, and Table 3.10, respectively.

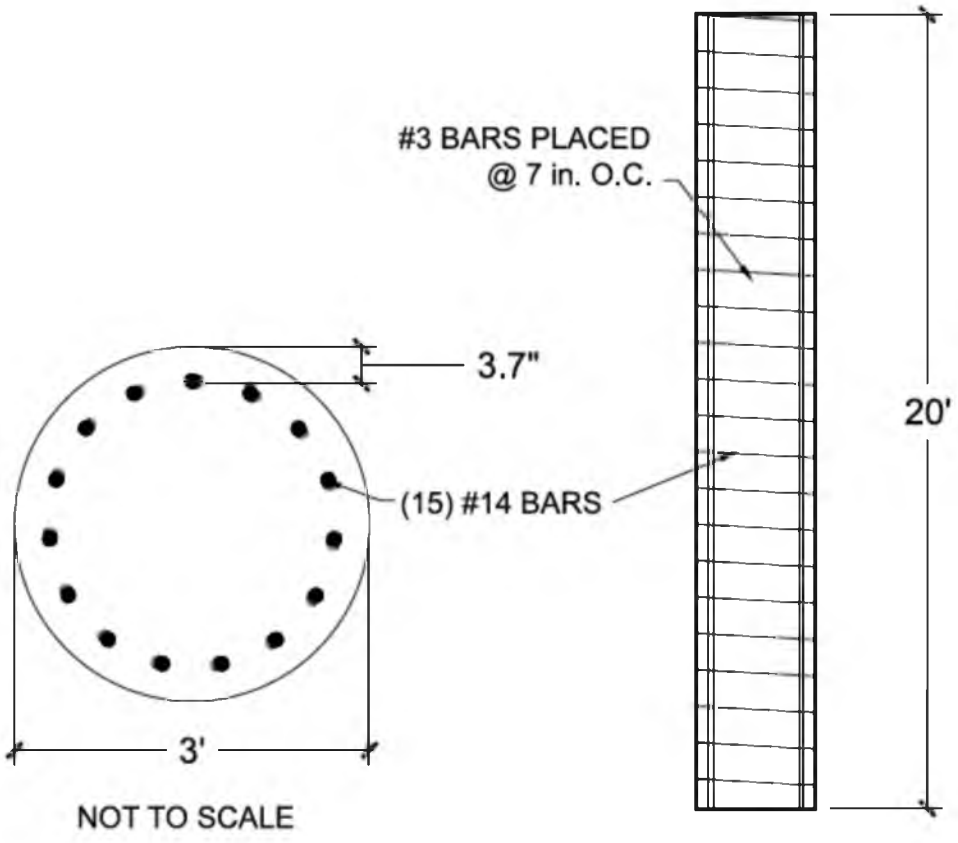

Figure 3.17. Schematic drawing of DS 11-1

Table 3.8. LPile foundation properties input for DS 11-1

Pile length =	20.00	ft
Pile diameter =	36	in.
Area =	1018	$in.^2$
Moment of inertia =	1319167	$in.^4$
Modulus of elasticity =	4030509	psi
Concrete comp. strength =	5000	psi
Longitudinal rebar =	15 #14	
Concrete cover to edge of bar =	2.85	in.
Rebar yield strength =	60000	psi
Rebar modulus of elasticity =	29000000	psi

Table 3.9. DFSAP foundation properties input for DS 11-1

Length of shaft =	20.00	ft
Length of shaft above ground =	0.00	ft
Outer diameter of shaft =	3.00	ft
Transverse steel ratio =	0.15	%
Concrete comp. strength =	5.00	ksi
Longitudinal steel ratio =	3.43	%
Yield stress of longitudinal steel =	60	ksi
Thickness of concrete cover =	2.85	in.

Table 3.10. MFAD foundation properties input for DS 11-1

Outer diameter of shaft =	3.00	ft
Stick up above ground level =	0.00	ft
Depth of embedment =	20.00	ft
Depth to GWT =	25	ft

3.5.1.3 Foundation Loading and Instrumentation

The lateral load was applied by a 200-kip hydraulic jack to the top of an integrated column at 10 ft above the ground surface. The load was applied by pulling the tops of the test foundation towards the top of the reaction foundation, which was placed 20 ft away. Additionally, a second 200-kip hydraulic jack was attached to a beam that was placed between the foundations near the ground surface. The action of the upper hydraulic ram pulling the foundations together and the lower hydraulic ram pushing them apart results in an increase in the applied moment to the top of the foundation, and increases the effective eccentricity of the total applied load to 80.

Lateral deflection at the ground surface was measured using two dial gauges placed diametrically along the line of loading. A plumb line was attached to the foundation to measure rotation at the top of the foundation. Soil pressure cells were placed in diametric pairs along the line of loading. The soil pressure cells were placed vertically along the entire depth of the foundation excavation.

The maximum applied horizontal load and overturning moment was approximately 24 kips and 1900 kip-ft, respectively. This load resulted in a maximum groundline deflection of approximately 1.9 in.

The top of the foundation was placed at the ground surface in the *LPile*, *DFSAP*, and *MFAD* models, and the equivalent loads from the load test were applied to the top of the foundation. The loads that were applied to the top of the foundation in each model are shown in Table 3.11.

Table 3.11. Loads applied to top of DS 11-1 in LPile, DFSAP, and MFAD

Load Number	LPile			DFSAP / MFAD		
	Lateral Load (lb)	Moment (lb-in.)	Axial Load (lb)	Lateral Load (kips)	Moment (kip-ft)	Axial Load (kips)
1	2500	2400000	0	2.50	200.00	0.00
2	5000	4800000	0	5.00	400.00	0.00
3	7500	7200000	0	7.50	600.00	0.00
4	10000	9600000	0	10.00	800.00	0.00
5	12500	12000000	0	12.50	1000.00	0.00
6	15000	14400000	0	15.00	1200.00	0.00
7	17500	16800000	0	17.50	1400.00	0.00
8	20000	19200000	0	20.00	1600.00	0.00
9	22500	21600000	0	22.50	1800.00	0.00
10	23900	22944000	0	23.90	1912.00	0.00

3.5.2 Load Test 18 near Los Angeles, CA

The results of a large-scale lateral load test program were presented by Bhushan, Haley, and Fong (1979). The load tests were conducted approximately 20 miles east of Los Angeles, CA. The soils at the site primarily consisted of sandy lean clay with medium to high plasticity. Two test foundations were constructed at the site, which had diameters of 2 ft and embedded depths of 15 ft. The *D/B* ratio for these foundations was 3.75. The only foundation from this load test program that met the experimental criteria was DS 18-2 because DS 18-1 was constructed with a bell at the bottom.

3.5.2.1 Soil Profile and Properties

The soil field investigation consisted of drilling two boreholes at the site. SPT testing was performed within each borehole to obtain SPT blowcounts and soil samples for laboratory testing. Laboratory testing included moisture content, Atterberg limits, density, unconfined compression testing, and unconsolidated-undrained (UU) triaxial

compression testing. The results of the field investigation and laboratory tests are shown in Table 3.12.

The information presented in Table 3.12 was used in conjunction with the methods outlined in Section 3.3 to estimate the values of the required soil properties for each analysis method. These values are presented in Table 3.13. It can be seen in Table 3.13 that ε_{50} was estimated using Figure 3.12 and the undrained shear strength of the soil despite the fact that values for ε_{50} were reported from laboratory testing. These values are presented so a comparison can be made between the measured value and the value estimated by *LPile*. The design values that were established from Table 3.13 are shown in Table 3.14. The discretization of sub-layers and the design values for each required soil property for *LPile*, *DFSAP*, and *MFAD* are shown in Table 3.15, Table 3.16, and Table 3.17, respectively.

Table 3.12. Results of field investigation and laboratory testing for Load Test 18 (Bhushan, Haley, & Fong, 1979)

Site	Sample Depth (ft)	SPT N Value	LL (%)	PI (%)	Minus #200 (%)	w_n (%)	ρ_d (pcf)	σ_3 (ksf)	σ_d (ksf)	ε_{50} (%)	Test Type
A	2	19	31	16	-	13	118	-	-	-	-
	4	34	39	21	76	16	111	0.72	10.8	0.7	UU
		-	43	25	79	18	109	1.44	11.2	0.9	UU
		-	46	28	76	18	110	2.88	12.3	1.0	UU
	6	35	41	24	-	16	112	-	-	-	-
	9	44	54	35	96	21	104	0	8.8	1.7	UC
	11	20	54	34	-	25	96	-	-	-	-
	14	20	44	31	84	19	106	0	3.6	0.8	UC

Notes

LL = Liquid Limit, PI = Plasticity Index, w_n = natural water content,
ρ_d = dry density, σ_3 = confining stress, σ_d = max. deviatoric stress,
UU = Unconsolidated Undrained triaxial test, UC = Unconfined Compression test

Table 3.13. Estimation of required soil properties for Load Test 18

Layer Depth												
Top (ft)	Bottom (ft)	w [1]	γ_d [1] (pcf)	γ [2] (pcf)	N [1] (blows/ft)	S_u [1] (ksf)	ε_{50} [1]	ε_{50} [3]	E_p [4] (ksi)	E_p [5] (ksi)	E_p [6] (ksi)	E_p [7] (ksi)
0.0	3.0	0.13	118	133	19	5.4	0.0070	0.0047	3.38	11.8	1.8	5.4
3.0	5.0	0.17	110	129	34	5.4	0.0070	0.0047	3.38	11.8	2.6	5.4
5.0	7.5	0.16	112	130	35	5.5	0.0075	0.0046	3.44	11.8	2.7	5.1
7.5	10.0	0.21	104	126	44	4.4	0.0170	0.0049	2.76	11.8	3.1	1.8
10.0	12.5	0.25	96	120	20	3.1	0.0125	0.0059	1.95	11.8	1.9	1.7
12.5	15.0	0.19	106	126	20	1.8	0.0080	0.0076	1.14	2.8	1.9	1.6

Notes

(1) From reported test data

(2) $\gamma = \gamma_d(1+w)$

(3) ε_{50} determined from LPile Technical Manual (2013)

(4) From Davidson (1982) for cohesive soils

(5) From Poulos & Davis (1980) for cohesive soils

(6) From Ohya et al. (1982) for cohesive soils

(7) Estimated as s_u / ε_{50}

Table 3.14. Design value of soil properties for Load Test 18

Layer Depth		γ	γ'	S_u		E_p
Top (ft)	Bottom (ft)	(pcf)	(pcf)	(ksf)	ε_{50}	(ksi)
0.0	3.0	133	133	5.4	0.0070	4.2
3.0	5.0	129	129	5.4	0.0070	4.5
5.0	7.5	130	130	5.5	0.0075	4.4
7.5	10.0	126	126	4.4	0.0170	3.0
10.0	12.5	120	120	3.1	0.0125	2.2
12.5	15.0	126	126	1.8	0.0080	1.8

Table 3.15. LPile sub-layer properties input for DS 18-2

	Layer Depth		γ	γ'	φ	S_u		k
LPile Soil Type	Top (ft)	Bottom (ft)	(pcf)	(pcf)	(deg)	(psf)	ε_{50}	(pci)
Stiff clay w/out free water	0.75	3.75	133	133	-	5400	0.0070	-
Stiff clay w/out free water	3.75	5.75	129	129	-	5400	0.0070	-
Stiff clay w/out free water	5.75	8.25	130	130	-	5500	0.0075	-
Stiff clay w/out free water	8.25	10.75	126	126	-	4400	0.0170	-
Stiff clay w/out free water	10.75	13.25	120	120	-	3100	0.0125	-
Stiff clay w/out free water	13.25	15.75	126	126	-	1800	0.0080	-

Table 3.16. DFSAP sub-layer properties input for DS 18-2

DFSAP Soil Type	Layer Thickness (ft)	γ' (pcf)	φ' (deg)	S_u (psf)	ε_{50}
Clay	3.0	133	-	5400	0.0070
Clay	2.0	129	-	5400	0.0070
Clay	2.5	130	-	5500	0.0075
Clay	2.5	126	-	4400	0.0170
Clay	2.5	120	-	3100	0.0125
Clay	2.5	126	-	1800	0.0080

Table 3.17. MFAD sub-layer properties input for DS 18-2

MFAD Layer Type	Depth to Bottom of Layer (ft)	γ (pcf)	φ (deg)	S_u (ksf)	E_p (ksi)
Soil	3.0	133	-	5.40	4.2
Soil	5.0	129	-	5.40	4.5
Soil	7.5	130	-	5.50	4.4
Soil	10.0	126	-	4.40	3.0
Soil	12.5	120	-	3.10	2.2
Soil	15.0	126	-	1.80	1.8

3.5.2.2 Foundation Properties

DS 18-2 had a diameter of 4 ft and an embedment depth of 15 ft, which results in a *D/B* ratio of 3.8. The longitudinal reinforcement was reported as #11 bars that resulted in a reinforcement ratio of about 3%. From the cross-sectional area of the foundation, the number of #11 bars was calculated to be 34. It was assumed that the longitudinal bars were placed 3.7 in. on center (o.c.) from the face of the foundation, which results in approximately 3 in. of clear concrete cover.

No further details were reported on the foundation properties; however, the test foundation was constructed as part of a testing program sponsored by the Southern California Edison Company for a new transmission line. Bhushan, Lee, and Grime (1981) presented a separate paper on several large-scale lateral load tests that were also conducted in 1979, which is the same year DS 18-2 was performed, as part of a test program sponsored by the Southern California Edison Company for a new transmission line project. Therefore, it is likely the properties of the foundations were similar. The modulus of elasticity and compressive strength of concrete was 4.33×10^6 psi and 5,770 psi, respectively, and these properties were used for DS-18.

It was not specified whether shear reinforcement, i.e., transverse reinforcement was used, so it was assumed that the minimum transverse steel reinforcement required by ACI 318-11 was placed over the entire length of the foundation. Assuming #4 bars are used for transverse reinforcement, the spacing was calculated to be 10 in. using Equation (3.3) and the transverse shear reinforcement ratio is 0.17%. The modulus of elasticity of the reinforcement is assumed to be 29,000 ksi and the yield strength is assumed to be 60,000 ksi. A schematic drawing of the foundation is shown in Figure 3.18. The foundation input properties for *LPile*, *DFSAP*, and *MFAD* are shown in Table 3.18, Table 3.19, and Table 3.20, respectively.

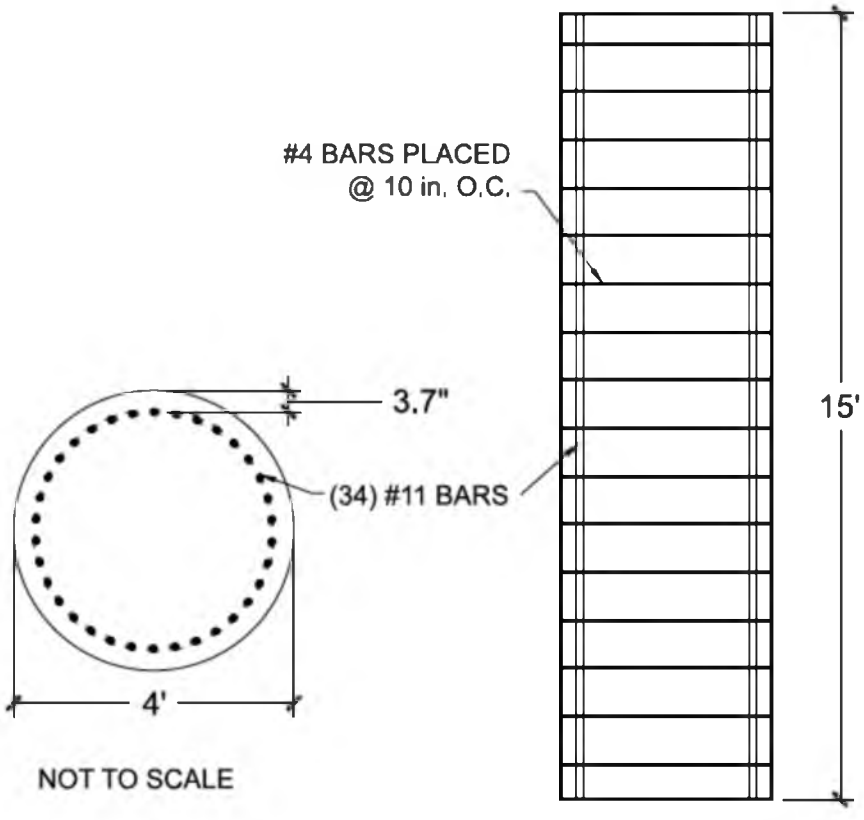

Figure 3.18. Schematic drawing of DS 18-2

Table 3.18. LPile foundation properties input for DS 18-2

Pile length =	15.75	ft
Pile diameter =	48	in.
Area =	1810	$in.^2$
Moment of inertia =	4169220	$in.^4$
Modulus of elasticity =	4329749	psi
Concrete comp. strength =	5770	psi
Longitudinal rebar =	34 #11	
Concrete cover to edge of bar =	3.00	in.
Rebar yield strength =	60000	psi
Rebar modulus of elasticity =	29000000	psi

Table 3.19. DFSAP foundation properties input for DS 18-2

Length of shaft =	15.75	ft
Length of shaft above ground =	0.75	ft
Outer diameter of shaft =	4.00	ft
Transverse steel ratio =	0.15	%
Concrete comp. strength =	5.77	ksi
Longitudinal steel ratio =	3.02	%
Yield stress of longitudinal steel =	60	ksi
Thickness of concrete cover =	3.00	in.

Table 3.20. MFAD foundation properties input for DS 18-2

Outer diameter of shaft =	4.00	ft
Stick up above ground level =	0.75	ft
Depth of embedment =	15.00	ft
Depth to GWT (1) =	999	ft

Notes

(1) GWT not reported and assumed deep

3.5.2.3 Foundation Loading and Instrumentation

The lateral load was applied by a 600-kip hydraulic jack to the top of the foundation at a point approximately 9 in. above the ground surface. The load was applied by jacking the test foundation against DS 18-1, which was located approximately 20 ft away.

Lateral deflection at the ground surface was measured using two dial gauges placed diametrically along the line of loading. A third dial gauge was placed approximately 3.5 ft above the ground surface, and was used to measure rotation of the top of the foundation by measuring displacement of a steel bar that extended vertically out of the foundation. All of the dial gauges were mounted on an independent support frame, and were accurate to the nearest ±0.001 in.

The maximum applied horizontal load and overturning moment was approximately 407 kips and 305 kip-ft, respectively. This load resulted in an initial groundline deflection of approximately 2.2 in. and a final measured groundline deflection of approximately 2.5 in. It should be noted that the authors reported the deflection of 2.5 in. as being "unstable", and therefore, it is likely this was the ultimate capacity of the foundation.

The top of the foundation was placed at 0.75 ft above the ground surface in the *LPile*, *DFSAP*, and *MFAD* models, and the equivalent loads from the load test were applied to the top of the foundation. The loads that were applied to the top of the foundation in each model are shown in Table 3.21.

Table 3.21. Loads applied to top of DS 18-2 in LPile, DFSAP, and MFAD

Load Number	LPile			DFSAP / MFAD		
	Lateral Load (lb)	Moment (lb-in.)	Axial Load (lb)	Lateral Load (kips)	Moment (kip-ft)	Axial Load (kips)
1	51781	0	0	51.78	0.00	0.00
2	86212	0	0	86.21	0.00	0.00
3	122078	0	0	122.08	0.00	0.00
4	188071	0	0	188.07	0.00	0.00
5	221544	0	0	221.54	0.00	0.00
6	256762	0	0	256.76	0.00	0.00
7	316862	0	0	316.86	0.00	0.00
8	341457	0	0	341.46	0.00	0.00
9	369288	0	0	369.29	0.00	0.00
10	406560	0	0	406.56	0.00	0.00

3.5.3 Load Test 19 near Los Angeles, CA

The results of a large-scale lateral load test program were presented by Bhushan, Lee, and Grime (1981). The test site was located approximately 42 miles east of Los Angeles, CA. The test site primarily consisted of sand and silty sand with variable amounts of gravel below 4 ft. The test foundations were 2 to 4 ft in diameter and had an embedment depth of 18 ft. The D/B ratio for these foundations ranged from 4.5 to 9. The foundations from this test site that met the experimental criteria were DS 19-1, DS 19-2, and DS 19-3.

The test site was further classified as site A, B, and C in the reference. DS 19-1 and DS 19-2 were located at site B, while DS 19-3 was located at site C. Where necessary, these sites will be referred to as site B or site C.

3.5.3.1 Soil Profile and Properties

A field investigation was performed to establish the stratigraphy of the site and the engineering properties of the soil. The field investigation included performing standard penetration testing (SPT) and cone penetration testing (CPT) at each test site. The engineering properties of the soil were estimated from laboratory tests where possible. Where lab test data were not available, CPT and SPT correlations were used. The generalized subsurface conditions are shown in Table 3.22. Note that the site is divided into site A, B, and C as previously discussed.

The information presented in Table 3.22 was used in conjunction with the methods outlined in Section 3.3 to estimate the values of the required soil properties for each analysis method. These values are presented in Table 3.23. The design values that were estimated from Table 3.23 are shown in Table 3.24.

Table 3.22. Generalized subsurface properties for Load Test 19 (Bhushan, Lee, & Grime, 1981)

Site	Soil Type	Depth (ft)	γ (pcf)	ϕ (deg)	D_r (%)	Test #
A	Sand (SP-SM)	0 - 8	105	38	55	1, 2, 3
	Sand (SP-SM)	8 - 15	110	40	67	
B	Silty sand (SM)	0 - 3	105	36	77	4, 5
	Silty sand (SM) w/ gravelly layers	3 - 18	105	42	88	
C	Silty sand (SM)	0 - 6	105	36	38	6, 7
	Silty sand (SM) w/ gravelly layers	6 - 18	105	42	92	

Notes
γ = total unit weight, ϕ = friction angle, D_r = relative density

Table 3.23. Estimation of required soil properties for Load Test 19

Layer Depth		γ [1]	ϕ [1]	D_R [1]	k [2]		N [3]	E_p [4]	E_p [5]	E_p [6]
Top (ft)	Bottom (ft)	(pcf)	(deg)	(%)	(pci)	σ_{v0}/P_a	(blows/ft)	(ksi)	(ksi)	(ksi)
0.0	3.0	105	36.0	77	230	0.07	10	3.3	0.6	0.6
3.0	18.0	105	42.0	88	305	0.52	20	4.4	1.0	2.0

Notes

(1) From reported test data

(2) From API (1993) using D_R

(3) From Holtz and Gibbs (1979)

(4) From Callanan and Kulhawy (1980)

(5) From Ohya et al. (1982)

(6) From Schmertmann (1970)

Table 3.24. Design value of soil properties for Load Test 19

Layer Depth		γ	γ'	ϕ	k	E_p
Top (ft)	Bottom (ft)	(pcf)	(pcf)	(deg)	(pci)	(ksi)
0.0	3.0	105	105	36.0	230	1.5
3.0	18.0	105	105	42.0	305	2.5

For site B, the discretization of sub-layers and the design values for each required soil property for *LPile*, *DFSAP*, and *MFAD* are shown in Table 3.25, Table 3.26, and Table 3.27, respectively. For site C, the discretization of sub-layers and the design values for each required soil property for *LPile*, *DFSAP*, and *MFAD* are shown in Table 3.28, Table 3.29, and Table 3.30, respectively.

3.5.3.2 Foundation Properties

The diameter of DS 19-1, DS 19-2, and DS 19-3 was 2 ft, 3 ft, and 3 ft, respectively, and the length of each foundation was 18 ft. The resulting *D/B* ratio for DS 19-1, DS 19-2, and DS 19-3 was 9, 6, and 6, respectively. The reinforcement and concrete properties were the same for each foundation at this site. Longitudinal reinforcement consisted of (14) #11 bars. The placement of the bars was not specified, so it was assumed that they were placed 3.5 in. on center (o.c.) from the face of the foundation, which results in clear concrete cover of approximately 3 in. It was also assumed that the longitudinal steel extended the entire length of the foundation. It was not specified whether shear reinforcement, i.e., transverse reinforcement, was used, so it was assumed that the minimum transverse steel reinforcement required by ACI 318-11 was placed over the entire length of the foundation. The minimum transverse steel reinforcement spacing was calculated from Equation (3.3) and by assuming that #3 bars

Table 3.25. LPile sub-layer properties input for DS 19-1 and DS 19-2

LPile Soil Type	Layer Depth Top (ft)	Layer Depth Bottom (ft)	γ (pcf)	γ' (pcf)	φ (deg)	S_u (psf)	ε_{50}	k (pci)
Sand (Reese)	0.0	3.0	105	105	36.0	-	-	230
Sand (Reese)	3.0	18.0	105	105	42.0	-	-	305

Table 3.26. DFSAP sub-layer properties input for DS 19-1 and DS 19-2

DFSAP Soil Type	Layer Thickness (ft)	γ' (pcf)	φ' (deg)	S_u (psf)	ε_{50}
Sand	3.0	105	36.0	-	-
Sand	15.0	105	42.0	-	-

Table 3.27. MFAD sub-layer properties input for DS 19-1 and DS 19-2

MFAD Layer Type	Depth to Bottom of Layer (ft)	γ (pcf)	φ (deg)	S_u (ksf)	E_p (ksi)
Soil	3.0	105	36.0	-	1.5
Soil	18.0	105	42.0	-	2.5

Table 3.28. LPile sub-layer properties input for DS 19-3

LPile Soil Type	Layer Depth Top (ft)	Layer Depth Bottom (ft)	γ (pcf)	γ' (pcf)	φ (deg)	S_u (psf)	ε_{50}	k (pci)
Sand (Reese)	0.0	3.0	105	105	36.0	-	-	55
Sand (Reese)	3.0	18.0	105	105	42.0	-	-	330

Table 3.29. DFSAP sub-layer properties input for DS 19-3

DFSAP Soil Type	Layer Thickness (ft)	γ' (pcf)	φ' (deg)	S_u (psf)	ε_{50}
Sand	3.0	105	36.0	-	-
Sand	15.0	105	42.0	-	-

Table 3.30. MFAD sub-layer properties input for DS 19-3

MFAD Layer Type	Depth to Bottom of Layer (ft)	γ (pcf)	φ (deg)	S_u (ksf)	E_p (ksi)
Soil	3.0	105	36.0	-	1.3
Soil	18.0	105	42.0	-	2.6

would be used. For this foundation, the center-to-center spacing of the transverse reinforcement is 11 inches, which results in a transverse reinforcement ratio of 0.13% for DS 19-1 and 0.10% for DS 19-2 and DS19-3. It should be noted that this also meets the maximum and minimum spacing requirements of ACI 318-11, which are not repeated here for the sake of brevity. It was also assumed that the elastic modulus of the rebar was 29,000 ksi and that the yield strength of the rebar was 60,000 ksi.

The modulus of elasticity was specified as 4.33 x 10^6 psi. The unconfined compressive strength of the concrete was not specified; however, it can be estimated from Equation (3.4). For an elastic modulus of 4.33 x 10^6 psi, the unconfined compressive strength of the concrete was calculated as 5,771 psi. A schematic of the foundation is shown in Figure 3.19.

For DS 19-1, the foundation input properties for *LPile*, *DFSAP*, and *MFAD* are shown in Table 3.31, Table 3.32, and Table 3.33, respectively. For DS 19-2 and DS 19-3, the foundation input properties for *LPile*, *DFSAP*, and *MFAD* are shown in Table 3.34, Table 3.35, and Table 3.36, respectively.

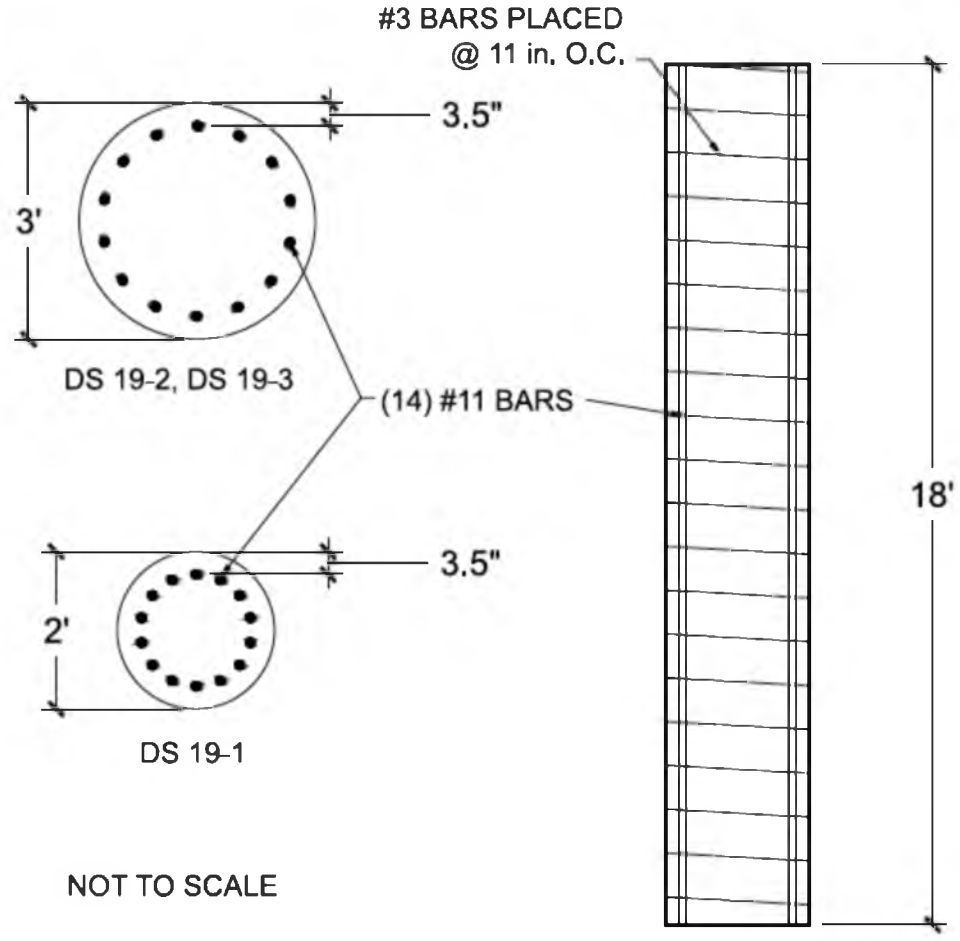

Figure 3.19. Schematic drawing of DS 19-1, DS 19-2, and DS 19-3

Table 3.31. LPile foundation properties input for DS 19-1

Pile length =	18.00	ft
Pile diameter =	24	in.
Area =	452	$in.^2$
Moment of inertia =	260576	$in.^4$
Modulus of elasticity =	4330125	psi
Concrete comp. strength =	5771	psi
Longitudinal rebar =	14 #11	
Concrete cover to edge of bar =	2.80	in.
Rebar yield strength =	60000	psi
Rebar modulus of elasticity =	29000000	psi

Table 3.32. DFSAP foundation properties input for DS 19-1

Length of shaft =	18.00	ft
Length of shaft above ground =	0.00	ft
Outer diameter of shaft =	2.00	ft
Transverse steel ratio =	0.13	%
Concrete comp. strength =	5.77	ksi
Longitudinal steel ratio =	5.07	%
Yield stress of longitudinal steel =	60	ksi
Thickness of concrete cover =	2.80	in.

Table 3.33. MFAD foundation properties input for DS 19-1

Outer diameter of shaft =	2.00	ft
Stick up above ground level =	0.00	ft
Depth of embedment =	18.00	ft
Depth to GWT (1) =	999	ft

Notes

(1) GWT not reported and assumed deep

Table 3.34. LPile foundation properties input for DS 19-2 and DS 19-3

Pile length =	18.00	ft
Pile diameter =	36	in.
Area =	1018	$in.^2$
Moment of inertia =	1319167	$in.^4$
Modulus of elasticity =	4330125	psi
Concrete comp. strength =	5771	psi
Longitudinal rebar =	14 #11	
Concrete cover to edge of bar =	2.80	in.
Rebar yield strength =	60000	psi
Rebar modulus of elasticity =	29000000	psi

Table 3.35. DFSAP foundation properties input for DS 19-2 and DS 19-3

Length of shaft =	18.00	ft
Length of shaft above ground =	0.00	ft
Outer diameter of shaft =	3.00	ft
Transverse steel ratio =	0.10	%
Concrete comp. strength =	5.77	ksi
Longitudinal steel ratio =	2.19	%
Yield stress of longitudinal steel =	60	ksi
Thickness of concrete cover =	2.80	in.

Table 3.36. MFAD foundation properties input for DS 19-2 and DS 19-3

Outer diameter of shaft =	3.00	ft
Stick up above ground level =	0.00	ft
Depth of embedment =	18.00	ft
Depth to GWT (1) =	999	ft

Notes

(1) GWT not reported and assumed deep

3.5.3.3 Foundation Loading and Instrumentation

The horizontal load was applied by using a 200-kip hydraulic ram to pull the tops of the test foundation and the reaction foundation together. The applied load was measured using a 200-kip load cell that was placed against the jacking plate. Dial gauges were placed in front of the foundation along the line of loading. These dial gauges were affixed to beams that were independently supported a minimum distance of 10 ft away from the foundations. The dial gauges were accurate to ± 0.001 in. and had a maximum range of 2 in. The maximum applied horizontal load for each foundation was 200 kips, which resulted in a maximum groundline deflection of approximately 1.7 in., 0.9 in., and 0.9 in. for DS 19-1, DS 19-2, and DS 19-3, respectively.

The top of the foundation was placed at the ground surface in the *LPile*, *DFSAP*, and *MFAD* models, and the equivalent loads from the load test were applied to the top of the foundation. The loads that were applied to the top of the foundation in each model are shown in Table 3.37.

3.5.4 Load Test 20 near Los Angeles, CA

The results of a large-scale lateral load test program were presented by Bhushan, Haley, and Fong (1979). The load tests were conducted approximately 20 miles east of Los Angeles, CA. The soils at the site primarily consisted of sandy lean clay. Six test foundations were constructed at the site, which had diameters ranging from 2 to 4 ft and lengths ranging from 9 to 15.5 ft, respectively, which resulted in *D/B* ratios ranging from 3.1 to 7.8. The foundations that met the experimental criteria at this site were DS 20-2, DS 20-4, DS 20-5, and DS 20-6.

3.5.4.1 Soil Profile and Properties

The soil field investigation consisted of drilling two boreholes at the site. SPT testing was performed within each borehole to obtain SPT N values and soil samples for laboratory testing. Laboratory testing included moisture content, Atterberg limits, density, unconfined compression testing, and unconsolidated-undrained (UU) triaxial compression testing. The results of the field investigation and laboratory tests are shown in Table 3.38.

The information presented in Table 3.38 was used in conjunction with the methods outlined in Section 3.3 to estimate the values of the required soil properties for each analysis method. These values are presented in Table 3.39.

Table 3.37. Loads applied to top of DS 19-1, DS 19-2, and DS 19-3 in LPile, DFSAP, and MFAD

Load Number	LPile			DFSAP / MFAD		
	Lateral Load (lb)	Moment (lb-in.)	Axial Load (lb)	Lateral Load (kips)	Moment (kip-ft)	Axial Load (kips)
1	20000	0	0	20.00	0.00	0.00
2	40000	0	0	40.00	0.00	0.00
3	60000	0	0	60.00	0.00	0.00
4	80000	0	0	80.00	0.00	0.00
5	100000	0	0	100.00	0.00	0.00
6	120000	0	0	120.00	0.00	0.00
7	140000	0	0	140.00	0.00	0.00
8	160000	0	0	160.00	0.00	0.00
9	180000	0	0	180.00	0.00	0.00
10	200000	0	0	200.00	0.00	0.00

Table 3.38. Results of field investigation and laboratory testing for Load Test 20 (Bhushan, Haley, & Fong, 1979)

Site	Sample Depth (ft)	SPT N Value	LL (%)	PI (%)	Minus #200 (%)	w_n (%)	ρ_d (pcf)	σ_3 (ksf)	σ_d (ksf)	ε_{50} (%)	Test Type
B	2	19	45	31	-	14	115	-	-	-	-
	4	30	44	28	70	13	88	0.72	6.6	0.60	UU
		-	46	29	88	14	92	1.44	9.6	0.80	UU
		-	40	23	75	14	102	2.88	14.6	0.80	UU
	5	32	-	-	-	15	97	0	4.6	0.76	UC
	6	22	-	-	-	28	92	-	-	-	-
	9	43	49	33	74	17	115	0	14.0	-	UC
	11	24	44	27	-	16	111	-	-	-	-
	14	31	-	-	-	18	102	0	3.9	-	UC
		-	31	16	60	16	104	0.72	4.9	0.60	UU
		-	33	19	70	16	107	1.44	7.7	0.70	UU
		-	35	21	76	18	112	2.88	11.8	1.10	UU

Notes

LL = Liquid Limit, PI = Plasticity Index, w_n = natural water content,

ρ_d = dry density, σ_3 = confining stress, σ_d = max. deviatoric stress,

UU = Unconsolidated Undrained triaxial test, UC = Unconfined Compression test

Table 3.39. Estimation of required soil properties for Load Test 20

Layer Depth												
Top (ft)	Bottom (ft)	w [1]	γ_d [1] (pcf)	γ [2] (pcf)	N [1] (blows/ft)	S_u [1] (ksf)	ε_{50} [1]	ε_{50} [3]	E_p [4] (ksi)	E_p [5] (ksi)	E_p [6] (ksi)	E_p [7] (ksi)
0.0	3.0	0.14	115	131	19	4.0	0.0060	0.0050	2.5	11.8	1.8	4.6
3.0	4.5	0.14	94	107	30	4.0	0.0070	0.0050	2.5	11.8	2.4	4.0
4.5	5.5	0.15	97	112	32	7.0	0.0070	0.0043	4.4	11.8	2.5	6.9
5.5	7.5	0.28	92	118	22	7.0	0.0070	0.0043	4.4	11.8	2.0	6.9
7.5	10.0	0.17	115	135	43	7.0	0.0060	0.0043	4.4	11.8	3.0	8.1
10.0	12.5	0.16	111	129	24	7.0	0.0070	0.0043	4.4	11.8	2.1	6.9
12.5	15.5	0.17	106	124	31	8.0	0.0070	0.0040	5.0	11.8	2.5	7.9

Notes

(1) From reported test data

(2) $\gamma = \gamma_d(1+w)$

(3) ε_{50} determined from LPile Technical Manual (2013)

(4) From Davidson (1982) for cohesive soils

(5) From Poulos & Davis (1980) for cohesive soils

(6) From Ohya et al. (1982) for cohesive soils

(7) Estimated as s_u / ε_{50}

It can be seen in Table 3.39 that ε_{50} was estimated using Figure 3.12 and the undrained shear strength of the soil despite the fact that values for ε_{50} were reported from laboratory testing. These values are presented so a comparison can be made between the measured value and the value estimated by *LPile*. The design values that were estimated from Table 3.39 are shown in Table 3.40. The discretization of sub-layers and the design values for each required soil property for *LPile*, *DFSAP*, and *MFAD* are shown in Table 3.41, Table 3.42, and Table 3.43, respectively.

3.5.4.2 Foundation Properties

For each foundation from this load test program, the modulus of elasticity and compressive strength of concrete was 4.33×10^6 psi and 5,770 psi, respectively, as discussed in Section 3.5.2.2. The modulus of elasticity and yield strength of the steel rebar reinforcement was 29,000 ksi and 60 ksi, respectively. The authors stated that #11 bars were used for longitudinal reinforcement and that the reinforcement ratio was approximately 3%. It was assumed that the longitudinal bars were placed 3.7 in. on center (o.c.) from the face of the foundation, which results in approximately 3 in. of clear concrete cover.

For DS 20-2, DS 20-4, DS 20-5, and DS 20-6, the foundation input properties for *LPile*, *DFSAP*, and *MFAD* are shown in Table 3.44, Table 3.45, and Table 3.46, respectively.

Table 3.40. Design value of soil properties for Load Test 20

Layer Depth		γ	γ'	S_u		E_p
Top (ft)	Bottom (ft)	(pcf)	(pcf)	(ksf)	ε_{50}	(ksi)
0.0	3.0	131	131	4.0	0.0060	3
3.0	4.5	107	107	4.0	0.0070	3
4.5	5.5	112	112	7.0	0.0070	4.6
5.5	7.5	118	118	7.0	0.0070	4.4
7.5	10.0	135	135	7.0	0.0060	5.2
10.0	12.5	129	129	7.0	0.0070	4.5
12.5	15.5	124	124	8.0	0.0070	5.1

Table 3.41. LPile sub-layer properties input for DS 20-2, DS 20-4, DS 20-5, and DS 20-6

	Layer Depth							
LPile Soil Type	Top (ft)	Bottom (ft)	γ (pcf)	γ' (pcf)	φ (deg)	S_u (psf)	ε_{50}	k (pci)
Stiff clay w/out free water	0.75	3.75	131	131	-	4000	0.0060	-
Stiff clay w/out free water	3.75	5.25	107	107	-	4000	0.0070	-
Stiff clay w/out free water	5.25	6.25	112	112	-	7000	0.0070	-
Stiff clay w/out free water	6.25	8.25	118	118	-	7000	0.0070	-
Stiff clay w/out free water	8.25	10.75	135	135	-	7000	0.0060	-
Stiff clay w/out free water	10.75	13.25	129	129	-	7000	0.0070	-
Stiff clay w/out free water	13.25	16.25	124	124	-	8000	0.0070	-

Table 3.42. DFSAP sub-layer properties input for DS 20-2, DS 20-4, DS 20-5, and DS 20-6

DFSAP Soil Type	Layer Thickness (ft)	γ' (pcf)	φ' (deg)	S_u (psf)	ε_{50}
Clay	3.0	131	-	4000	0.0060
Clay	1.5	107	-	4000	0.0070
Clay	1.0	112	-	7000	0.0070
Clay	2.0	118	-	7000	0.0070
Clay	2.5	135	-	7000	0.0060
Clay	2.5	129	-	7000	0.0070
Clay	3.0	124	-	8000	0.0070

Table 3.43. MFAD sub-layer properties input for DS 20-2, DS 20-4, DS 20-5, and DS 20-6

MFAD Layer Type	Depth to Bottom of Layer (ft)	γ (pcf)	φ (deg)	S_u (ksf)	E_p (ksi)
Soil	3.0	131	-	4.00	3.0
Soil	4.5	107	-	4.00	3.0
Soil	5.5	112	-	7.00	4.6
Soil	7.5	118	-	7.00	4.4
Soil	10.0	135	-	7.00	5.2
Soil	12.5	129	-	7.00	4.5
Soil	15.5	124	-	8.00	5.1

Table 3.44. LPile foundation properties input for DS 20-2, DS 20-4, DS 20-5, and DS 20-6

Description	DS 20-2		DS 20-4		DS 20-5		DS 20-6	
Pile length =	13.25	ft	16.25	ft	9.75	ft	16.25	ft
Pile diameter =	48	in.	48	in.	24	in.	24	in.
Area =	1810	$in.^2$	1810	$in.^2$	452	$in.^2$	452	$in.^2$
Moment of inertia =	4169220	$in.^4$	4169220	$in.^4$	260576	$in.^4$	260576	$in.^4$
Modulus of elasticity =	4329749	psi	4329749	psi	4329749	psi	4329749	psi
Concrete comp. strength =	5770	psi	5770	psi	5770	psi	5770	psi
Longitudinal rebar =	34 #11		34 #11		9 #11		9 #11	
Concrete cover to edge of bar =	3.00	in.	3.00	in.	3.00	in.	3.00	in.
Rebar yield strength =	60000	psi	60000	psi	60000	psi	60000	psi
Rebar modulus of elasticity =	$29x10^6$	psi	$29x10^6$	psi	$29x10^6$	psi	$29x10^6$	Psi

Table 3.45. DFSAP foundation properties input for DS 20-2, DS 20-4, DS 20-5, and DS 20-6

Description	DS 20-2		DS 20-4		DS 20-5		DS 20-6	
Length of shaft =	13.25	ft	16.25	ft	9.75	ft	16.25	ft
Length of shaft above ground =	0.75	ft	0.75	ft	0.75	ft	0.75	ft
Outer diameter of shaft =	4.00	ft	4.00	ft	2.00	ft	2.00	ft
Transverse steel ratio =	0.15	%	0.15	%	0.13	%	0.13	%
Concrete comp. strength =	5.77	ksi	5.77	ksi	5.77	ksi	5.77	ksi
Longitudinal steel ratio =	3.02	%	3.02	%	3.20	%	3.20	%
Yield stress of longitudinal steel =	60.0	ksi	60.0	ksi	60.0	ksi	60.0	ksi
Thickness of concrete cover =	3.00	in.	3.00	in.	3.00	in.	3.00	in.

Table 3.46. MFAD foundation properties input for DS 20-2, DS 20-4, DS 20-5, and DS 20-6

Description	DS 20-2		DS 20-4		DS 20-5		DS 20-6	
Outer diameter of shaft =	4.00	ft	4.00	ft	2.00	ft	2.00	ft
Stick up above ground level =	0.75	ft	0.75	ft	0.75	ft	0.75	ft
Depth of embedment =	12.50	ft	15.50	ft	9.00	ft	15.50	ft
Depth to GWT (1) =	999	ft	999	ft	999	ft	999	ft

Notes

(1) GWT not reported and assumed deep

3.5.4.3 Foundation Loading and Instrumentation

The load testing apparatus and instrumentation was described previously in Section 3.5.2.3.

The maximum applied horizontal load and overturning moment that was applied to DS 20-2 was approximately 391 kips and 294 kip-ft, respectively. This load resulted in measured groundline deflection of approximately 3.95 in. The maximum applied horizontal load and overturning moment that was applied to DS 20-4 was approximately 449 kips and 337 kip-ft, respectively. This load resulted in an initial groundline deflection of approximately 2.2 in. and a final measured groundline deflection of approximately 2.9 in. The maximum applied horizontal load and overturning moment that was applied to DS 20-5 was approximately 160 kips and 120 kip-ft, respectively. This load resulted in measured groundline deflection of approximately 1.4 in. The maximum applied horizontal load and overturning moment that was applied to DS 20-6 was approximately 334 kips and 250 kip-ft, respectively. This load resulted in an initial groundline deflection of approximately 3.0 in. and a final measured groundline deflection of approximately 3.9 in. It should be noted that the authors reported the final deflections of DS 20-4 and DS 20-6 as being “unstable”, and therefore, it is likely these foundations

had reached their ultimate capacity.

The top of the foundation was placed at 0.75 ft above the ground surface in the *LPile*, *DFSAP*, and *MFAD* models, and the equivalent loads from the load test were applied to the top of the foundation. The loads that were applied to the top of the foundation in each *LPile* model are shown in Table 3.47 and the loads that were applied to the top of the foundation in in each *DFSAP* and *MFAD* model are shown in Table 3.48.

3.5.5 Load Test 22 at College Station, TX

The results of a large-scale lateral load test program, which was conducted at the Texas A&M University Research and Extension Center near College Station, TX, was presented by Bierschwale, Coyle, and Bartoskewitz (1981) and Kasch et al. (1977). The soils at the site consisted of approximately 5 ft of stiff sandy lean clay underlain by a thick stratum of very stiff fat clay. The fat clay was slickensided and overconsolidated due to desiccation below 10 ft. The test foundations were comprised of three instrumented drilled shafts with diameters ranging from 2.5 to 3 ft and embedment depths ranging from 15 to 20 ft. The *D/B* ratio for these foundations ranged from 5 to 6.7. The foundations that met the experimental criteria were DS 22-1 and DS 22-2.

3.5.5.1 Soil Profile and Properties

A field investigation was performed to establish the stratigraphy of the site, the groundwater table location, and the engineering properties of the soil. The field investigation was conducted by drilling three boreholes and performing one Texas cone penetrometer (TCP) test. A groundwater observation well was also installed at the site to monitor long-term groundwater conditions. The engineering properties of the soil were

Table 3.47. Loads applied to top of DS 20-2, DS 20-4, DS 20-5, and DS 20-6 in LPile

Load Number	DS 20-2			DS 20-4			DS 20-5			DS 20-6		
	Lateral Load (lb)	Moment (lb-in.)	Axial Load (lb)	Lateral Load (lb)	Moment (lb-in.)	Axial Load (lb)	Lateral Load (lb)	Moment (lb-in.)	Axial Load (lb)	Lateral Load (lb)	Moment (lb-in.)	Axial Load (lb)
1	69899	0	0	74418	0	0	21604	0	0	45602	0	0
2	110374	0	0	112314	0	0	36867	0	0	68177	0	0
3	152114	0	0	169545	0	0	55323	0	0	95881	0	0
4	194486	0	0	246111	0	0	76384	0	0	118421	0	0
5	243183	0	0	309786	0	0	100672	0	0	142000	0	0
6	284936	0	0	383343	0	0	115673	0	0	176782	0	0
7	315311	0	0	449323	0	0	129000	0	0	210167	0	0
8	337804	0	0	-	-	-	146982	0	0	252623	1	0
9	365943	0	0	-	-	-	160318	0	0	290346	2	0
10	391463	0	0	-	-	-	-	-	-	309219	3	0

Table 3.48. Loads applied to top of DS 20-2, DS 20-4, DS 20-5, and DS 20-6 in DFSAP and MFAD

Load Number	DS 20-2			DS 20-4			DS 20-5			DS 20-6		
	Lateral Load (kips)	Moment (kip-ft)	Axial Load (kips)	Lateral Load (kips)	Moment (kip-ft)	Axial Load (kips)	Lateral Load (kips)	Moment (kip-ft)	Axial Load (kips)	Lateral Load (kips)	Moment (kip-ft)	Axial Load (kips)
1	70	0	0	74	0	0	22	0	0	46	0	0
2	110	0	0	112	0	0	37	0	0	68	0	0
3	152	0	0	170	0	0	55	0	0	96	0	0
4	194	0	0	246	0	0	76	0	0	118	0	0
5	243	0	0	310	0	0	101	0	0	142	0	0
6	285	0	0	383	0	0	116	0	0	177	0	0
7	315	0	0	449	0	0	129	0	0	210	0	0
8	338	0	0	-	-	-	147	0	0	253	0	0
9	366	0	0	-	-	-	160	0	0	290	0	0
10	391	0	0	-	-	-	-	-	-	309	0	0

estimated from the results of the TCP test and laboratory tests. Laboratory testing included soil classification, Atterberg limits, moisture contents, densities, miniature torvane tests, and unconfined compression tests that were performed on specimens trimmed from thin-wall tube samples. The generalized subsurface conditions, as presented by Bierschwale, Coyle, and Bartoskewitz (1981), are shown in Figure 3.20.

The information presented in Figure 3.20 was used in conjunction with the methods outlined in Section 3.3 to estimate the values of the required soil properties for each analysis method. These values are presented in Table 3.49, and the design values are presented in Table 3.50.

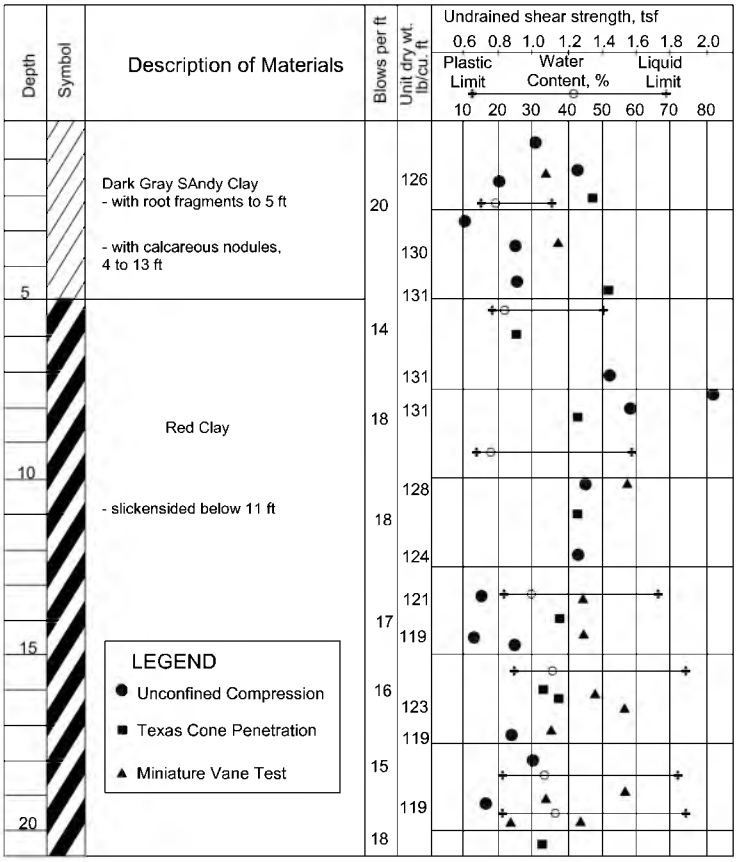

Figure 3.20. Generalized subsurface conditions for Load Test 22 (Bierschwale, Coyle, & Bartoskewitz, 1981)

Table 3.49. Estimation of required soil properties for Load Test 22

Layer Depth		γ [(1)]	N [(1)]	S_u [(1)]		E_p [(3)]	E_p [(4)]	E_p [(5)]	E_p [(6)]
Top (ft)	Bottom (ft)	(pcf)	(blows/ft)	(ksf)	ε_{50} [(2)]	(ksi)	(ksi)	(ksi)	(ksi)
0.0	2.5	126	20	2.2	0.0068	1.4	3.8	1.9	2.2
2.5	3.0	130	20	1.2	0.0094	0.8	1.1	1.9	0.9
3.0	5.0	130	20	2.2	0.0068	1.4	3.8	1.9	2.2
5.0	6.5	131	14	1.8	0.0076	1.1	2.4	1.5	1.6
6.5	7.5	131	14	2.9	0.0061	1.8	11.8	1.5	3.3
7.5	8.0	131	18	4.1	0.0050	2.6	11.8	1.8	5.7
8.0	10.5	130	18	2.9	0.0061	1.8	11.8	1.8	3.3
10.5	12.5	126	18	2.5	0.0065	1.6	5.8	1.8	2.7
12.5	15.0	120	17	2.0	0.0070	1.3	2.9	1.7	2.0
15.0	21.0	120	16	2.5	0.0065	1.6	5.8	1.6	2.7

Notes

(1) From reported test data

(2) ε_{50} determined from LPile Technical Manual (2013)

(3) From Davidson (1982) for cohesive soils

(4) From Poulos & Davis (1980) for cohesive soils

(5) From Ohya et al. (1982) for cohesive soils

(6) Estimated as s_u / ε_{50}

Table 3.50. Design value of soil properties for Load Test 22

Layer Depth		γ	γ'	S_u		E_p
Top (ft)	Bottom (ft)	(pcf)	(pcf)	(ksf)	ε_{50}	(ksi)
0.0	2.5	126	126	2.2	0.0068	2.2
2.5	3.0	130	130	1.2	0.0094	1.4
3.0	5.0	130	130	2.2	0.0068	2.2
5.0	6.5	131	131	1.8	0.0076	1.7
6.5	7.5	131	131	2.9	0.0061	2.6
7.5	8.0	131	131	4.1	0.0050	4.0
8.0	10.5	130	130	2.9	0.0061	2.7
10.5	12.5	126	126	2.5	0.0065	2.4
12.5	15.0	120	120	2.0	0.0070	2.0
15.0	21.0	120	58	2.5	0.0065	2.4

It should also be noted that the location of the groundwater table was reported as being between 15 and 18 ft below the ground surface. The design groundwater table for this investigation was chosen as 15 ft. The discretization of sub-layers and the design values for each required soil property for *LPile*, *DFSAP*, and *MFAD* are shown in Table 3.51, Table 3.52, and Table 3.53, respectively.

DS 22-1 had a diameter of 3 ft and an embedment depth of 20 ft, which results in a *D/B* ratio of 6.7. The unconfined compressive strength of the concrete was 3,000 psi, and the modulus of elasticity was estimated to be 3.12×10^6 psi using Equation (3.4). Longitudinal reinforcement consisted of (12) #11 bars and (12) 1.5 in. diameter anchor bolts. The #11 bars extended the entire length of the foundation, while the anchor bolts were terminated at 8 ft below the top of the foundation. The anchor bolts were placed at 2 in. o.c. and 6 in. o.c., respectively, from the face of the foundation. Spiral transverse reinforcement consisting of a #3 bar was placed with a 6 in. pitch over the entire length of the foundation. A 12WF120 column was attached to the top of the foundation, and the load was applied horizontally to the column at 2.6 ft above the top of the foundation.

Table 3.51. LPile sub-layer properties input for DS 22-1 and DS 22-2

LPile Soil Type	Layer Depth Top (ft)	Layer Depth Bottom (ft)	γ (pcf)	γ' (pcf)	φ (deg)	S_u (psf)	ε_{50}	k (pci)
Stiff clay w/out free water	0.0	2.5	126	126	-	2200	0.0068	-
Stiff clay w/out free water	2.5	3.0	130	130	-	1200	0.0094	-
Stiff clay w/out free water	3.0	5.0	130	130	-	2200	0.0068	-
Stiff clay w/out free water	5.0	6.5	131	131	-	1800	0.0076	-
Stiff clay w/out free water	6.5	7.5	131	131	-	2900	0.0061	-
Stiff clay w/out free water	7.5	8.0	131	131	-	4100	0.0050	-
Stiff clay w/out free water	8.0	10.5	130	130	-	2900	0.0061	-
Stiff clay w/out free water	10.5	12.5	126	126	-	2500	0.0065	-
Stiff clay w/out free water	12.5	15.0	120	120	-	2000	0.0070	-
Stiff clay w/out free water	15.0	21.0	120	58	-	2500	0.0065	-

Table 3.52. DFSAP sub-layer properties input for DS 22-1 and DS 22-2

DFSAP Soil Type	Layer Thickness (ft)	γ' (pcf)	φ' (deg)	S_u (psf)	ε_{50}
Clay	2.5	126	-	2200	0.0068
Clay	0.5	130	-	1200	0.0094
Clay	2.0	130	-	2200	0.0068
Clay	1.5	131	-	1800	0.0076
Clay	1.0	131	-	2900	0.0061
Clay	0.5	131	-	4100	0.0050
Clay	2.5	130	-	2900	0.0061
Clay	2.0	126	-	2500	0.0065
Clay	2.5	120	-	2000	0.0070
Clay	6.0	58	-	2500	0.0065

Table 3.53. MFAD sub-layer properties input for DS 22-1 and DS 22-2

MFAD Layer Type	Depth to Bottom of Layer (ft)	γ (pcf)	φ (deg)	S_u (ksf)	E_p (ksi)
Soil	2.5	126	-	2.20	2.2
Soil	3.0	130	-	1.20	1.4
Soil	5.0	130	-	2.20	2.2
Soil	6.5	131	-	1.80	1.7
Soil	7.5	131	-	2.90	2.6
Soil	8.0	131	-	4.10	4.0
Soil	10.5	130	-	2.90	2.7
Soil	12.5	126	-	2.50	2.4
Soil	15.0	120	-	2.00	2.0
Soil	21.0	120	-	2.50	2.4

3.5.5.2 Foundation Properties

DS 22-2 had a diameter of 3 ft and an embedment depth of 15 ft, which results in a *D/B* ratio of 5. The unconfined compressive strength of the concrete was 4,130 psi, and the modulus of elasticity was estimated to be 3.66 x 10^6 psi using Equation (3.4). Longitudinal reinforcement consisted of (12) #11 bars and (12) 1.5 in. diameter anchor bolts that extended the entire length of the foundation. The anchor bolts were placed at 2 in. o.c. and 6 in. o.c., respectively, from the face of the foundation. Spiral transverse reinforcement consisting of a #3 bar was placed with a 2 in. pitch over the upper 6 ft of the foundation and a 6 in. pitch over the remaining length of the foundation. A 12WF120 column was attached to the top of the foundation, and the load was applied horizontally to the column at 2.6 ft above the top of the foundation.

It was assumed that the elastic modulus of the rebar was 29,000 ksi and that the yield strength of the rebar was 60,000 ksi for both test foundations. A schematic of DS 22-1 and DS 22-2 is shown in Figure 3.21.

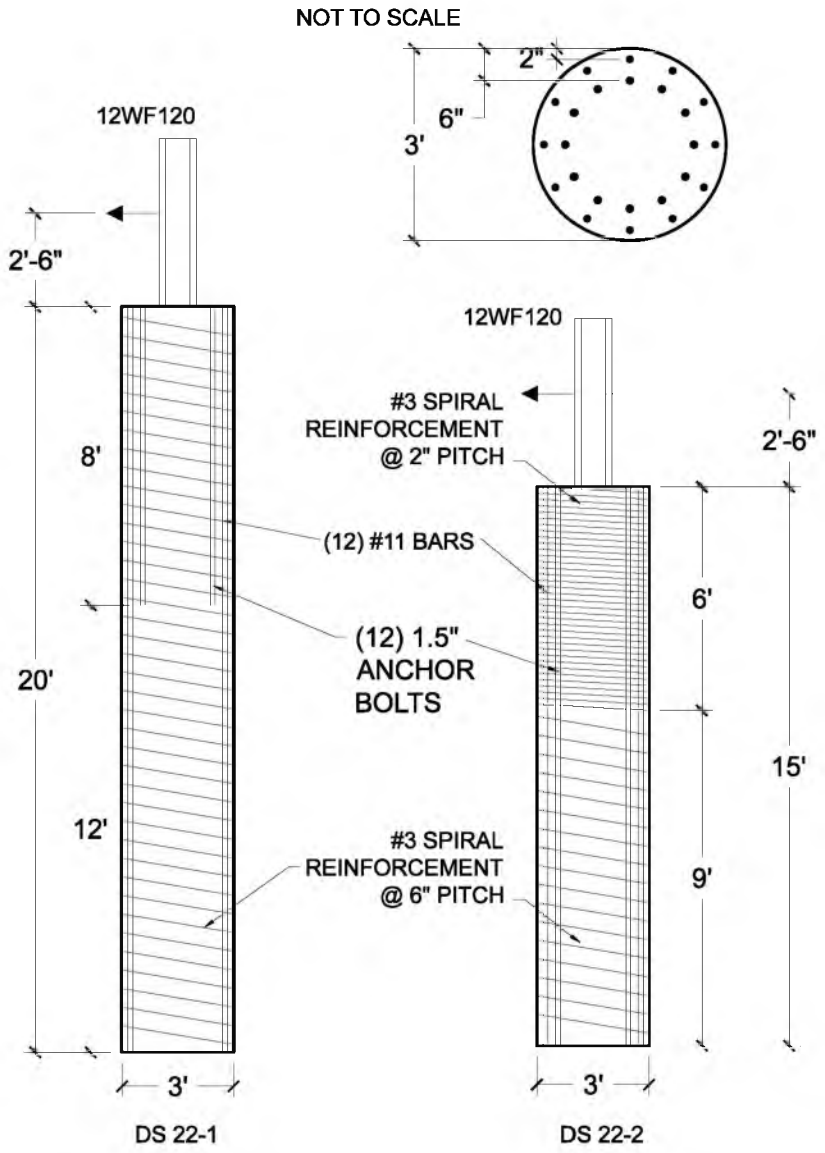

Figure 3.21. Schematic drawing of DS 22-2

For DS 22-1, the foundation input properties for *LPile*, *DFSAP*, and *MFAD* are shown in Table 3.54, Table 3.55, and Table 3.56, respectively. For DS 22-2, the foundation input properties for *LPile*, *DFSAP*, and *MFAD* are shown in Table 3.57, Table 3.58, and Table 3.59, respectively.

It should be noted that the rebar configuration shown in Table 3.54 and Table 3.57 does not match the description given in Section 0. This is because *LPile* does not

Table 3.54. LPile foundation properties input for DS 22-1

Pile length =	20.00	ft
Pile diameter =	36	in.
Area =	1018	$in.^2$
Moment of inertia =	1319167	$in.^4$
Modulus of elasticity =	3122019	psi
Concrete comp. strength =	3000	psi
Longitudinal rebar (0 - 8') =	12 #14	
Longitudinal rebar (8' - 20') =	12 #11	
Concrete cover to edge of bar =	1.30	in.
Rebar yield strength =	60000	psi
Rebar modulus of elasticity =	29000000	psi

Table 3.55. DFSAP foundation properties input for DS 22-1

Length of shaft =	20.00	ft
Length of shaft above ground =	0.00	ft
Outer diameter of shaft =	3.00	ft
Transverse steel ratio =	0.19	%
Concrete comp. strength =	3.00	ksi
Longitudinal steel ratio (0 - 8') =	2.72	%
Longitudinal steel ratio (8' - 20') =	1.87	%
Yield stress of longitudinal steel =	60	ksi
Thickness of concrete cover =	1.30	in.

allow the placement of rebar at more than one distance away from the center of the foundation. As such, the moment-curvature diagram for the actual configuration of the rebar and anchor bolts was computed manually using MATLAB. The size of the rebar in the *LPile* model was adjusted until the moment-curvature diagrams matched reasonably well, and the rebar that was chosen to represent both the actual #11 rebar and the 1.5 in. diameter anchor bolts was #14 bars.

Table 3.56. MFAD foundation properties input for DS 22-1

Outer diameter of shaft =	3.00	ft
Stick up above ground level =	0.00	ft
Depth of embedment =	20.00	ft
Depth to GWT =	15	ft

Table 3.57. LPile foundation properties input for DS 22-2

Pile length =	15.00	ft
Pile diameter =	36	in.
Area =	1018	$in.^2$
Moment of inertia =	1319167	$in.^4$
Modulus of elasticity =	3663109	psi
Concrete comp. strength =	4130	psi
Longitudinal rebar =	12 #14	
Concrete cover to edge of bar =	1.15	in.
Rebar yield strength =	60000	psi
Rebar modulus of elasticity =	29000000	psi

Table 3.58. DFSAP foundation properties input for DS 22-2

Length of shaft =	15.00	ft
Length of shaft above ground =	0.00	ft
Outer diameter of shaft =	3.00	ft
Transverse steel ratio =	0.58	%
Concrete comp. strength =	4.13	ksi
Longitudinal steel ratio =	2.72	%
Yield stress of longitudinal steel =	60	ksi
Thickness of concrete cover =	1.15	in.

Table 3.59. MFAD foundation properties input for DS 22-2

Outer diameter of shaft =	3.00	ft
Stick up above ground level =	0.00	ft
Depth of embedment =	15.00	ft
Depth to GWT =	15	ft

3.5.5.3 Foundation Loading and Instrumentation

The horizontal load was applied to the top of the foundation by a winch and pulley system. The load was applied approximately 2.5 ft above the ground to a wide-flanged beam that was attached to the top of the foundation. The applied load was measured using a 200 kip capacity strain gauge load cell that was accurate to ± 0.036 kips. Lateral deflection at the ground surface was measured using two dial gauges placed on opposite sides of the foundation along the line of loading. The dial gauges were accurate to ± 0.001 in. The rotation of the top of foundation was measured using a tiltmeter that was placed on the wide flange beam that was affixed to the top of the foundation. The tiltmeter was accurate to ± 0.016 degrees. Soil pressure cells were placed along the front and back of the foundation excavation with respect to the direction of the applied load. The soil pressure cells were placed vertically along the entire depth of the foundation excavation. Additionally, two soil pressure cells were placed on either side of one of the center cells so all three cells were on the same horizontal plane. These two cells were placed at 30 and 45 degrees, respectively, from the line of loading on the loaded side of the foundation.

The top of the foundation was placed at the ground surface in the *LPile*, *DFSAP*, and *MFAD* models, and the equivalent loads from the load test were applied to the top of the foundation. The maximum horizontal and moment load applied to DS 22-1 was approximately 169 kips and 423 kip-ft, respectively, resulting in maximum groundline deflection of approximately 3.2 in. The maximum horizontal and moment load applied to DS 22-2 was approximately 127 kips and 318 kip-ft, respectively, resulting in maximum groundline deflection of approximately 1.5 in. The loads that were applied to DS 22-1 and DS 22-2 in each model are shown in Table 3.60 and Table 3.61, respectively.

Table 3.60. Loads applied to top of DS 22-1 in LPile, DFSAP, and MFAD

Load Number	LPile			DFSAP / MFAD		
	Lateral Load (lb)	Moment (lb-in.)	Axial Load (lb)	Lateral Load (kips)	Moment (kip-ft)	Axial Load (kips)
1	16171	485142	0	16.17	40.43	0.00
2	25821	774618	0	25.82	64.55	0.00
3	40011	1200315	0	40.01	100.03	0.00
4	49354	1480629	0	49.35	123.39	0.00
5	66277	1988298	0	66.28	165.69	0.00
6	84806	2544183	0	84.81	212.02	0.00
7	99308	2979249	0	99.31	248.27	0.00
8	113782	3413472	0	113.78	284.46	0.00
9	127876	3836274	0	127.88	319.69	0.00
10	143518	4305531	0	143.52	358.79	0.00
11	156678	4700334	0	156.68	391.69	0.00
12	169000	5070000	0	169.00	422.50	0.00

Table 3.61. Loads applied to top of DS 22-2 in LPile, DFSAP, and MFAD

Load Number	LPile			DFSAP / MFAD		
	Lateral Load (lb)	Moment (lb-in.)	Axial Load (lb)	Lateral Load (kips)	Moment (kip-ft)	Axial Load (kips)
1	20000	600000	0	20.00	50.00	0.00
2	30000	900000	0	30.00	75.00	0.00
3	40000	1200000	0	40.00	100.00	0.00
4	50000	1500000	0	50.00	125.00	0.00
5	60000	1800000	0	60.00	150.00	0.00
6	70000	2100000	0	70.00	175.00	0.00
7	80000	2400000	0	80.00	200.00	0.00
8	90000	2700000	0	90.00	225.00	0.00
9	100000	3000000	0	100.00	250.00	0.00
10	110000	3300000	0	110.00	275.00	0.00
11	120000	3600000	0	120.00	300.00	0.00
12	127000	3810000	0	127.00	317.50	0.00

3.5.6 Load Test 23 in Ontario, Canada

The results of a large-scale lateral load test program were presented by Ismael and Klym (1981). The load tests were conducted at a site located in Ontario, Canada. The soils at the site within the depth of the foundation consisted of dense sand with silt and trace clay. Two identical test foundations were constructed with diameters of 3 ft and embedment depths of 21 ft, which resulted in a *D/B* ratio of 7. Both foundations DS 23-1 and 23-2 met the experimental criteria and will be used in this investigation.

3.5.6.1 Soil Profile and Properties

A field investigation was performed to establish the stratigraphy of the site, the groundwater table location, and the engineering properties of the soil. The field investigation consisted of drilling one borehole to a depth of 61.5 ft and performing SPT tests and dynamic cone penetration tests. Samples were recovered at 5 ft intervals for laboratory testing. Laboratory testing included soil classification, moisture contents, densities, and hydrometer tests. The engineering properties of the soil were estimated from the results of the in-situ tests and the laboratory tests. The methods outlined in Section 3.3.3 were used in conjunction with the reported in-situ test data and laboratory data to estimate the values of the required soil properties for each analysis method. These values are presented in Table 3.62. It can be seen in Table 3.62 that there are multiple values for some of the soil parameters. The design value was estimated from the range of values for each parameter, which is shown in Table 3.63. The discretization of sub-layers and the design values for each required soil property for *LPile*, *DFSAP*, and *MFAD* are shown in Table 3.64, Table 3.65, and Table 3.66, respectively.

Table 3.62. Estimation of required soil properties for Load Test 23

Layer Depth		N [1]		γ_d [2]	γ [3]		ϕ [4]	ϕ [5]	ϕ [6]	D_R [7]	k [8]	k [9]	E_p [10]	E_p [11]	E_p [12]
Top (ft)	Bottom (ft)	(blows/ft)	w [1]	(pcf)	(pcf)	σ_{v0}/P_a	(deg)	(deg)	(deg)	(%)	(pci)	(pci)	(ksi)	(ksi)	(ksi)
0.0	2.0	20	0.205	110	133	0.06	-	33.1	38.9	91	186	94	1.8	1.0	0.4
2.0	7.5	20	0.205	110	133	0.30	-	33.1	38.9	91	186	94	4.4	1.0	1.8
7.5	12.5	24	0.195	110	131	0.63	-	34.3	39.9	86	166	106	4.0	1.1	1.4
12.5	17.5	17	0.199	110	132	0.94	42.4	32.2	38.0	70	105	137	4.8	0.9	2.2
17.5	21.0	6	0.210	100	121	1.19	32.3	28.7	32.1	66	95	49	5.9	0.4	2.9

Notes

(1) From reported test data

(2) From Kulhawy and Mayne (1990)

(3) $\gamma = \gamma_d(1+w)$

(4) From Schmertmann (1975)

(5) From Peck, Hanson, and Thornburn (1974)

(6) From Meyerhoff (1956)

(7) From Holtz and Gibbs (1979)

(8) From API (1993) using D_R

(9) From API (1993) using ϕ

(10) From Callanan and Kulhawy (1980)

(11) From Ohya et al. (1982)

(12) From Schmertmann (1970)

Table 3.63. Design value of soil properties for Load Test 23

Layer Depth		γ	γ'	ϕ	k	E_p
Top (ft)	Bottom (ft)	(pcf)	(pcf)	(deg)	(pci)	(ksi)
0.0	2.0	133	133	36	140	1.1
2.0	7.5	133	70	36	140	2.2
7.5	12.5	131	69	37	136	2.0
12.5	17.5	132	69	39	121	2.4
17.5	21.0	121	59	32	72	2.9

Table 3.64. LPile sub-layer properties input for DS 23-1 and DS 23-2

	Layer Depth							
LPile Soil Type	Top (ft)	Bottom (ft)	γ (pcf)	γ' (pcf)	φ (deg)	S_u (psf)	ε_{50}	k (pci)
Sand	0.0	2.0	133	133	36.0	-	-	140
Sand	2.0	7.5	133	70	36.0	-	-	140
Sand	7.5	12.5	131	69	37.0	-	-	136
Sand	12.5	17.5	132	69	39.0	-	-	121
Sand	17.5	21.0	121	59	32.0	-	-	72

Table 3.65. LPile sub-layer properties input for DS 23-1 and DS 23-2

DFSAP Soil Type	Layer Thickness (ft)	γ' (pcf)	φ' (deg)	S_u (psf)	ε_{50}
Sand	2.0	133	36.0	-	-
Sand	5.5	70	36.0	-	-
Sand	5.0	69	37.0	-	-
Sand	5.0	69	39.0	-	-
Sand	3.5	59	32.0	-	-

Table 3.66. LPile sub-layer properties input for DS 23-1 and DS 23-2

MFAD Layer Type	Depth to Bottom of Layer (ft)	γ (pcf)	φ (deg)	S_u (ksf)	E_p (ksi)
Soil	2.0	133	36.0	-	1.1
Soil	7.5	133	36.0	-	2.2
Soil	12.5	131	37.0	-	2.0
Soil	17.5	132	39.0	-	2.4
Soil	21.0	121	32.0	-	2.9

3.5.6.2 Foundation Properties

As previously noted, the test foundations DS 23-1 and DS 23-2 were identical. The diameter and embedment depth of the test foundations was 21 ft and 7 ft, respectively, which resulted in a *D/B* ratio of 7. The unconfined compressive strength of the concrete was 3,000 psi. The modulus of elasticity was estimated to be 3.12 x 10^6 psi using Equation (3.4). The longitudinal reinforcement consisted of (8) #11 bars placed at 3 in. o.c. from the face of the foundation, which results in a reinforcement ratio of 1.24%. It was not specified whether shear reinforcement, i.e., transverse reinforcement, was used, so it was assumed that the minimum transverse steel reinforcement required by ACI 318-11 was placed over the entire length of the foundation. Assuming #3 bars are used for transverse reinforcement, the spacing was calculated to be 8.5 in. using Equation (3.3) and the transverse shear reinforcement ratio is 0.13%. The modulus of elasticity of the reinforcement is assumed to be 29,000 ksi and the yield strength is assumed to be 60,000 ksi. A schematic drawing of the foundation is shown in Figure 3.22. For DS 23-1 and DS 23-2, the foundation input properties for *LPile*, *DFSAP*, and *MFAD* are shown in Table 3.67, Table 3.68, and Table 3.69, respectively.

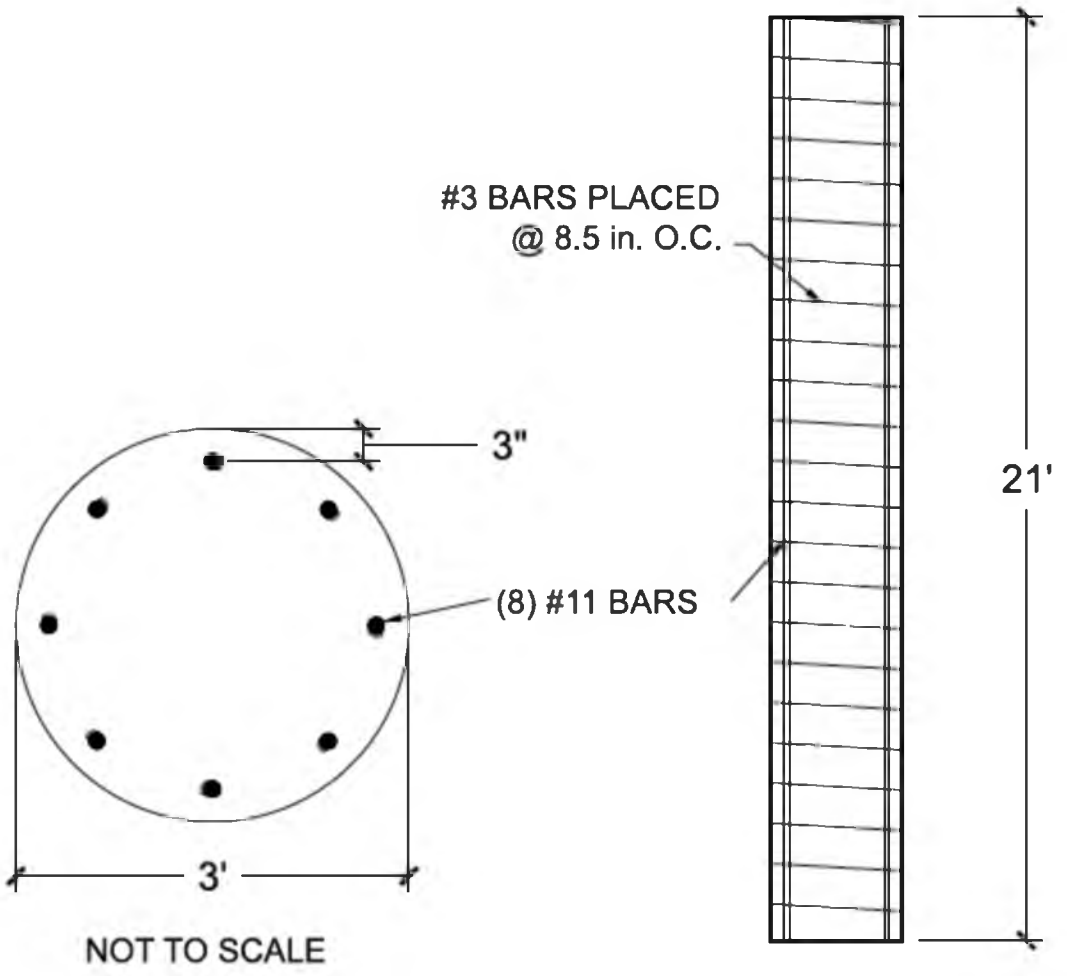

Figure 3.22. Schematic drawing of DS 23-1 and DS 23-2

Table 3.67. LPile foundation properties input for DS 23-1 and DS 23-2

Pile length =	21	ft
Pile diameter =	36	in.
Area =	1018	$in.^2$
Moment of inertia =	1319167	$in.^4$
Modulus of elasticity =	3122019	psi
Concrete comp. strength =	3000	psi
Longitudinal rebar =	8 #11	
Concrete cover to edge of bar =	2.30	in.
Rebar yield strength =	60000	psi
Rebar modulus of elasticity =	29000000	psi

Table 3.68. DFSAP foundation properties input for DS 23-1 and DS 23-2

Length of shaft =	21.00	ft
Length of shaft above ground =	0.00	ft
Outer diameter of shaft =	3.00	ft
Transverse steel ratio =	0.13	%
Concrete comp. strength =	3.00	ksi
Longitudinal steel ratio =	1.24	%
Yield stress of longitudinal steel =	60	ksi
Thickness of concrete cover =	2.30	in.

Table 3.69. MFAD foundation properties input for DS 23-1 and DS 23-2

Outer diameter of shaft =	3.00	ft
Stick up above ground level =	0.00	ft
Depth of embedment =	21.00	ft
Depth to GWT =	2	ft

3.5.6.3 Foundation Loading and Instrumentation

The lateral load was applied by jacking the two foundations apart with two 200-kip hydraulic jacks placed in series and a reaction beam placed between the two foundations. The load was applied to the foundations at the ground surface, and as such, there was no applied moment. Lateral deflection of each foundation at the ground surface was measured using a dial gauge that was placed behind the foundation in the line of loading. Strain gauges were placed in diametric pairs at three elevations along the foundation to measure bending strain during loading. Soil pressure cells were installed at the soil-foundation interface of both foundations to measure the soil pressure that develops during loading. Two soil pressure cells were placed on the back of the foundation, i.e., the side opposite the loading jack, in the line of loading at depths of 2 ft

and 10 ft. Two additional soil pressure cells were placed on the front of the foundation in the line of loading at depths of 15 ft and 20 ft. An inclinometer casing was placed along the entire length of DS 23-2 to allow measurement of the slope of the foundation.

The maximum applied horizontal load that was applied to both foundations was 120 kips, which resulted in groundline deflections of approximately 1.76 and 2.31 in. for DS 23-1 and DS 23-2, respectively. The top of the foundation was placed at the ground surface in the *LPile*, *DFSAP*, and *MFAD* models, and the equivalent loads from the load test were applied to the top of the foundation. The loads applied to the top of the DS 23-1 and DS 23-2 in each model are shown in Table 3.70 and Table 3.71, respectively.

Table 3.70. Loads applied to top of DS 23-1 in LPile, DFSAP, and MFAD

	LPile			DFSAP / MFAD		
Load Number	Lateral Load (lb)	Moment (lb-in.)	Axial Load (lb)	Lateral Load (kips)	Moment (kip-ft)	Axial Load (kips)
1	19752	0	0	19.75	0.00	0.00
2	35716	0	0	35.72	0.00	0.00
3	52717	0	0	52.72	0.00	0.00
4	72414	0	0	72.41	0.00	0.00
5	86097	0	0	86.10	0.00	0.00
6	96033	0	0	96.03	0.00	0.00
7	103925	0	0	103.92	0.00	0.00
8	110013	0	0	110.01	0.00	0.00
9	120000	0	0	120.00	0.00	0.00

Table 3.71. Loads applied to top of DS 23-2 in LPile, DFSAP, and MFAD

Load Number	LPile			DFSAP / MFAD		
	Lateral Load (lb)	Moment (lb-in.)	Axial Load (lb)	Lateral Load (kips)	Moment (kip-ft)	Axial Load (kips)
1	13784	0	0	13.78	0.00	0.00
2	21631	0	0	21.63	0.00	0.00
3	29646	0	0	29.65	0.00	0.00
4	37660	0	0	37.66	0.00	0.00
5	43170	0	0	43.17	0.00	0.00
6	57779	0	0	57.78	0.00	0.00
7	73323	0	0	73.32	0.00	0.00
8	94076	0	0	94.08	0.00	0.00
9	101097	0	0	101.10	0.00	0.00
10	112000	0	0	112.00	0.00	0.00
11	120000	0	0	120.00	0.00	0.00

3.5.7 Load Test 75 in Hawthorne, California

The results of a large-scale lateral load test program were presented by Janoyan, Stewart, and Wallace (2001). The load test was conducted at a site in Hawthorne, CA. The soils at the site primarily consisted of stiff clay with interbedded layers of silt and sand. The test foundation had a diameter and embedded depth of 6.5 ft and 48 ft, respectively, which resulted in a D/B ratio of 7.4. It should be noted that the test foundation was constructed with an integrated concrete column, which had a diameter and length of 6 ft and 40 ft, respectively.

3.5.7.1 Soil Profile and Properties

The soil field investigation was extensive, and included four seismic cone penetration test (SCPT) soundings, four CPT soundings, three rotary-wash borings with SPT testing, down-hole suspension logging of shear wave velocities, pressuremeter

testing (PMT), and excavation mapping of one test pit. Samples for laboratory testing were obtained from the borings using thin-walled Pitcher tube samplers and split-barrel samplers and were hand-carved from the test pit. Laboratory testing included moisture content, Atterberg limits, sieve and hydrometer, one-dimensional consolidation, and UU triaxial compression testing. A generalized soil profile is shown along with the results of the field investigation and laboratory tests in Figure 3.23.

The information presented in Figure 3.23 was used in conjunction with the methods outlined in Section 3.3 to estimate the values of the required soil properties for each analysis method. These values are presented in Table 3.72

It can be seen in Table 3.72 that ε_{50} was estimated using Figure 3.12 and reported values of s_u despite the fact that values for ε_{50} were reported from laboratory testing. These values are presented so a comparison can be made between the measured value and the value estimated by *LPile*. The design values that were estimated from Table 3.72 are shown in Table 3.73, respectively.

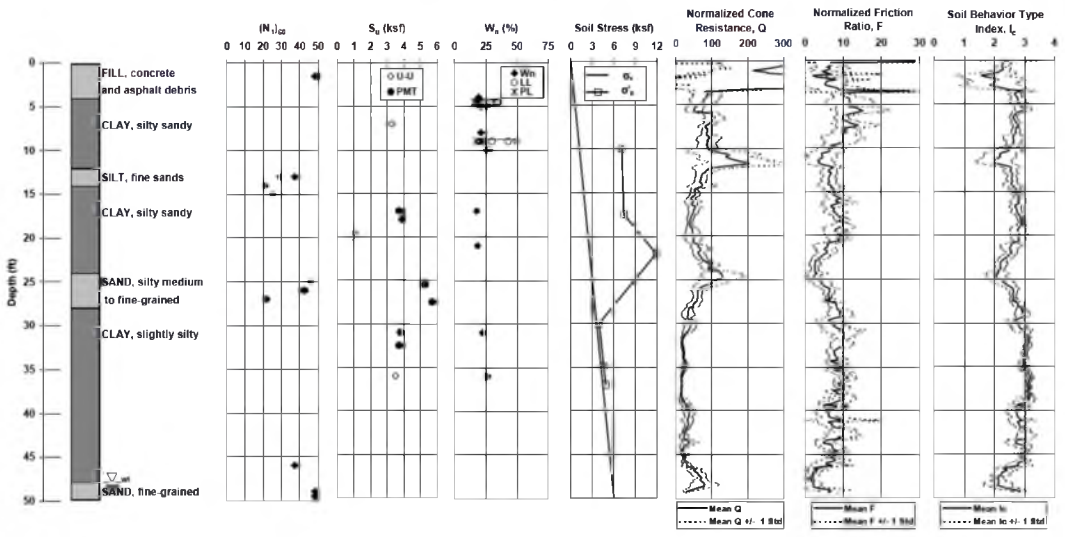

Figure 3.23. Generalized soil profile and results from laboratory tests and field investigation for Load Test 75 (Janoyan, Stewart, & Wallace, 2001)

Table 3.72. Estimation of required soil properties for Load Test 75

Layer Depth		q_c [1]	γ [1]		S_u [1]				E_p [4]	E_p [5]	E_p [6]	E_p [7]
Top (ft)	Bottom (ft)	(ksf)	(lb/ft^3)	σ_{v0}/P_a	(ksf)	N [2]	ε_{50} [1]	ε_{50} [3]	(ksi)	(ksi)	(ksi)	(ksi)
0.0	3.0	80	120	0.09	-	-	-	-	-	-	-	-
3.0	11.0	100	120	0.40	3.25	24	0.003	0.0058	2.1	11.8	2.1	7.5
11.0	12.5	250	120	0.67	-	-	-	-	-	-	-	-
12.5	22.5	120	120	0.99	2.75	29	0.005	0.0063	1.7	8.9	2.4	3.8
22.5	27.5	230	120	1.42	-	-	-	-	-	-	-	-
27.5	48.0	120	120	2.14	3.50	29	0.004	0.0055	2.2	11.8	2.4	6.1
48.0	50.0	300	120	2.78	-	-	-	-	-	-	-	-

Layer Depth			ϕ [8]	ϕ [9]	ϕ [10]	ϕ [11]	ϕ [12]	ϕ [13]	D_R [14]	D_R [15]	k [16]	k [17]	E_p [18]	E_p [19]	E_p [20]
Top (ft)	Bottom (ft)	N [1]	(deg)	(deg)	(deg)	(deg)	(deg)	(deg)	(%)	(%)	(pci)	(pci)	(ksi)	(ksi)	(ksi)
0.0	3.0	48	-	40.4	43.8	34.6	47.9	40.8	91	32	140	340	6.6	1.7	6.6
3.0	11.0	-	-	-	-	-	-	-	-	-	-	-	-	-	-
11.0	12.5	28	45.8	35.4	40.8	39.9	41.6	41.4	70	66	175	300	4.0	1.2	2.6
12.5	22.5	-	-	-	-	-	-	-	-	-	-	-	-	-	-
22.5	27.5	38	44.3	38.1	42.5	39.4	41.1	39.2	66	64	160	310	5.5	1.5	3.5
27.5	48.0	-	-	-	-	-	-	-	-	-	-	-	-	-	-
48.0	50.0	44	46.1	39.5	43.3	41.3	42.5	38.8	66	71	180	320	6.0	1.6	4.1

(1) From reported test data
(2) From Kulhawy and Mayne (1990)
(3) ε50 determined from LPile Technical Manual (2013)
(4) From Davidson (1982) for cohesive soils
(5) From Poulos & Davis (1980) for cohesive soils
(6) From Ohya et al. (1982) for cohesive soils
(7) Estimated as s_u / ε_{50}
(8) From Schmertmann (1975)
(9) From Peck, Hanson, and Thornburn (1974)
(10) From Meyerhoff (1956) using SPT data
(11) From Meyerhoff (1956) using CPT data
(12) From Robertson and Campanella (1983) using CPT data
(13) From Kulhawy and Mayne (1990)
(14) From Holtz and Gibbs (1979)
(15) From Meyerhoff (1956) using CPT data
(16) From API (1993) using D_R
(17) From API (1993) using ϕ
(18) From Callanan and Kulhawy (1980)
(19) From Ohya et al. (1982)
(20) From Schmertmann (1970)

Table 3.73. Design value of soil properties for Load Test 75

Layer Depth		γ	γ'	ϕ	S_u		k	E_p
Top (ft)	Bottom (ft)	(pcf)	(pcf)	(deg)	(ksf)	ε_{50}	(pci)	(ksi)
0.0	3.0	120	120	43	-	-	240	5.0
3.0	11.0	120	120	-	3.25	0.003	-	4.5
11.0	12.5	120	120	41	-	-	235	2.6
12.5	22.5	120	120	-	2.75	0.005	-	3.0
22.5	27.5	120	120	42	-	-	235	3.5
27.5	48.0	120	120	-	3.50	0.004	-	4.1
48.0	50.0	120	58	42	-	-	250	3.9

3.5.7.2 Foundation Properties

The test foundation was constructed as a drilled shaft with an integrated concrete column. The diameter and embedded depth of the drilled shaft was 6.5 ft and 48 ft, respectively, which resulted in a *D/B* ratio of 7.4. The diameter and length of the concrete column was 6 ft and 40 ft, respectively. Unconfined compression tests were performed on several concrete cylinders, and the average unconfined compressive strength and modulus of elasticity were determined to be 6,100 psi and 3.5 x 10^6 psi, respectively. A steel reinforcement cage was constructed from 36 #14 longitudinal reinforcement bars and #8 transverse reinforcement hoops spaced at 6 in. o.c. The resulting longitudinal and transverse steel reinforcement ratio was 1.72% and 0.6%, respectively. The longitudinal bars were placed in bundled pairs at 7.85 in. o.c. from the face of the foundation, and 5.85 in. o.c. from the face of the concrete column, which resulted in the desired clear concrete cover of 7 in. and 4 in., respectively. Laboratory strength tests were performed on several samples of the rebar, and the average yield strength and modulus of elasticity of the rebar were determined to be 72 ksi and 29,000 ksi, respectively. A schematic drawing of the foundation is shown in Figure 3.24.

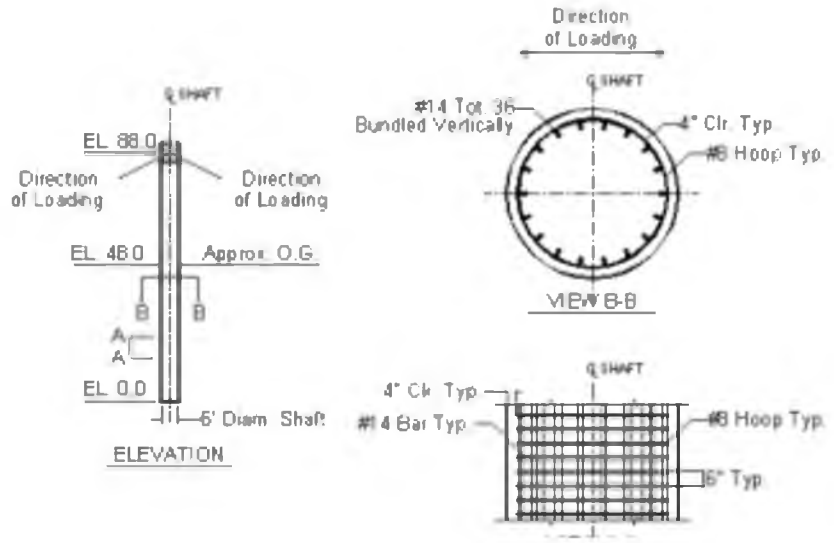

Figure 3.24. Schematic drawing of DS 75-1 (Janoyan, Stewart, & Wallace, 2001)

The foundation input properties for *LPile*, *DFSAP*, and *MFAD* are shown in Table 3.74, Table 3.75, and Table 3.76, respectively.

3.5.7.3 Foundation Loading and Instrumentation

The lateral load was applied to the top of the concrete column by a system of hydraulic jacks, loading frames, and steel cables. An embankment was constructed on opposite sides of the foundation that sloped upwards towards the top of the column. A loading frame was constructed on each embankment, and four hydraulic rams with capacity of 100 kips each were attached to the loading frames. The applied load was transferred from the hydraulic rams to the top of the concrete column through a steel cable. A load cell was placed between the hydraulic rams and the steel cable to measure the applied load at the top of the concrete column for each loading increment. A schematic of the loading system is shown in Figure 3.25.

Table 3.74. LPile foundation properties input for DS 75-1

Pile length =	48	ft
Pile diameter =	78	in.
Pile area =	4778	$in.^2$
Pile moment of inertia =	29071557	$in.^4$
Column length =	40	ft
Column diameter =	72	in.
Column area =	4072	$in.^2$
Column moment of inertia =	21106677	$in.^4$
Modulus of elasticity =	3500000	psi
Concrete comp. strength =	6100	psi
Longitudinal rebar =	36 #14	
Concrete cover to edge of bar (Pile) =	8.00	in.
Concrete cover to edge of bar (Col.) =	5.00	in.
Rebar yield strength =	71000	psi
Rebar modulus of elasticity =	29000000	psi

Table 3.75. DFSAP foundation properties input for DS 75-1

Length of concrete column =	40.00	ft
Outer diameter of concrete column =	6.00	ft
Trans. steel ratio of conc. column =	0.58	%
Long. steel ratio of conc. column =	2.03	%
Thickness of conc. cover (column) =	5.00	in.
Outer diameter of shaft =	6.50	ft
Transverse steel ratio of shaft =	0.55	%
Concrete comp. strength =	6.10	ksi
Longitudinal steel ratio of shaft =	1.72	%
Yield stress of longitudinal steel =	71	ksi
Thickness of concrete cover (shaft) =	8.00	in.

Table 3.76. MFAD foundation properties input for DS 75-1

Outer diameter of column =	6.00	ft
Outer diameter of shaft =	6.50	ft
Stick up above ground level =	40.00	ft
Depth of embedment =	48.00	ft
Depth to GWT =	48	ft

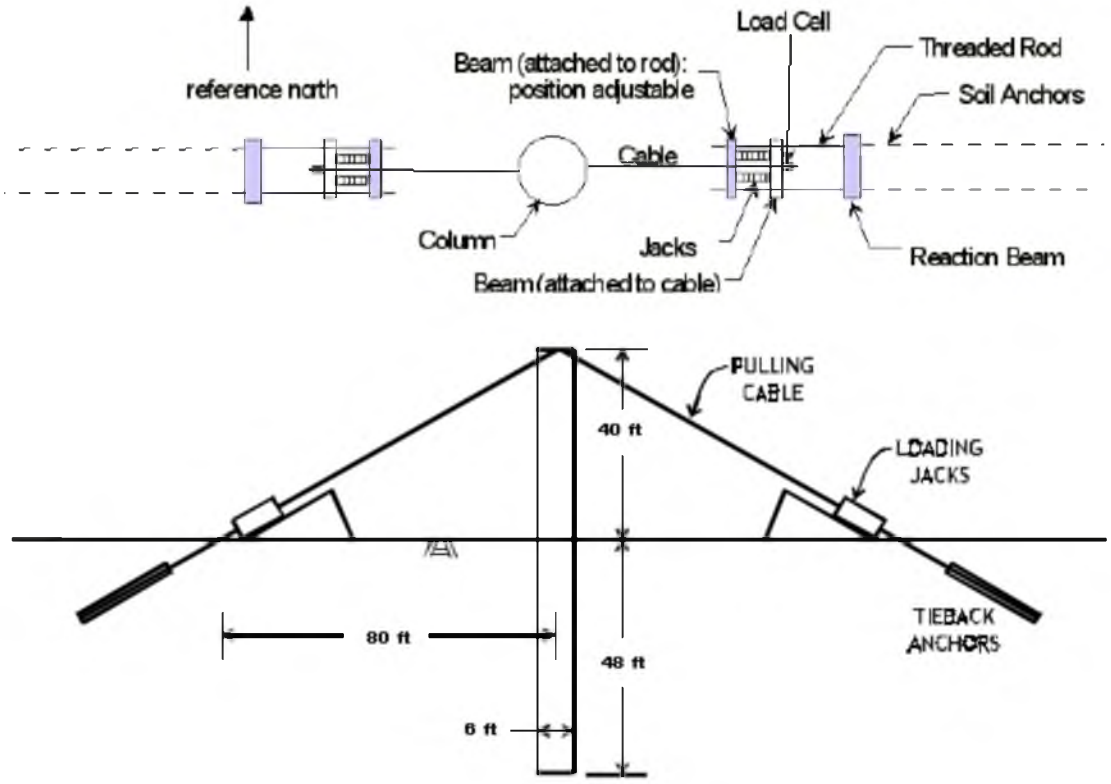

Figure 3.25. Schematic of loading system for DS 75-1 (Janoyan, Stewart, & Wallace, 2001)

Lateral deflection of the top of the concrete column was measured manually at each loading increment using a total station. The slope of the foundation was measured using 11 inclinometers placed down the center of the foundation. The bending strain was measured near the extreme fibers of the foundation using 32 fiber optic sensors, 60 electrical resistance strain gauges, and 32 extensometers. An additional 16 electrical resistance strain gauges were placed on the transverse reinforcement to measure the strains that develop within the transverse reinforcement during loading.

Soil pressure cells were installed at the soil-foundation interface of the foundation to measure the soil pressure that develops during loading. A total of 24 soil pressure cells were placed along the length of the foundation between depths of 3 ft and 45 ft at an

interval of 7 ft. At depths of 3, 10, and 17 ft, a soil pressure cell was placed on both sides of the foundation in the line of loading, and two additional soil pressure cells were placed on the loaded face of the foundation on either side of the center cell at angles of 30 and 60 degrees from the line of loading. At depths of 24, 31, 38, and 45 ft, a soil pressure cell was placed on both sides of the foundation in the line of loading.

The maximum applied horizontal and axial loads that were applied to the top of the concrete column were approximately 320 kips ad 150 kips, respectively. This applied load resulted in a maximum groundline displacement of approximately 6.9 in.

The models in *LPile*, *DFSAP*, and *MFAD* were set up with two different configurations. In the first configuration, the integrated concrete column was included in the model, and the lateral and axial loads were applied to the top of the integrated column at 40 ft above the ground surface. The applied loads for this configuration are shown in Table 3.77. In the second configuration, the integrated concrete column was not included in the model, and lateral and axial loads were applied to the top of the foundation at the ground surface, along with the moment caused by the laterally applied load and the p-Δ effect caused by deflection of the top of the integrated column. The applied loads for this configuration are shown in Table 3.78.

The pile deflections for the two model configurations in each analysis method were similar, and using either modeling approach did not appear to have a notable difference on the results.

3.5.8 Load Test 76 in Houston, TX

The results of a large-scale lateral load test program were presented by O'Neill, Vipulanandan, and Hassan (2000). The load tests were conducted at the National

Table 3.77. Loads applied to top of DS 75-1 in LPile, DFSAP, and MFAD when integrated column is included in the model

Load Number	LPile			DFSAP / MFAD		
	Lateral Load (lb)	Moment (lb-in.)	Axial Load (lb)	Lateral Load (kips)	Moment (kip-ft)	Axial Load (kips)
1	50000	0	23438	50.00	0.00	23.44
2	100000	0	46875	100.00	0.00	46.88
3	152000	0	71250	152.00	0.00	71.25
4	192000	0	90000	192.00	0.00	90.00
5	216000	0	101250	216.00	0.00	101.25
6	267000	0	125156	267.00	0.00	125.16
7	300000	0	140625	300.00	0.00	140.63
8	320000	0	150000	320.00	0.00	150.00

Table 3.78. Loads applied to top of DS 75-1 in LPile, DFSAP, and MFAD when integrated column is not included in the model

Load Number	LPile			DFSAP / MFAD		
	Lateral Load (lb)	Moment (lb-in.)	Axial Load (lb)	Lateral Load (kips)	Moment (kip-ft)	Axial Load (kips)
1	50000	24023438	23438	50.00	2001.95	23.44
2	100000	48093750	46875	100.00	4007.81	46.88
3	152000	73245000	71250	152.00	6103.75	71.25
4	192000	92700000	90000	192.00	7725.00	90.00
5	216000	104591250	101250	216.00	8715.94	101.25
6	267000	129661875	125156	267.00	10805.16	125.16
7	300000	146531250	140625	300.00	12210.94	140.63
8	320000	157200000	150000	320.00	13100.00	150.00

Geotechnical Experimentation Site – University of Houston (NGES-UH) in Houston, Texas. The soils at the site primarily consisted of stiff overconsolidated clay overlying stiff sandy clay with seams of sand. Two of the test foundations had diameters of 1.5 ft and two had diameters of 3.0 ft. Two of the test foundations had lengths of 20 ft and two had lengths of 35 ft. The resulting in *D/B* ratios for the test foundations ranged from 6.7 to 23.4. The only foundation from this load test program that met the experimental criteria was DS 76-1. The other foundations did not meet the experimental criteria because their *D/B* ratios were too high.

3.5.8.1 Soil Profile and Properties

The field investigation was not discussed in the paper presented by O'Neill, Vipulanandan, and Hassan (2000). Instead, the authors state that considerable information about the site is available in other references. A generalized subsurface profile is shown along with the results of a CPT sounding in Figure 3.26. It should be noted that the embedment depth of DS 76-1 is 20 ft (6.1 m), and as such, the foundation is only embedded within the overconsolidated lean clay layer.

The authors report that s_u and ε_{50} for this layer is 2.2 ksf and 0.007, respectively. The methods outlined in Section 3.3 were used to estimate the remaining values of the required soil properties for each analysis method. These values are presented in Table 3.79. The design values for the subsurface profile are shown in Table 3.80.

3.5.8.2 Foundation Properties

The test foundation was constructed as an augered cast-in-place foundation, which is technically different than a drilled shaft. The primary difference is that grout is

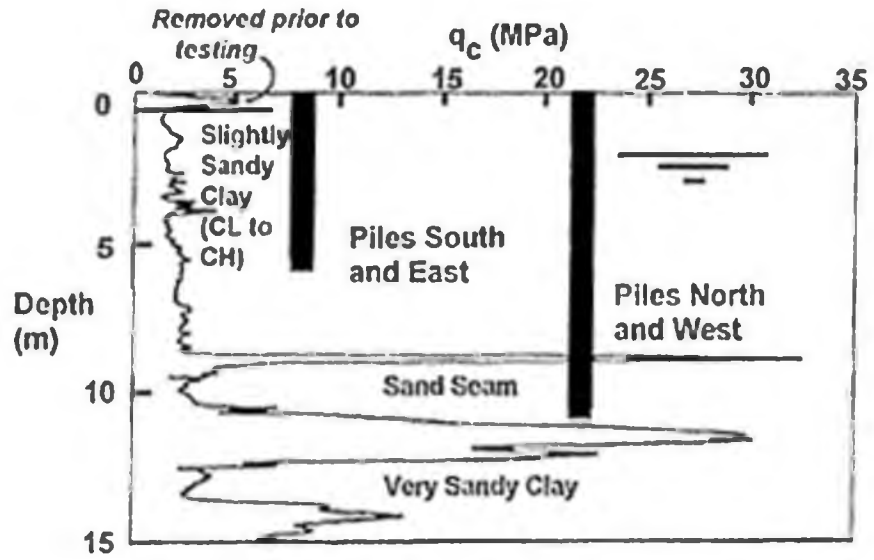

Figure 3.26. Generalized subsurface profile for Load Test 76 (O'Neill, Vipulanandan, & Hassan, 2000)

Table 3.79. Estimation of required soil properties for Load Test 76

Layer Depth		γ [1]	q_c [1]	S_u [1]			E_p [3]	E_p [4]	E_p [5]	E_p [6]
Top (ft)	Bottom (ft)	(pcf)	(ksf)	(ksf)	ε_{50} [1]	ε_{50} [2]	(ksi)	(ksi)	(ksi)	(ksi)
0.0	23.0	125	**28**	2.2	0.0070	0.0069	1.3	3.5	0.8	2.1

Notes

(1) From reported test data

(2) From LPile Technical Manual (2013)

(3) From Davidson (1982) for cohesive soils

(4) From Poulos and Davis (1980) for cohesive

(5) From Ohya et al. (1982) for cohesive soils

(6) Estimated as s_u / ε_{50}

Table 3.80. Design value of soil properties for Load Test 76

Layer Depth		γ	γ'	S_u		E_p
Top (ft)	Bottom (ft)	(pcf)	(pcf)	(ksf)	ε_{50}	(ksi)
0.0	23.0	125	125	2.2	0.0070	2.0

used instead of concrete, and the grout is pumped into the hole as the auger is retracted. The grout has similar compressibility to concrete, but the rupture strength is somewhat less. The design procedure and overall behavior is essentially the same as a drilled shaft.

The diameter and embedded depth of the test foundation was 3.0 ft and 20.0 ft, respectively, which resulted in a *D/B* ratio of 6.7. The engineering properties of the grout were by performing laboratory tests on 12 cylinders. The unconfined compressive strength and rupture strength of the grout was reported as 5,350 psi and 285 psi, respectively. The modulus of elasticity of the grout was reported as 4.05×10^6 psi.

A steel reinforcement cage was constructed from 8 #10 longitudinal reinforcement bars and #4 transverse reinforcement hoops spaced at 9 in. o.c. The resulting longitudinal and transverse steel reinforcement ratio was 1.0% and 0.2%, respectively. The longitudinal bars were placed at 6.1 in. o.c. from the face of the foundation, which resulted in 5 in. of clear concrete cover. Laboratory strength tests were performed on samples of the rebar, and the average yield strength and modulus of elasticity of the rebar were determined to be 70 ksi and 30,800 ksi, respectively. A schematic drawing of the foundation is shown in Figure 3.27.

3.5.8.3 Foundation Loading and Instrumentation

The lateral load was applied to the top of the foundation by placing a hydraulic jack in between the test foundation and the reaction foundation and jacking the foundations apart. The capacity of the hydraulic jack was not specified. The slope of the foundation was measured along the length of the foundation using an inclinometer placed along the neutral axis. No other instrumentation was reported.

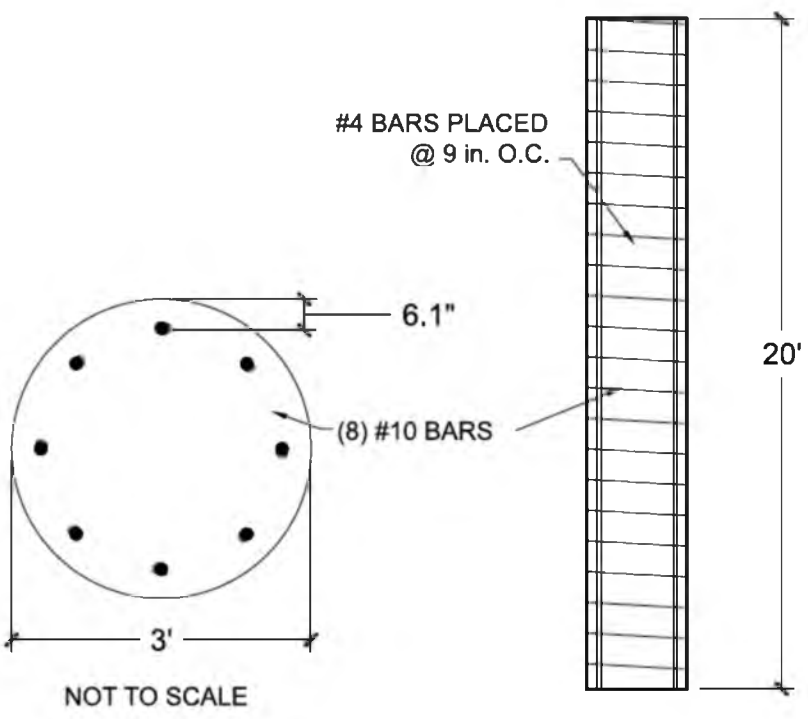

Figure 3.27. Schematic drawing of DS 76-1

The maximum applied horizontal load to the top of DS 76-1 was approximately 117 kips, which resulted in a groundline deflection of approximately 1.0 in. The top of the foundation was placed at 0.5 ft above the ground surface in the *LPile*, *DFSAP*, and *MFAD* models, and the equivalent loads from the load test were applied to the top of the foundation. The loads that were applied to the top of the foundation in each model are shown in Table 3.81.

The moment-curvature curve that is generated by *LPile* is generated from user-defined values of cross-sectional geometry of the pile, longitudinal rebar configuration, unconfined compressive strength of the concrete, yield strength of the longitudinal rebar, and the modulus of elasticity of the longitudinal rebar. The moment-curvature curve is also a function of the modulus of elasticity of the concrete and the rupture strength of the concrete; however, these values are calculated internally by *LPile* using Equations (3.4)

Table 3.81. Loads applied to top of DS 22-1 in LPile, DFSAP, and MFAD

Load Number	LPile			DFSAP / MFAD		
	Lateral Load (lb)	Moment (lb-in.)	Axial Load (lb)	Lateral Load (kips)	Moment (kip-ft)	Axial Load (kips)
1	25376	0	0	25.38	0.00	0.00
2	45034	0	0	45.03	0.00	0.00
3	55097	0	0	55.10	0.00	0.00
4	66505	0	0	66.51	0.00	0.00
5	79453	0	0	79.45	0.00	0.00
6	94120	0	0	94.12	0.00	0.00
7	105818	0	0	105.82	0.00	0.00
8	117372	0	0	117.37	0.00	0.00

and (3.5), respectively, and cannot be modified by the analyst. This can be problematic if these values were established from laboratory testing and differ from the values estimated by Equations (3.4) and (3.5), which is the case for the current load test.

It is not clear from the *DFSAP* documentation how the moment-curvature curve is established in *DFSAP*; however, the inputs are identical to the inputs in *LPile*, and the resulting moment-curvature curves are very similar to the curves generated by *LPile*. It is assumed that a similar section analysis is performed, and that the elastic modulus and rupture strength of concrete is calculated internally using Equations (3.4) and (3.5), respectively.

Because the measured values of modulus of elasticity and rupture strength of the grout used to construct DS 76-1 cannot be used by *LPile* or *DFSAP* to compute the correct moment-curvature curve, the moment-curvature curve was generated manually. A sectional analysis that is similar to the one performed by *LPile* was performed using MATLAB. Moment-curvature curves were generated using Equations (3.4) and (3.5) for the modulus of elasticity and the rupture strength of the grout, respectively, and the

values that were specified in Section 3.5.8.2. A moment-curvature curve was also generated using *LPile* and *DFSAP* so a comparison could be made between the four methods. These curves are shown in Figure 3.28.

The results shown in Figure 3.28 show that the moment-curvature curves are very similar for all four methods. The most noticeable difference between these curves is the presence of a dip after the initial linear portion of the curve for the manually generated curves and the curve generated by *DFSAP*. This dip begins to form at the onset of tensile cracking in the extreme fibers of the concrete when the tensile stress exceeds its rupture strength. As the bending curvature increases, the crack propagates towards the neutral axis, and the area of concrete in the compressive region decreases. Closer inspection of the data revealed that the compressive stress in the concrete also increases with increasing curvature, but at a slower rate than the propagation of the tensile crack; therefore, the moment capacity decreases until the crack propagation stabilizes and the compressive stress in the concrete begins to increase at a faster rate. It is not apparent from the *LPile* documentation why this decrease does not occur in the curve generated by *LPile*. Regardless, the results shown in Figure 3.28 show that the moment-curvature curve generated in MATLAB from the reported grout properties is reasonable, and that some degree of error will only be introduced in sections with curvature values less than approximately 3.5×10^{-5} rad/in.

The analyst has the option of specifying a user-defined moment-curvature relationship in *LPile*. Unfortunately, it is not possible to specify a user-defined moment-curvature relationship in *DFSAP*. As such, the *LPile* analysis was performed using this user-defined moment-curvature relationship and the *DFSAP* analysis was performed using the internally generated moment-curvature curve.

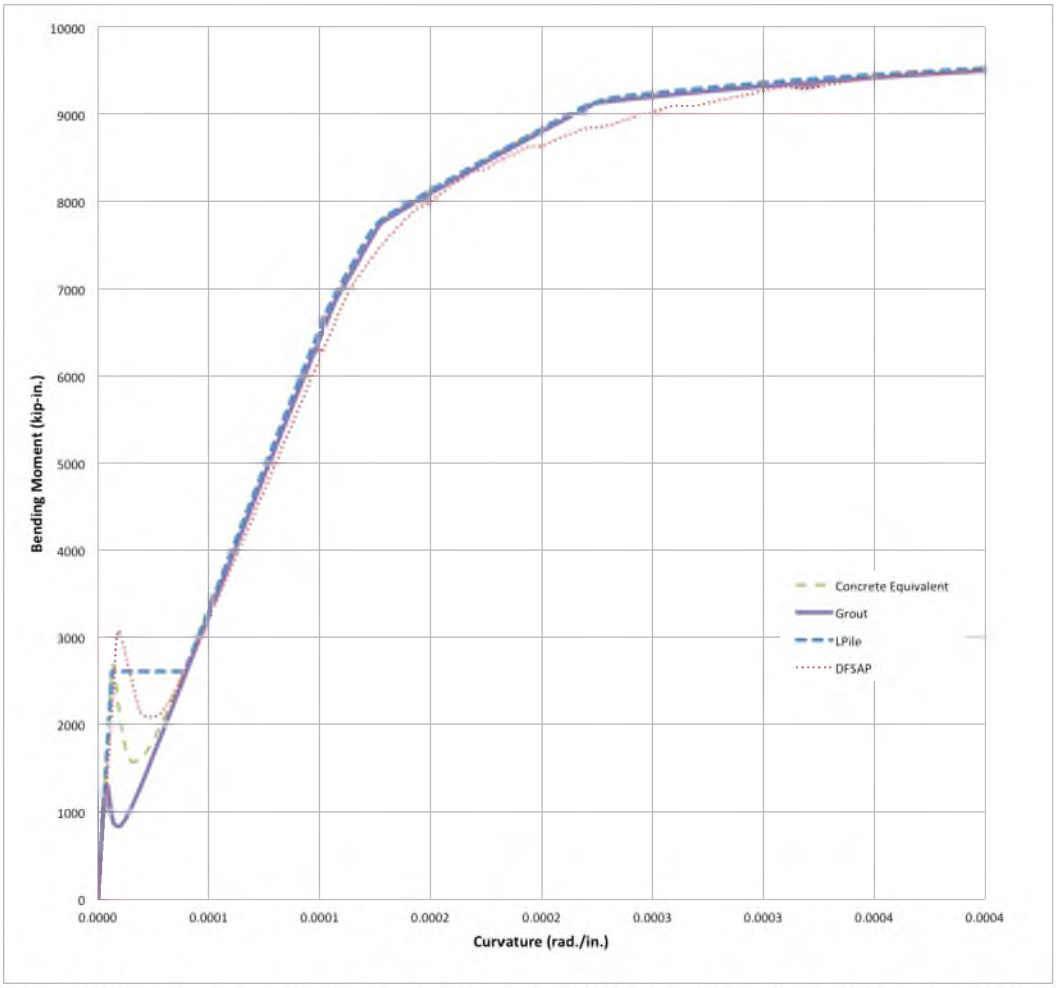

Figure 3.28. Moment-Curvature curves for DS 76-1 from four different methods

3.6 Parametric Study

A parametric study was performed to gain insight into how the input parameters affected the results of each analysis method. The parametric study was limited to two large-scale load tests to limit the scope and complexity of the parametric study. The two large-scale load tests that were chosen were DS 19-2 and DS 76-1. These load tests were chosen because each was embedded in an entirely granular or cohesive soil, their *D/B* ratios were similar, the strength parameters were specified in the literature, i.e., correlations did not have to be used to infer the strength properties, and their subsurface profiles were represented by only one and two sub-layers, respectively.

Parametric studies become more complex as the number of evaluated parameters increases and as the number of values that each parameter can take increases because the total number of simulations that must be performed is the product of the number of values of each parameter. As such, it was decided to limit the parametric study to cases where the subsurface soil profile was represented by only one sub-layer. DS 76-1 was the only large-scale load test that was conducted in a purely cohesive soil that was represented by one sub-layer, and there were no such tests in granular soils; however, DS 19-2 was conducted in two similar sub-layers of granular soil, so it was chosen to represent granular soils in the parametric study.

As discussed in Sections 2.3 and 2.5, it has been suggested that the diameter and rigidity of the foundation affects the response. As such, it was desirable to conduct the parametric study on two foundations with similar diameters and D/B ratios. DS 19-2 and DS 76-1 both have a diameter of 3 ft and a D/B ratio of 6.0 and 6.7, respectively. Additional geometric affects will not be considered in the parametric study.

As shown in Section 3.5.3, DS 19-2 was embedded in a purely granular soil that was idealized as two sub-layers. The soil properties that were included in the parametric study were ϕ and E_p for the *MFAD* model, ϕ and ε_{50} for the *DFSAP* model, and ϕ and k for the *LPile* model. As shown in Section 3.5.8, DS 76-1 was embedded in a purely cohesive soil that was idealized as a single homogeneous layer. The soil properties that were included in the parametric study were s_u and E_p for the *MFAD* model, and s_u and ε_{50} for the *DFSAP* and *LPile* models.

Upper bound and lower bound values were estimated for each of these soil properties, and the analysis was repeated for each upper bound and lower bound value while using the "best-estimate" values from the original analysis for the rest of the input

parameters. The assumption that is made using this approach is that the other parameters are reasonably accurate and that the results of each analysis are independent of the rest of the input parameters. To help validate this assumption, and to provide additional insight into the sensitivity of each model to these parameters, the deflection of the top of the foundation was estimated for a single load over a reasonable range for each parameter. In general, the constant load that was applied to the top of the foundation was the largest load reported in the test data because preliminary analyses showed that sensitivity increases with increasing load; however, the load was reduced for some of the sensitivity analyses due to some form of failure of the system or failure of the analysis method to obtain a solution.

4 RESULTS

Recall from Section 3.5 that 15 large-scale load tests were selected for analysis in this investigation. Of these large-scale load tests, eight were conducted in cohesive soils (DS 18-2, DS 20-2, DS 20-4, DS 20-5, DS 20-6, DS 22-1, DS 22-2, DS 76-1), six were conducted in granular soils (DS 11-1, DS 19-1, DS 19-2, DS 19-3, DS 23-1, DS 23-2), and one was conducted in alternating layers of granular and cohesive soils (DS 75-1). The results for each large-scale load test and analysis method are presented in this section. The results of the sensitivity analysis in which the soil properties for each model were increased and decreased by one standard deviation from the "best-estimate" values are also presented in this section.

In general, curves for applied lateral load vs. groundline deflection are presented for each analysis method using "best-estimate" input parameters, followed by a plot of predicted groundline deflection vs. measured groundline deflection in log-log scale. These plots are presented in log-log scale because the load-deflection curves generally increase exponentially with increasing applied load, and log-log scale shows the differences between the experimental and analytical results over the entire range of loading more clearly. It should be noted that each log-log scale plot of results shows a so-called line of equivalency, which is where the experimentally-observed groundline deflection is equal to the predicted groundline deflection from analysis. Data points that plot above this line represent analytical results that are conservative, while data points

that plot below this line represent analytical results that are unconservative. The figures presenting the results of the "best-estimate" input parameters are followed by a plot for each analysis method showing the results for ± 1 standard deviation of input parameters.

4.1 Load Test 11 Results

The lateral load vs. groundline deflection curves from the experimental and analytical results for DS 11-1 are presented in Figure 4.1a. The experimentally-observed groundline deflection is plotted against the predicted groundline deflection from each analysis method for DS 11-1 in Figure 4.1b.

The results shown in Figure 4.1a and Figure 4.1b show that *LPile* overpredicted groundline deflection for the entire range of loads used in the analysis. The *DFSAP* results are generally in good agreement with the experimentally-observed results at relatively small magnitudes of applied load, but tend to become increasingly unconservative with increasing lateral load. The *MFAD* results are in good agreement with the experimentally-observed results over the entire range of applied load. For this experiment, *LPile* estimated the most groundline deflection and *DFSAP* estimated the least groundline deflection over the entire range of applied load.

The lateral load vs. groundline deflection curves from the experimental and analytical results for DS 11-1 using soil input properties with ±1 standard deviation from the "best-estimate" values are presented in Figure 4.2. These results show that increasing or decreasing the soil input properties by one standard deviation does not result in equivalent deviation from the best-estimate input property values, but instead results in considerably more pile head deflection when soil input properties are reduced by one standard deviation. For this experiment, *MFAD* was the most sensitive to the change in

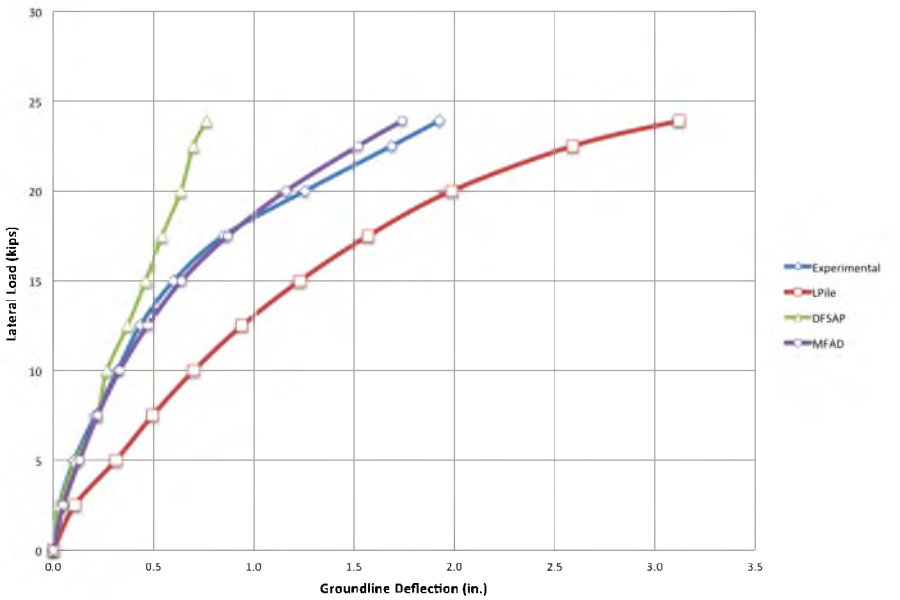

(a)

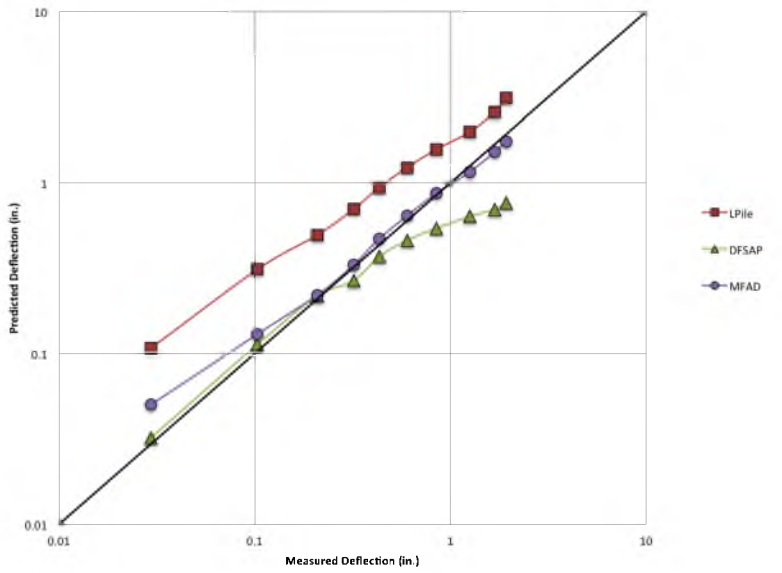

(b)

Figure 4.1. DS 11-1 results showing a) lateral load vs. groundline deflection curves, and b) predicted vs. measured groundline deflection curves in log-log scale

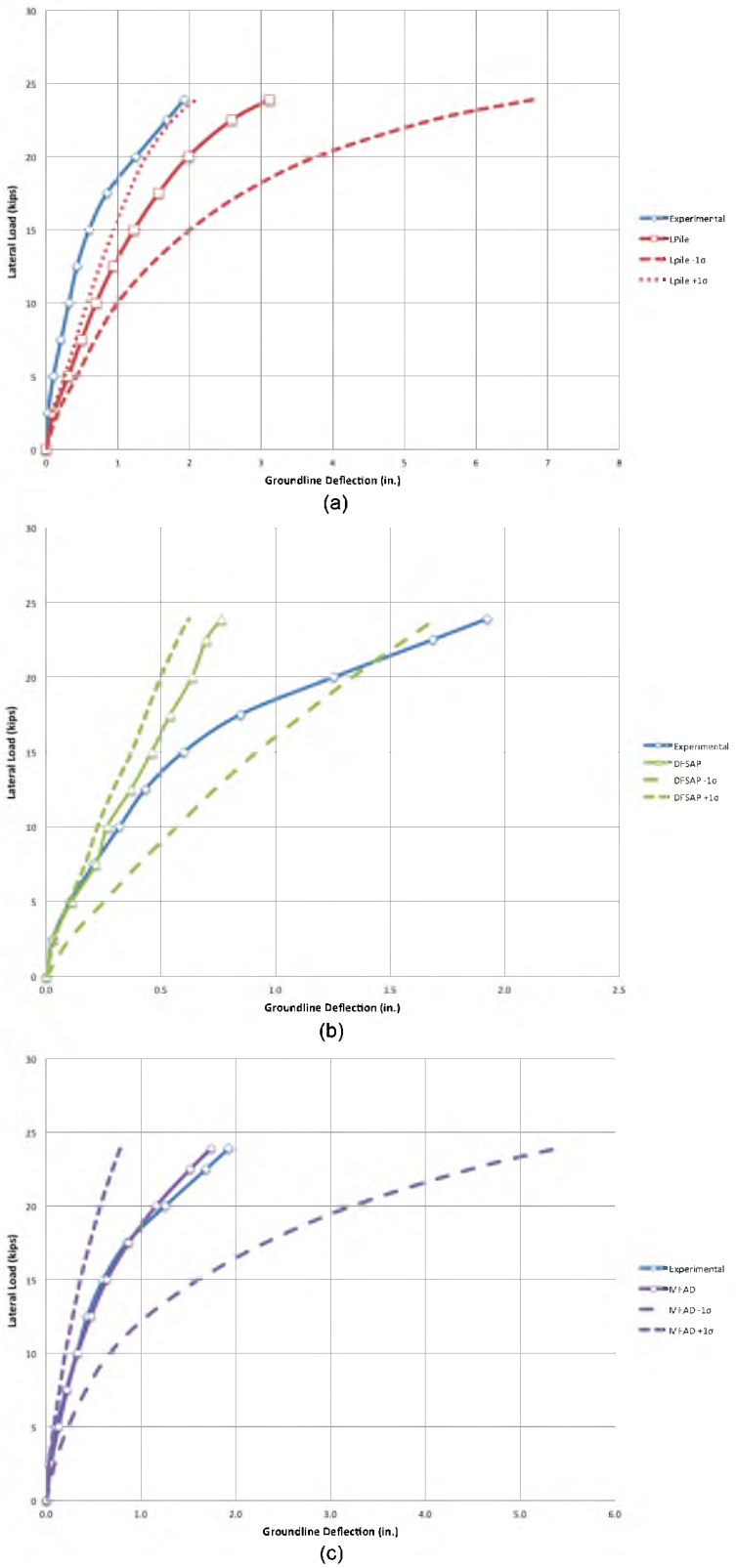

Figure 4.2. Load-deflection curves for DS 11-1 using ± 1 standard deviation input parameters for a) LPile, b) DFSAP, and c) MFAD models

soil input properties, while *DFSAP* was the least sensitive to the change in soil input properties. *MFAD* and *LPile* both exhibited higher sensitivity as the applied load increased, while *DFSAP* sensitivity exhibited little change over the entire range of applied load.

4.2 Load Test 18 Results

The lateral load vs. groundline deflection curves from the experimental and analytical results for DS 18-2 are presented in Figure 4.3a. The experimentally-observed groundline deflection is plotted against the predicted groundline deflection from each analysis method for DS 18-2 in Figure 4.3b.

The results shown in Figure 4.3a and Figure 4.3b show that *LPile* initially underpredicted groundline deflection and then overpredicted groundline deflection at larger magnitudes of applied load. The *DFSAP* results are generally in good agreement with the experimentally-observed results with only slight overprediction of groundline deflection at the initial applied load. The results show that *MFAD* slightly underpredicted groundline deflection over the entire range of applied load, and that the error between estimated and predicted groundline deflection did not change with applied load. For this experiment, *LPile* estimated the most groundline deflection and *MFAD* estimated the least groundline deflection for measured deflection greater than approximately 0.3 inches. It should be noted that *DFSAP* was unable to converge on a solution for loads greater than 257 kips.

The lateral load vs. groundline deflection curves from the experimental and analytical results for DS 18-2 using soil input properties with ±1 standard deviation from the "best-estimate" values are presented in Figure 4.4. These results show that increasing

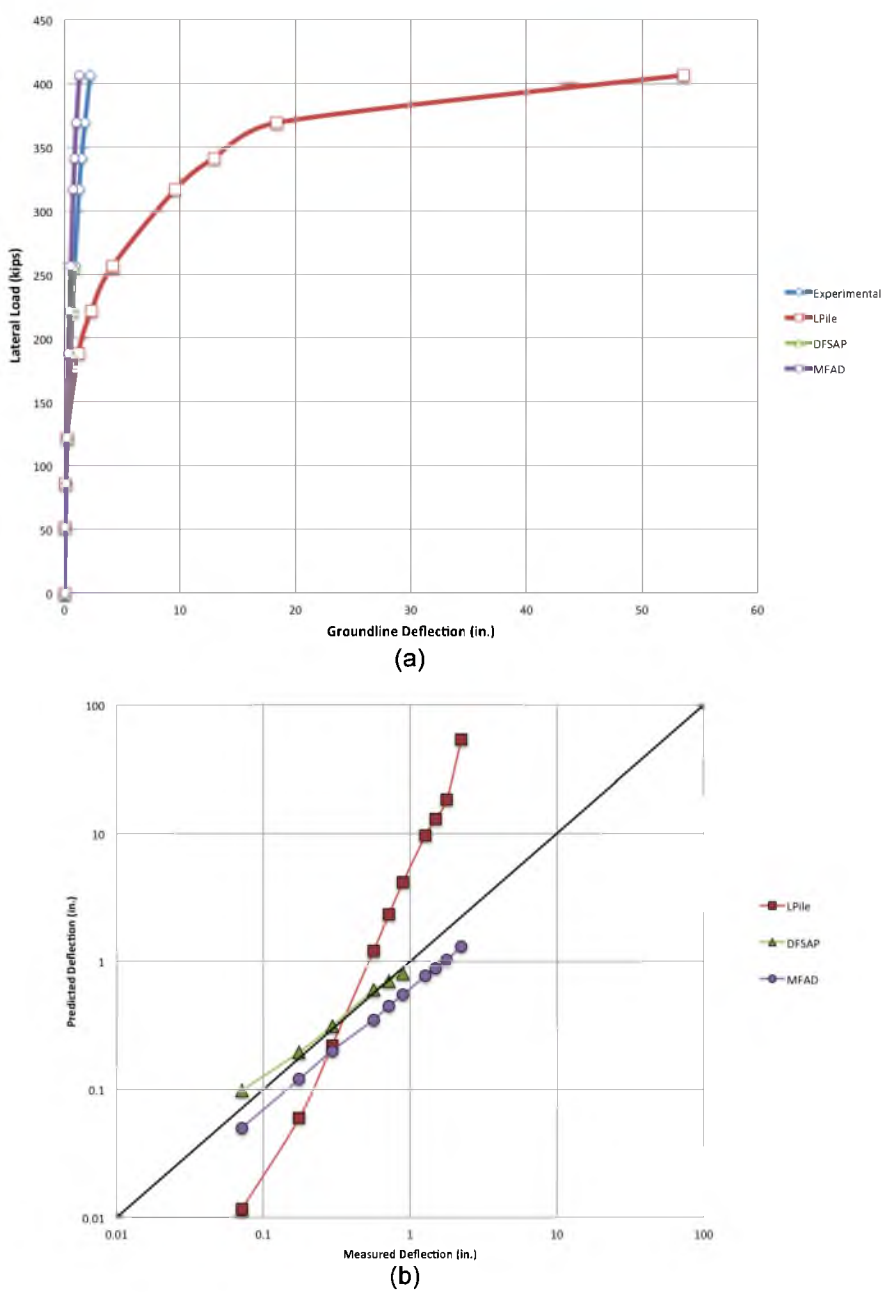

Figure 4.3. DS 18-2 results showing a) lateral load vs. groundline deflection curves, and b) predicted vs. measured groundline deflection curves in log-log scale

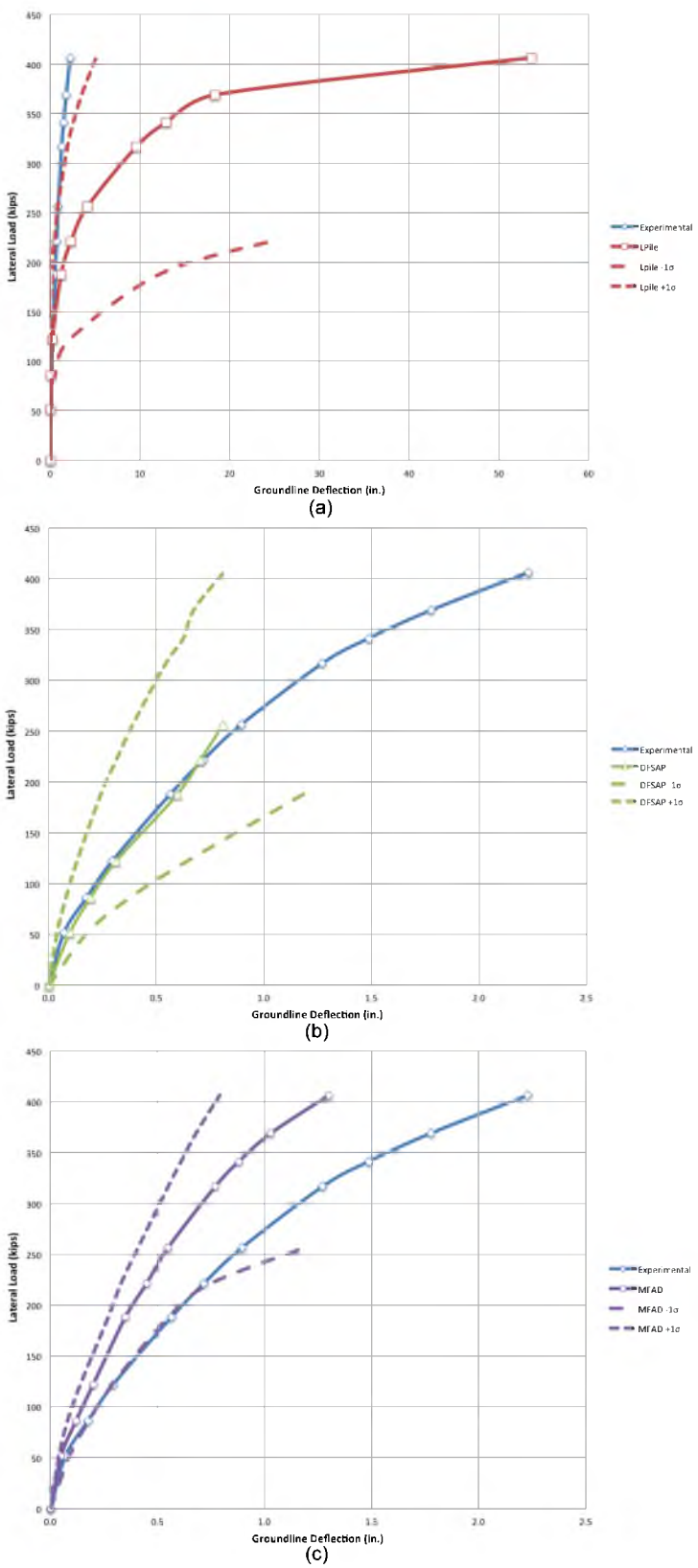

Figure 4.4. Load-deflection curves for DS 18-2 using ± 1 standard deviation input parameters for a) LPile, b) DFSAP, and c) MFAD models Load Test 19 Results

or decreasing the soil input properties by one standard deviation does not result in equivalent deviation from the best-estimate input property values, but instead results in considerably more pile head deflection when soil input properties are reduced by one standard deviation. For this experiment, *LPile* was the most sensitive to the change in soil input properties, while *MFAD* was slightly less sensitive than *DFSAP* to change in soil input properties. *MFAD* and *DFSAP* exhibited minor change in sensitivity over the entire range of applied load, while *LPile* exhibited increasing sensitivity to soil input properties with increasing load. It should be noted that all three analysis methods failed to reach solutions before the ultimate applied load of 407 kips for soil input properties of -1 standard deviation.

4.3 Load Test 19 Results

The lateral load vs. groundline deflection curves from the experimental and analytical results for DS 19-1 are presented in Figure 4.5a. The experimentally-observed groundline deflection is plotted against the predicted groundline deflection from each analysis method for DS 19-1 in Figure 4.5b.

The results shown in Figure 4.5a and Figure 4.5b show that *LPile* overpredicted groundline deflection for the entire range of loads used in the analysis. With the exception of the initial applied load, *MFAD* and *DFSAP* both overpredicted groundline deflection for the entire range of applied load. The deviation between measured groundline deflection and predicted groundline deflection increased for all three analysis methods with increasing applied load. For this experiment, *LPile* estimated the most groundline deflection and *DFSAP* estimated the least groundline deflection over the entire range of applied load. It should be noted that *LPile* was unable to converge on a

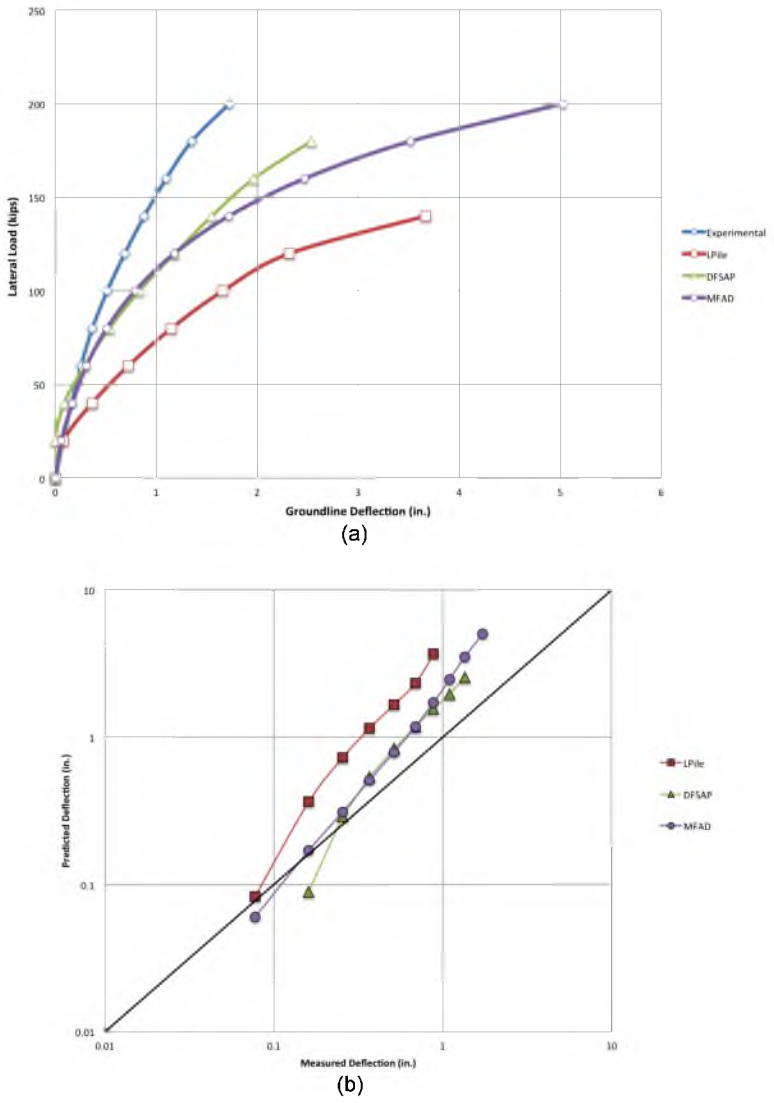

Figure 4.5. DS 19-1 results showing a) lateral load vs. groundline deflection curves, and b) predicted vs. measured groundline deflection curves in log-log scale

solution for loads greater than 140 kips and *DFSAP* was unable to converge on a solution for loads greater than 180 kips.

The lateral load vs. groundline deflection curves from the experimental and analytical results for DS 19-1 using soil input properties with ±1 standard deviation from the "best-estimate" values are presented in Figure 4.6. These results show that increasing or decreasing the soil input properties by one standard deviation does not result in

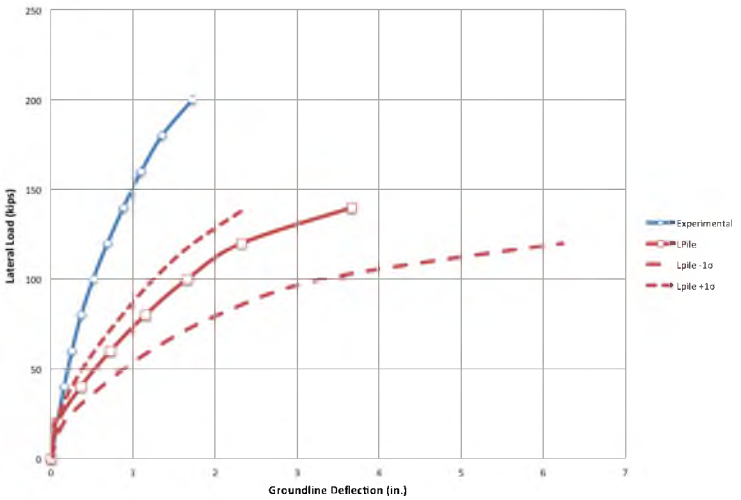

(a)

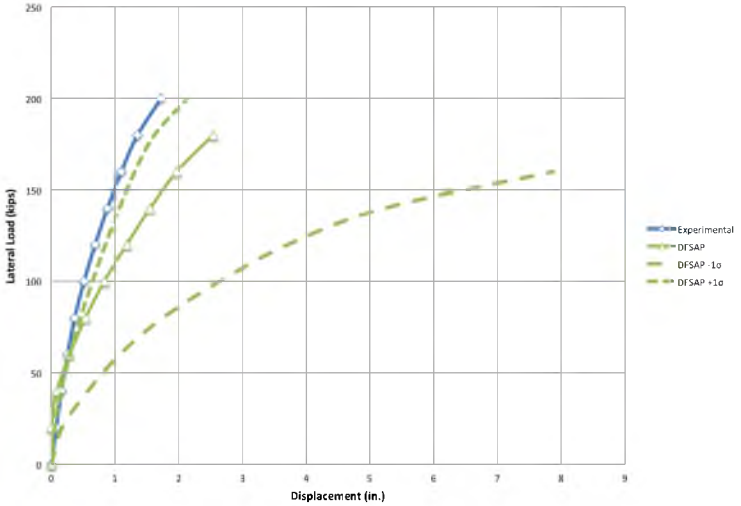

(b)

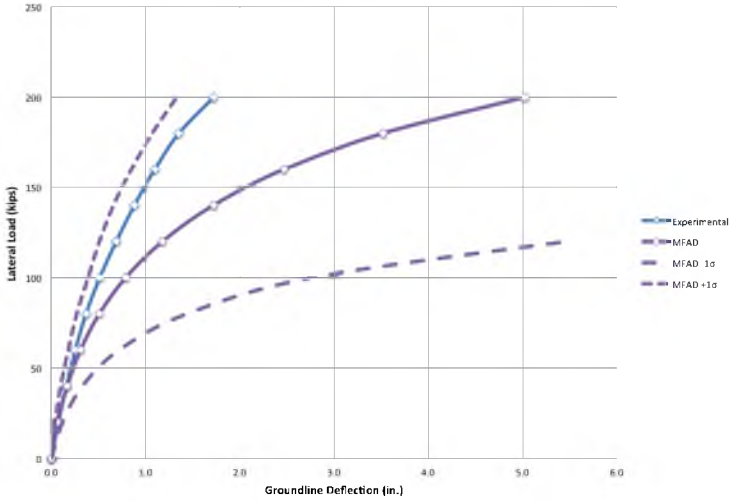

(c)

Figure 4.6. Load-deflection curves for DS 19-1 using ± 1 standard deviation input parameters for a) LPile, b) DFSAP, and c) MFAD models

equivalent deviation from the best-estimate input property values, but instead results in considerably more pile head deflection when soil input properties are reduced by one standard deviation. For this experiment, *MFAD* was the most sensitive to the change in soil input properties, while *LPile* was the least sensitive to the change in soil input properties. All three analysis methods exhibited higher sensitivity to soil input properties with increasing applied load; however, *MFAD* exhibited considerably higher sensitivity to soil input properties than the other two methods. It should be noted that all three analysis methods failed to reach solutions before the ultimate applied load of 200 kips for soil input properties of -1 standard deviation.

The lateral load vs. groundline deflection curves from the experimental and analytical results for DS 19-2 are presented in Figure 4.7a. The experimentally-observed groundline deflection is plotted against the predicted groundline deflection from each analysis method for DS 19-2 in Figure 4.7b.

The results shown in Figure 4.7a and Figure 4.7b show that all three analysis methods overpredicted groundline deflection for the entire range of applied load. The deviation between measured groundline deflection and predicted groundline deflection from *LPile* and *MFAD* increased with increasing applied load. For this experiment, *LPile* estimated the most groundline deflection and *DFSAP* estimated the least groundline deflection for measured groundline deflection greater than approximately 0.2 inches.

The lateral load vs. groundline deflection curves from the experimental and analytical results for DS 19-2 using soil input properties with ±1 standard deviation from the "best-estimate" values are presented in Figure 4.8. These results show that increasing or decreasing the soil input properties by one standard deviation does not result in equivalent deviation from the best-estimate input property values, but instead results in

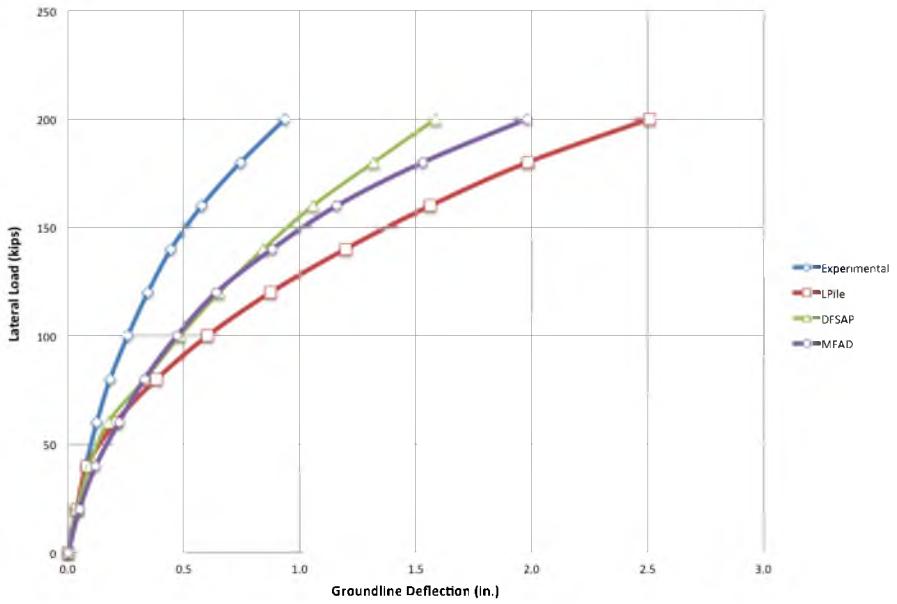

(a)

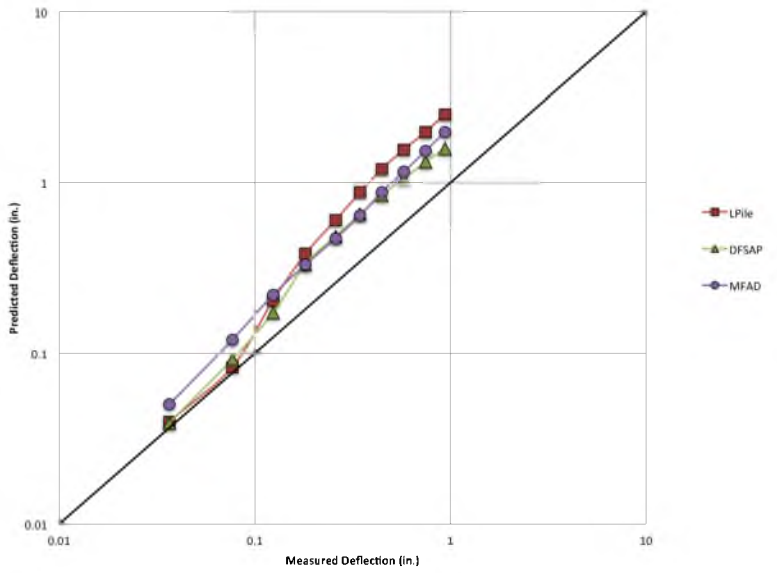

(b)

Figure 4.7. DS 19-2 results showing a) lateral load vs. groundline deflection curves, and b) predicted vs. measured groundline deflection curves in log-log scale

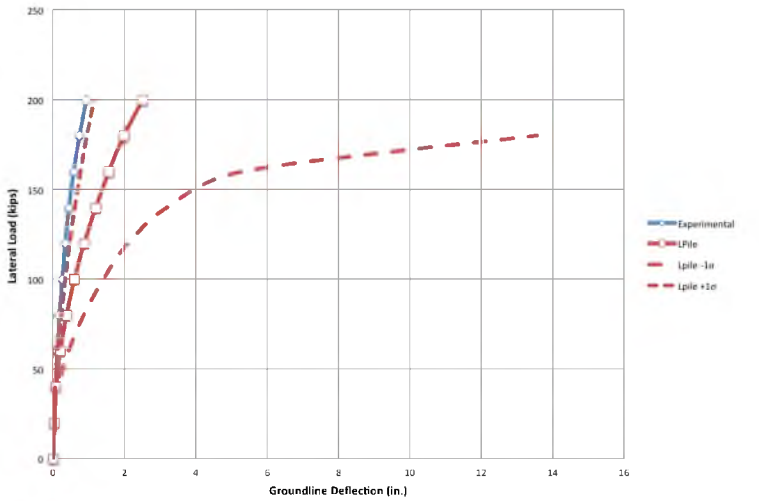

(a)

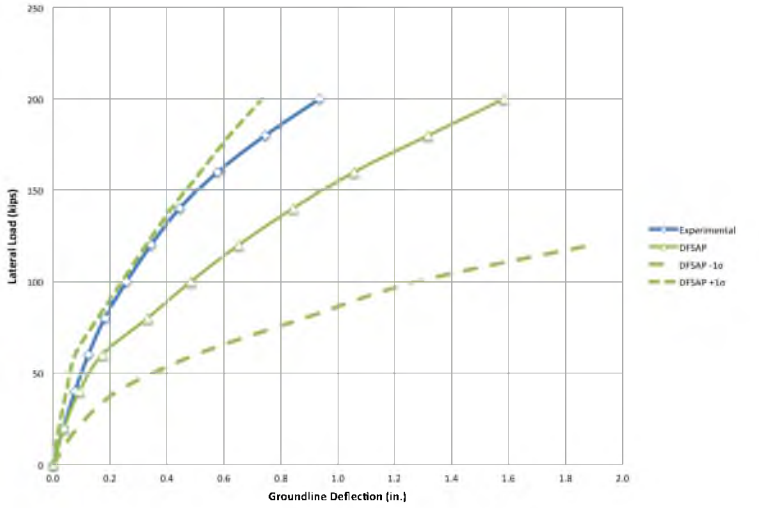

(b)

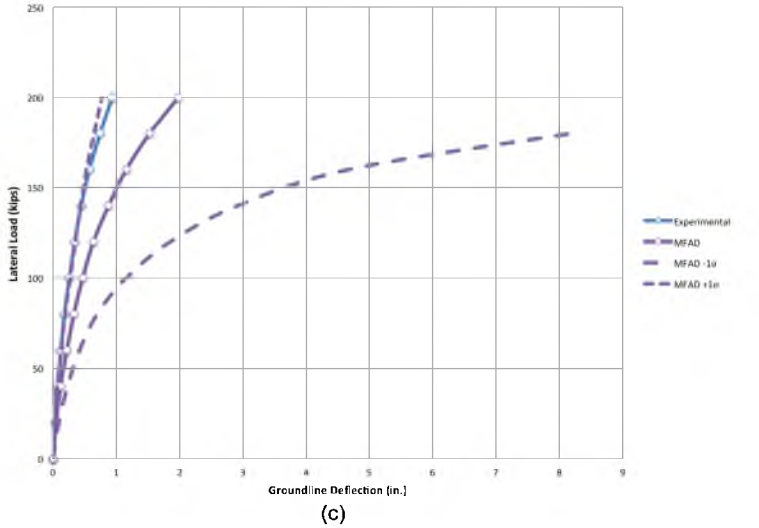

(c)

Figure 4.8. Load-deflection curves for DS 19-2 using ± 1 standard deviation input parameters for a) LPile, b) DFSAP, and c) MFAD models

considerably more pile head deflection when soil input properties are reduced by one standard deviation. For this experiment, *MFAD* was the most sensitive to the change in soil input properties, while *LPile* was the least sensitive to the change in soil input properties. All three analysis methods exhibited higher sensitivity to soil input properties with increasing applied load. It should be noted that all three analysis methods failed to reach solutions before the ultimate applied load of 200 kips for soil input properties of -1 standard deviation.

The lateral load vs. groundline deflection curves from the experimental and analytical results for DS 19-3 are presented in Figure 4.9a. The experimentally-observed groundline deflection is plotted against the predicted groundline deflection from each analysis method for DS 19-3 in Figure 4.9b. The results shown in Figure 4.9a and Figure 4.9b show that all three analysis methods overpredicted groundline deflection for the entire range of applied load. The deviation between measured groundline deflection and predicted groundline deflection from *LPile* and *MFAD* slightly increased with increasing applied load. For this experiment, *LPile* estimated the most groundline deflection and *DFSAP* estimated the least groundline deflection for measured groundline deflection greater than approximately 0.1 inches.

The lateral load vs. groundline deflection curves from the experimental and analytical results for DS 19-3 using soil input properties with ±1 standard deviation from the "best-estimate" values are presented in Figure 4.10. These results show that increasing or decreasing the soil input properties by one standard deviation does not result in equivalent deviation from the best-estimate input property values, but instead results in considerably more pile head deflection when soil input properties are reduced by one standard deviation. For this experiment, *MFAD* was the most sensitive to the

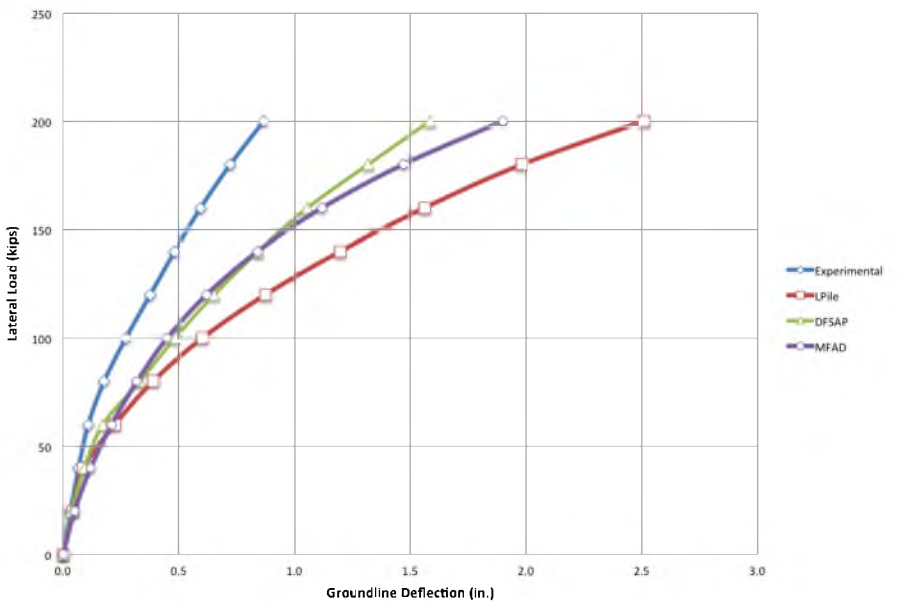

(a)

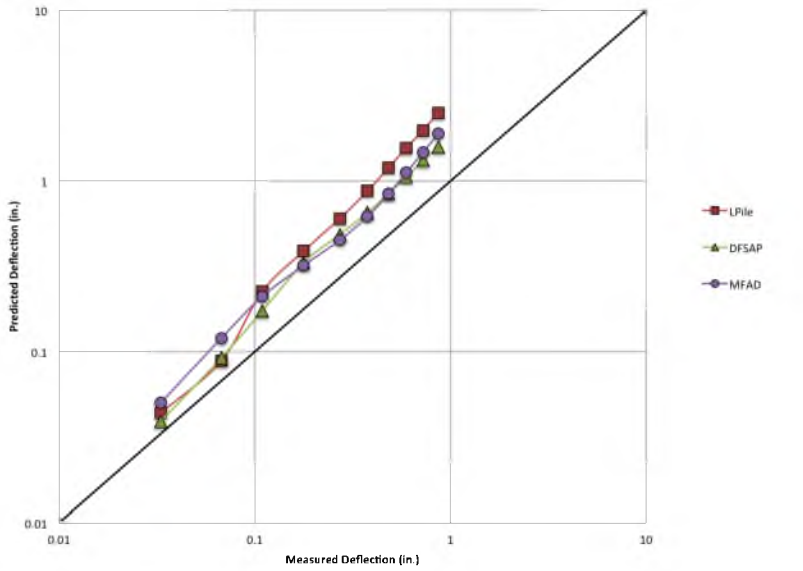

(b)

Figure 4.9. DS 19-3 results showing a) lateral load vs. groundline deflection curves, and b) predicted vs. measured groundline deflection curves in log-log scale

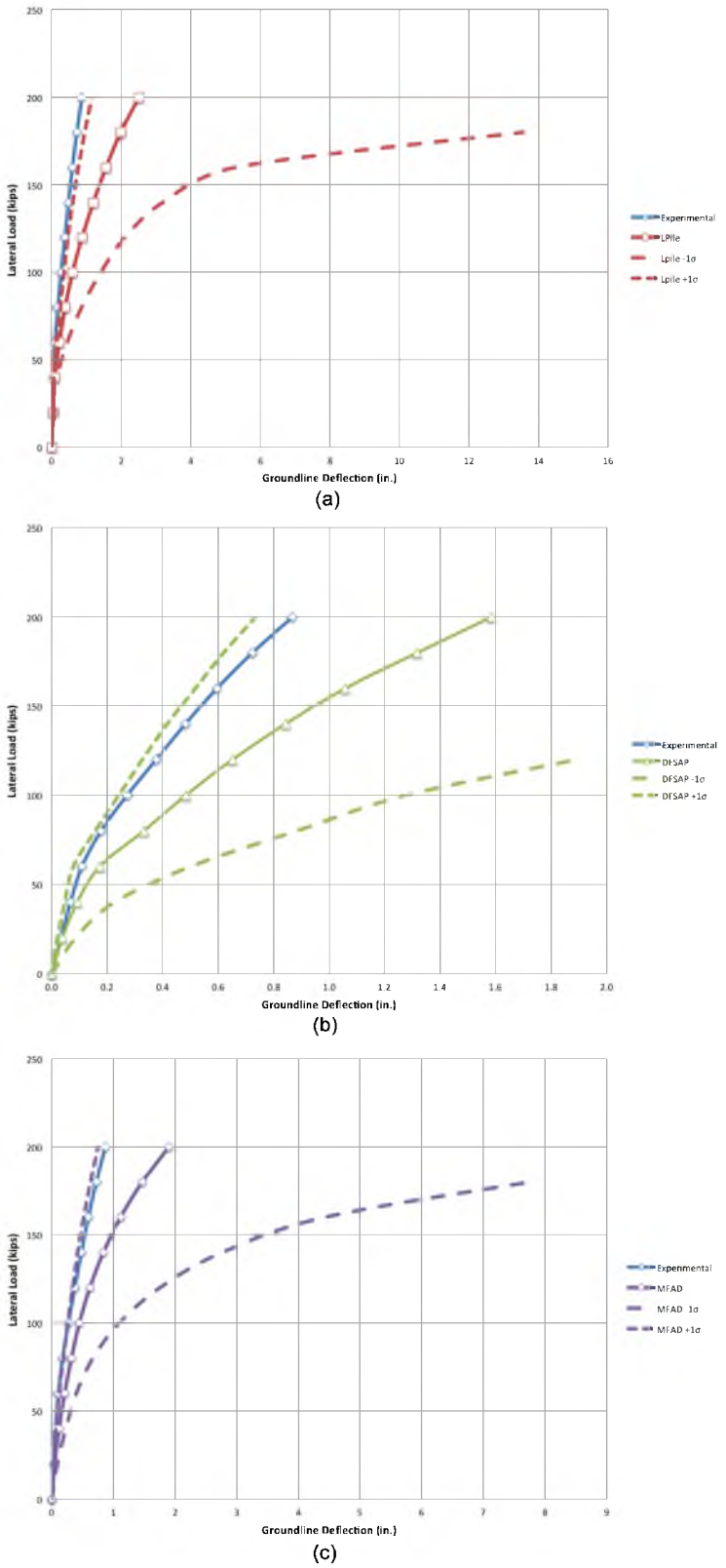

Figure 4.10. Load-deflection curves for DS 19-3 using ± 1 standard deviation input parameters for a) LPile, b) DFSAP, and c) MFAD models

change in soil input properties, while *LPile* was the least sensitive to the change in soil input properties. All three analysis methods exhibited higher sensitivity to soil input properties with increasing applied load. It should be noted that all three analysis methods failed to reach solutions before the ultimate applied load of 200 kips for soil input properties of -1 standard deviation.

4.3.1 Parametric Study

The parameters that were included in the parametric study for *LPile* were ϕ and k. The results of the *LPile* analyses for the upper bound, lower bound, and best-estimate values of ϕ and k are shown in Figure 4.11 and Figure 4.12, respectively. The parameters that were included in the parametric study for *DFSAP* were ϕ and ε_{50}. The results of the *DFSAP* analyses for the upper bound, lower bound, and best-estimate values of ϕ and ε_{50} are shown in Figure 4.13 and Figure 4.14, respectively. The parameters that were included in the parametric study for *MFAD* were ϕ and E_p. The results of the *MFAD* analyses for the upper bound, lower bound, and best-estimate values of ϕ and E_p are shown in Figure 4.15 and Figure 4.16, respectively.

The sensitivity analysis for ϕ was performed by applying a constant lateral load to the top of the foundation and incrementally increasing ϕ for each simulation. The range of ϕ that was chosen for the sensitivity analysis was 34 to 48 degrees. The lateral load that was applied to the top of the foundation in the *LPile* and *DFSAP* models was 100 kips, and the lateral load that was applied to the top of the foundation in the *MFAD* model was 150 kips. The difference is due to the fact that the foundation failed at 150 kips in *LPile* and *DFSAP*, so the load was reduced for these models.

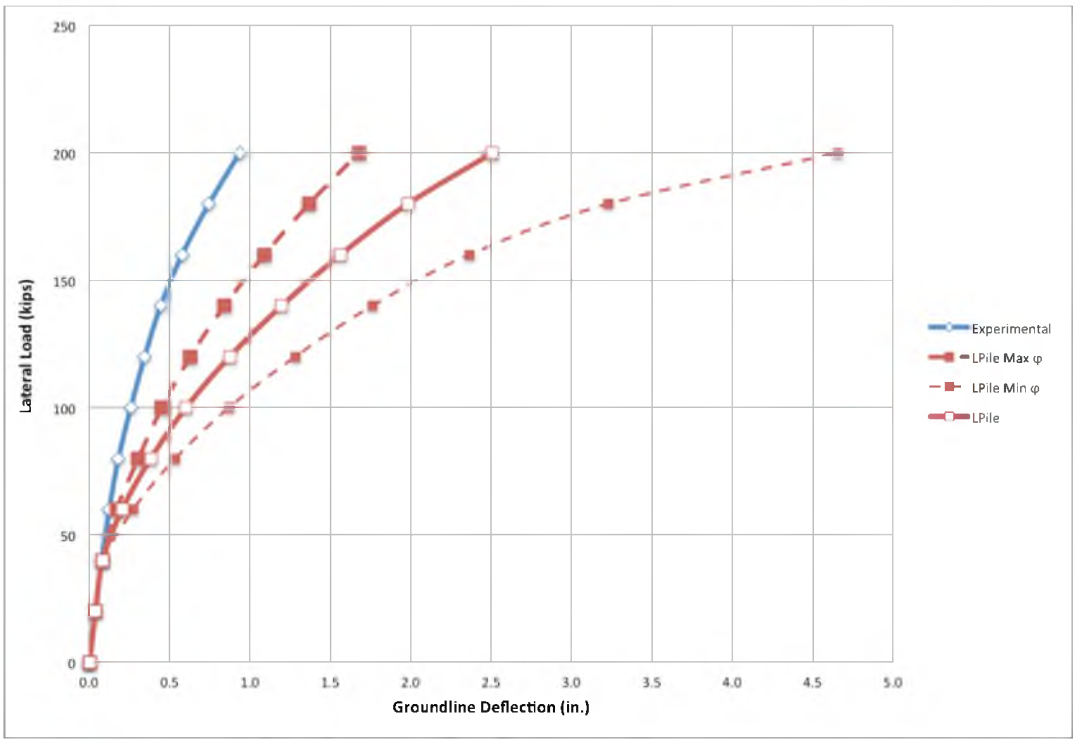

Figure 4.11. Results of LPile analysis of DS 19-2 for upper bound, lower bound, and best-estimate values of ϕ

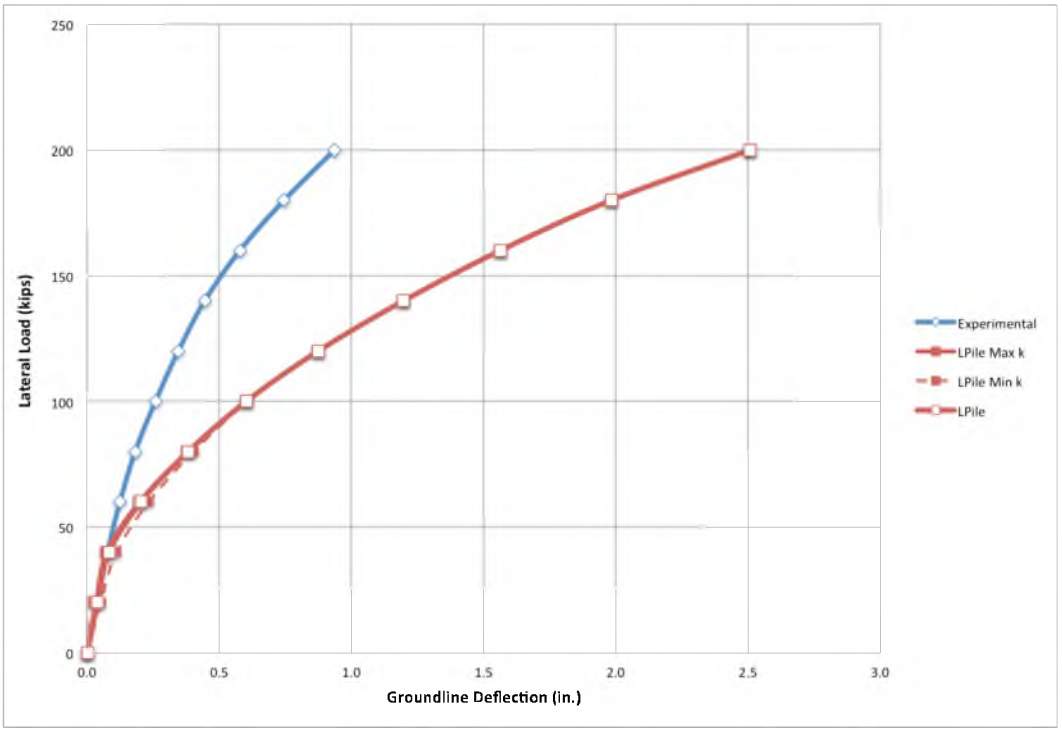

Figure 4.12. Results of LPile analysis of DS 19-2 for upper bound, lower bound, and best-estimate values of k

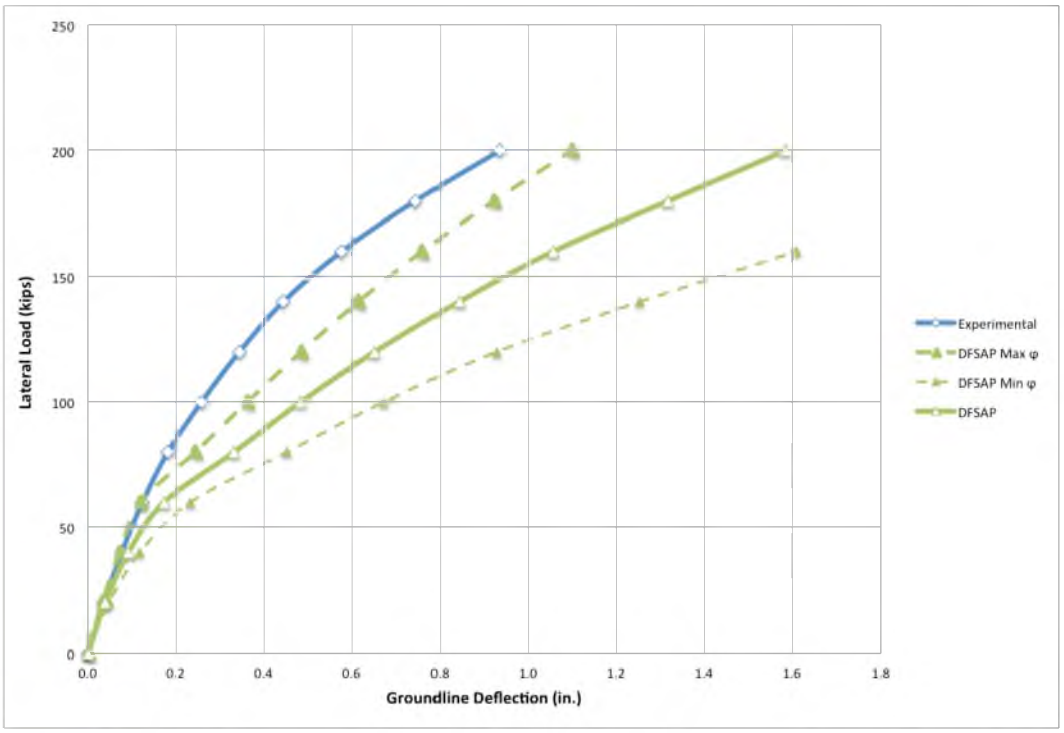

Figure 4.13. Results of DFSAP analysis of DS 19-2 for upper bound, lower bound, and best-estimate values of ϕ

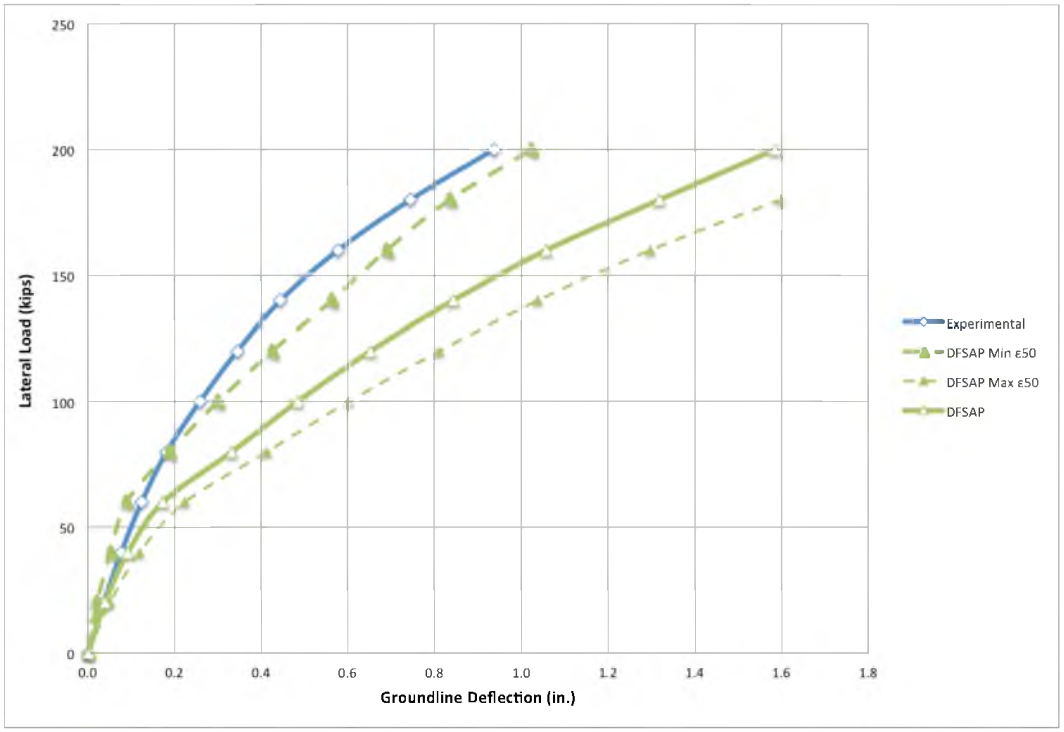

Figure 4.14. Results of DFSAP analysis of DS 19-2 for upper bound, lower bound, and best-estimate values of ε_{50}

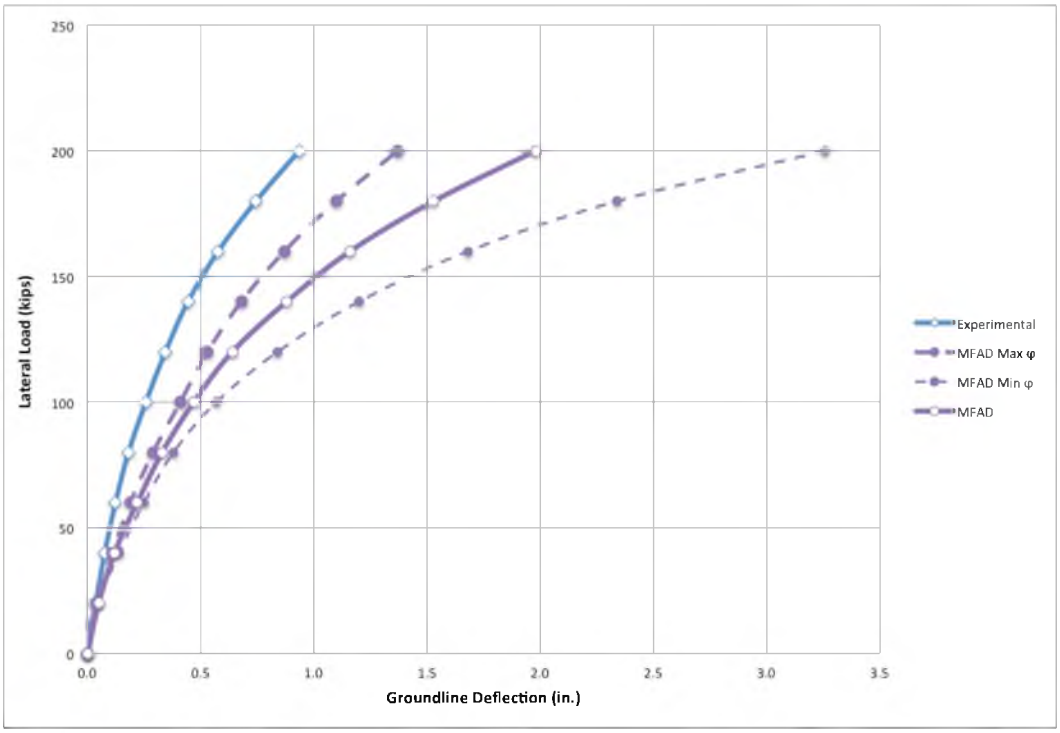

Figure 4.15. Results of MFAD analysis of DS 19-2 for upper bound, lower bound, and best-estimate values of ϕ

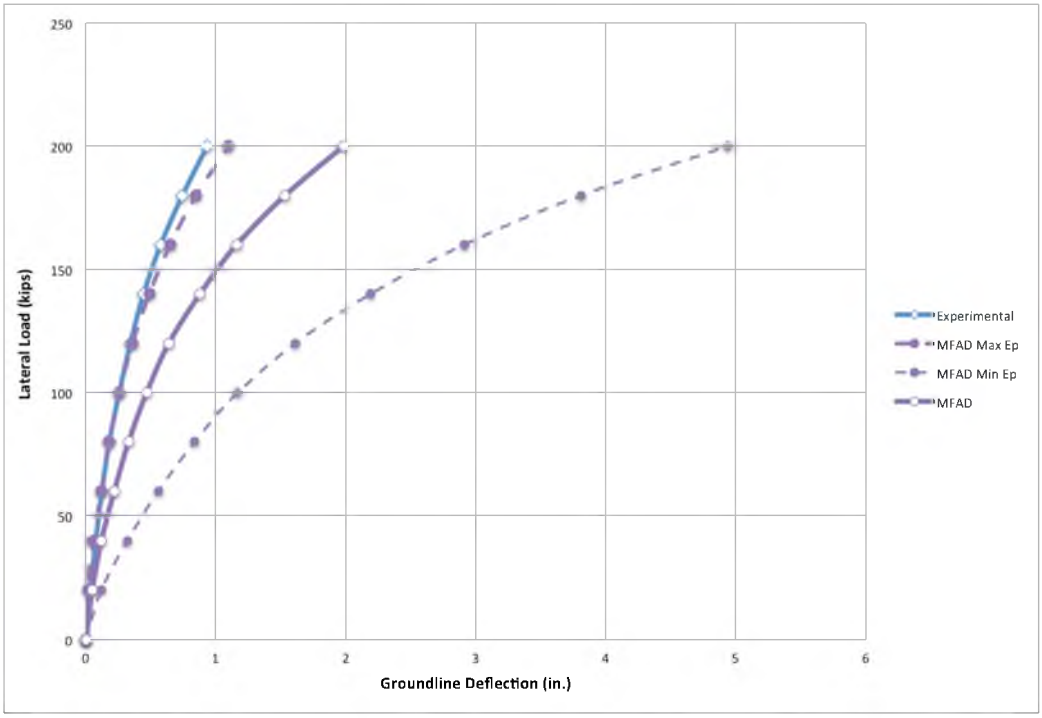

Figure 4.16. Results of MFAD analysis of DS 19-2 for upper bound, lower bound, and best-estimate values of E_p

The *LPile* simulations that were performed at each incremental value of ϕ were performed for three values of k to gain insight into the sensitivity of the model to k, and to identify whether the sensitivity of ϕ was dependent upon k. The values of k that were used for the sensitivity analysis were 100, 200, and 400 pci, which are within the expected range of k for the specified range of ϕ. A plot of pile head deflection vs. ϕ for each *LPile* simulation is shown in Figure 4.17. The same figure is also shown in log-log scale in Figure 4.18. It should be noted that the two sub-layers for DS 19-2 were combined into a single layer to facilitate isolation of the parameters of interest.

The *DFSAP* simulations that were performed at each incremental value of ϕ were performed at four values of ε_{50} to gain insight into the sensitivity of the model to ε_{50}, and to identify whether the sensitivity of ϕ was dependent upon ε_{50}. The values of ε_{50} that were used for the sensitivity analysis were 0.001, 0.002, 0.004, and 0.008, which are within the expected range of ε_{50} for the specified range of ϕ. A plot of pile head deflection vs. ϕ for each *DFSAP* simulation is shown in Figure 4.19. The same figure is also shown in log-log scale in Figure 4.20.

The *MFAD* simulations that were performed at each incremental value of ϕ were performed at four values of E_p to gain insight into the sensitivity of the model to E_p, and to identify whether the sensitivity of ϕ was dependent upon E_p. The values of E_p that were used for the sensitivity analysis were 0.5, 1.0, 2.0, and 4.0 ksi, which are within the expected range of E_p for the specified range of ϕ. A plot of pile head deflection vs. ϕ for each *MFAD* simulation is shown in Figure 4.21. The same figure is also shown in log-log scale in Figure 4.22.

The results of the sensitivity analysis for ϕ showed that the *LPile* results were not very sensitive to k; however, *DFSAP* and *MFAD* models were sensitive to ε_{50} and E_p,

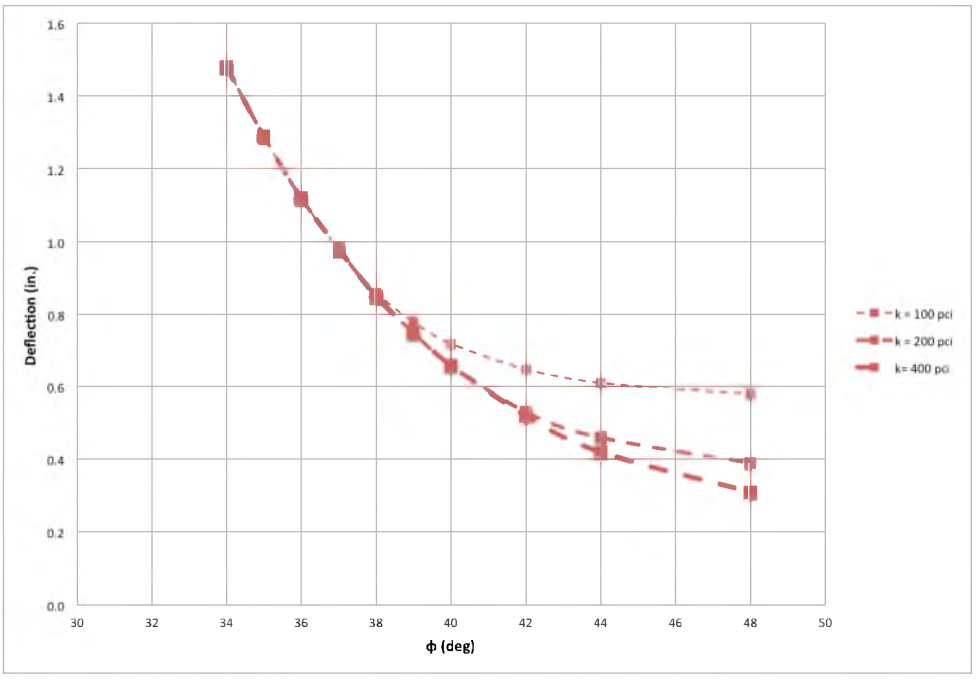

Figure 4.17. Results of LPile sensitivity analysis for ϕ ranging from 34 to 48 degrees and k ranging from 100 to 400 pci

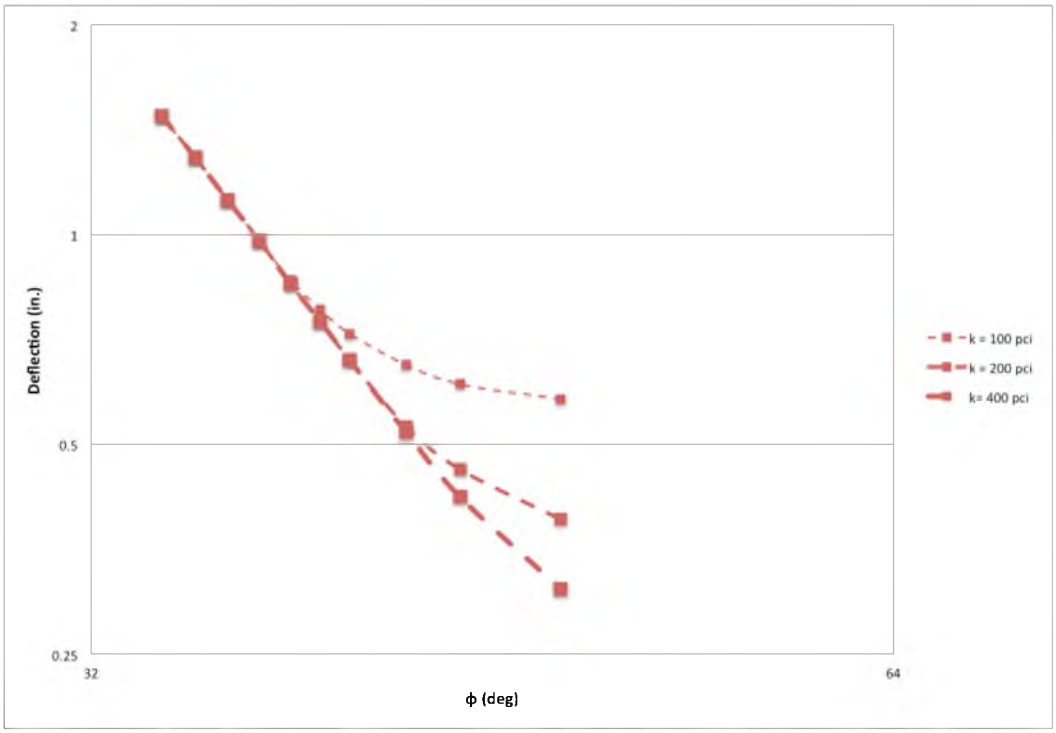

Figure 4.18. Results of LPile sensitivity analysis for ϕ ranging from 34 to 48 degrees and k ranging from 100 to 400 pci in log-log scale

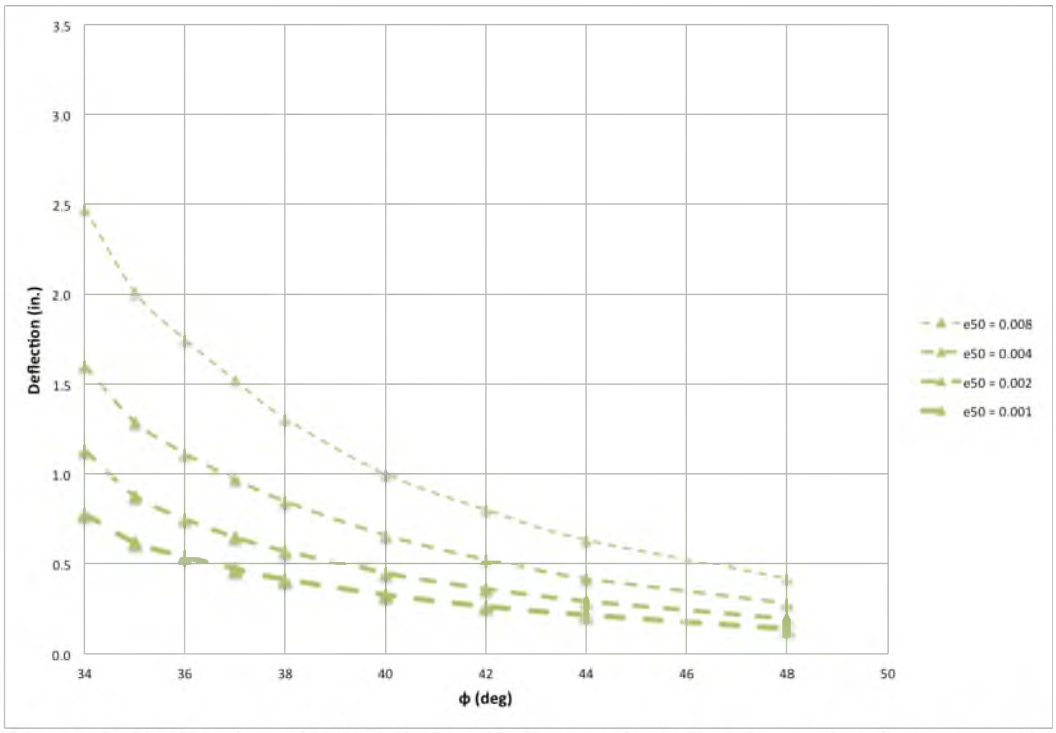

Figure 4.19. Results of DFSAP sensitivity analysis for ϕ ranging from 34 to 48 degrees and ε_{50} ranging from 0.001 to 0.008

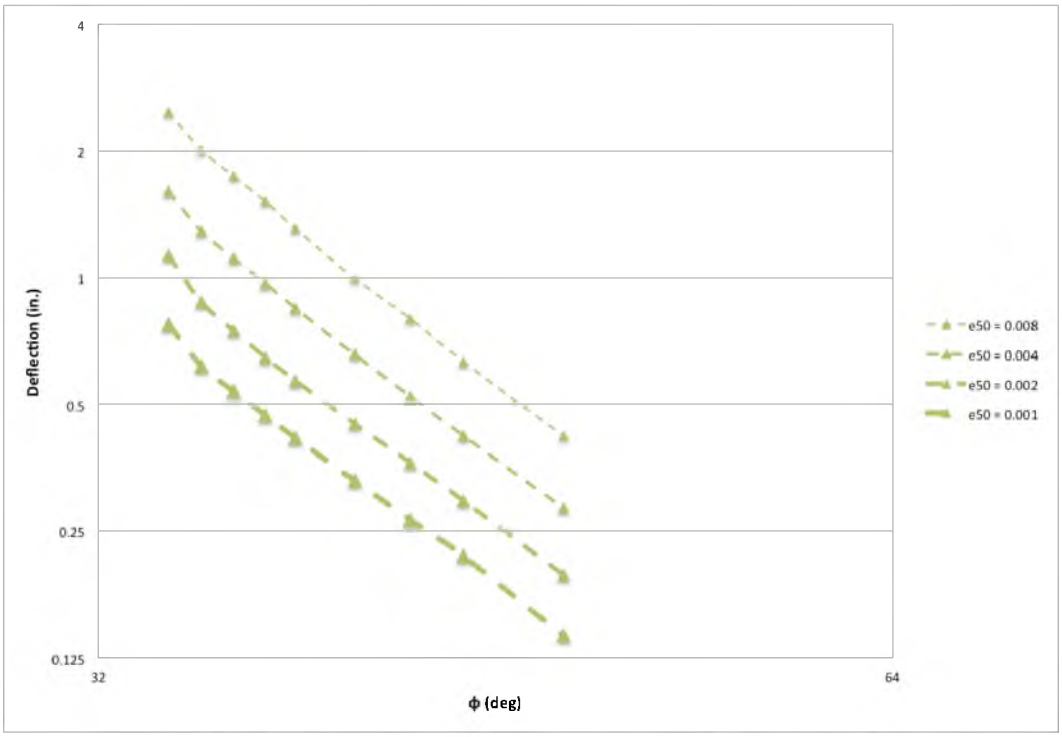

Figure 4.20. Results of DFSAP sensitivity analysis for ϕ ranging from 34 to 48 degrees and ε_{50} ranging from 0.001 to 0.008 in log-log scale

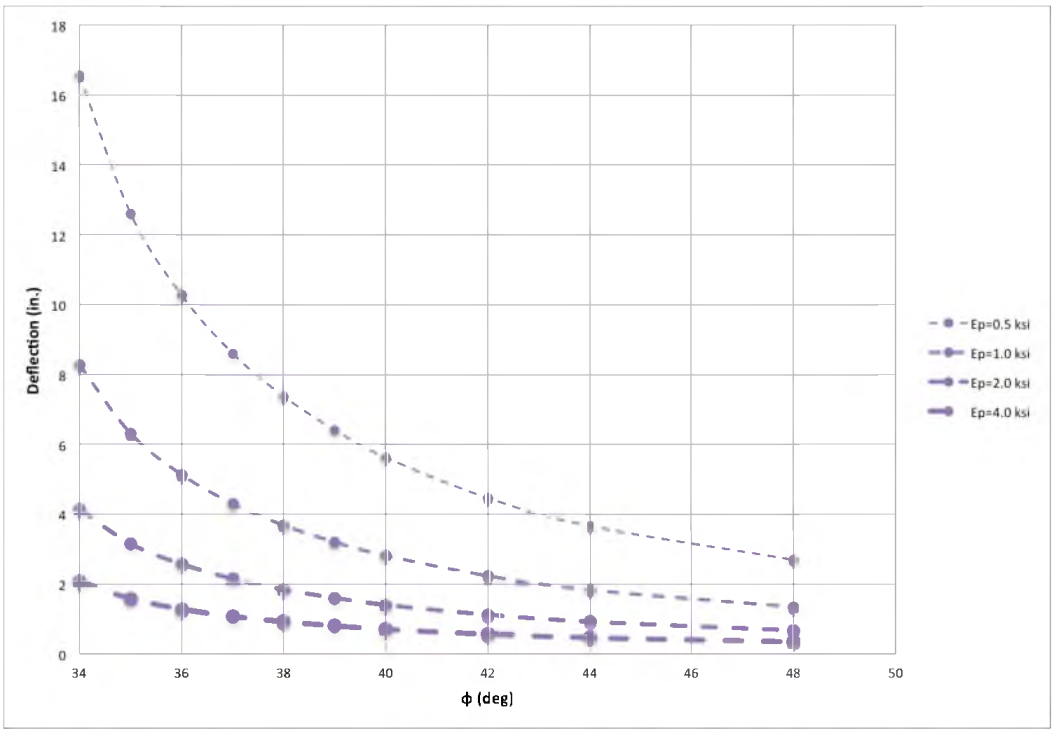

Figure 4.21. Results of MFAD sensitivity analysis for ϕ ranging from 34 to 48 degrees and E_p ranging from 0.5 to 4.0 ksi

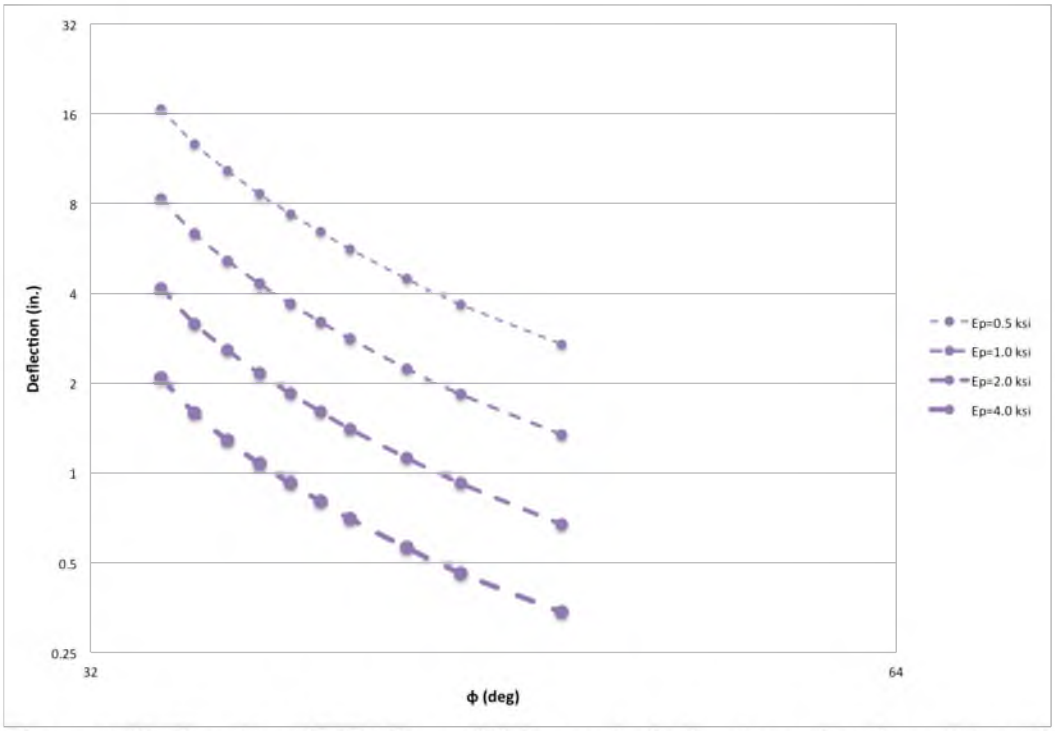

Figure 4.22. Results of MFAD sensitivity analysis for ϕ ranging from 34 to 48 degrees and E_p ranging from 0.5 to 4.0 ksi in log-log scale

respectively. As such, additional sensitivity analyses were performed to gain insight into the sensitivity of the *DFSAP* model to ε_{50} and of the *MFAD* model to E_p. For these sensitivity analyses, ϕ was held constant at 34, 38, 42, and 48 degrees, and ε_{50} and E_p were increased incrementally from 0.001 to 0.008 and 0.5 to 6.0 ksi, respectively. The results of deflection vs. ε_{50} for the *DFSAP* simulations are shown in Figure 4.23. The results of deflection vs. E_p for the *MFAD* simulations are shown in Figure 4.24. Additionally, the results shown in Figure 4.24 have been reproduced in log-log scale in Figure 4.25.

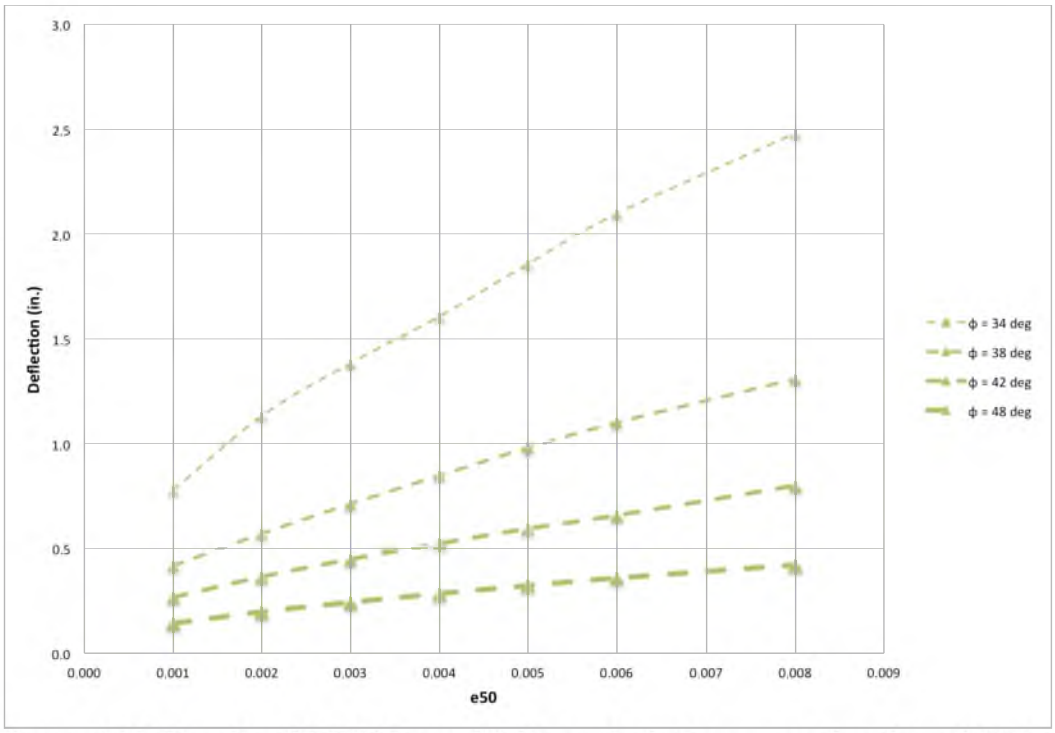

Figure 4.23. Results of DFSAP sensitivity analysis for ε_{50} ranging from 0.001 to 0.008 and ϕ ranging from 34 to 48 degrees

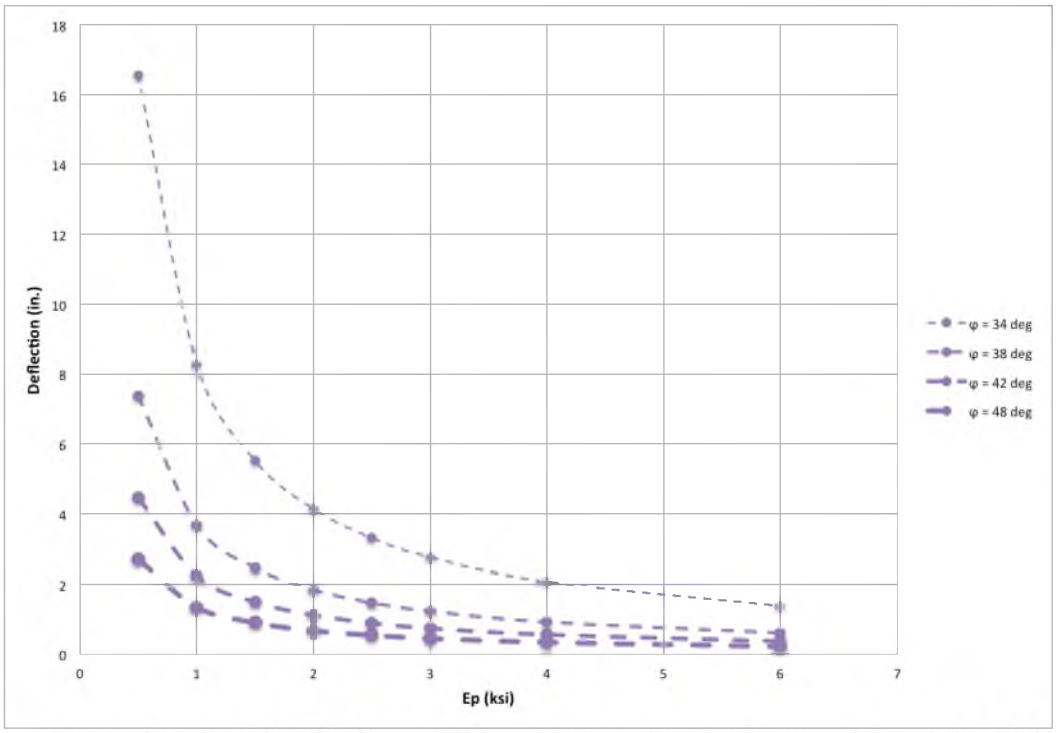

Figure 4.24. Results of MFAD sensitivity analysis for E_p ranging from 0.5 to 6.0 ksi and ϕ ranging from 34 to 48 degrees

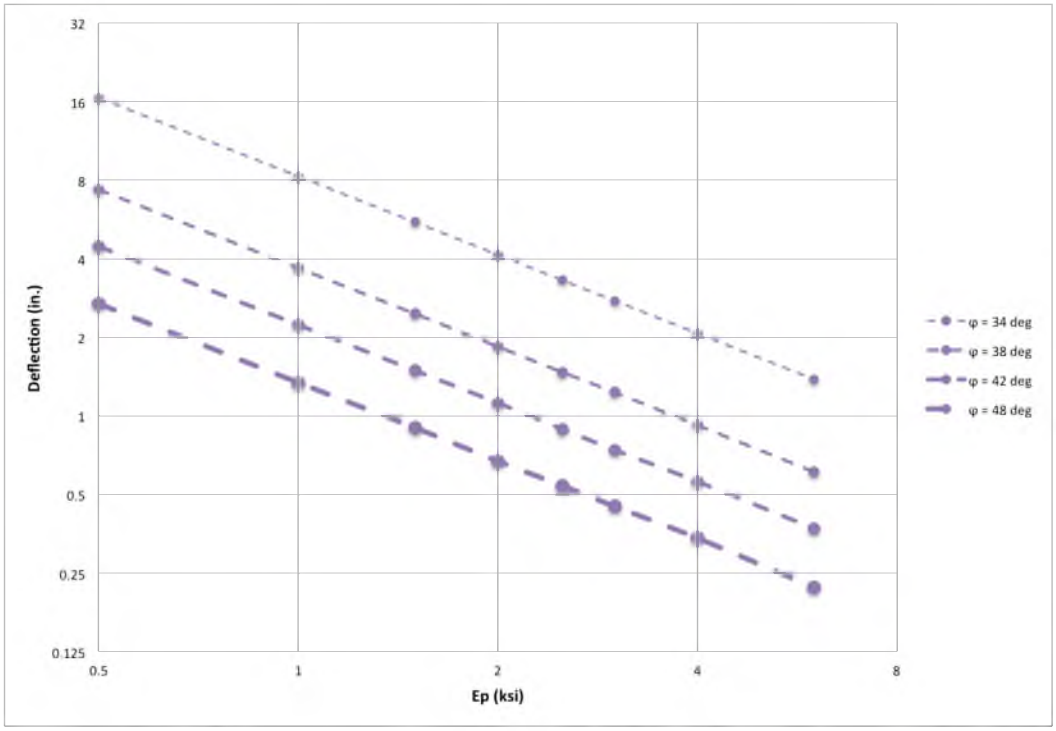

Figure 4.25. Results of MFAD sensitivity analysis for E_p ranging from 0.5 to 6.0 ksi and ϕ ranging from 34 to 48 degrees in log-log scale

4.4 Load Test 20 Results

The lateral load vs. groundline deflection curves from the experimental and analytical results for DS 20-2 are presented in Figure 4.26a. The experimentally-observed groundline deflection is plotted against the predicted groundline deflection from each analysis method for DS 20-2 in Figure 4.26b.

The results shown in Figure 4.26a and Figure 4.26b show that *LPile* initially underpredicted groundline deflection and then overpredicted groundline deflection at larger magnitudes of applied load. With the exception of the initial load, both *DFSAP* and *MFAD* underpredicted groundline deflection over the entire range of applied load. The error between estimated and predicted groundline deflection increased considerably for *LPile* and slightly for *DFSAP* and *MFAD* with increasing applied load. For this experiment, *LPile* estimated the most groundline deflection and *MFAD* estimated the least groundline deflection for measured deflection greater than approximately 0.1 inches. It should be noted that *DFSAP* estimated slightly more groundline deflection that *MFAD* at maximum applied load of 391 kips; however, the groundline deflection estimated by *DFSAP* at this load is virtually the same as the groundline deflection estimated at 367 kips as shown in Figure 4.27b. It appears a numerical error in *DFSAP* is causing the same groundline deflections to be estimated at the two different loads. It should also be noted that *LPile* was unable to converge on a solution for applied loads greater than 338 kips.

The lateral load vs. groundline deflection curves from the experimental and analytical results for DS 20-2 using soil input properties with ±1 standard deviation from the "best-estimate" values are presented in Figure 4.27. These results show that increasing or decreasing the soil input properties by one standard deviation does not

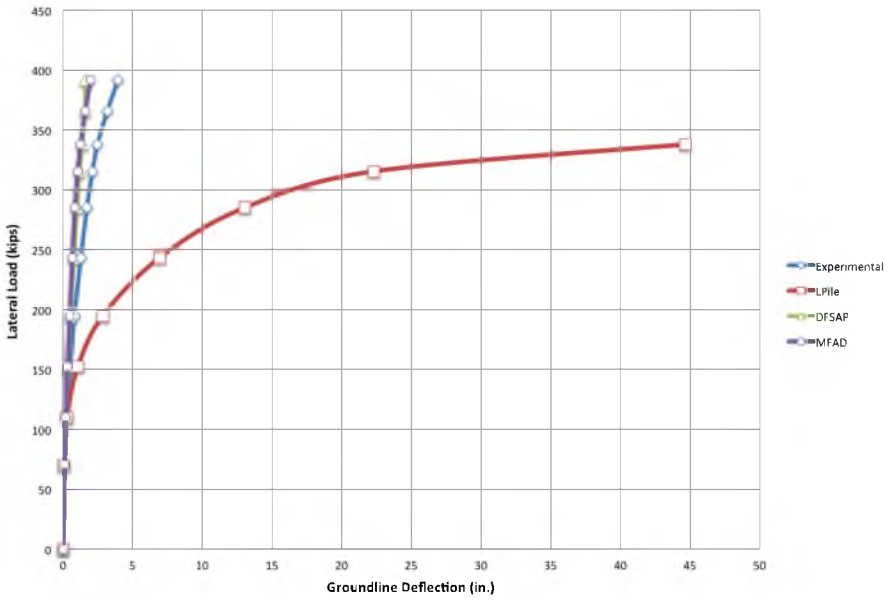

(a)

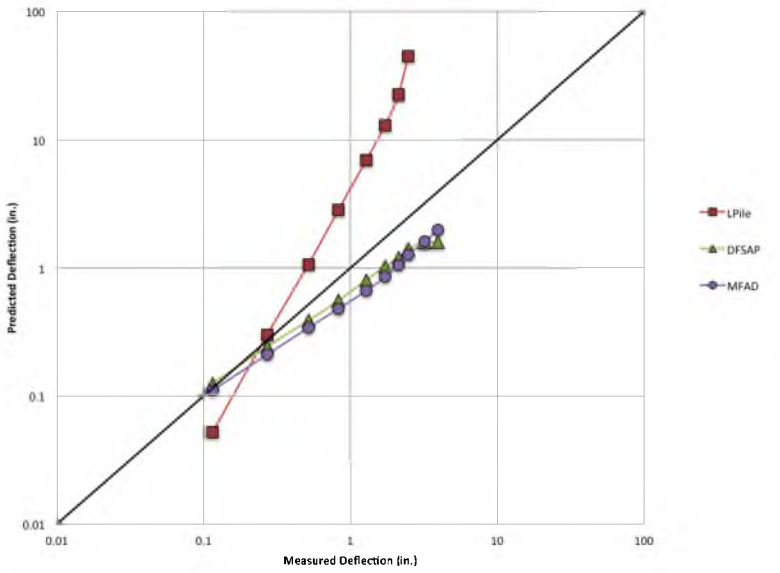

(b)

Figure 4.26. DS 20-2 results showing a) lateral load vs. groundline deflection curves, and b) predicted vs. measured groundline deflection curves in log-log scale

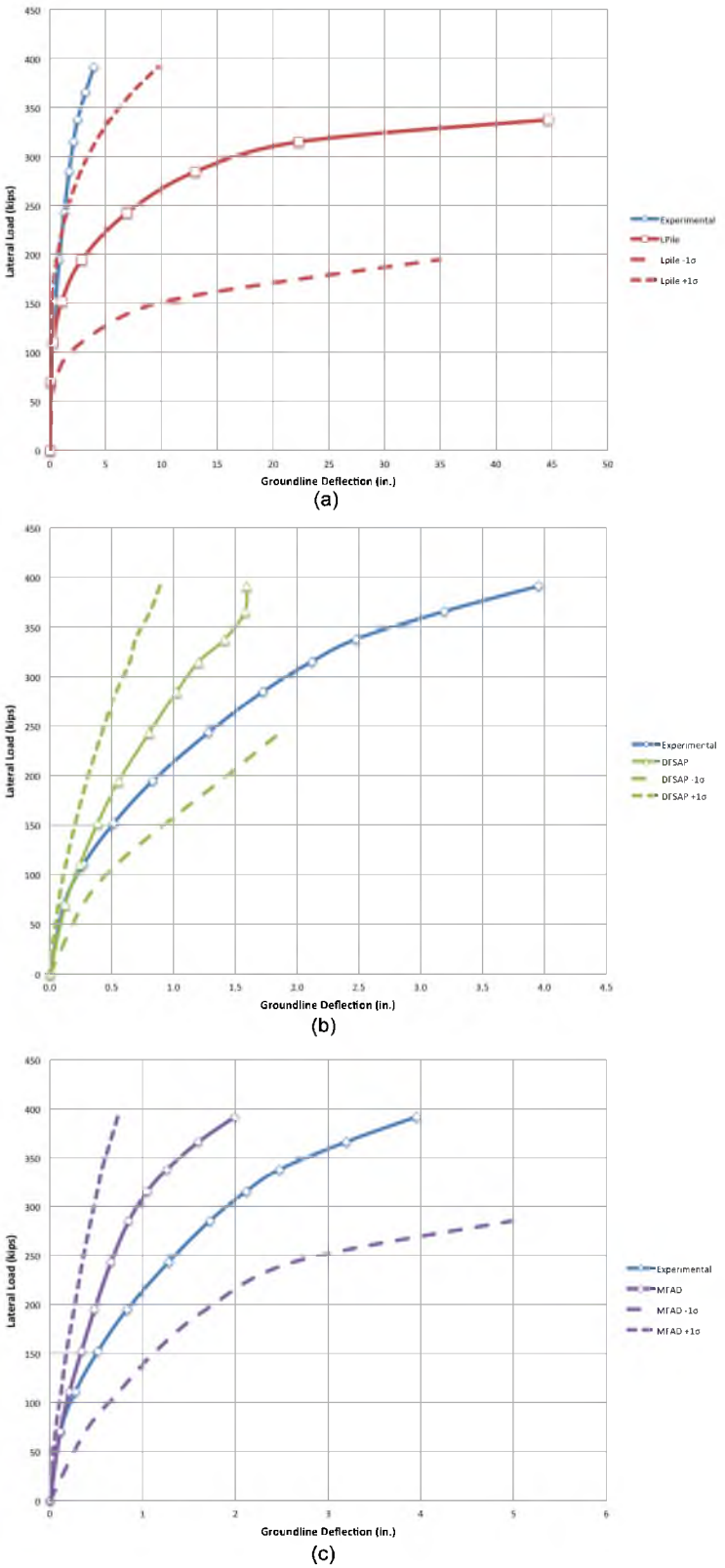

Figure 4.27. Load-deflection curves for DS 20-2 using ± 1 standard deviation input parameters for a) LPile, b) DFSAP, and c) MFAD models

result in equivalent deviation from the best-estimate input property values, but instead results in considerably more pile head deflection when soil input properties are reduced by one standard deviation. For this experiment, *LPile* was the most sensitive to the change in soil input properties and *DFSAP* was the least sensitive to change in soil input properties. *LPile* and *MFAD* exhibited an increase in sensitivity with increasing applied load, while *DFSAP* exhibited only minor changes in sensitivity over the range of applied load. It should be noted that all three analysis methods failed to reach solutions before the ultimate applied load of 449 kips for soil input properties of -1 standard deviation.

The lateral load vs. groundline deflection curves from the experimental and analytical results for DS 20-4 are presented in Figure 4.28a. The experimentally-observed groundline deflection is plotted against the predicted groundline deflection from each analysis method for DS 20-4 in Figure 4.28b.

The results shown in Figure 4.28a and Figure 4.28b show that *LPile* initially underpredicted groundline deflection and then overpredicted groundline deflection at larger magnitudes of applied load. With the exception of the initial load, *DFSAP* underpredicted groundline deflection over the entire range of applied load. *MFAD* also underpredicted the groundline deflection over the entire range of applied load. The error between estimated and predicted groundline deflection increased considerably for *LPile* and remained fairly constant for *DFSAP* and *MFAD* with increasing applied load. for this experiment, *LPile* estimated the most groundline deflection and *MFAD* estimated the least groundline deflection for measured deflection greater than approximately 0.4 inches.

The lateral load vs. groundline deflection curves from the experimental and analytical results for DS 20-4 using soil input properties with ±1 standard deviation from the "best-estimate" values are presented in Figure 4.29. These results show that

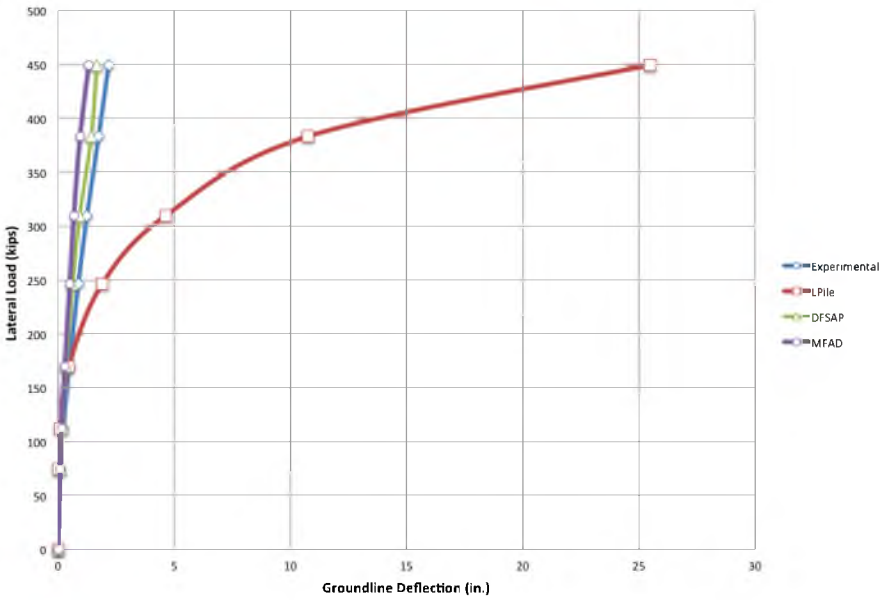

(a)

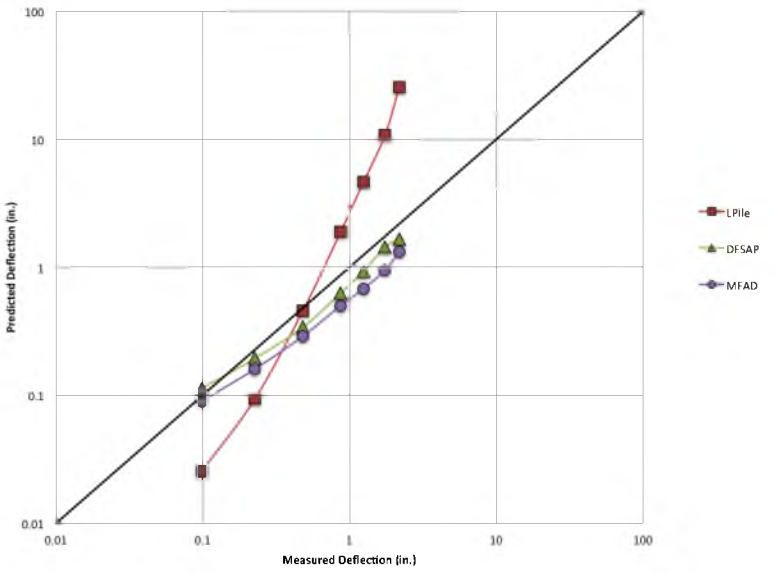

(b)

Figure 4.28. DS 20-4 results showing a) lateral load vs. groundline deflection curves, and b) predicted vs. measured groundline deflection curves in log-log scale

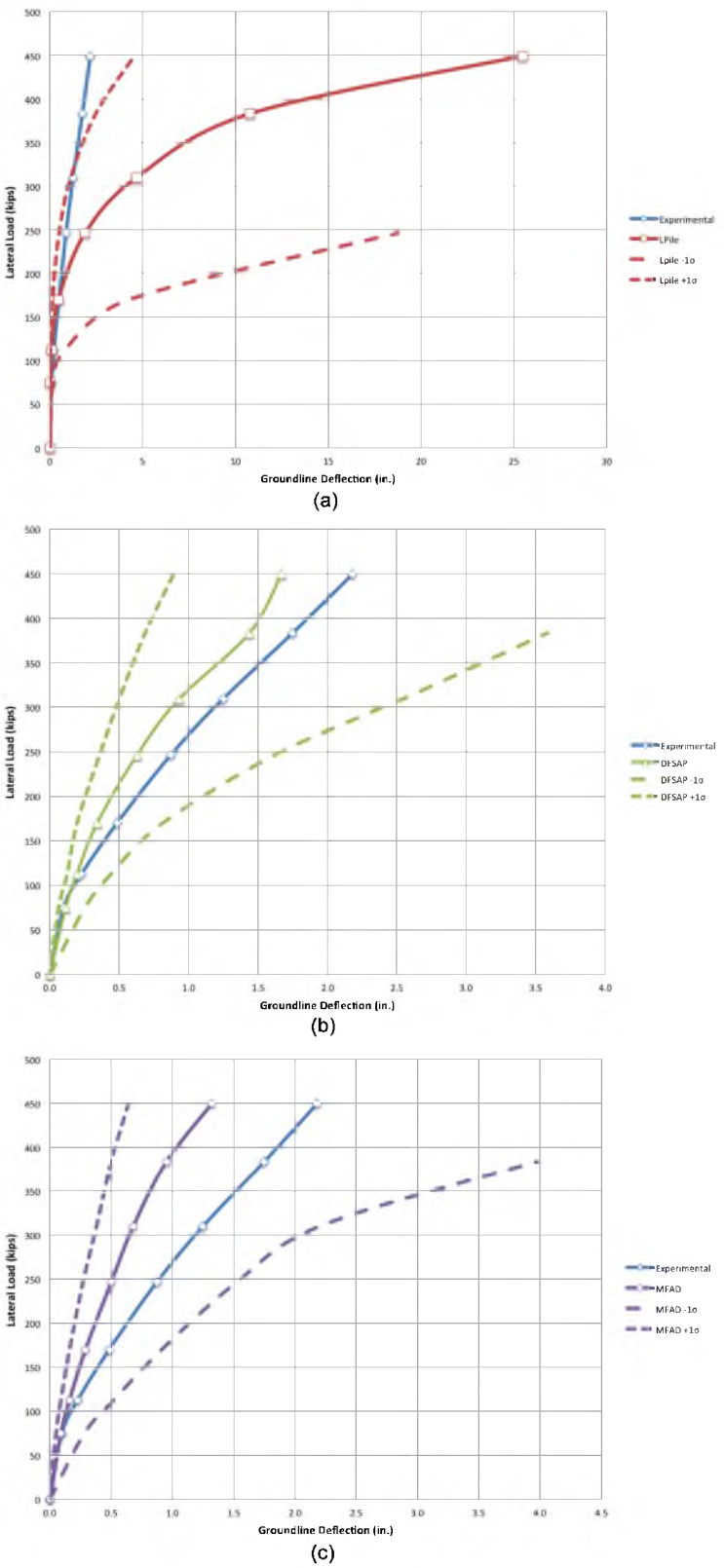

Figure 4.29. Load-deflection curves for DS 20-4 using ± 1 standard deviation input parameters for a) LPile, b) DFSAP, and c) MFAD models

increasing or decreasing the soil input properties by one standard deviation does not result in equivalent deviation from the best-estimate input property values, but instead results in considerably more pile head deflection when soil input properties are reduced by one standard deviation. For this experiment, *LPile* was the most sensitive to the change in soil input properties and *DFSAP* was the least sensitive to change in soil input properties. *LPile* exhibited considerable increase in sensitivity with increasing applied load, while *MFAD* exhibited moderate increase in sensitivity with increasing applied load. *DFSAP* exhibited only minor changes in sensitivity over the range of applied load. It should be noted that all three analysis methods failed to reach solutions before the ultimate applied load of 449 kips for soil input properties of -1 standard deviation.

The lateral load vs. groundline deflection curves from the experimental and analytical results for DS 20-5 are presented in Figure 4.30a. The experimentally-observed groundline deflection is plotted against the predicted groundline deflection from each analysis method for DS 20-5 in Figure 4.30b.

The results shown in Figure 4.30a and Figure 4.30b show that *LPile* underpredicted groundline deflection for the initial increment of applied load and then overpredicted groundline deflection at larger magnitudes of applied load. Both *DFSAP* and *MFAD* overpredicted groundline deflection over the entire range of applied load. the deviation between predicted and observed groundline deflection for *MFAD* increased slightly at larger magnitudes of applied load.

For this experiment, *LPile* estimated the most groundline deflection and *MFAD* estimated the least groundline deflection for measured deflection greater than approximately 0.1 inches. It should be noted that *LPile* and *DFSAP* both failed to obtain solutions for the maximum experimental load of 160 kips. *LPile* failed to converge on a

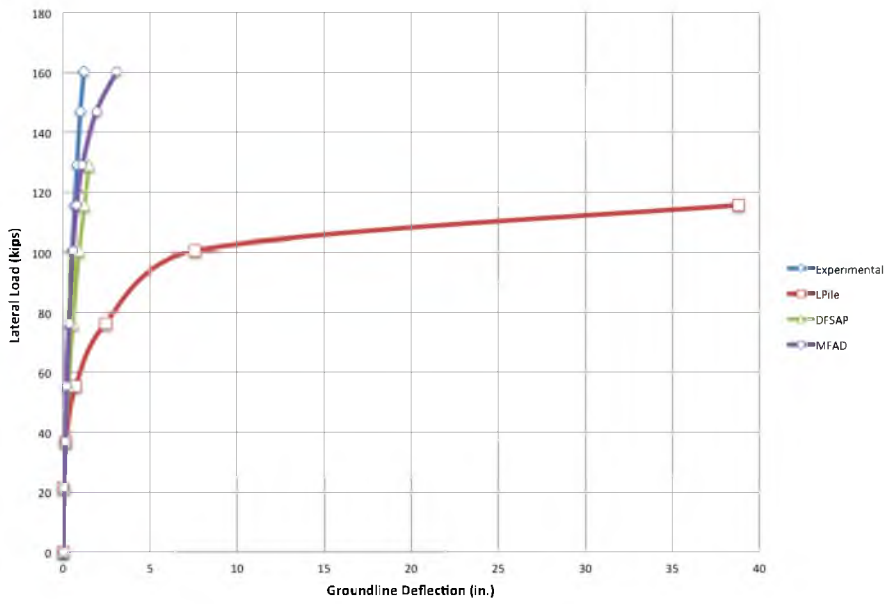

(a)

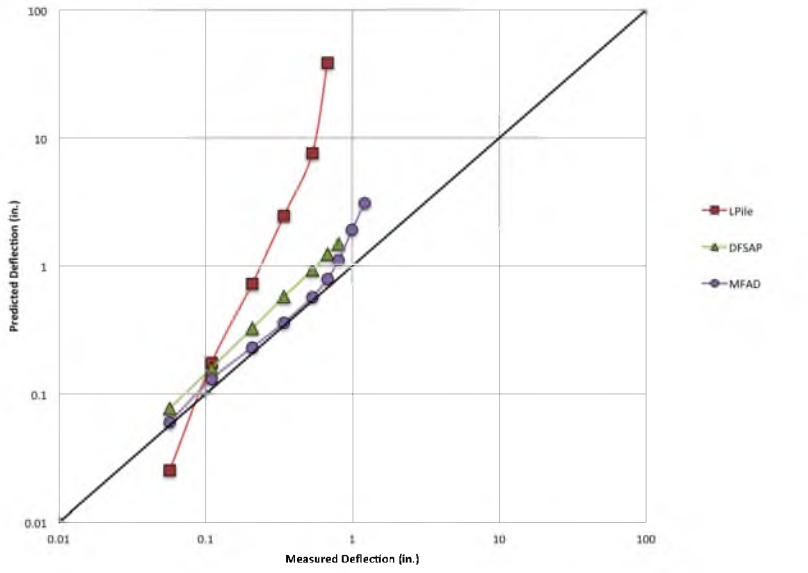

(b)

Figure 4.30. DS 20-5 results showing a) lateral load vs. groundline deflection curves, and b) predicted vs. measured groundline deflection curves in log-log scale

solution beyond 116 kips, and *DFSAP* failed to converge on a solution beyond 129 kips.

The lateral load vs. groundline deflection curves from the experimental and analytical results for DS 20-5 using soil input properties with ±1 standard deviation from the "best-estimate" values are presented in Figure 4.31. These results show that increasing or decreasing the soil input properties by one standard deviation does not result in equivalent deviation from the best-estimate input property values, but instead results in considerably more pile head deflection when soil input properties are reduced by one standard deviation. For this experiment, *LPile* was the most sensitive to the change in soil input properties and *DFSAP* was the least sensitive to change in soil input properties. *LPile* exhibited considerable increase in sensitivity with increasing applied load, while *MFAD* and *DFSAP* exhibited moderate increase in sensitivity with increasing applied load. It should be noted that all three analysis methods failed to reach solutions before the ultimate applied load of 160 kips for soil input properties of -1 standard deviation.

The lateral load vs. groundline deflection curves from the experimental and analytical results for DS 20-6 are presented in Figure 4.32a. The experimentally-observed groundline deflection is plotted against the predicted groundline deflection from each analysis method for DS 20-6 in Figure 4.32b.

The results shown in Figure 4.32a and Figure 4.32b show that *LPile* overpredicted groundline deflection for the entire range of applied load and that the deviation between observed and predicted groundline deflection increased slightly with increasing applied load. *DFSAP* overpredicted groundline deflection over the entire range of applied load and the deviation between predicted and groundline deflection remained fairly constant over the range of applied load. *MFAD* underpredicted groundline deflection over the

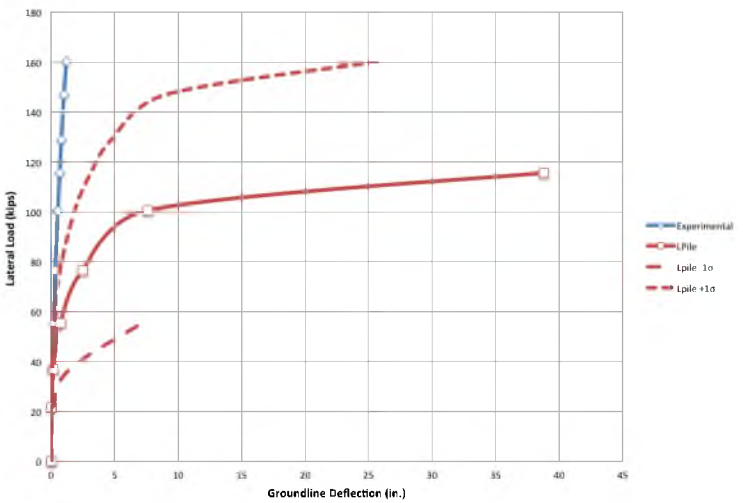

(a)

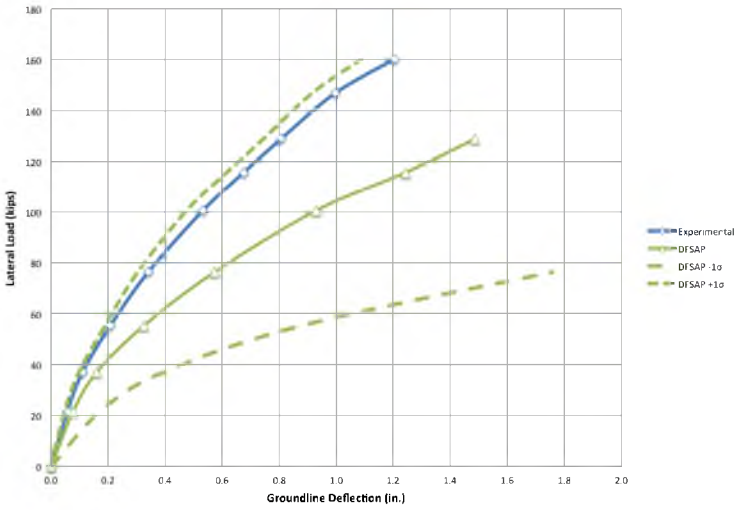

(b)

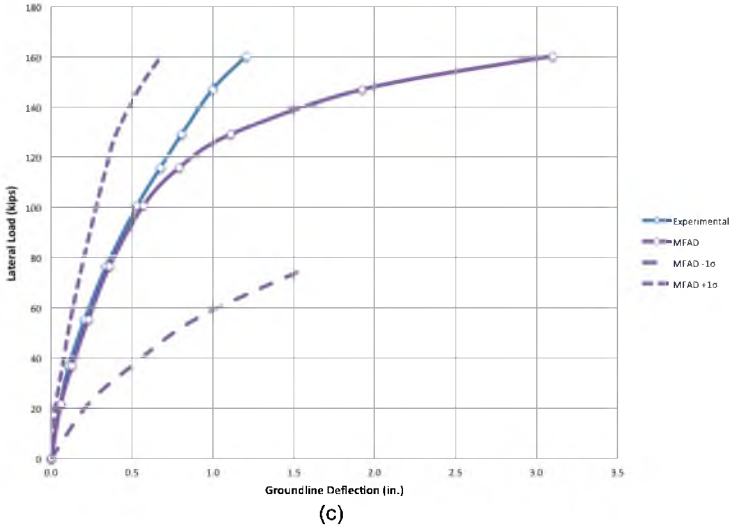

(c)

Figure 4.31. Load-deflection curves for DS 20-5 using ± 1 standard deviation input parameters for a) LPile, b) DFSAP, and c) MFAD models

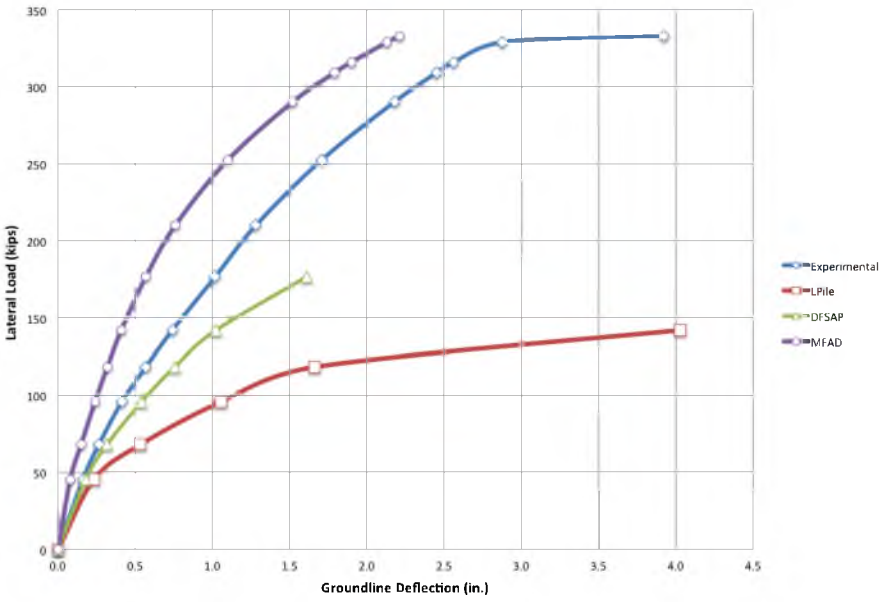

(a)

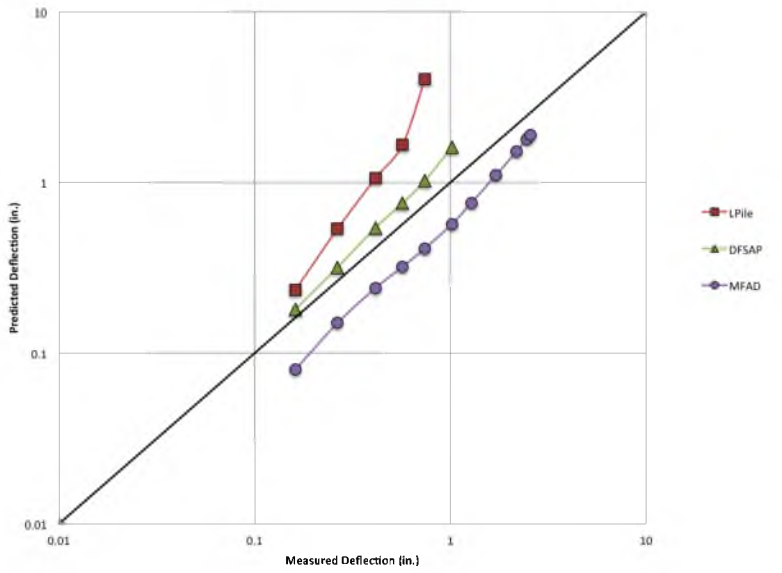

(b)

Figure 4.32. DS 20-6 results showing a) lateral load vs. groundline deflection curves, and b) predicted vs. measured groundline deflection curves in log-log scale

entire range of applied load, and the deviation between observed and predicted groundline deflection decreased slightly with increasing applied load. For this experiment, *LPile* estimated the most groundline deflection and *MFAD* estimated the least groundline deflection for measured deflection at all increments of applied load. It should be noted that *LPile* and *DFSAP* both failed to obtain solutions for the maximum experimental load of 333 kips. *LPile* failed to converge on a solution beyond 142 kips, and *DFSAP* failed to converge on a solution beyond 177 kips.

The lateral load vs. groundline deflection curves from the experimental and analytical results for DS 20-6 using soil input properties with ±1 standard deviation from the "best-estimate" values are presented in Figure 4.33.

As with previous simulations, these results show that *LPile* overpredicted groundline deflection for the entire range of applied load and that the deviation between observed and predicted groundline deflection increased slightly with increasing applied load. *DFSAP* overpredicted groundline deflection over the entire range of applied load and the deviation between predicted and groundline deflection remained fairly constant over the range of applied load. *MFAD* underpredicted groundline deflection over the entire range of applied load, and the deviation between observed and predicted groundline deflection decreased slightly with increasing applied load. For this experiment, *LPile* estimated the most groundline deflection and *MFAD* estimated the least groundline deflection for measured deflection at all increments of applied load. It should be noted that *LPile* and *DFSAP* both failed to obtain solutions for the maximum experimental load of 333 kips. *LPile* failed to converge on a solution beyond 142 kips, and *DFSAP* failed to converge on a solution beyond 177 kips.

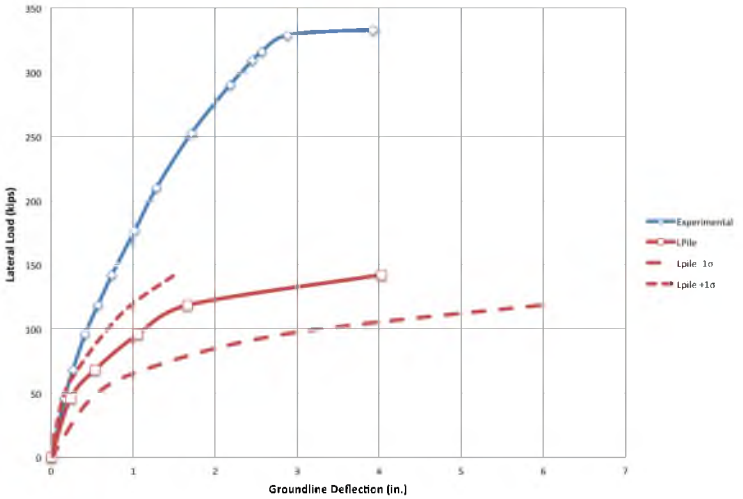

(a)

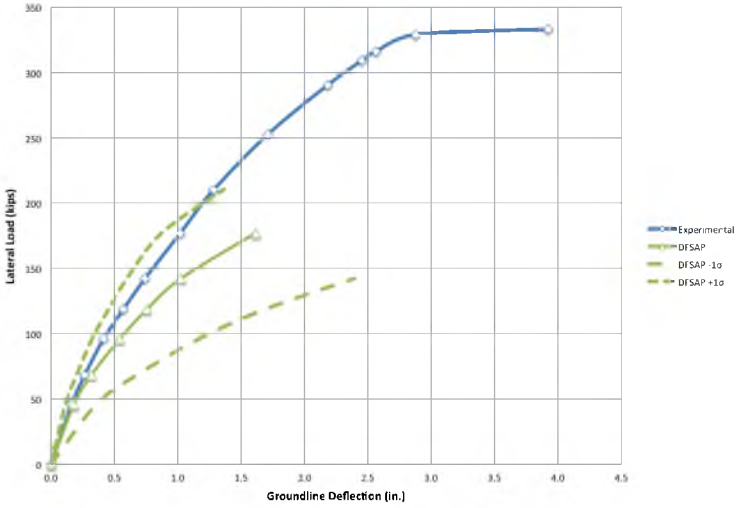

(b)

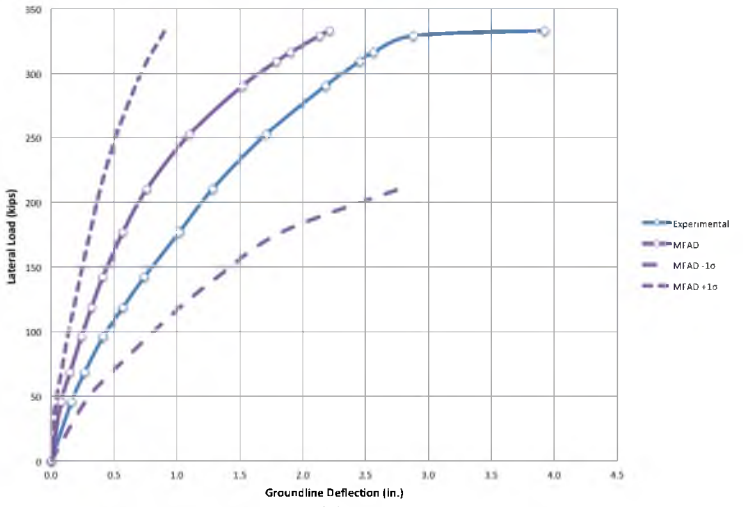

(c)

Figure 4.33. Load-deflection curves for DS 20-6 using ± 1 standard deviation input parameters for a) LPile, b) DFSAP, and c) MFAD models

4.5 Load Test 22 Results

The lateral load vs. groundline deflection curves from the experimental and analytical results for DS 22-1 are presented in Figure 4.34a. The experimentally-observed groundline deflection is plotted against the predicted groundline deflection from each analysis method for DS 22-1 in Figure 4.34b.

The results shown in Figure 4.34a and Figure 4.34b show that *LPile* initially underpredicted groundline deflection and then overpredicted groundline deflection at larger magnitudes of applied load. The results show that *DFSAP* initially overpredicted groundline deflection and then underpredicted groundline deflection with increasing applied load. With the exception of the initial increment of applied load, *MFAD* underpredicted groundline deflection for the entire range of applied load. For this experiment, *LPile* estimated the most groundline deflection and *MFAD* estimated the least groundline deflection for measured deflection greater than approximately 0.4 inches.

The lateral load vs. groundline deflection curves from the experimental and analytical results for DS 22-1 using soil input properties with ±1 standard deviation from the "best-estimate" values are presented in Figure 4.35. As with previous load test simulations, considerably more pile head deflection occurs when soil input properties are reduced by one standard deviation. For this experiment, *LPile* was the most sensitive to the change in soil input properties and *DFSAP* was the least sensitive to change in soil input properties. *LPile* and *MFAD* exhibited a considerable increase in sensitivity with increasing applied load, while *DFSAP* exhibited only a minor increase in sensitivity with increasing applied load. It should be noted that all three analysis methods failed to reach solutions before the ultimate applied load of 169 kips for soil input properties of -1 standard deviation.

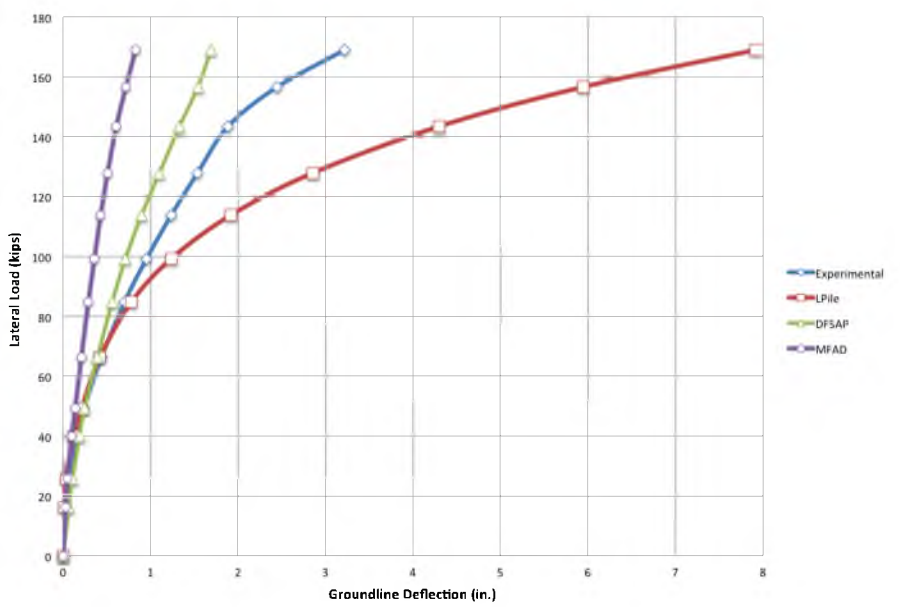

(a)

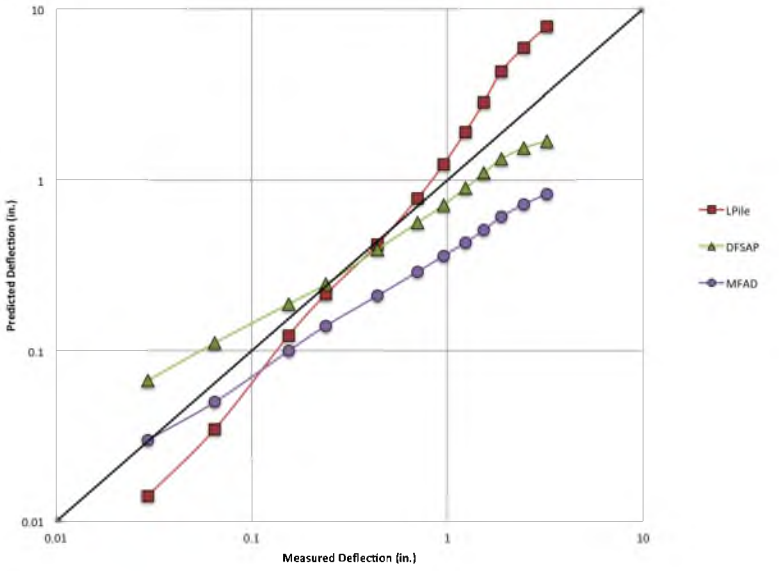

(b)

Figure 4.34. DS 22-1 results showing a) lateral load vs. groundline deflection curves, and b) predicted vs. measured groundline deflection curves in log-log scale

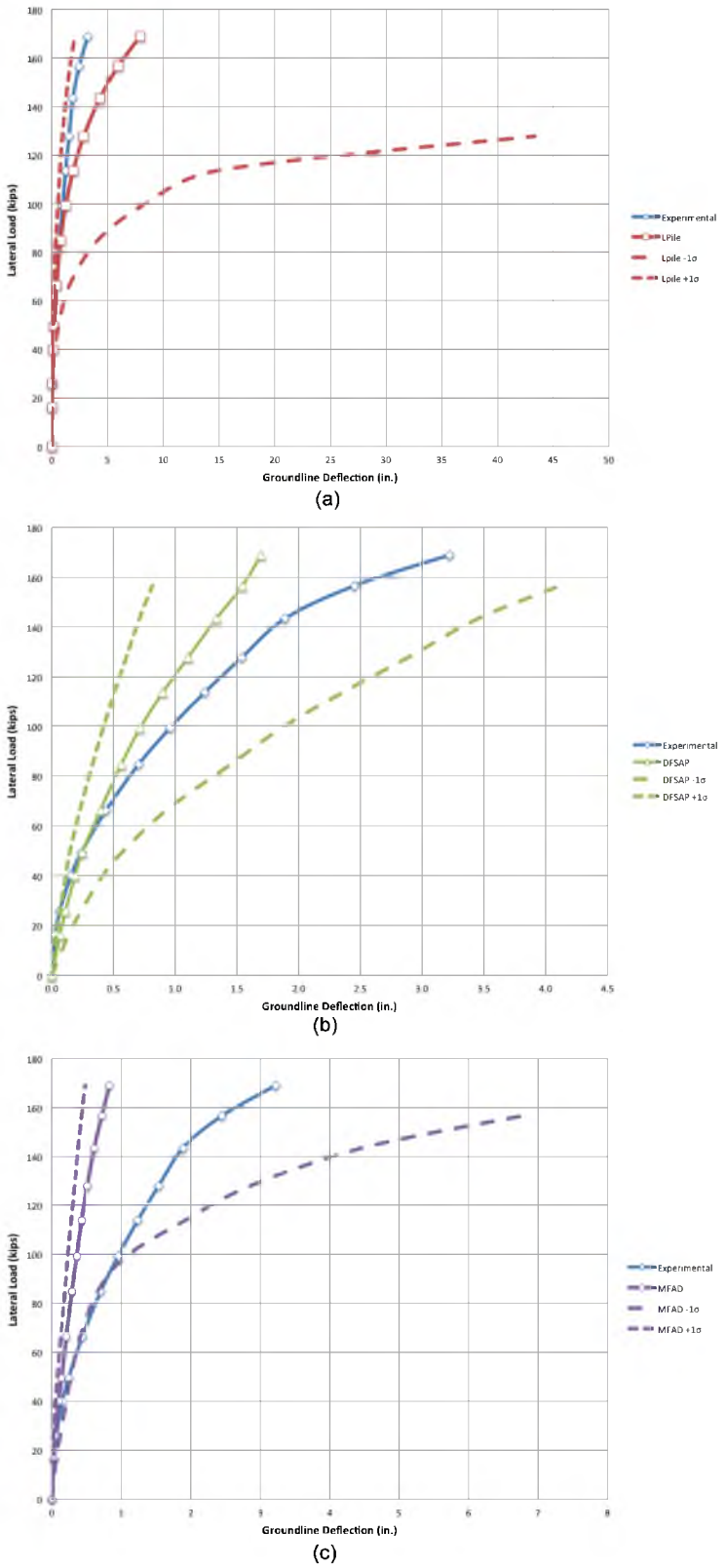

Figure 4.35. Load-deflection curves for DS 22-1 using ± 1 standard deviation input parameters for a) LPile, b) DFSAP, and c) MFAD models

The lateral load vs. groundline deflection curves from the experimental and analytical results for DS 22-2 are presented in Figure 4.36a. The experimentally-observed groundline deflection is plotted against the predicted groundline deflection from each analysis method for DS 22-2 in Figure 4.36b.

The results shown in Figure 4.36a and Figure 4.36b show that *LPile* initially underpredicted groundline deflection and then overpredicted groundline deflection at larger magnitudes of applied load. The results show that *DFSAP* initially overpredicted groundline deflection and then underpredicted groundline deflection with increasing applied load. With the exception of the initial increment of applied load, *MFAD* underpredicted groundline deflection for the entire range of applied load. For this experiment, *LPile* estimated the most groundline deflection and *MFAD* estimated the least groundline deflection for measured deflection greater than approximately 0.3 inches.

The lateral load vs. groundline deflection curves from the experimental and analytical results for DS 22-2 using soil input properties with ±1 standard deviation from the "best-estimate" values are presented in Figure 4.37. These results show that increasing or decreasing the soil input properties by one standard deviation does not result in equivalent deviation from the best-estimate input property values, but results in considerably more pile head deflection when soil input properties are reduced by one standard deviation. For this experiment, *LPile* was the most sensitive to the change in soil input properties and *DFSAP* was the least sensitive to change in soil input properties. *LPile* and *MFAD* exhibited a considerable increase in sensitivity with increasing applied load, while *DFSAP* exhibited only a minor increase in sensitivity with increasing applied load. It should be noted that all three analysis methods failed to reach solutions before the ultimate applied load of 127 kips for soil input properties of -1 standard deviation.

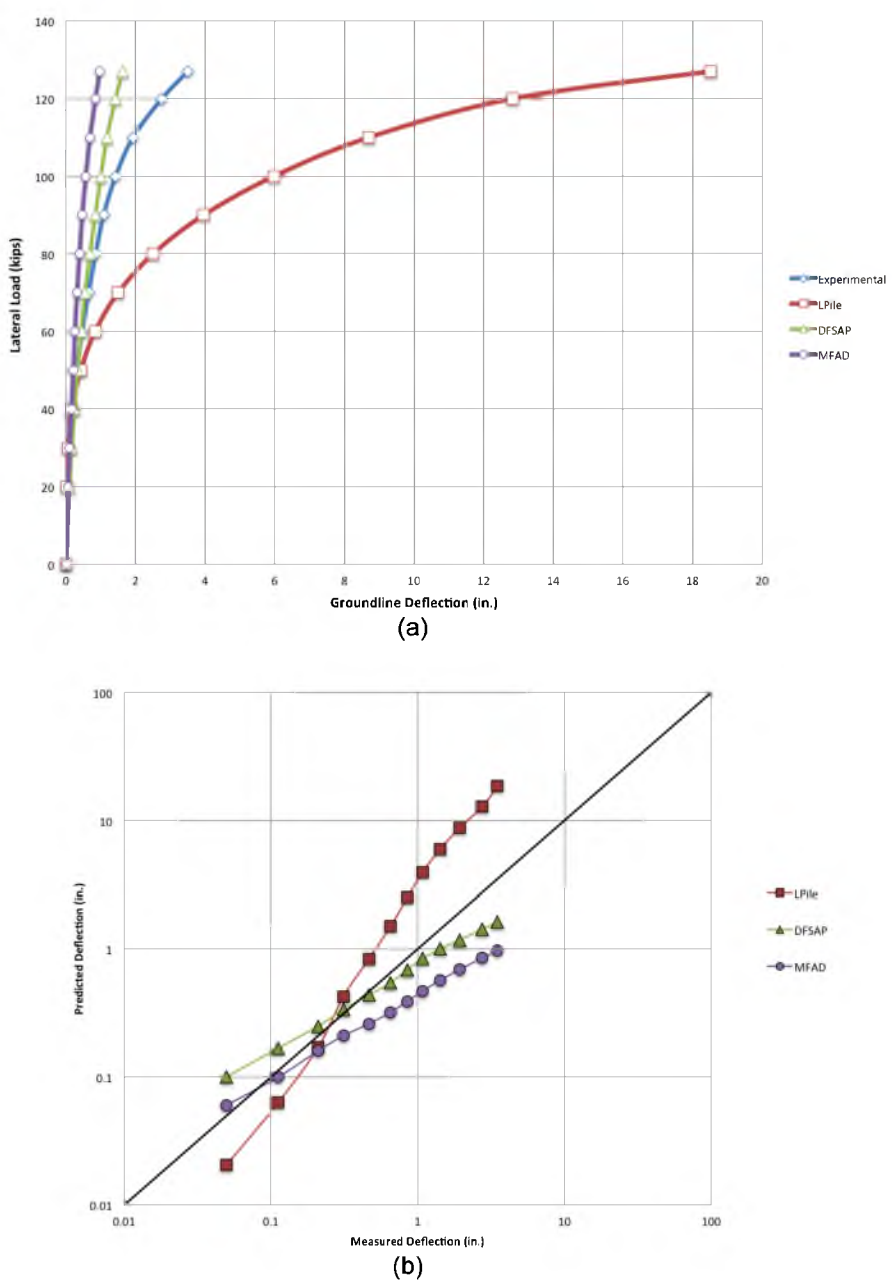

Figure 4.36. DS 22-2 results showing a) lateral load vs. groundline deflection curves, and b) predicted vs. measured groundline deflection curves in log-log scale

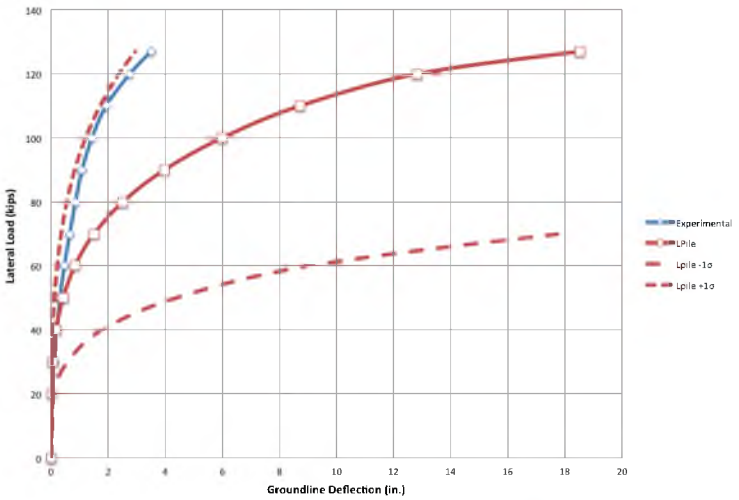

(a)

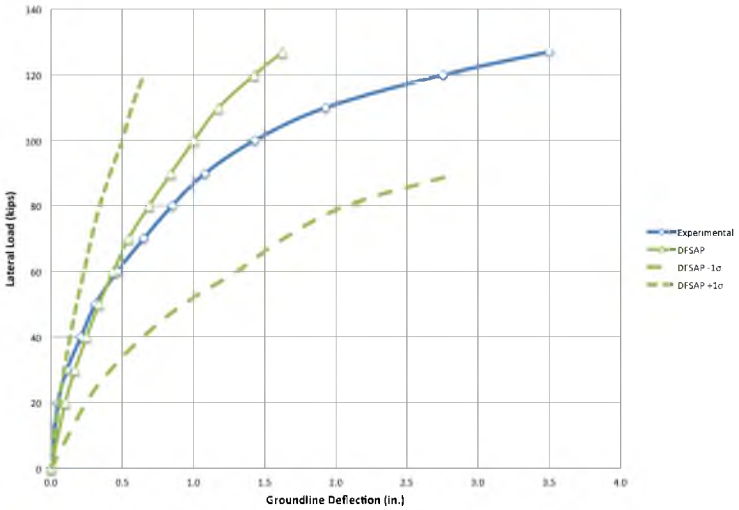

(b)

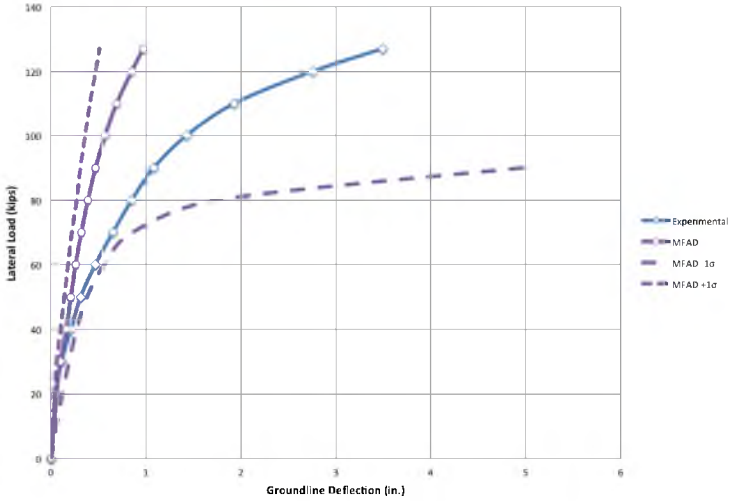

(c)

Figure 4.37. Load-deflection curves for DS 22-2 using ± 1 standard deviation input parameters for a) LPile, b) DFSAP, and c) MFAD models

4.6 Load Test 23 Results

The lateral load vs. groundline deflection curves from the experimental and analytical results for DS 23-1 are presented in Figure 4.38a. The experimentally-observed groundline deflection is plotted against the predicted groundline deflection from each analysis method for DS 23-1 in Figure 4.38b.

The results shown in Figure 4.38a and Figure 4.38b show that *LPile* initially underpredicted groundline deflection and then overpredicted groundline deflection with an increase in applied load. Both *DFSAP* and *MFAD* underpredicted groundline deflection for the entire range of applied load. With the exception of the second increment of applied load, *LPile* estimated the most groundline deflection and *MFAD* estimated the least groundline deflection for the range of applied load in this experiment.

The lateral load vs. groundline deflection curves from the experimental and analytical results for DS 23-1 using soil input properties with ±1 standard deviation from the "best-estimate" values are presented in Figure 4.39. These results show that increasing or decreasing the soil input properties by one standard deviation does not result in equivalent deviation from the best-estimate input property values, but instead results in considerably more pile head deflection when soil input properties are reduced by one standard deviation. For this experiment, *MFAD* was the most sensitive to change in soil input properties, while *LPile* was the least sensitive to the change in soil input properties. All three analysis methods exhibited higher sensitivity to soil input properties with increasing applied load; however, *MFAD* exhibited considerably higher sensitivity to soil input properties than the other two methods. It should be noted that all three analysis methods failed to reach solutions before the ultimate applied load of 120 kips for soil input properties of -1 standard deviation.

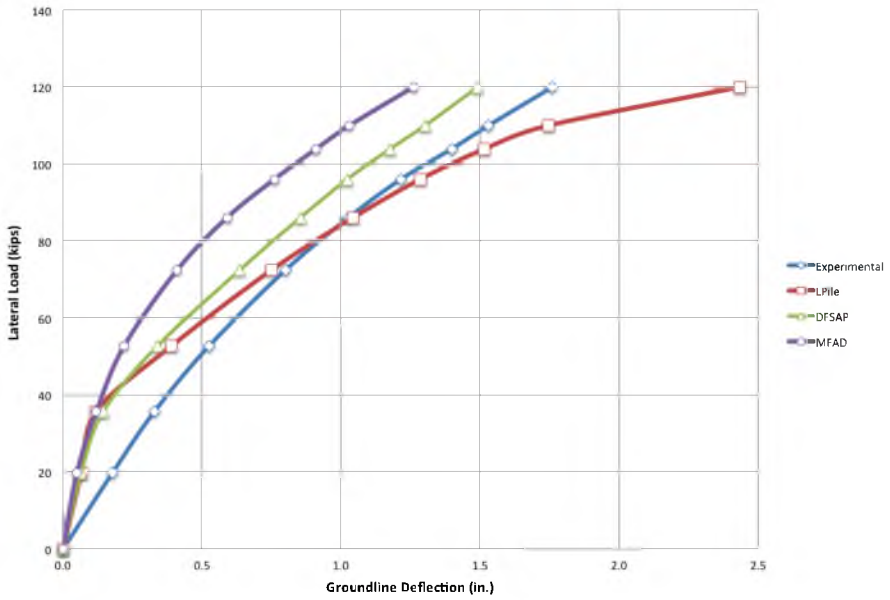

(a)

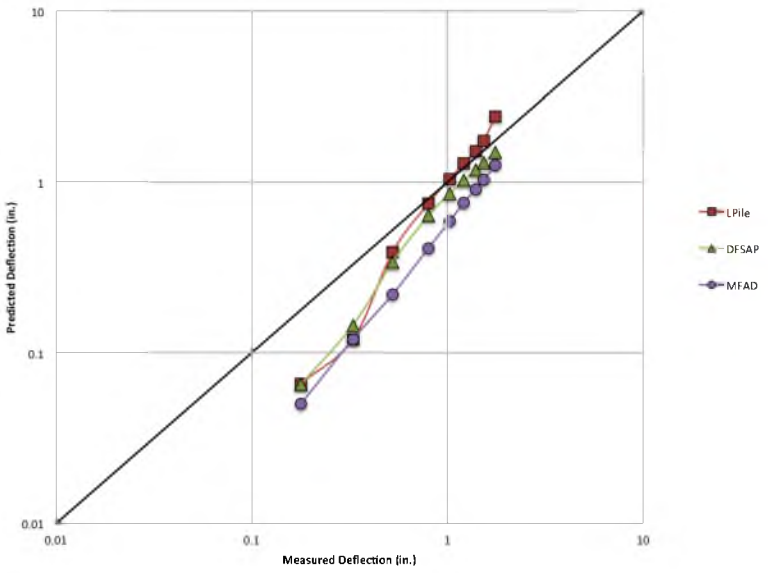

(b)

Figure 4.38. DS 23-1 results showing a) lateral load vs. groundline deflection curves, and b) predicted vs. measured groundline deflection curves in log-log scale

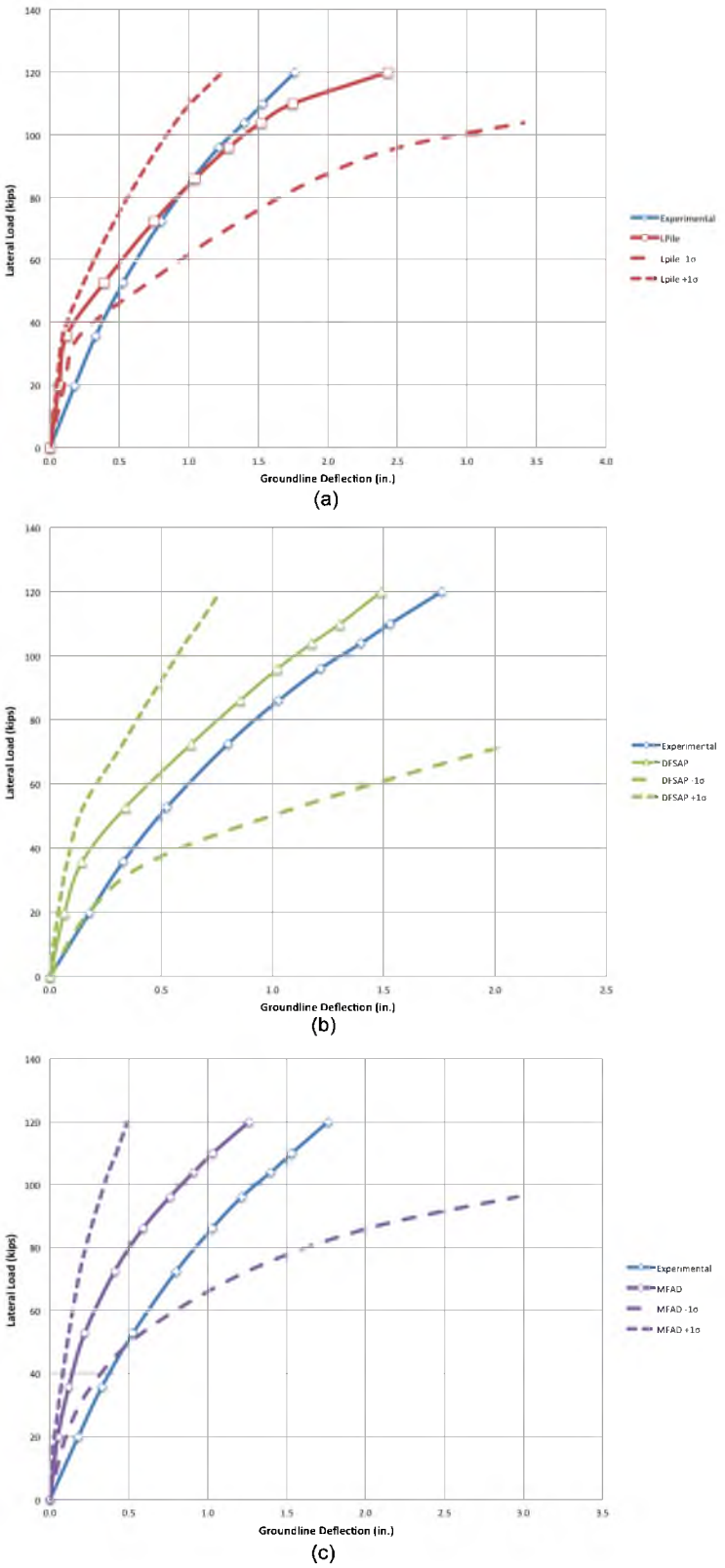

Figure 4.39. Load-deflection curves for DS 23-1 using ± 1 standard deviation input parameters for a) LPile, b) DFSAP, and c) MFAD models

The lateral load vs. groundline deflection curves from the experimental and analytical results for DS 23-2 are presented in Figure 4.40a. The experimentally-observed groundline deflection is plotted against the predicted groundline deflection from each analysis method for DS 23-2 in Figure 4.40b.

The results shown in Figure 4.40a and Figure 4.40b show that, with the exception of the initial and final increments of applied load, *LPile* underpredicted groundline deflection over the entire range of applied load. It should be noted that this experiment was the only experiment in this investigation in which *LPile* underpredicted groundline deflection for the majority of the range of applied load. *DFSAP* underpredicted groundline deflection for all but the first two increments of applied load. With the exception of the initial load increment, *MFAD* underpredicted groundline deflection for the entire range of applied load. For this experiment, *LPile* generally estimated the most groundline deflection and *MFAD* estimated the least groundline deflection.

The lateral load vs. groundline deflection curves from the experimental and analytical results for DS 23-2 using soil input properties with ±1 standard deviation from the "best-estimate" values are presented in Figure 4.41. As with previous load tests, considerably more pile head deflection occurs when soil input properties are reduced by one standard deviation. For this experiment, *MFAD* was the most sensitive to change in soil input properties, while *LPile* was the least sensitive to the change in soil input properties. All three analysis methods exhibited higher sensitivity to soil input properties with increasing applied load; however, *MFAD* exhibited considerably higher sensitivity to soil input properties than the other two methods. It should be noted that all three analysis methods failed to reach solutions before the ultimate applied load of 120 kips for soil input properties of -1 standard deviation.

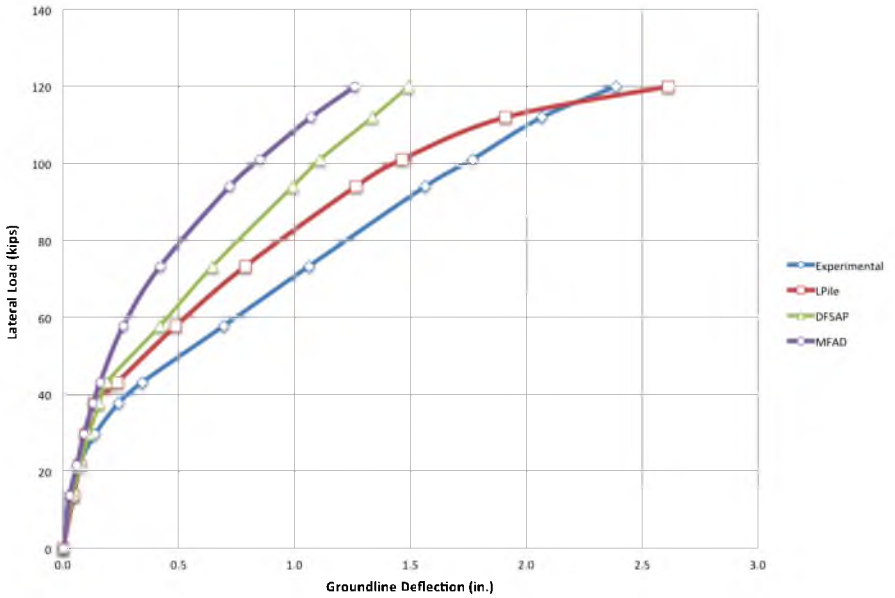

(a)

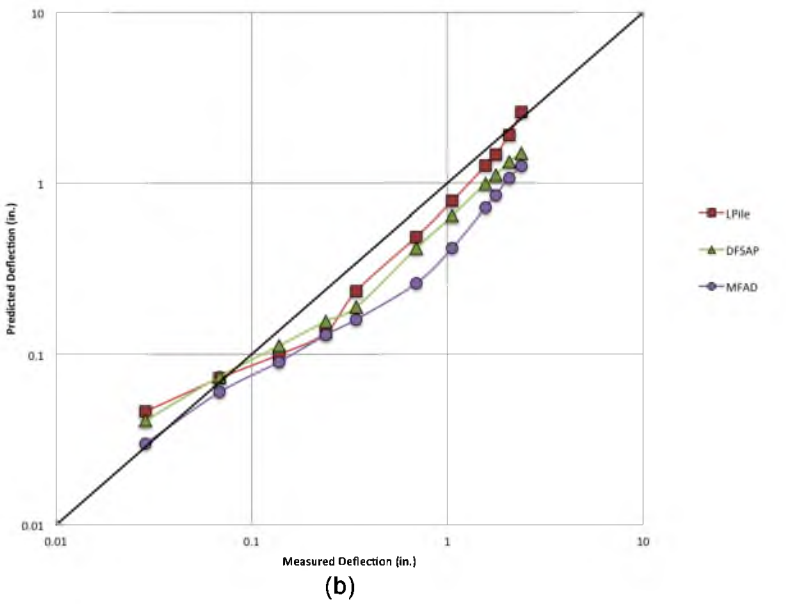

(b)

Figure 4.40. DS 23-2 results showing a) lateral load vs. groundline deflection curves, and b) predicted vs. measured groundline deflection curves in log-log scale

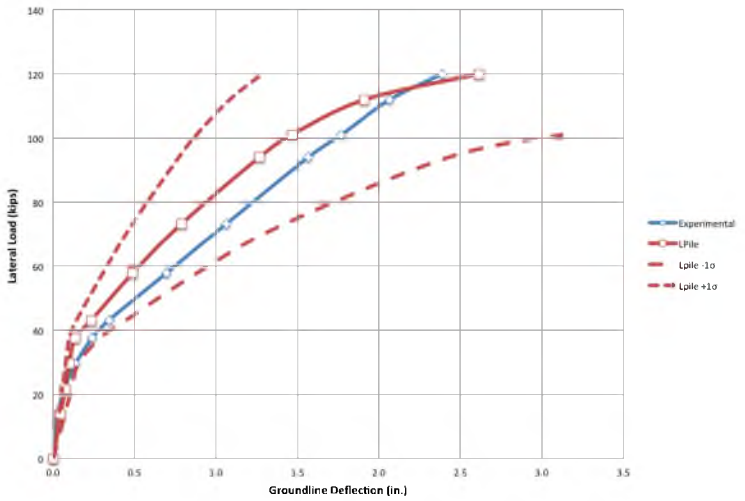

(a)

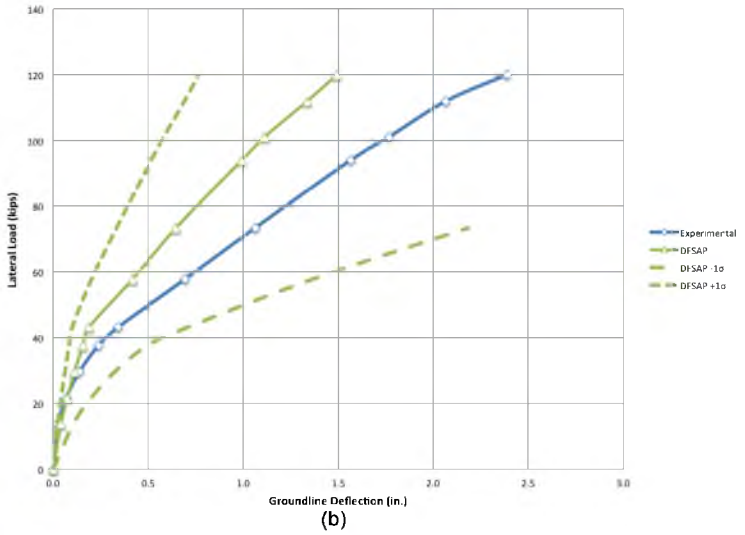

(b)

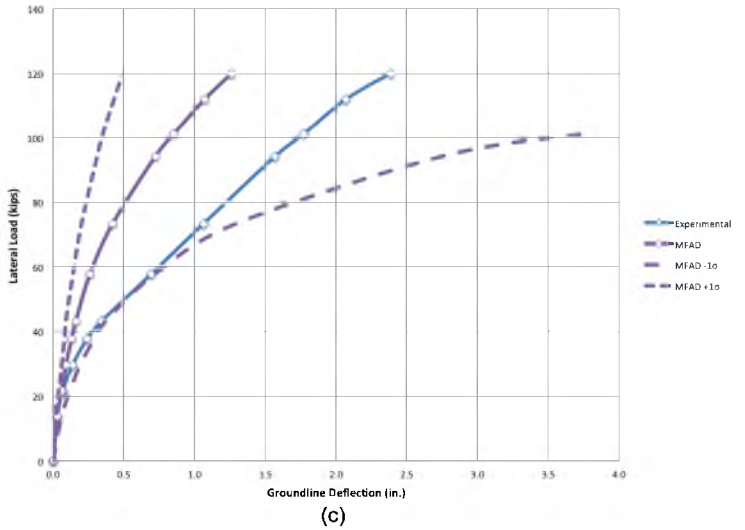

(c)

Figure 4.41. Load-deflection curves for DS 23-2 using ± 1 standard deviation input parameters for a) LPile, b) DFSAP, and c) MFAD models

4.7 Load Test 75 Results

The lateral load vs. groundline deflection curves from the experimental and analytical results for DS 75-1 are presented in Figure 4.42a. The experimentally-observed groundline deflection is plotted against the predicted groundline deflection from each analysis method for DS 75-1 in Figure 4.42b.

The results shown in Figure 4.42a and Figure 4.42b show that all three analysis methods underpredicted the groundline deflection for the initial increment of applied load. Both *LPile* and *DFSAP* overpredicted groundline deflection for all subsequent increments of applied load, while *MFAD* underpredicted groundline deflection for all subsefor all subsequent increments of applied load. It should be noted that *LPile* and *DFSAP* failed to converge on a solution for loads greater than 267 kips.

The lateral load vs. groundline deflection curves from the experimental and analytical results for DS 75-1 using soil input properties with ±1 standard deviation from the "best-estimate" values are presented in Figure 4.43. These results show that increasing or decreasing the soil input properties by one standard deviation does not result in equivalent deviation from the best-estimate input property values, but instead results in considerably more pile head deflection when soil input properties are reduced by one standard deviation. For this experiment, *MFAD* was the most sensitive to the change in soil input properties, while *LPile* and *DFSAP* exhibited very similar sensitivity to change in soil input properties over the entire range of applied load. None of the analysis methods appeared to show any correlation between sensitivity to soil input properties and magnitude of applied load. It should be noted that all three analysis methods failed to reach solutions before the ultimate applied load of 320 kips for soil input properties of -1 standard deviation.

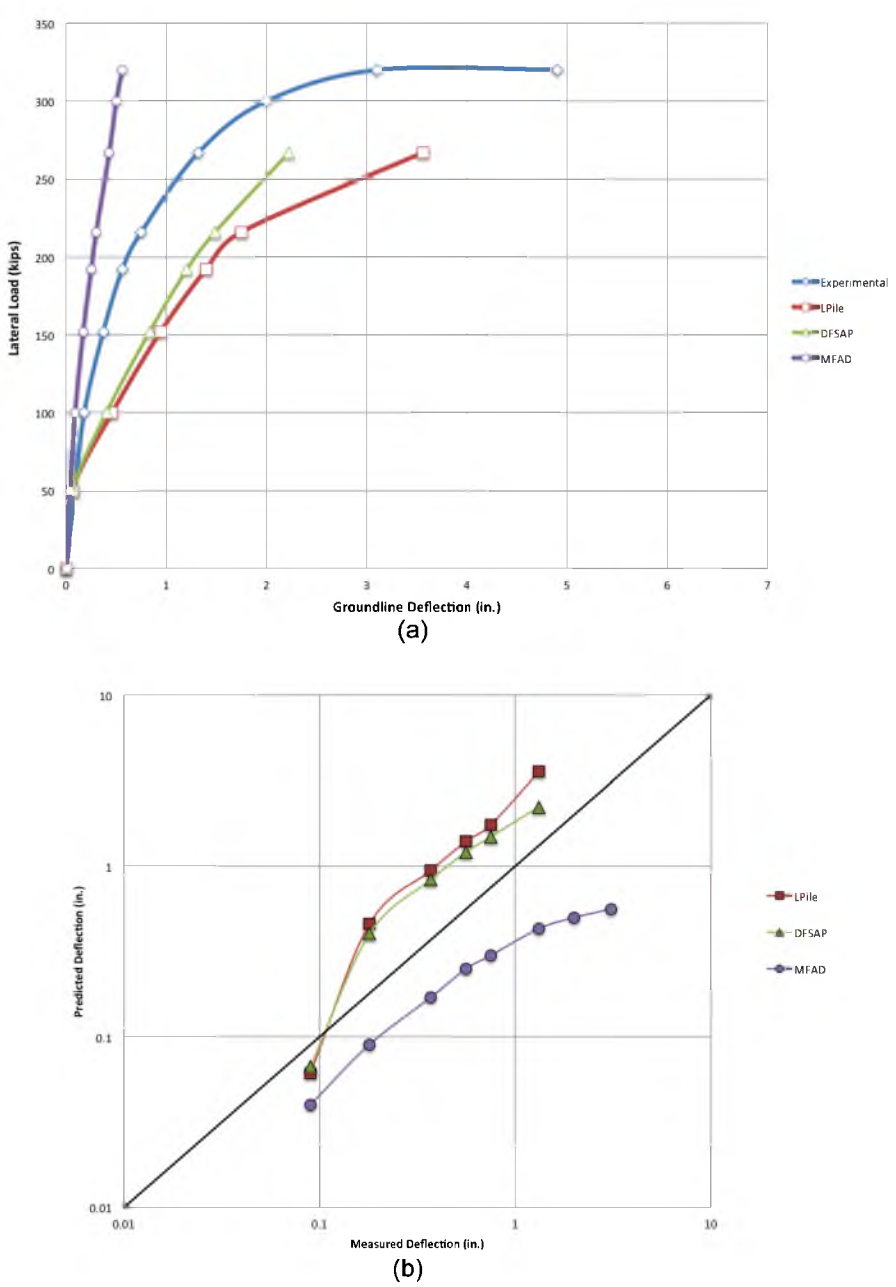

Figure 4.42. DS 75-1 results showing a) lateral load vs. groundline deflection curves, and b) predicted vs. measured groundline deflection curves in log-log scale

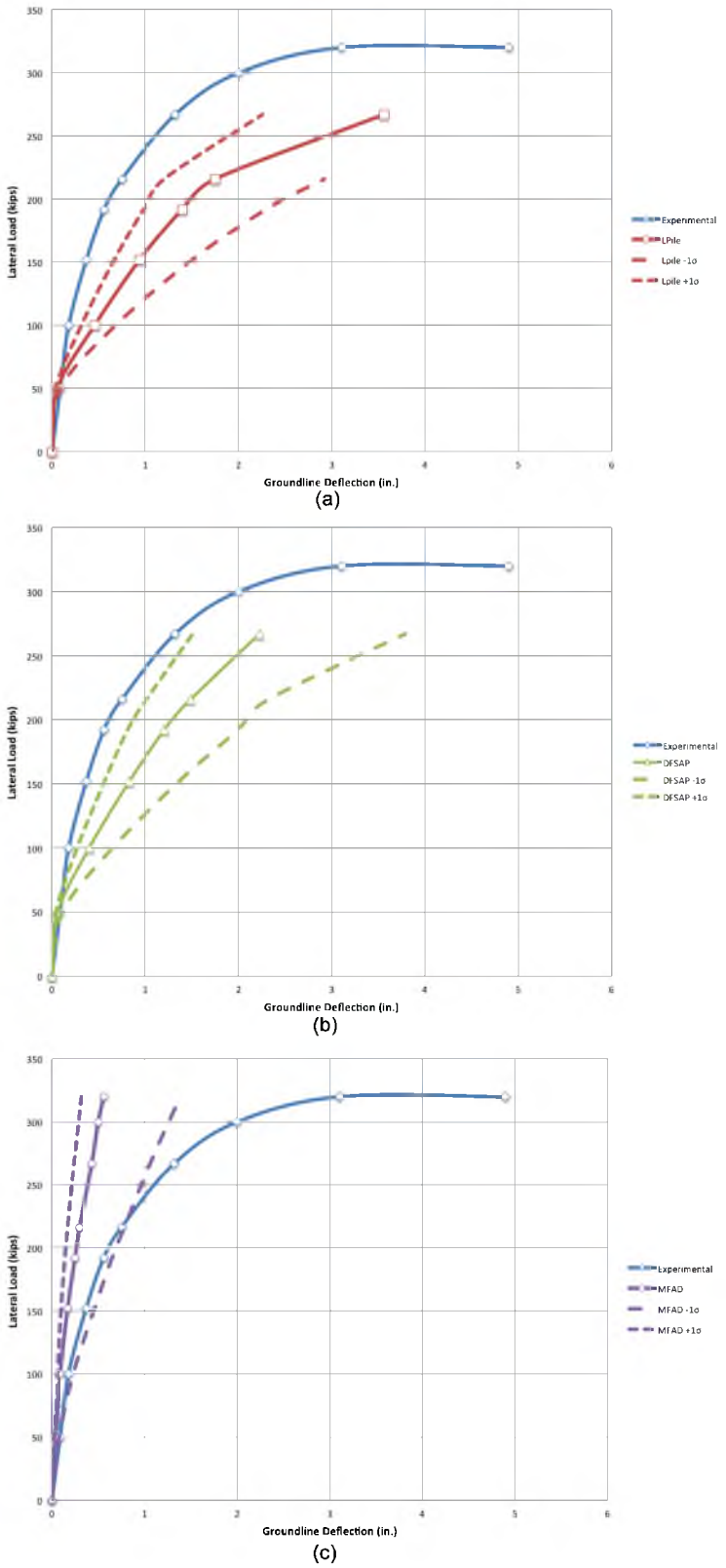

Figure 4.43. Load-deflection curves for DS 75-1 using ± 1 standard deviation input parameters for a) LPile, b) DFSAP, and c) MFAD models

4.8 Load Test 76 Results

The lateral load vs. groundline deflection curves from the experimental and analytical results for DS 76-1 are presented in Figure 4.44a. The experimentally-observed groundline deflection is plotted against the predicted groundline deflection from each analysis method for DS 76-1 in Figure 4.44b.

The results shown in Figure 4.44a and Figure 4.44b show that *LPile* initially underpredicted groundline deflection and then overpredicted groundline deflection at larger magnitudes of applied load. These results show that *DFSAP* overpredicted groundline deflection for the entire range of applied load, while *MFAD* initially overpredicted groundline deflection and then underpredicted groundline deflection at larger magnitudes of applied load. With the exception of the first increment of applied load, *LPile* estimated the most groundline deflection and *MFAD* estimated the least amount of groundline deflection for this experiment.

The lateral load vs. groundline deflection curves from the experimental and analytical results for DS 76-1 using soil input properties with ±1 standard deviation from the "best-estimate" values are presented in Figure 4.45. These results show that increasing or decreasing the soil input properties by one standard deviation does not result in equivalent deviation from the best-estimate input property values, but instead results in considerably more pile head deflection when soil input properties are reduced by one standard deviation. For this experiment, *LPile* was the most sensitive to the change in soil input properties and *MFAD* was the least sensitive to change in soil input properties. *LPile* exhibited considerable increase in sensitivity to soil input properties as the magnitude of applied load increased, while *MFAD* and *DFSAP* exhibited only minor differences in sensitivity over the entire range of applied load. It should be noted that this

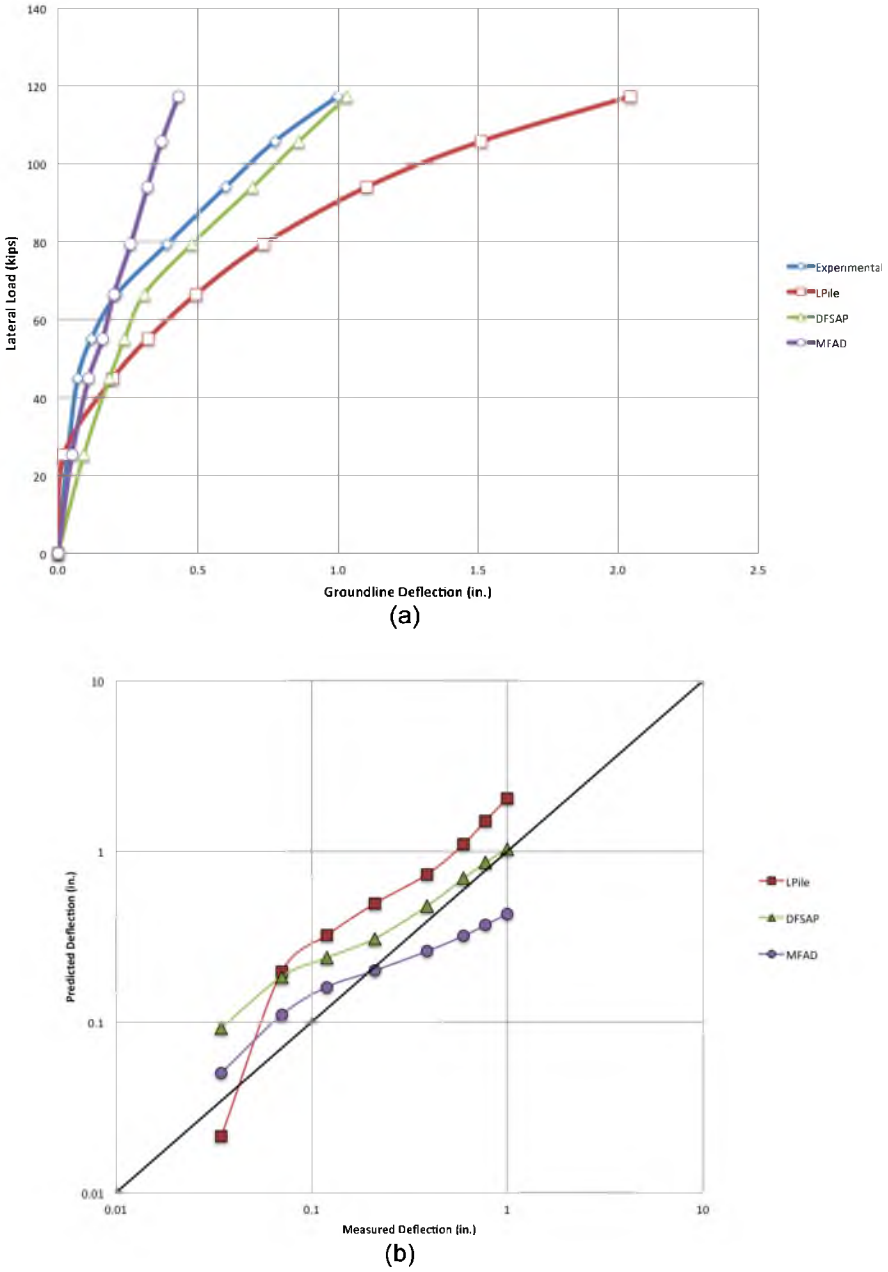

Figure 4.44. DS 76-1 results showing a) lateral load vs. groundline deflection curves, and b) predicted vs. measured groundline deflection curves in log-log scale

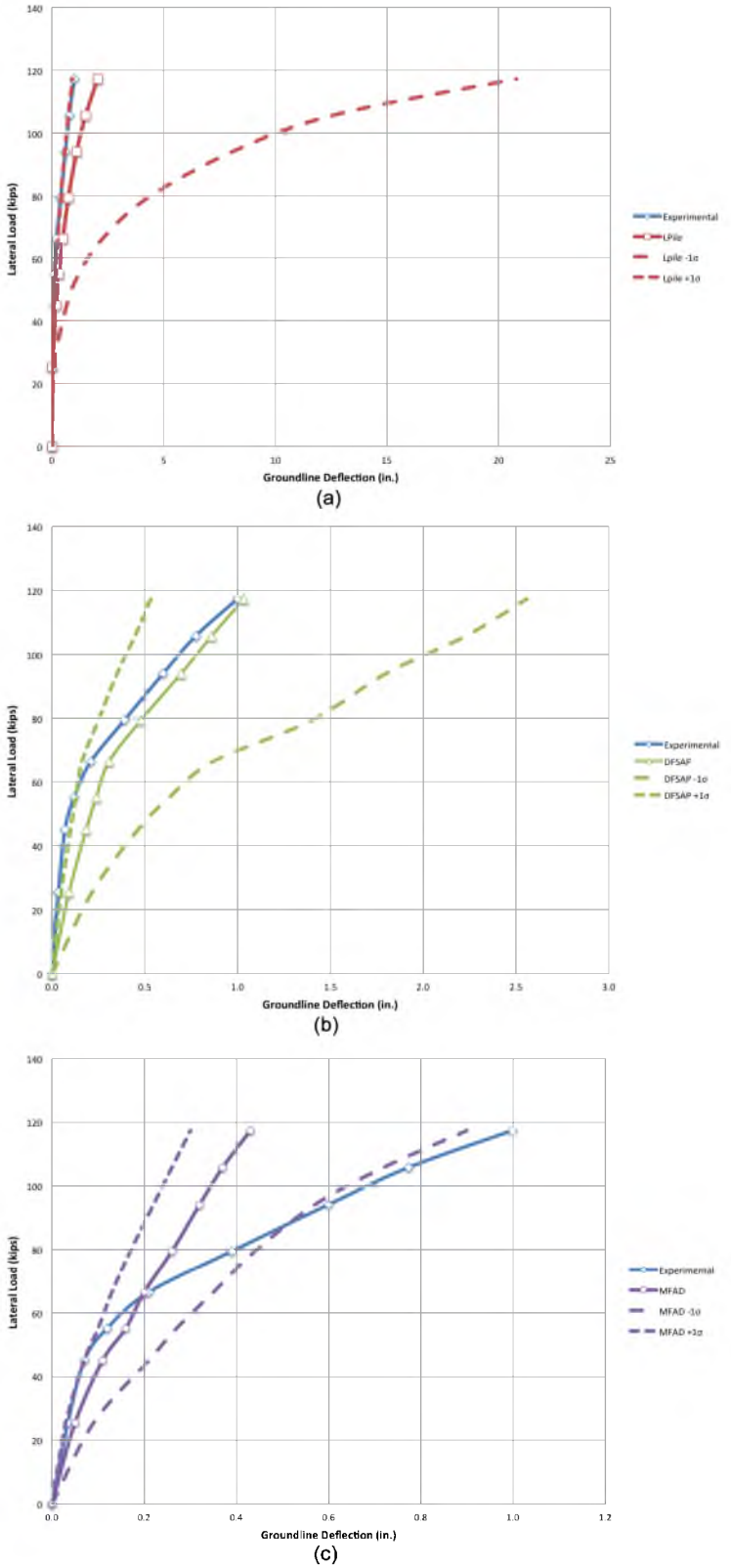

Figure 4.45. Load-deflection curves for DS 76-1 using ± 1 standard deviation input parameters for a) LPIle, b) DFSAP, and c) MFAD models

experiment was the only experiment in this investigation where solutions were obtained for all three analysis methods at the maximum applied load for soil input properties of -1 standard deviation. The maximum applied load for this experiment only resulted in 1 inch of pile head deflection, and it is therefore likely that this experiment was terminated well below the ultimate capacity of the foundation.

4.8.1 Parametric Study

The parameters that were included in the parametric study for *LPile* and *DFSAP* were s_u and ε_{50}. The results of the *LPile* analyses for the upper bound, lower bound, and best-estimate values of s_u and ε_{50} are shown in Figure 4.46 and Figure 4.47, respectively. The results of the *DFSAP* analyses for the upper bound, lower bound, and best-estimate values of s_u and ε_{50} are shown in Figure 4.48 and Figure 4.49, respectively.

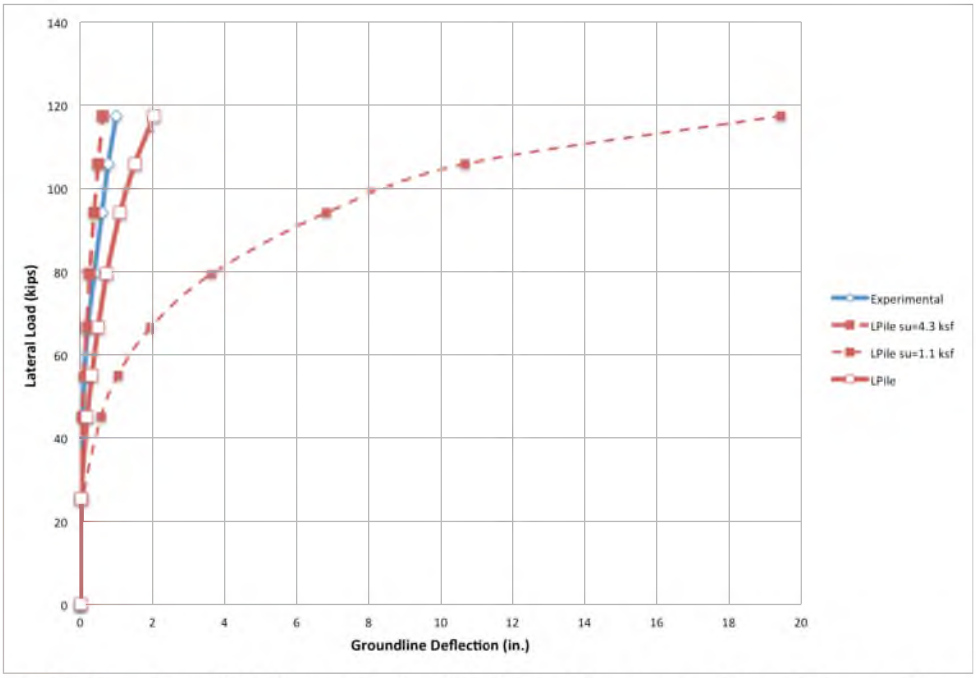

Figure 4.46. Results of LPile analysis of DS 76-1 for upper bound, lower bound, and best-estimate values of s_u

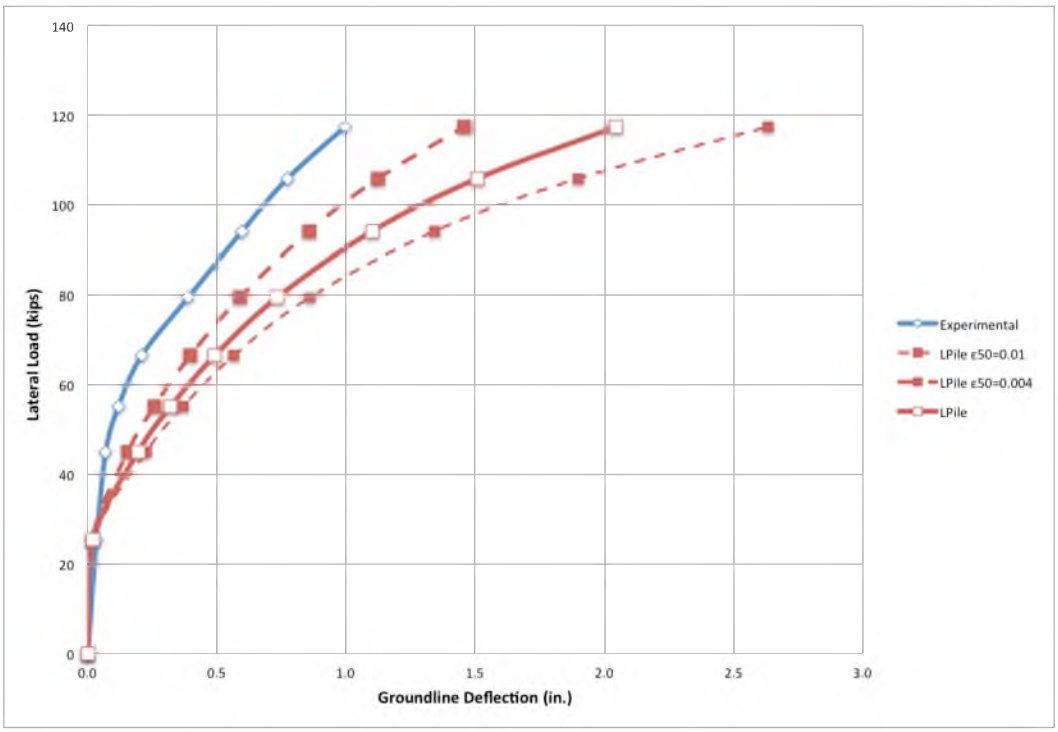

Figure 4.47. Results of LPile analysis of DS 76-1 for upper bound, lower bound, and best-estimate values of ε_{50}

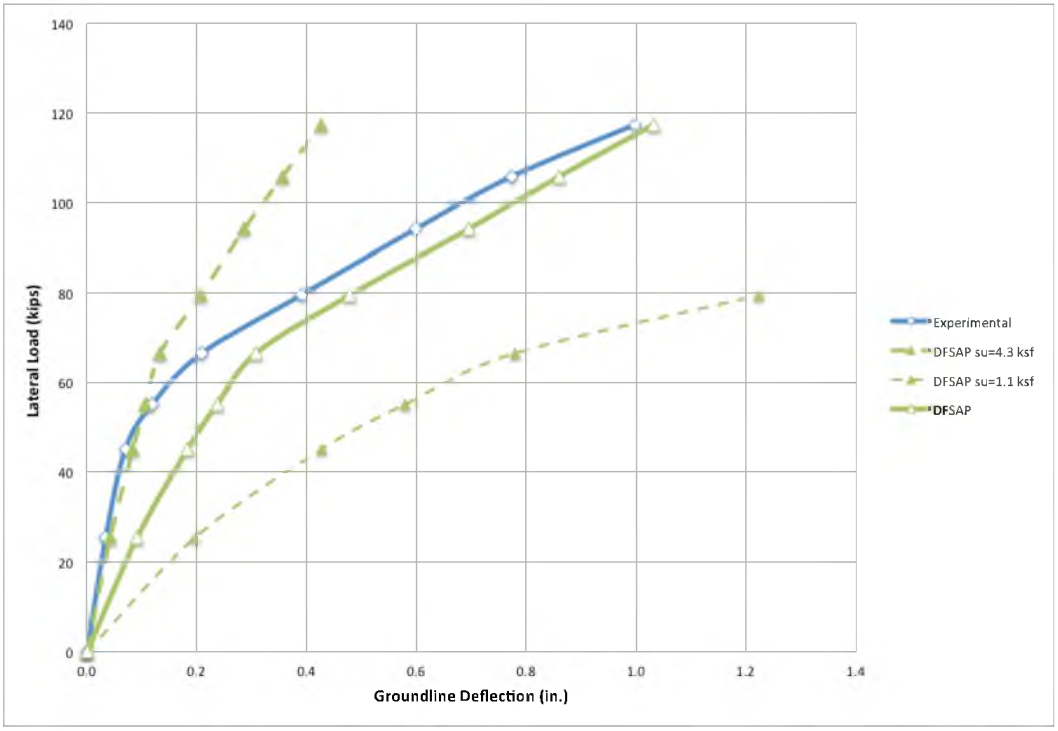

Figure 4.48. Results of DFSAP analysis of DS 76-1 for upper bound, lower bound, and best-estimate values of s_u

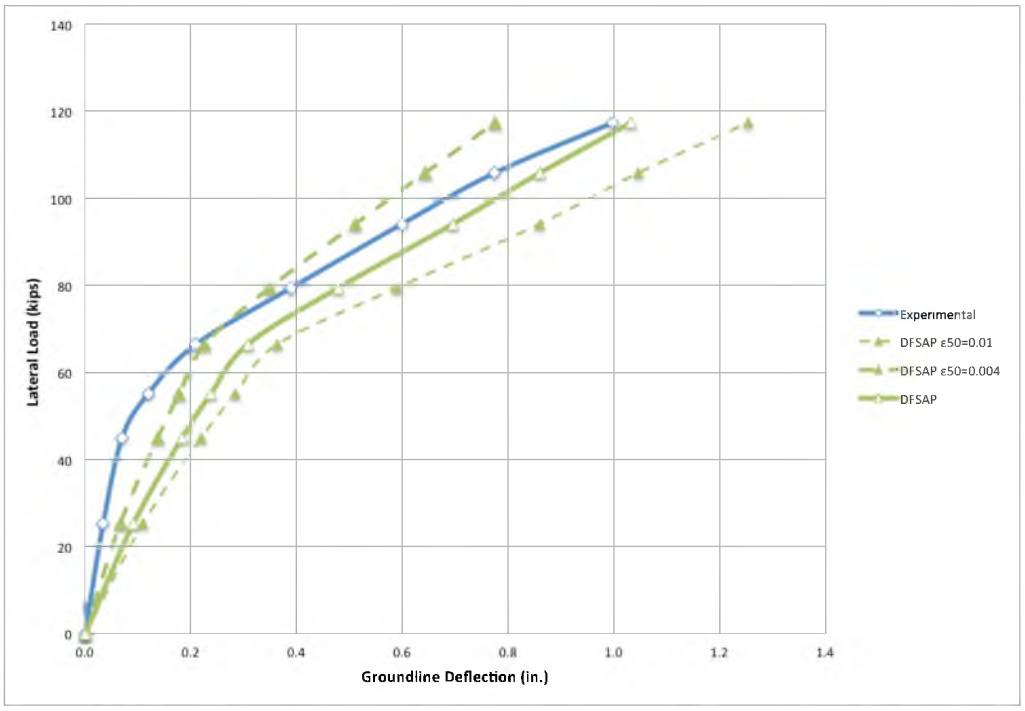

Figure 4.49. Results of DFSAP analysis of DS 76-1 for upper bound, lower bound, and best-estimate values of ε_{50}

The parameters that were included in the parametric study for *MFAD* were s_u and E_p. The results of the *MFAD* analyses for the upper bound, lower bound, and best-estimate values of s_u and E_p are shown in Figure 4.50 and Figure 4.51, respectively.

The sensitivity analysis for s_u was performed by applying a constant lateral load to the top of the foundation and incrementally increasing s_u for each simulation. The range of s_u that was chosen for the sensitivity analysis was 1.0 to 6.0 ksf. The lateral load that was applied to the top of the foundation in each model was the maximum reported load of 117 kips.

The *LPile* and *DFSAP* simulations that were performed at each incremental value of s_u were performed for four values of ε_{50} to gain insight into the sensitivity of the model to ε_{50}, and to identify whether the sensitivity of s_u was dependent upon ε_{50}. The values of ε_{50} that were used for the sensitivity analysis were 0.004, 0.006, 0.008, and 0.01, which

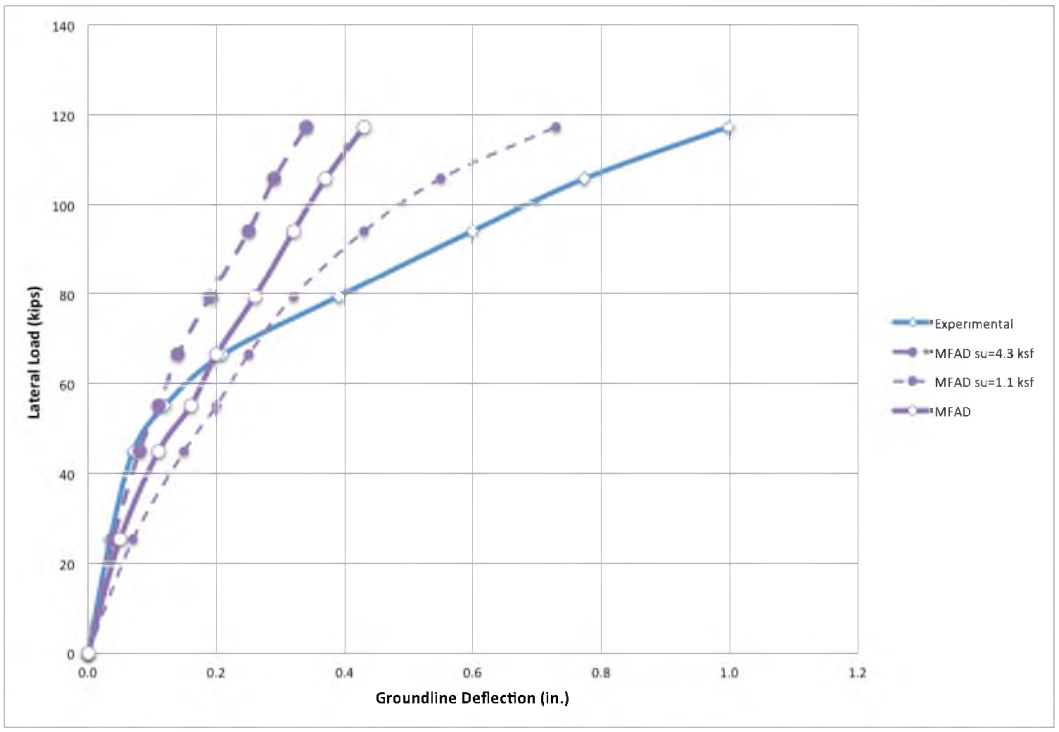

Figure 4.50. Results of MFAD analysis of DS 76-1 for upper bound, lower bound, and best-estimate values of s_u

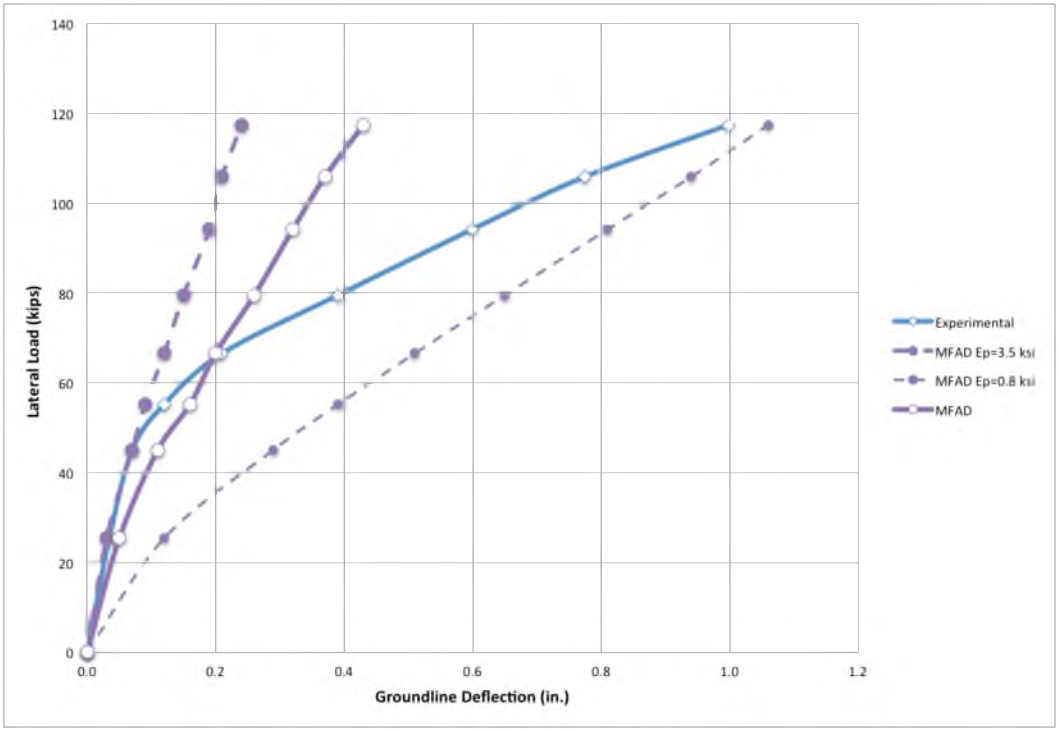

Figure 4.51. Results of MFAD analysis of DS 76-1 for upper bound, lower bound, and best-estimate values of E_p

are within the expected range of ε_{50} for the specified range of s_u. A plot of pile head deflection vs. s_u for each *LPile* simulation is shown in Figure 4.52. The same figure is also shown in log-log scale in Figure 4.53. It should be noted that the minimum value of s_u for this sensitivity analysis was 1.1 ksf because it was not possible to obtain an *LPile* solution for all values of ε_{50} at 1.0 ksf.

A plot of pile head deflection vs. s_u for each *DFSAP* simulation is shown in Figure 4.54. The same figure is also shown in log-log scale in Figure 4.55. It should be noted that the minimum value of s_u for this sensitivity analysis was 1.3 ksf because it was not possible to obtain a *DFSAP* solution for all values of ε_{50} at 1.0 ksf.

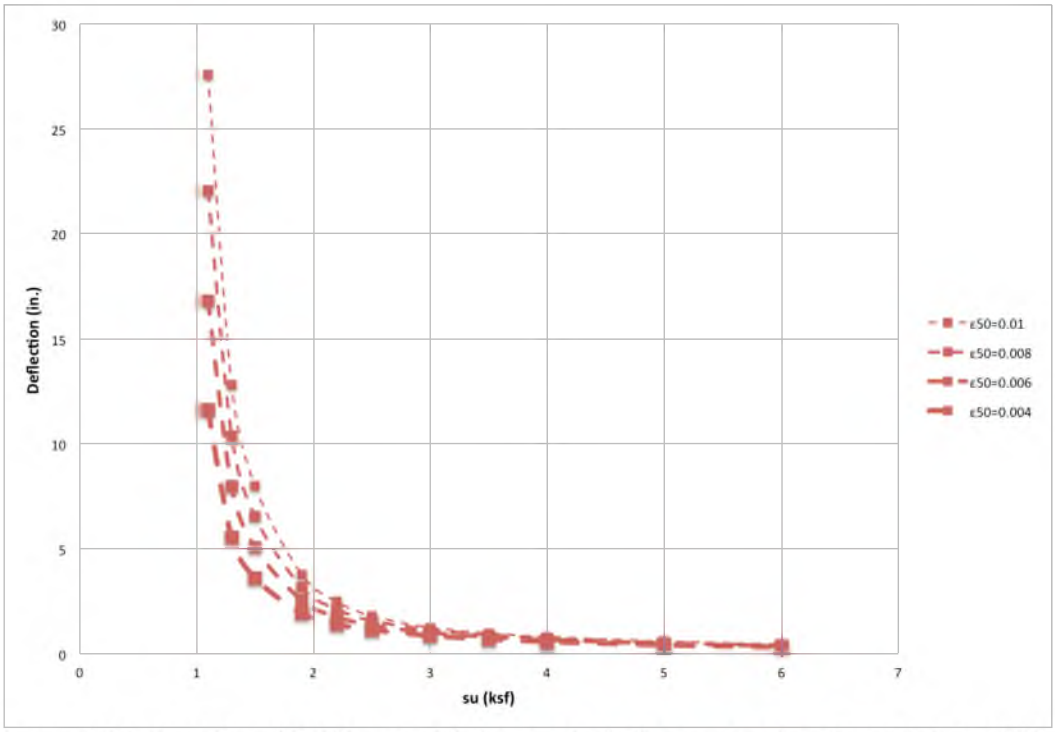

Figure 4.52. Results of LPile sensitivity analysis for s_u ranging from 1.1 to 6.0 ksf and ε_{50} ranging from 0.004 to 0.01

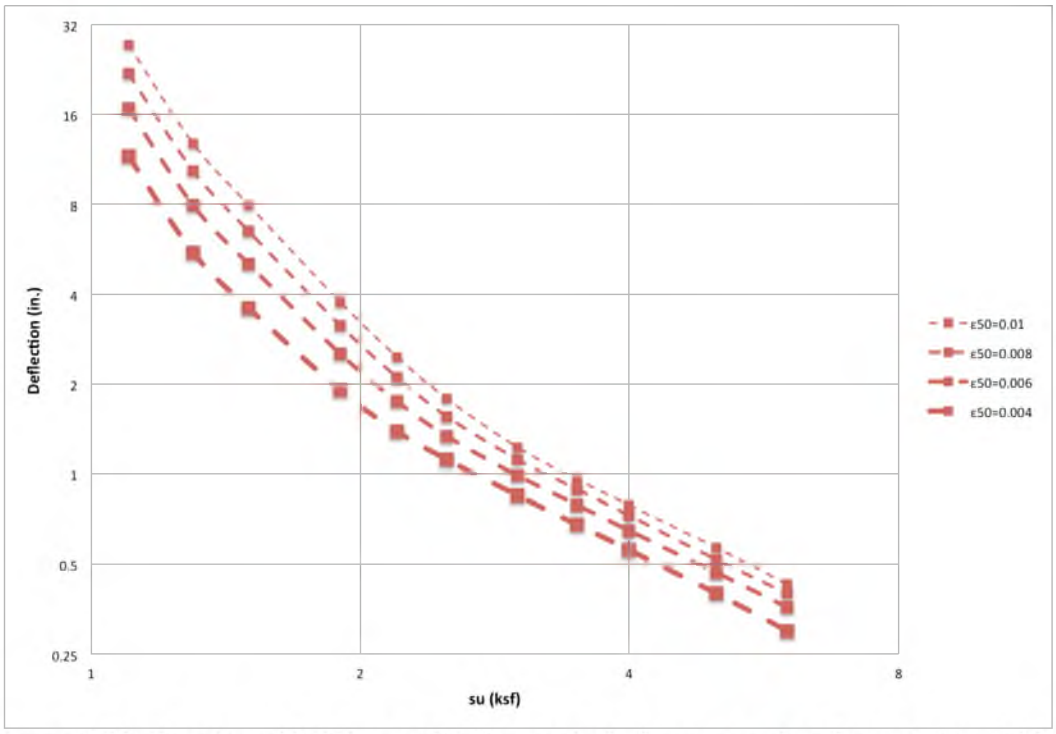

Figure 4.53. Results of LPile sensitivity analysis for s_u ranging from 1.1 to 6.0 ksf and ε_{50} ranging from 0.004 to 0.01 in log-log scale

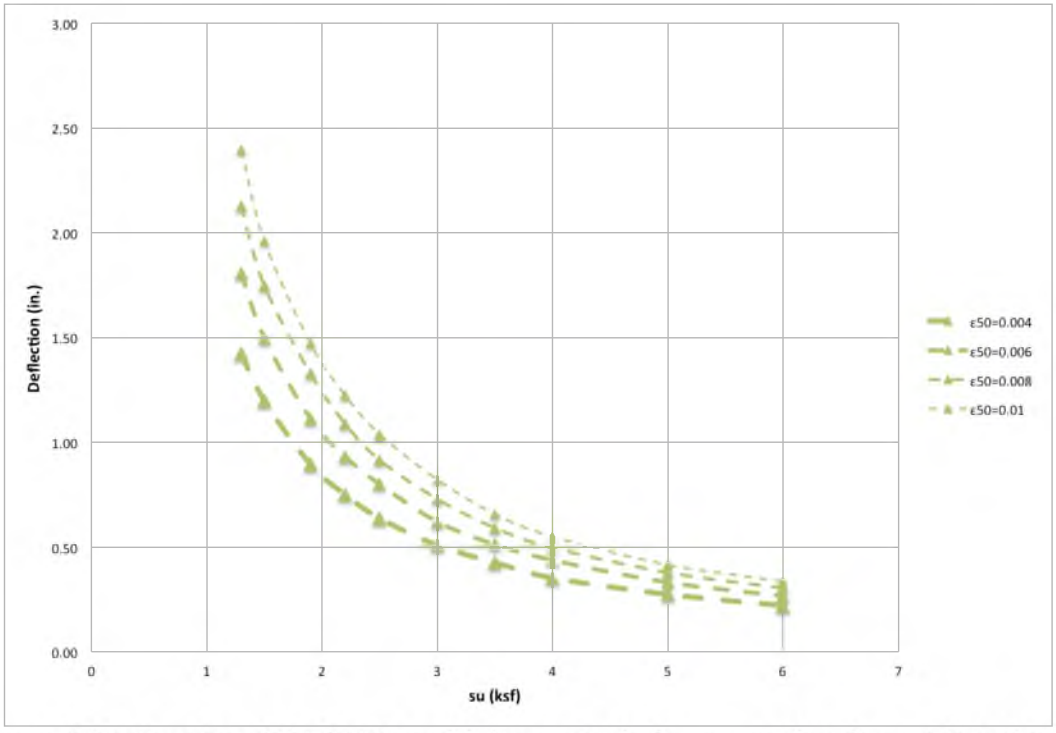

Figure 4.54. Results of DFSAP sensitivity analysis for s_u ranging from 1.3 to 6.0 ksf and ε_{50} ranging from 0.004 to 0.01

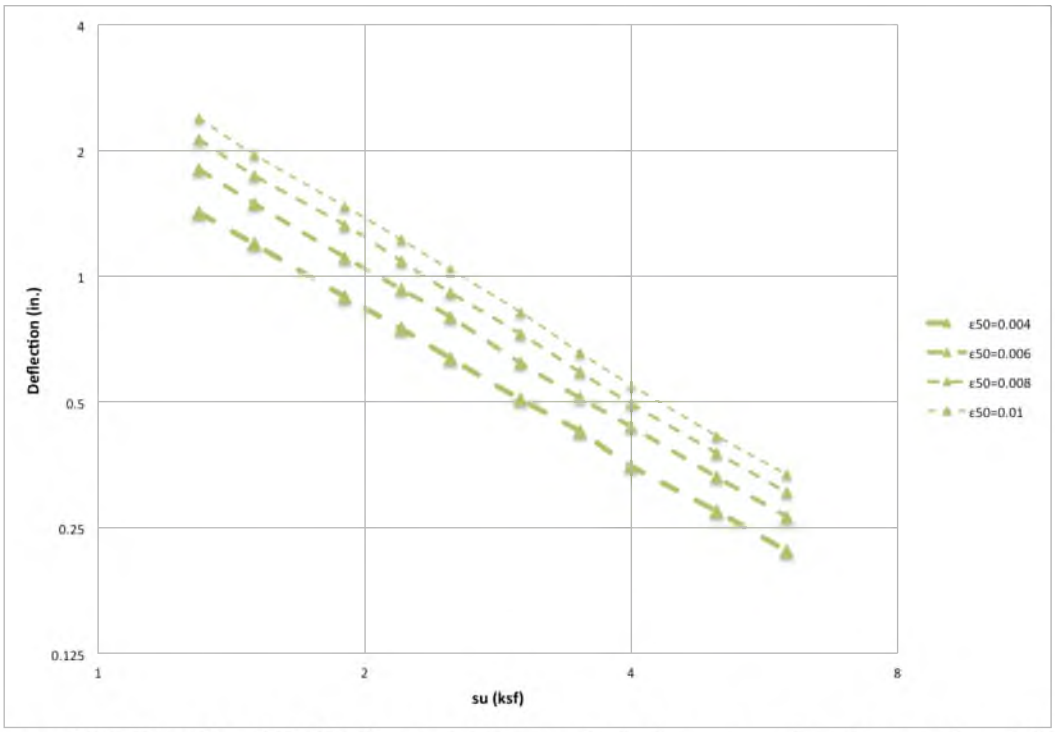

Figure 4.55. Results of DFSAP sensitivity analysis for s_u ranging from 1.3 to 6.0 ksf and ε_{50} ranging from 0.004 to 0.01 in log-log scale

The *MFAD* simulations that were performed at each incremental value of s_u were performed at four values of E_p to gain insight into the sensitivity of the model to E_p, and to identify whether the sensitivity of s_u was dependent upon E_p. The values of E_p that were used for the sensitivity analysis were 1.0, 2.0, 3.0, and 4.0 ksi, which are within the expected range of E_p for the specified range of s_u. A plot of pile head deflection vs. s_u for each *MFAD* simulation is shown in Figure 4.56. The same figure is also shown in log-log scale in Figure 4.57.

The results of the sensitivity analysis showed that both *LPile* and *DFSAP* were sensitive to ε_{50}, and that the *MFAD* model was sensitive to E_p. As such, additional sensitivity analyses were performed to gain insight into the sensitivity of the *LPile* and *DFSAP* models to ε_{50} and of the *MFAD* model to E_p. For these sensitivity analyses, s_u

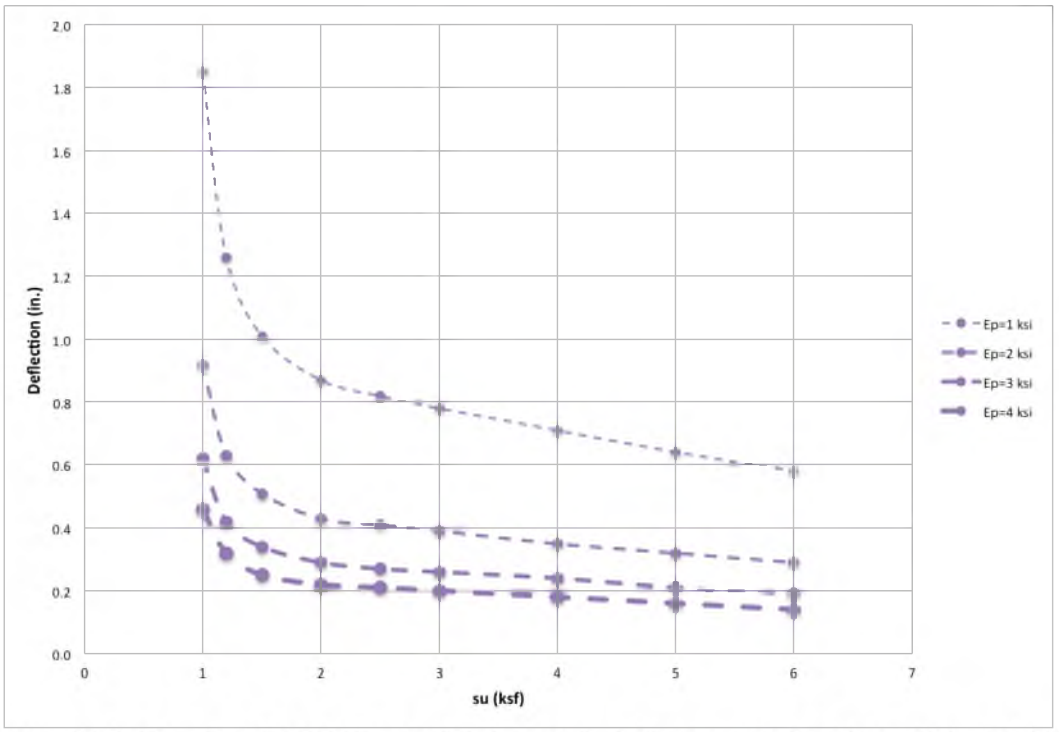

Figure 4.56. Results of MFAD sensitivity analysis for s_u ranging from 1.0 to 6.0 ksf and E_p ranging from 1.0 to 4.0 ksi

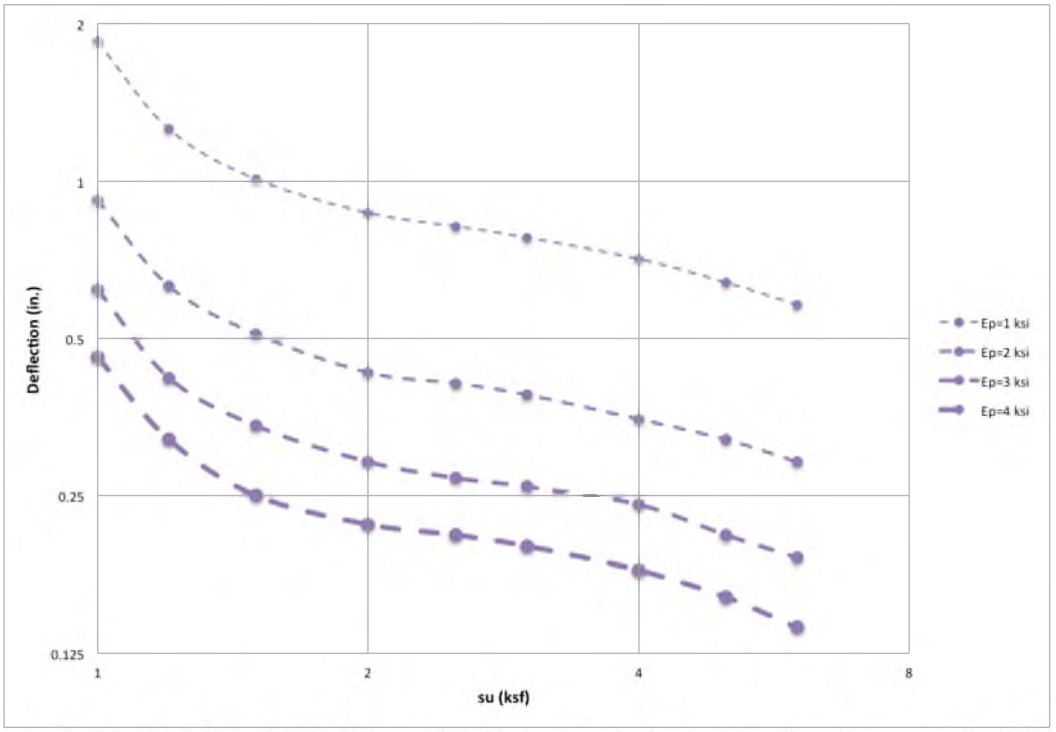

Figure 4.57. Results of MFAD sensitivity analysis for s_u ranging from 1.0 to 6.0 ksf and E_p ranging from 1.0 to 4.0 ksi in log-log scale

was held constant at 1.5, 3.0, 4.5, and 6.0 ksf for the *LPile* and *DFSAP* simulations, and at 1.0, 2.0, and 4.0 ksf for the *MFAD* simulations. The value of ε_{50} was incrementally increased from 0.004 to 0.01 and E_p was incrementally increased from 1.0 to 6.0.

The results of deflection vs. ε_{50} for the *LPile* and *DFSAP* simulations are shown in Figure 4.58 and Figure 4.59, respectively. The results of deflection vs. E_p for the *MFAD* simulations are shown in Figure 4.60. Additionally, the results shown in Figure 4.60 are reproduced in log-log scale in Figure 4.61.

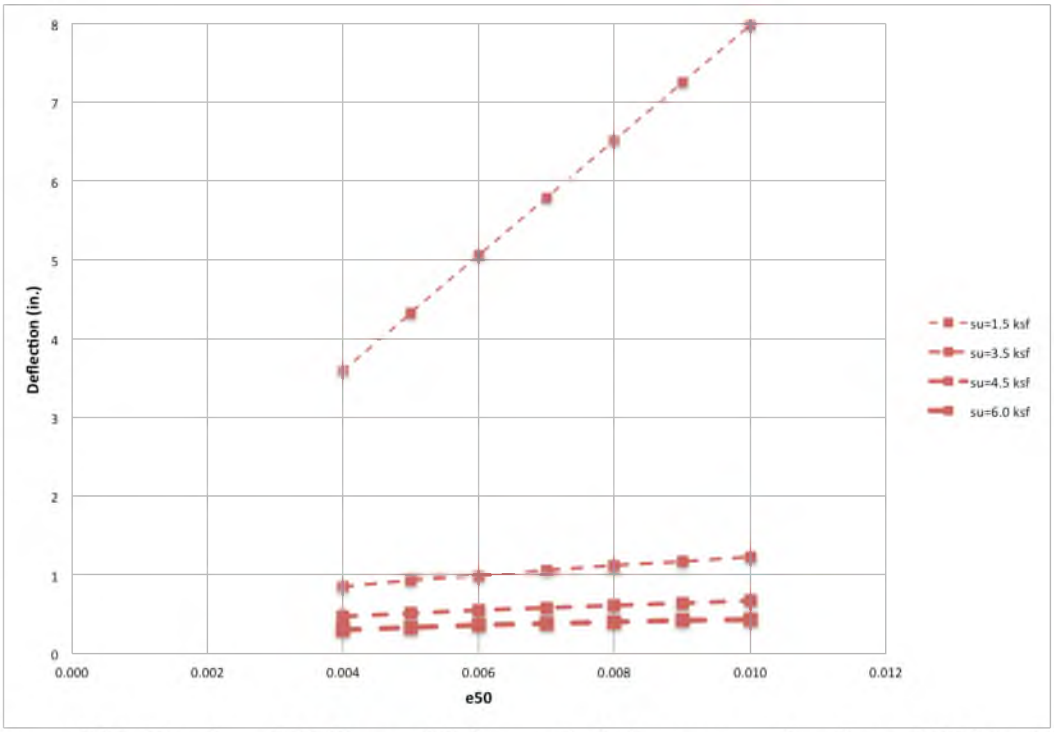

Figure 4.58. Results of LPile sensitivity analysis for ε_{50} ranging from 0.004 to 0.01 and s_u ranging from 1.5 to 6.0 ksf

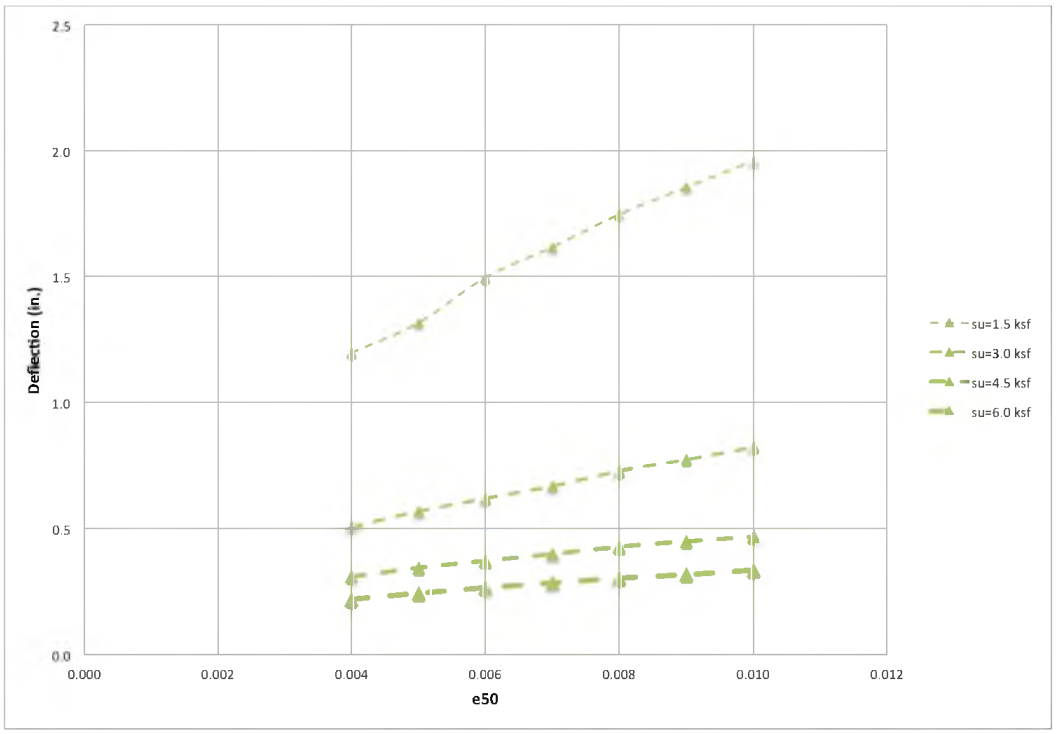

Figure 4.59. Results of DFSAP sensitivity analysis for ε_{50} ranging from 0.004 to 0.01 and s_u ranging from 1.5 to 6.0 ksf

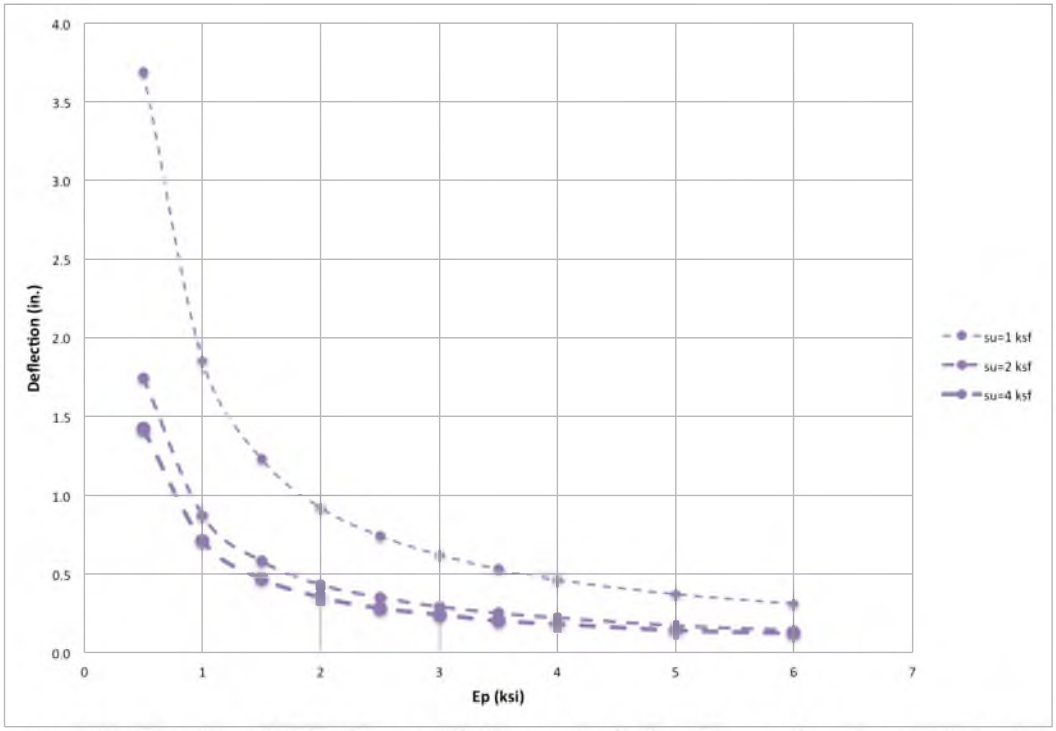

Figure 4.60. Results of MFAD sensitivity analysis for E_p ranging from 1.0 to 4.0 ksi and s_u ranging from 1.0 to 4.0 ksf

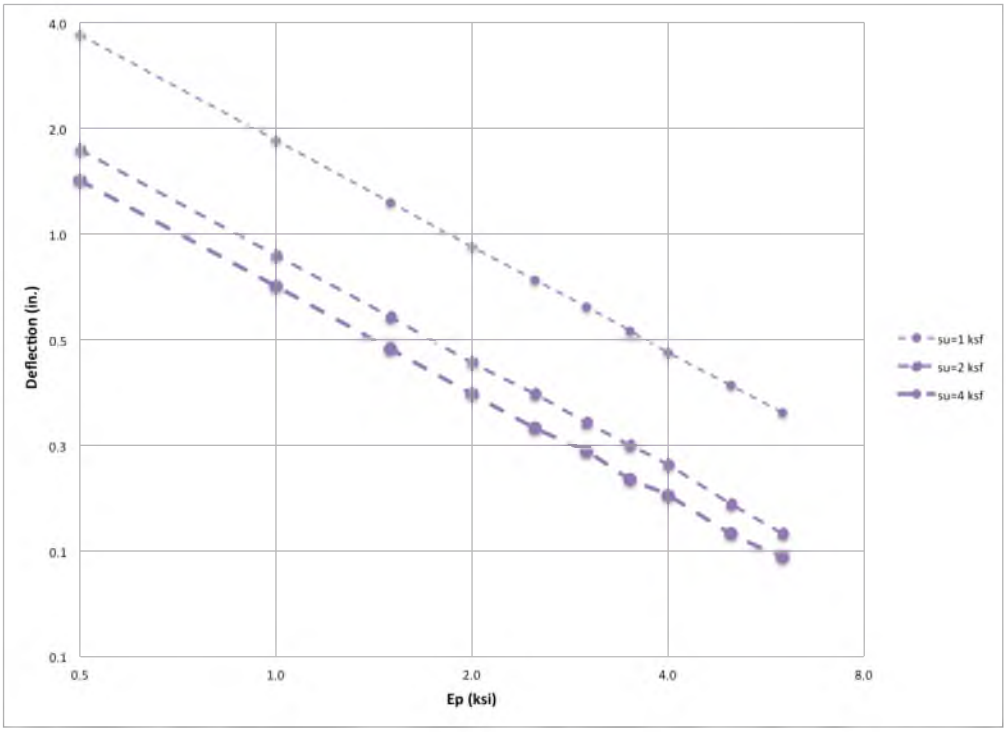

Figure 4.61. Results of MFAD sensitivity analysis for E_p ranging from 1.0 to 4.0 ksi and s_u ranging from 1.0 to 4.0 ksf in log-log scale

5 DISCUSSION

Recall from Section 3.5 that 15 large-scale load tests were selected for analysis in this investigation. Of these large-scale load tests, eight were conducted in cohesive soils (DS 18-2, DS 20-2, DS 20-4, DS 20-5, DS 20-6, DS 22-1, DS 22-2, DS 76-1), six were conducted in granular soils (DS 11-1, DS 19-1, DS 19-2, DS 19-3, DS 23-1, DS 23-2), and one was conducted in alternating layers of granular and cohesive soils (DS 75-1). This section contains a discussion of the results for each large-scale load test presented in Section 4 and the implications for the accuracy of each analysis method.

The method that is used to perform a robust analysis of a laterally loaded drilled shaft foundation must generally account for the behavior of the foundation, the soil, and the interface between the foundation and the soil under combined lateral loads, axial loads, and overturning moments. The inaccuracy of the results of a particular analysis method generally result from 1) the inaccuracy of the techniques used to model the behavior of the foundation, the soil, or the soil-foundation interface; and 2) the inaccuracy of the input parameters for the model. Because limited data were available for most of the large-scale load tests reported in the literature, it is difficult to assess the accuracy of the input properties for the analysis methods used in this investigation. As such, it is difficult to definitively state whether the disparity between the predicted and observed results is attributable to the inaccuracy of the analysis method or the inaccuracy of the input properties; however, it is likely the "true" value of soil input properties used

for this investigation are within ± 1 standard deviation of the "best-estimate" values. As such, the experimental load-deflection curves should be bounded by the load-deflection curves from the analyses that were performed using ±1 standard deviation soil input properties for a particular analysis method if that analysis method is accurately capturing the behavior of the load test. If not, it is reasonable to conclude that the particular analysis method is not modeling that particular load test accurately. Furthermore, if all three analysis methods are significantly higher or lower than the experimentally-observed results, it is reasonable to conclude that the "best-estimate" input parameters are likely not very accurate.

Comparisons between the experimentally-observed results and the results of each analysis method using "best-estimate" properties and ±1 standard deviation soil input properties are presented in this section, along with a discussion of how the results of the three analysis methods considered in this investigation compared with each other. Further discussion of the influence of the rigidity of the foundations, i.e., *D/B* ratio, the soil input properties, and the regression analysis of the combined results for granular and cohesive soils is also presented in this section.

5.1 Discussion of LPile Results

5.1.1 Granular Soils

The results from the *LPile* analyses of the large-scale load tests performed in granular soils show that the overall behavior for each test was similar; however, there were differences in each test that were difficult to observe by looking at the results of each test individually. As such, the predicted groundline deflections from each *LPile* analysis were plotted against the measured groundline deflections from each load test

performed in granular soil to show the combined results. These results are shown in Figure 5.1 along with the R^2 value and best-fit line from a simple linear regression analysis. Note that these figures are similar to the log-log scale plots shown in Section 4, and the diagonal line represents the line of equivalency of measured and predicted values.

The regression line for the *LPile* results shown in Figure 5.1 is steeper than the line of equivalency, which suggests that the differences between observed and predicted results are not independent from the magnitude of the applied load. Closer inspection of this figure shows that the regression line crosses the line of equivalency at approximately 0.07 inches, which means that predicted values of groundline deflection greater than 0.07 inches tend to be conservative. This value of deflection is much less than the tolerable

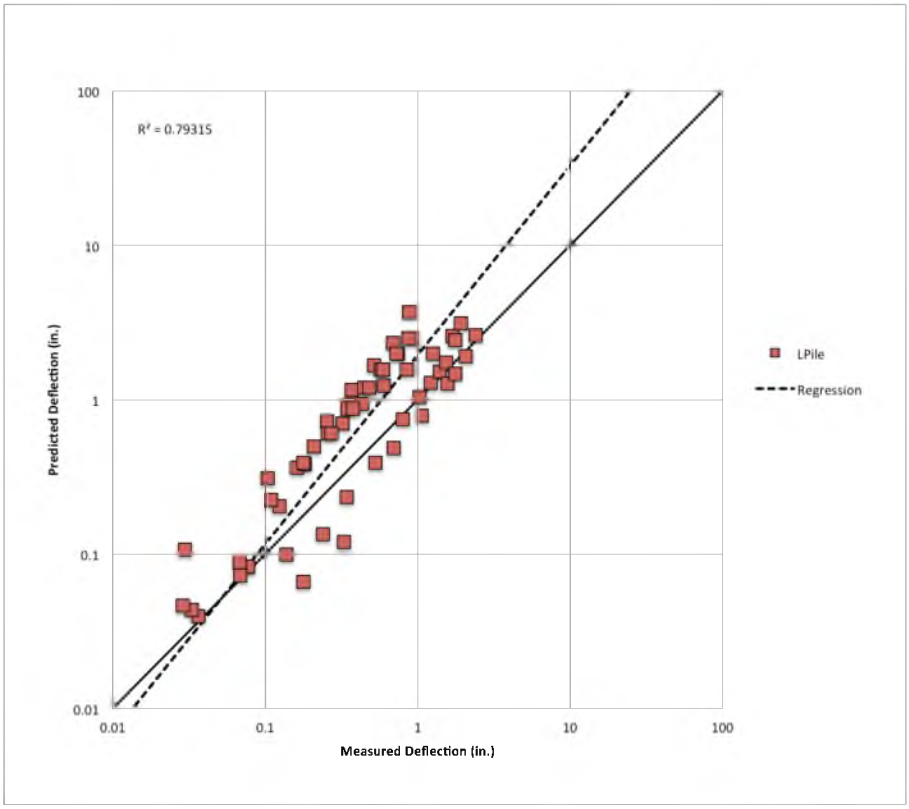

Figure 5.1. Combined LPile analysis results of predicted vs. measured groundline deflection for large-scale load tests performed in granular soils

groundline deflection for most structures; therefore, it can be said that these results show that *LPile* tends to overpredict groundline deflection and that this tendency increases with increasing magnitude of applied load. It should be noted, however, that *LPile* analyses for foundations of structures with *very* low tolerance for movement, such as those reported by Bhushan and Askari (1984), could be unconservative.

The results of the *LPile* analyses performed for each load test using soil input properties with ±1 standard deviation from the "best-estimate" values show that increasing or decreasing the soil input properties by one standard deviation does not result in equivalent deviation from the best-estimate input property values, but instead results in considerably more pile head deflection when soil input properties are reduced by one standard deviation.

The results of the parametric study for DS 19-2 presented in Section 4 help to illustrate the change in pile head deflection with variation in soil input parameters for load tests conducted in granular soils. Figure 4.17 and Figure 4.18 show how pile head deflection changes with variation in ϕ and k. These figures show that the change in pile head deflection increases exponentially with decreasing values of ϕ and that the change in pile head deflection is somewhat dependent on k; however, the curves for the three values of k shown in Figure 4.17 and Figure 4.18 converge as ϕ decreases. Therefore, pile head deflection is not dependent on k over the entire range of possible values of ϕ. Furthermore, the sensitivity of pile head deflection to ϕ decreases with increasing k.

The results of these analyses suggest *LPile* is most sensitive to ϕ and that sensitivity increases exponentially with decreasing values of ϕ. Furthermore, the sensitivity analysis results for DS 19-2 suggest that the sensitivity of *LPile* to ϕ increases with increasing magnitude of applied load, while sensitivity to k decreased with increase

in applied load. The results of the ±1 standard deviation of soil input properties analyses discussed previously in Section 4 for each load test show similar trends of increasing sensitivity to soil input properties for all load tests; thus, it is reasonable to conclude that the sensitivity of *LPile* to ϕ and k shown in the parametric study results for DS 19-2 are not unique to DS 19-2.

5.1.2 Cohesive Soils

The results from the *LPile* analyses of the large-scale load tests performed in cohesive soils show that the overall behavior for each test was similar; however, there were differences in each test that were difficult to observe by looking at the results of each test individually. As such, the predicted groundline deflections from each *LPile* analysis were plotted against the measured groundline deflections from each load test performed in cohesive soil to show the combined results. These results are shown in Figure 5.2 along with the R^2 value and best-fit line from a simple linear regression analysis. Note that these figures are similar to the log-log scale plots shown in Section 4, and the diagonal line represents the line of equivalency of measured and predicted values. The regression line for the *LPile* results shown in Figure 5.2 is steeper than the line of equivalency, which suggests that the differences between observed and predicted results are not independent from the magnitude of the applied load. Closer inspection of this figure shows that the regression line crosses the line of equivalency at approximately 0.25 inches, which means that predicted values of groundline deflection greater than 0.25 inches tend to be conservative. Although *LPile* tends to predict very conservative groundline defection as load magnitude increases, these results show there is a reasonable chance that small groundline deflections predicted by *LPile* will be unconservative.

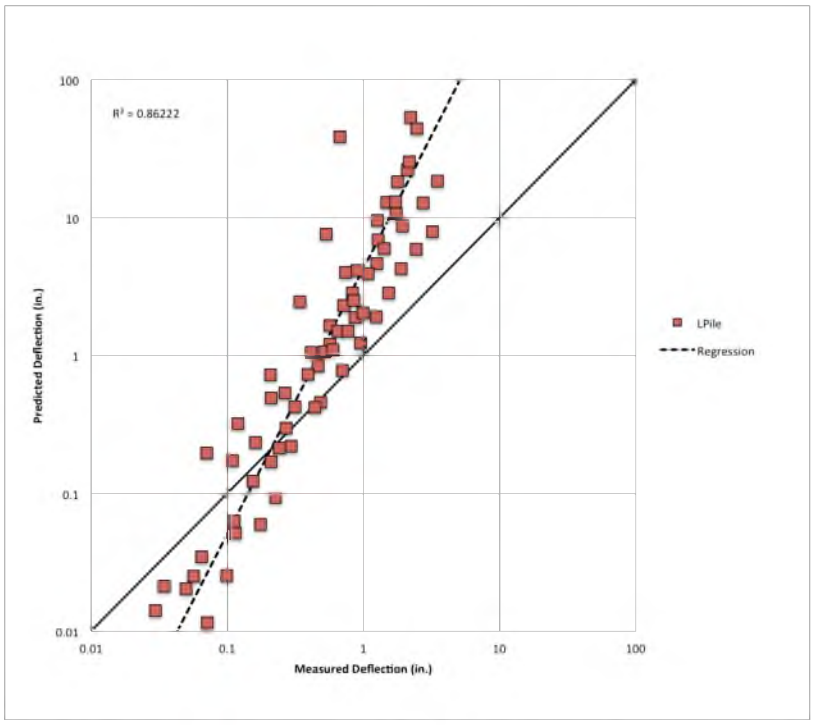

Figure 5.2. Combined LPile analysis results of predicted vs. measured groundline deflection for large-scale load tests performed in cohesive soils

The results of the *LPile* analyses performed for each load test using soil input properties with ±1 standard deviation from the "best-estimate" values show that increasing or decreasing the soil input properties by one standard deviation does not result in equivalent deviation from the best-estimate input property values, but instead results in considerably more pile head deflection when soil input properties are reduced by one standard deviation.

The results of the parametric study for DS 76-1 presented in Section 4 help to illustrate the change in pile head deflection with variation in soil input parameters for load tests conducted in cohesive soils. Figure 4.52 and Figure 4.53 show how pile head deflection changes with variation in s_u and ε_{50}. These figures show that the change in pile head deflection increases exponentially with decreasing values of s_u. The change in groundline deflection is dependent on ε_{50}, and deflection increases linearly with

increasing values of ε_{50} as shown in Figure 4.58. Closer inspection of Figure 4.58 shows that groundline deflection is only moderately sensitive to ε_{50}; however, it is important to notice that groundline deflection increases rapidly as s_u decreases. This presents a potentially serious problem if *LPile* analyses are performed using the values of ε_{50} calculated by *LPile* instead of values estimated from laboratory or in-situ tests. As shown in Figure 3.12, *LPile* calculates ε_{50} as a function of s_u only, and this value increases rapidly with decreasing s_u. Therefore, the groundline deflections predicted by *LPile* for small values of s_u can potentially become excessively large very quickly.

The results of these analyses suggest *LPile* is most sensitive to s_u and that sensitivity increases exponentially with decreasing values of s_u. Furthermore, the sensitivity analysis results for DS 76-1 suggest that the sensitivity of *LPile* to s_u increases considerably with increasing magnitude of applied load, while sensitivity to ε_{50} showed only minor variation with increase in applied load. The results of the ±1 standard deviation of soil input properties analyses discussed previously in Section 4 for each load test show similar trends of increasing sensitivity to soil input properties for all load tests; thus, it is reasonable to conclude that the sensitivity of *LPile* to s_u and ε_{50} shown in the parametric study results for DS 76-1 are not unique to DS 76-1.

5.2 Discussion of DFSAP Results

5.2.1 Granular Soils

The results from the *DFSAP* analyses of the large-scale load tests performed in granular soils show that the overall behavior for each test was similar; however, there were differences in each test that were difficult to observe by looking at the results of each test individually. As such, predicted groundline deflections from each *DFSAP*

analysis were plotted against the measured groundline deflections from each load test performed in granular soil to show the combined results. These results are shown in Figure 5.1 along with the R^2 value and best-fit line from a simple linear regression analysis. Note that these figures are similar to the log-log scale plots shown in Section 4, and the diagonal line represents the line of equivalency of measured and predicted values.

The regression line for the *DFSAP* results shown in Figure 5.3 is slightly steeper than the line of equivalency. As discussed for the *LPile* analyses, this suggests that the differences between observed and predicted results are not independent from the magnitude of the applied load; however, the regression line is not much steeper than the line of equivalency, and thus dependency of the results on load magnitude is generally small. This trend from the regression line is in good agreement with the results of each load test discussed in Section 4.

The *DFSAP* regression line crosses the line of equivalency at approximately 0.18 inches, which means that predicted values of groundline deflection greater than 0.18 inches tend to be conservative. Although *DFSAP* tends to predict conservative groundline defection as load magnitude increases, these results show there is still considerable chance that the groundline deflection predicted by *DFSAP* will be unconservative.

The results of the *LPile* analyses performed for each load test using soil input properties with ±1 standard deviation from the "best-estimate" values show that increasing or decreasing the soil input properties by one standard deviation does not result in equivalent deviation from the best-estimate input property values, but instead results in considerably more pile head deflection when soil input properties are reduced by one standard deviation.

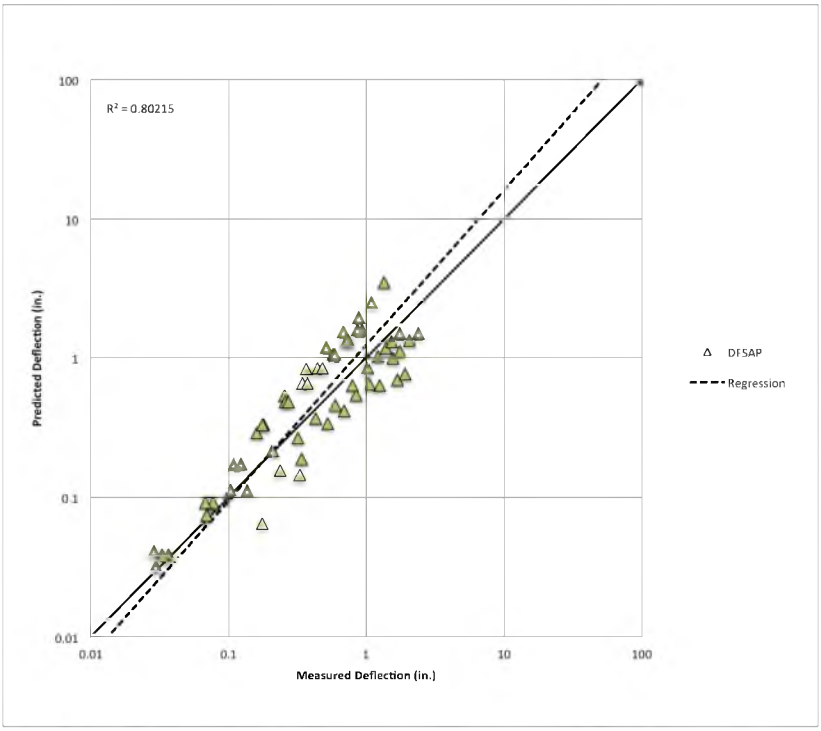

Figure 5.3. Combined DFSAP analysis results of predicted vs. measured groundline deflection for large-scale load tests performed in granular soils

The results of the parametric study for DS 19-2 presented in Section 4 help to illustrate the change in pile head deflection with variation in soil input parameters for load tests conducted in granular soils. Figure 4.19 and Figure 4.20 show how pile head deflection changes with variation in ϕ and ε_{50}. These figures show that the change in pile head deflection increases exponentially with decreasing values of ϕ. The change in pile head deflection is dependent on ε_{50}, and deflection increases linearly with increasing values of ε_{50} as shown in Figure 4.23.

The results of these analyses suggest *DFSAP* is most sensitive to ϕ and that sensitivity increases exponentially with decreasing values of ϕ. Furthermore, the sensitivity analysis results for DS 19-2 suggest that the sensitivity of *DFSAP* to ϕ increases with increasing magnitude of applied load, while sensitivity to ε_{50} showed

minor variation with increase in applied load. The results of the ±1 standard deviation of soil input properties analyses discussed previously in Section 4 for each load test show similar trends of increasing sensitivity to soil input properties for all load tests; thus, it is reasonable to conclude that the sensitivity of *DFSAP* to ϕ and ε_{50} shown in the parametric study results for DS 19-2 are not unique to DS 19-2.

5.2.2 Cohesive Soils

The results from the *DFSAP* analyses of the large-scale load tests performed in cohesive soils show that the overall behavior for each test was similar; however, there were differences in each test that were difficult to observe by looking at the results of each test individually. As such, the predicted groundline deflections from each *DFSAP* analysis were plotted against the measured groundline deflections from each load test performed in cohesive soil to show the combined results. These results are shown in Figure 5.4 along with the R^2 value and best-fit line from a simple linear regression analysis. Note that these figures are similar to the log-log scale plots shown in Section 4, and the diagonal line represents the line of equivalency of measured and predicted values.

The regression line for the *DFSAP* results shown in Figure 5.4 is shallower than the line of equivalency, which suggests that the differences between observed and predicted results are not independent from the magnitude of the applied load. Closer inspection of this figure shows that the regression line crosses the line of equivalency at approximately 0.53 inches, which means that predicted values of groundline deflection greater than 0.53 inches tend to be unconservative. These results show there is a reasonable chance that *DFSAP* analysis results for drilled shafts in cohesive soils will be unconservative.

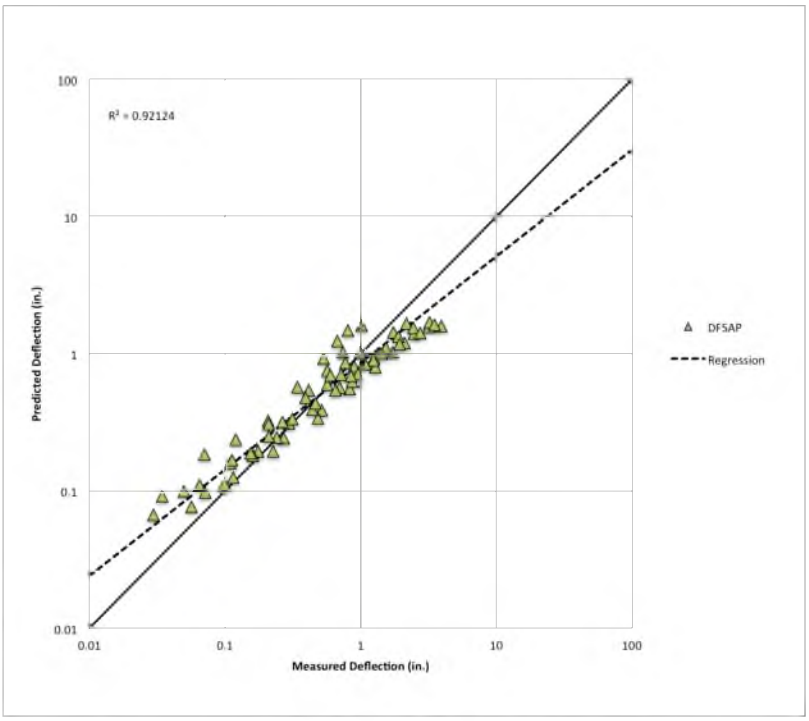

Figure 5.4. Combined DFSAP analysis results of predicted vs. measured groundline deflection for large-scale load tests performed in cohesive soils

The results of the *DFSAP* analyses performed for each load test using soil input properties with ±1 standard deviation from the "best-estimate" values show that increasing or decreasing the soil input properties by one standard deviation does not result in equivalent deviation from the best-estimate input property values, but instead results in considerably more pile head deflection when soil input properties are reduced by one standard deviation.

The results of the parametric study for DS 76-1 presented in Section 4 help to illustrate the change in pile head deflection with variation in soil input parameters for load tests conducted in cohesive soils. Figure 4.54 and Figure 4.55 show how pile head deflection changes with variation in s_u and ε_{50}. These figures show that the change in pile head deflection increases exponentially with decreasing values of s_u. The change in groundline deflection is dependent on ε_{50}, and deflection increases linearly with

increasing values of ε_{50} as shown in Figure 4.59.

The results of these analyses suggest *DFSAP* is most sensitive to s_u and that sensitivity increases exponentially with decreasing values of s_u. Furthermore, the sensitivity analysis results for DS 76-1 suggest that the sensitivity of *DFSAP* to both s_u and ε_{50} showed only minor variation with increase in applied load. The results of the ±1 standard deviation of soil input properties analyses discussed previously in Section 4 for each load test show similar trends; thus, it is reasonable to conclude that the sensitivity of *DFSAP* to s_u and ε_{50} shown in the parametric study results for DS 76-1 are not unique to DS 76-1.

5.3 Discussion of MFAD Results

5.3.1 Granular Soils

The results from the *MFAD* analyses of the large-scale load tests performed in granular soils show that the overall behavior for each test was similar; however, there were differences in each test that were difficult to observe by looking at the results of each test individually. As such, predicted groundline deflections from each *MFAD* analysis were plotted against the measured groundline deflections from each load test performed in granular soil to show the combined results. These results are shown in Figure 5.5 along with the R^2 value and best-fit line from a simple linear regression analysis. Note that these figures are similar to the log-log scale plots shown in Section 4, and the diagonal line represents the line of equivalency of measured and predicted values.

The regression line for the *MFAD* results shown in Figure 5.5 is slightly steeper than the line of equivalency. As discussed for the *LPile* analyses, this suggests that the

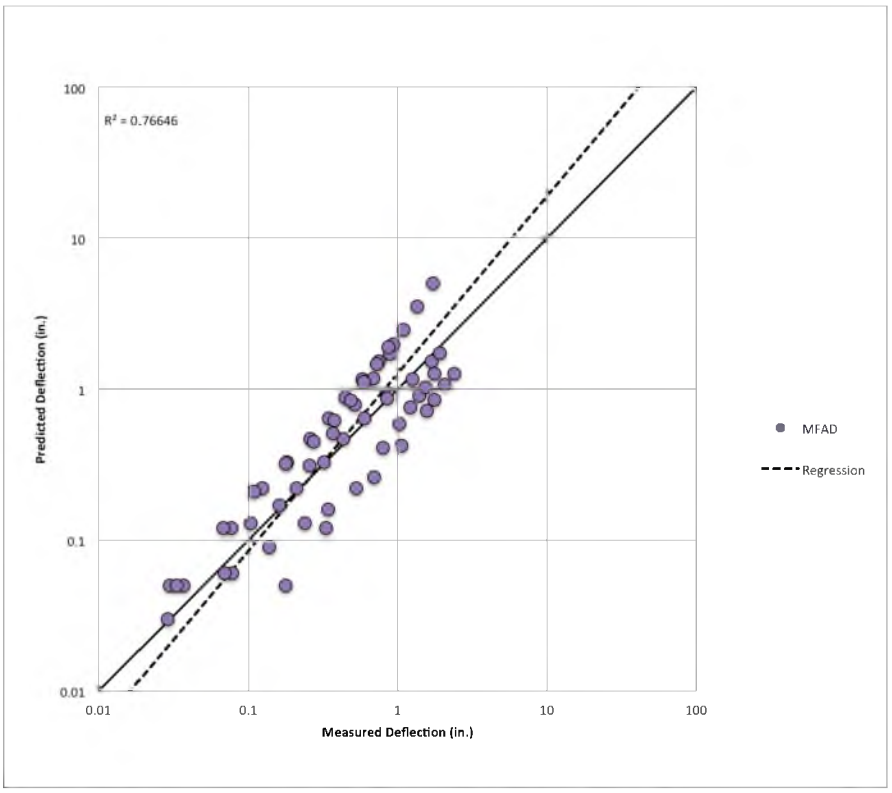

Figure 5.5. Combined MFAD analysis results of predicted vs. measured groundline deflection for large-scale load tests performed in granular soils

differences between observed and predicted results are not independent from the magnitude of the applied load. This trend from the regression line is in good agreement with the results of each load test discussed in Section 4.

The *MFAD* regression line crosses the line of equivalency at approximately 0.25 inches, which means that predicted values of groundline deflection greater than 0.25 inches tend to be conservative. Although *MFAD* tends to predict conservative groundline defection as load magnitude increases, these results show there is still considerable chance that the groundline deflection predicted by *MFAD* will be unconservative.

The results of the *MFAD* analyses performed for each load test using soil input properties with ±1 standard deviation from the "best-estimate" values show that increasing or decreasing the soil input properties by one standard deviation does not

result in equivalent deviation from the best-estimate input property values, but instead results in considerably more pile head deflection when soil input properties are reduced by one standard deviation.

The results of the parametric study for DS 19-2 presented in Section 4 help to illustrate the change in pile head deflection with variation in soil input parameters for load tests conducted in granular soils. Figure 4.21 and Figure 4.22 show how pile head deflection changes with variation in ϕ and E_p. These figures show that the change in pile head deflection increases exponentially with decreasing values of ϕ. The change in pile head deflection is dependent on E_p, and Figure 4.24 shows that deflection is inversely proportional to E_p.

The results of these analyses suggest *MFAD* is most sensitive to ϕ and that sensitivity increases exponentially with decreasing values of ϕ. Furthermore, the sensitivity analysis results for DS 19-2 suggest that the sensitivity of *MFAD* to both ϕ and E_p increase with increasing magnitude of applied load. The results of the ±1 standard deviation of soil input properties analyses discussed previously in Section 4 for each load test show similar trends of increasing sensitivity to soil input properties for all load tests; thus, it is reasonable to conclude that the sensitivity of *MFAD* to ϕ and E_p shown in the parametric study results for DS 19-2 are not unique to DS 19-2.

5.3.2 Cohesive Soils

The results from the *MFAD* analyses of the large-scale load tests performed in cohesive soils show that the overall behavior for each test was similar; however, there were differences in each test that were difficult to observe by looking at the results of each test individually. As such, the predicted groundline deflections from each *MFAD*

analysis were plotted against the measured groundline deflections from each load test performed in cohesive soil to show the combined results. These results are shown in Figure 5.6 along with the R^2 value and best-fit line from a simple linear regression analysis. Note that these figures are similar to the log-log scale plots shown in Section 4, and the diagonal line represents the line of equivalency of measured and predicted values.

The regression line for the *MFAD* results shown in Figure 5.6 is shallower than the line of equivalency, which suggests that the differences between observed and predicted results are not independent from the magnitude of the applied load. Closer inspection of this figure shows that the regression line does not cross the line of equivalency beyond 0.01 inches, which means that the predicted values of groundline

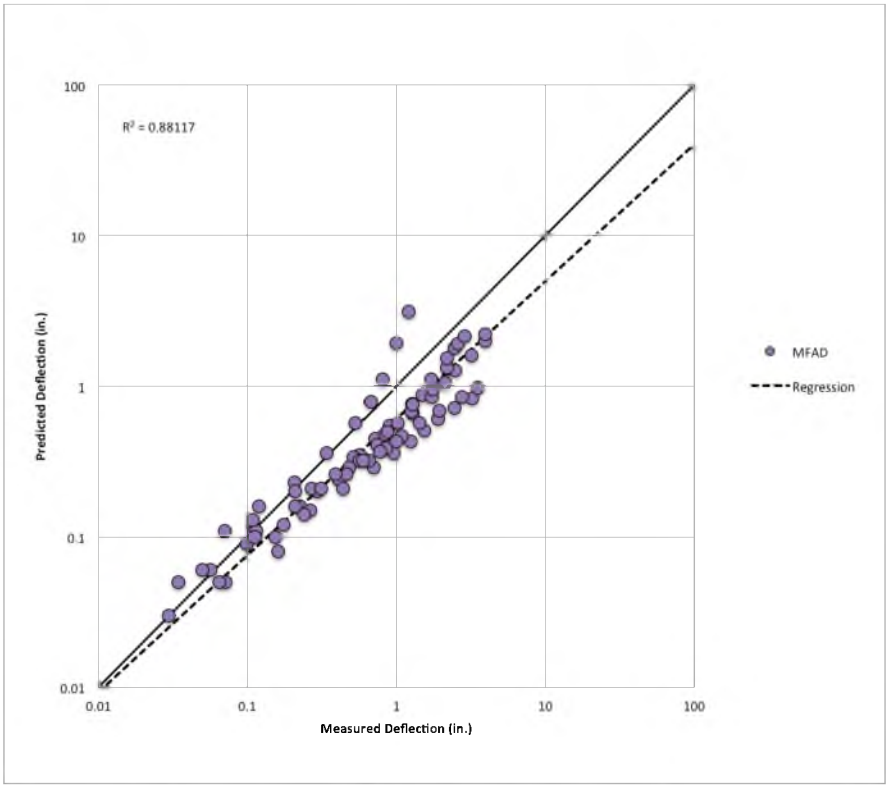

Figure 5.6. Combined MFAD analysis results of predicted vs. measured groundline deflection for large-scale load tests performed in cohesive soils

deflection tend to be unconservative. With the exception of DS 20-5 and a small number of initial loading increments for other load tests, *MFAD* was unconservative for all of the load tests performed in cohesive soils. These results show there is a strong chance that *MFAD* analysis results for drilled shafts in cohesive soils will be unconservative.

The results of the *MFAD* analyses performed for each load test using soil input properties with ±1 standard deviation from the "best-estimate" values show that increasing or decreasing the soil input properties by one standard deviation does not result in equivalent deviation from the best-estimate input property values, but instead results in considerably more pile head deflection when soil input properties are reduced by one standard deviation.

The results of the parametric study for DS 76-1 presented in Section 4 help to illustrate the change in pile head deflection with variation in soil input parameters for load tests conducted in cohesive soils. Figure 4.56, Figure 4.57, and Figure 4.59 show how pile head deflection changes with variation in s_u and E_p. These figures show that the change in pile head deflection increases exponentially with decreasing values of s_u and E_p.

The results of these analyses suggest *MFAD* is most sensitive to E_p and that sensitivity increases exponentially with decreasing values of s_u. The sensitivity analysis results for DS 76-1 suggest that the sensitivity of *MFAD* to both s_u and E_p showed only minor variation with increase in applied load; however, the results of the ±1 standard deviation of soil input properties analyses discussed previously in Section 4 for each load test showed variable behavior with increase in applied load. Additional investigation is necessary to determine the degree to which the results of the parametric study for DS 76-1 are representative of general behavior of the *MFAD* model.

5.4 Comparison of Analysis Methods

5.4.1 Granular Soils

It can be seen in Figure 5.1, Figure 5.3, and Figure 5.5 that all three analysis methods yield fairly similar results in granular soils; however, there are differences in the results that warrant further discussion. In general, the regression analyses for the three methods shown in these figures are very similar with similar slopes and R^2 values. The slope of the regression line for all three analysis methods is steeper than the slope of the line of equivalency, which suggests the results from all three analysis methods are somewhat dependent upon load magnitude. *LPile* has the steepest slope of the three methods, suggesting it has the greatest dependency on load magnitude, while *DFSAP* has the slope closes to 1, suggesting it has the least dependency on load magnitude. This observation of the regression analyses is consistent with the observations made in the results presented in in Section 4.

In general, *LPile* tended to predict the most groundline deflection while *DFSAP* tended to predict the least amount of groundline deflection. For the six load tests performed in granular soils, *LPile* estimated the most groundline deflection for all six analyses, while *DFSAP* estimated the least amount of groundline deflection in six of the analyses. *LPile* conservatively overpredicted groundline deflection at the maximum increment of applied load for each load test. Although the regression lines shown in Figure 5.3 and Figure 5.5 show that *DFSAP* and *MFAD* tend to overpredict groundline deflection at maximum applied load, only three of the six (DS 11-1, DS 23-1, and DS 23-2) load test analyses for each of these methods actually resulted in overpredicted groundline deflection estimates for the maximum increment of applied load.

The results of the ± 1 standard deviation soil input properties presented in Section

4 show that, with the exception of DS 23-1 and DS 23-2, the experimentally-observed load-deflection curves are stiffer than the all of the -1 standard deviation curves for *LPile* in granular soils. For DS 11-1, the experimentally-observed load-deflection curve is bounded by the ± 1 standard deviation load-deflection curves for *MFAD* and *DFSAP*. This suggests the best-estimate soil input properties for DS 11-1 are reasonably accurate, and that *LPile* is not accurately modeling the behavior of this load test. The experimental load-deflection curve for 19-1 is only bounded by *MFAD* and is slightly softer than the -1 standard deviation curve from *DFSAP*. Likewise, the experimental load-deflection curves for DS 19-2 and DS 19-3 are bounded by the *DFSAP* and *MFAD* ± 1 standard deviation load-deflection curves; however, they are very close to the -1 standard deviation curve. This suggests the best-estimate soil input properties for the soil properties at site for DS 19-1, DS 19-2, and DS 19-3 might be slightly lower than their true values. The experimental load-deflection curves are in good agreement with all three analysis methods for DS 23-1 and DS 23-2, which suggests that the best-estimate soil properties are reasonable and that each analysis method is accurately modeling these load tests. It should be noted, however, that the first two loading increments are not bounded by *LPile* or *MFAD*, which may indicate that k or E_p, respectively, are slightly stiffer than their true values. Regardless, minor adjustments in these values would still yield good agreement in the results over the rest applied load increments.

The results for DS 11-1 and DS 23-2 suggest there might be some dependency of the models on the mode of application of the applied load, i.e.,the combination of lateral load and overturning moment. The drilled shafts tested for DS 11-1 and DS 23-2 were very similar in that their length, diameter, and *D/B* ratios were approximately 20 ft, 3 ft, and 7, respectively. Furthermore, both load tests were performed in what can generally

be described as dense fine sand. DS 11-1 was loaded to just under 2 inches of groundline deflection, while DS 23-2 was loaded to just over 2 inches of groundline deflection. The observed results and the results from each of the analysis methods shown in Section 4.1 and 4.6 show somewhat surprisingly different behavior for such similar test conditions. The difference in behavior seems to be attributable to the difference in loading mechanism. The loads applied to DS 11-1 were applied through a load frame that generated relatively small lateral loads and very large overturning moments, which was equivalent to applying the lateral load 80 feet above the ground surface. The lateral loads applied to DS 23-2 were applied at the ground surface, which resulted in large lateral loads and no overturning moment. The results for DS 11-1 are in very good agreement with the *MFAD* results, while the *DFSAP* results are unconservative and generally do not match the overall behavior of the observed results. It would be reasonable to hypothesize that the difference in the *DFSAP* results might be due to overly stiff soil input properties; however, the results of the ±1 standard deviation sensitivity analyses shown in Figure 4.2b show that *DFSAP* still does not quite capture the observed behavior even with softer soil input properties. The rest of the large-scale load tests performed in granular soils (DS 19-1, DS 19-2, DS 19-3, DS 23-1) were performed with little or no overturning moment, and the ±1 standard deviation sensitivity analyses show that *DFSAP* captures the general behavior of these tests reasonably well. Therefore, it appears *DFSAP* has a more difficult time capturing the behavior of foundations that are loaded with large overturning moments. It is not surprising that the *MFAD* results are in good agreement with the experimental results of DS 11-1 considering *MFAD* was developed from the results of large-scale load tests that were performed with large overturning moments. From the results of these load tests and for reasons stated in this discussion, it appears

MFAD is a more appropriate model for drilled shafts with large overturning moments than *DFSAP*. The results form the *LPile* analysis were very similar for both load tests, which suggests this model is not as sensitive to large overturning moments as *DFSAP* or *MFAD*; however, as previously noted, *LPile* overpredicted deflection for this load test despite what appear to be reasonably accurate values for the best-estimate soil input parameters. This suggests *LPile* may tend to overpredict pile head deflection for foundations with large overturning moments.

The error of each analysis method was calculated for each increment of applied load for all of the load tests performed in granular soils. In order to gain insight into the effect of the rigidity of the pile on the results, i.e., the *D/B* ratio, the average error from each analysis method for each load test was plotted against the *D/B* ratio of the test foundation in Figure 5.7.

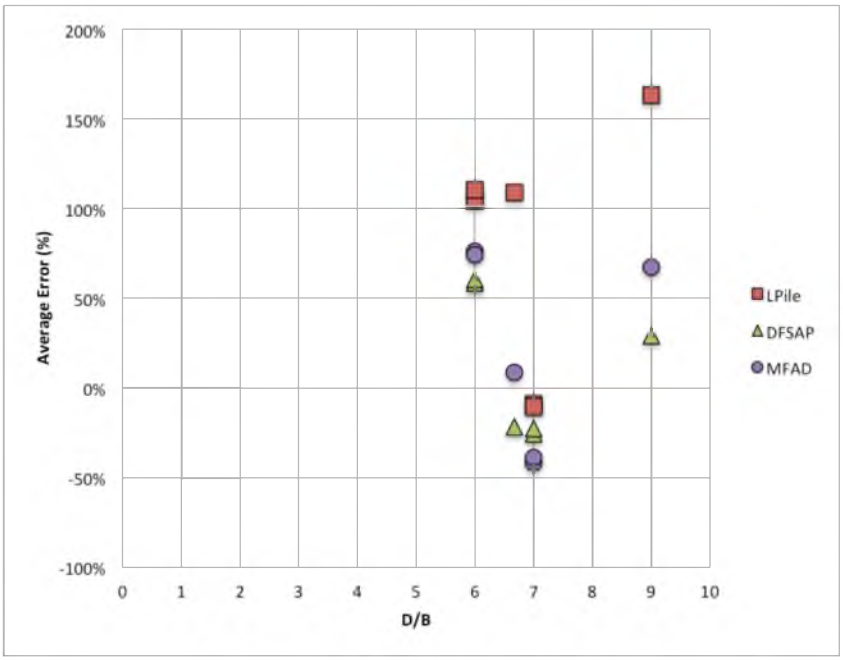

Figure 5.7. Average error from each load test performed in granular soils vs. D/B ratio for LPile, DFSAP, and MFAD

Figure 5.7 shows that the load tests considered in this investigation do not demonstrate any clear trend in the accuracy of the results as a function of the *D/B* ratio of the foundation. Furthermore, these results do not show that any particular model is clearly more accurate than the others; however, with the exception of DS 23-1 and DS 23-2, the average error for *LPile* is larger than the average error for *DFSAP* or *MFAD*. The average error for *MFAD* tends to be slightly larger than the average error for *DFSAP*.

The results of the ±1 standard deviation of soil input properties for each analysis method considered in this investigation show increasing or decreasing the soil input properties by one standard deviation does not result in equivalent deviation from the best-estimate input property values, but instead results in considerably more pile head deflection when soil input properties are reduced by one standard deviation. All three analysis methods were most sensitive to ϕ with pile head deflection increasing exponentially with decreasing values of ϕ. As such, very small reductions in ϕ tend to result in considerable increase in prediction of pile head deflection. This is particularly true for *MFAD*, but perhaps more important for *LPile* considering *LPile* already shows a tendency to overestimate deflection in granular soils.

5.4.2 Cohesive Soils

It can be seen in Figure 5.2, Figure 5.4, and Figure 5.6 that *DFSAP* and *MFAD* yielded similar results in cohesive soils; however, *LPile* showed a tendency to predict considerably more deflection than the other two methods. The slope of the regression line for all three methods is different than the line of equivalency, which suggests the results from all three analysis methods are somewhat dependent upon load magnitude. *LPile* has the steepest slope of the three methods, suggesting it has the greatest

dependency on load magnitude, while *MFAD* has the slope closes to 1, suggesting it has the least dependency on load magnitude. This observation of the regression analyses is consistent with the observations made in the results presented in in Section 4.

In general, *LPile* tended to predict the most groundline deflection while *MFAD* tended to predict the least amount of groundline deflection. For the eight load tests performed in granular soils, *LPile* predicted the most groundline deflection for all eight analyses. *MFAD* predicted the least amount of groundline deflection for all but the final load increment of DS 20-2.

The results of the ± 1 standard deviation soil input properties presented in Section 4 show that, with the exception of DS 22-1 and DS 22-2, the experimentally-observed load-deflection curves are stiffer than the all of the -1 standard deviation curves for *LPile* in cohesive soils. For DS 18-2, DS 20-2, DS 20-4, and DS 20-5, the LPile results are bounded for some of the intermediate increments of applied load, but become much softer than the -1 standard deviation curves at larger increments of applied load. All of experimental load-deflection curves were generally bounded by the ± 1 standard deviation load-deflection curves for *MFAD* and *DFSAP*. The experimentally-observed deflections exceeded the +1 standard deviation deflection values from *MFAD* for the last three increments of applied load for DS 76-1. This suggests that the best-estimate soil input properties for all of the load tests conducted in cohesive soils are reasonably accurate, and therefore, *LPile* is not accurately modeling the behavior of the load tests performed in cohesive soils.

There were no load tests performed in cohesive soils with large overturning moments; therefore, it is not possible to identify differences in the three analysis methods for the foundations with large overturning moments. DS 75-1 was performed in

alternating layers of granular and cohesive soil, but most of the soil profile consisted of cohesive soils. This was the only other load test considered in this investigation where the foundation was subjected to a large overturning moment. The results of the analyses shown in Figure 4.42 and Figure 4.43 show that *LPile* and *DFSAP* both overestimated groundline deflection and that neither method was able to achieve solutions for load increments greater than 267 kips. *MFAD* underestimated groundline deflection for the entire range of applied load. The ± 1 standard deviation of soil input properties show that the -1 standard deviation results for *DFSAP* and the +1 standard deviation results for *MFAD* are both in reasonably good agreement with the experimentally-observed results. It should be noted that *DFSAP* still failed to estimate groundline deflection greater than 267 kips, and *MFAD* still tended to underestimate groundline deflection at the maximum applied load of 320 kips. This makes sense because this load test was carried out to large-strain failure of the drilled shaft, and neither *DFSAP* nor *MFAD* are designed to model drilled shafts once failure has occurred. At failure, *MFAD* tends to underestimate deflection due to cracking and, in this case, rupture of the foundation reinforcement, while *DFSAP* will not converge upon a solution. In general, these results show that *MFAD* does a reasonable job of estimating pile deflection for foundations embedded in mostly cohesive soils and subjected to large overturning moments for the same reasons stated for granular soils. It should be noted that the results for the best-estimate soil properties were unconservative, and potential problems can arise if soil input properties are too stiff. *DFSAP* also appeared to do a reasonable job of estimating pile deflection for foundations embedded in mostly cohesive soils and subjected to large overturning moments, which was not the case in granular soils. These results suggest that foundations of this type can be analyzed using both *MFAD* and *DFSAP* with reasonable

estimates of input properties, and the actual pile deflection is likely to be bounded by the estimation of deflection from these two methods.

The error of each analysis method was calculated for each increment of applied load for all of the load tests performed in granular soils. In order to gain insight into the effect of the rigidity of the pile on the results, i.e., the *D/B* ratio, the average error from each analysis method for each load test was plotted against the *D/B* ratio of the test foundation in Figure 5.8. This figure shows that *DFSAP* and *MFAD* do not exhibit clear trends in the accuracy of the results as a function of the *D/B* ratio of the foundation; however, it appears the error of the *DFSAP* results may increase slightly with increasing *D/B* ratio. The *LPile* results shown in this figure suggest that the accuracy of *LPile* decreases with decreasing *D/B* ratio. Although there appears to be an identifiable trend, it is the author's opinion that there are insufficient data to establish a reliable predictor of

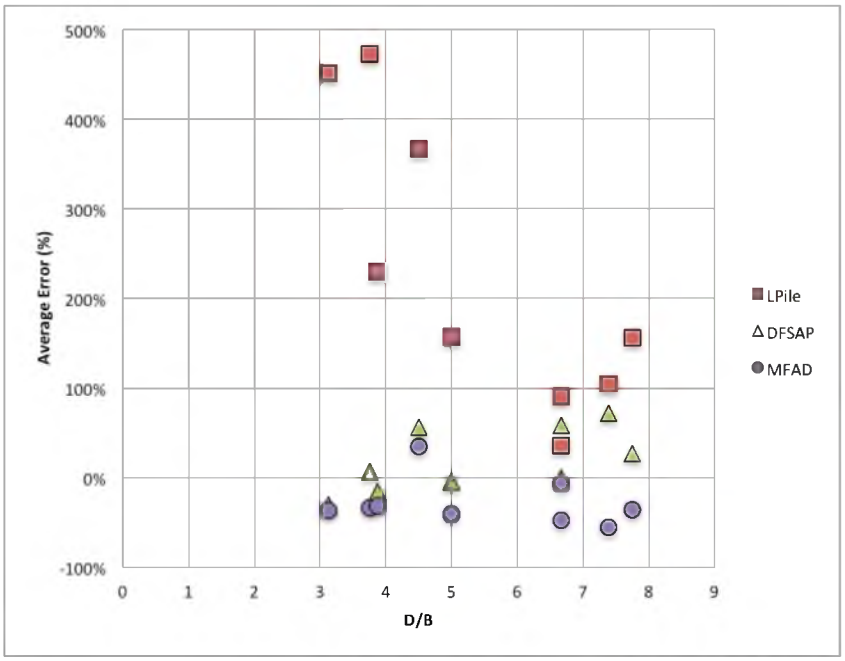

Figure 5.8. Average error from each load test performed in cohesive soils vs. D/B ratio for LPile, DFSAP, and MFAD

foundation response as a function of *D/B* ratio. In general, the average error of *MFAD* and *DFSAP* appears to be very similar, while the average error of *LPile* is considerably larger for all but one (DS 22-1) large-scale load test.

The *LPile* results are particularly interesting because, as discussed in Section 2.4.2.2, the *p-y* curve for stiff clay was derived from the results of a large-scale load test performed on a drilled shaft in stiff clay. For the load tests considered in this investigation, it would be reasonable to assume that the *LPile* results for all of the load tests performed in cohesive soils would be in good agreement with experimentally-observed results considering the only major difference between these load tests and the load tests performed to establish the stiff clay *p-y* curve is the rigidity of the foundation. Recall from Section 2.4.2.2 that the *D/B* ratio of the drilled shaft used in the formulation of the stiff clay *p-y* curve was 16.8, which is at least double the *D/B* ratios shown in Figure 5.8. This provides further evidence that the accuracy of *LPile* for drilled shafts in cohesive soils is not independent of *D/B*, and that accuracy should improve as the foundation behaves more like a flexible foundation.

As discussed in Section 2.4.2.1, the coefficient of 2.5 in Equation (2.27) was recommended by Skempton (1951) for D/B ratios greater than 10; however, reduced values were suggested for D/B ratios less than 10. By reducing 2.5 in Equation (2.27), y50 is reduced, and thus p in Equation (2.29) increases. This increase in p would reduce the deflection estimates and thus improve the accuracy of the LPile model for stiff clays where the D/B ratio of the foundation is less than 10. Kulhawy and Chen (1995) also note that Broms' (1964b) recommended value of Np = 9 in Equation (2.24) is probably too low for drilled shaft foundations given their rough surface, and that a value closer to 12 is more appropriate. Unfortunately, it is not possible to manually change the

coefficient of 2.5 or the value of N_p in *LPile* to account for drilled shafts with lower *D/B* ratios. One possible solution is to manually compute the *p-y* curves with modified input parameters and then enter them as user-defined *p-y* curves in *LPile*; however, this was not done for this investigation.

The results of the ±1 standard deviation of soil input properties for each analysis method considered in this investigation show increasing or decreasing the soil input properties by one standard deviation does not result in equivalent deviation from the best-estimate input property values, but instead results in considerably more pile head deflection when soil input properties are reduced by one standard deviation. All three analysis methods were most sensitive to s_u with pile head deflection increasing exponentially with decreasing values of s_u. As such, very small reductions in s_u tend to result in considerable increase in prediction of pile head deflection for all three methods. Both *DFSAP* and *LPile* exhibited the most sensitivity to changes in s_u, while *MFAD* was appears to be the most sensitive to changes in E_p. *LPile* and *DFSAP* were both sensitive to changes in ε_{50}, with pile deflection increasing linearly with decreasing s_u. In general, *LPile* was much more sensitive to input properties than *DFSAP* or *MFAD*. With the exception of DS 76-1, *DFSAP* was the least sensitive to change in soil input properties. All three analysis methods demonstrated increasing sensitivity with increasing magnitude of applied load with *LPile* exhibiting considerable dependency on load magnitude, *MFAD* exhibiting moderate to considerable dependency on load magnitude, and *DFSAP* exhibiting minor dependency on load magnitude.

In general, the soil input properties for each load test performed in cohesive soils were reasonably accurate. *DFSAP* and *MFAD* both provided results in fairly good agreement with experimentally-observed results, while *LPile* tended to underpredict

groundine deflection for the initial increments of applied load and then sharply overpredict groundline deflection with increasing load magnitude. The groundline deflection predicted by *LPile* using -1 standard deviation soil input properties was larger than all of the experimentally-observed groundline deflections with the exception of DS 22-1 and DS 22-2. For these two load tests, *LPile* estimated slightly less groundline deflection using -1 standard deviation soil input properties. With the exception of DS 22-1 and DS 76-1, the deflection estimated by *LPile* using -1 standard deviation soil input properties was larger than the groundline deflection estimated by *DFSAP* using best-estimate soil input properties. *MFAD* was consistently unconservative for each load test performed in cohesive soils with the exception of DS 76-1. *DFSAP* was not consistently conservative or unconservative and generally had small values of error between observed and predicted results. The biggest concern with *DFSAP* in cohesive soils is that three of the analyses (DS 18-2, DS 20-5, DS 20-6) failed before reaching the maximum applied load. If *DFSAP* were used to design DS 18-2, DS 20-5, or DS 20-6 for large magnitudes of applied load, the end result would have been a recommendation for a larger foundation as the solutions would not have been achieved for the larger magnitudes of applied load.

5.5 Regression Analysis and Reliability

The recommendations for use of each analysis method to this point have been somewhat qualitative instead of quantitative. Although the results of this investigation thus far provide insight into the relative accuracy of each model and guidelines have been given regarding the use of each model for different soil types and loading conditions, there is still a lack of more qualitative data regarding the uncertainty of each analysis method. Recall from previous discussion that the uncertainty inherent in each analysis

method is a function of the uncertainty associated with the input properties and the uncertainty associated with the model's ability to accurately capture the behavior of the foundation. The uncertainty associated with the input parameters can be estimated by performing sensitivity analyses of the input parameters, while the model uncertainty can be estimated from the results of each analysis method. The model uncertainty is estimated from the regression analysis performed on the combined results presented in Section 5.1 through 5.3 of this thesis. From the model uncertainty and the uncertainty of the input parameters for each model, it is possible to estimate the overall reliability of the design.

For the purposes of this discussion, the reliability R of the design is the probability that the deflection of the foundation will be less than the design deflection of the foundation. From the results of cohesive soils, it is clear that the actual deflection of a foundation designed using *LPile* will be much less than the actual deflection of a foundation designed using *MFAD* if the same limiting design deflection is used in both models. As such, the reliability of the two models is clearly different, with the reliability of *LPile* being much higher. The problem is that the designer does not know quantitatively what the reliability of any of the analysis methods presented in this investigation will be for a particular type of soil because it is assumed that the predicted deflection is also the most likely deflection of the actual foundation. More importantly, this precludes the designer from choosing the level of reliability of their design in the same way that one would choose a factor of safety. This problem can be addressed by estimating the error of each analysis method from the observed and predicted results and the results of the regression analyses presented in Section 5.1 through 5.3. The parametric equation for the best-fit regression line shown in these figures is

$$\log(\delta_{predicted}) = a * \log(\delta_{measured}) + b \quad \textbf{(5.1)}$$

where:

$\delta_{predicted}$ = pile deflection predicted by analysis method

$\delta_{measured}$ = measured pile deflection from large-scale load test

a = linear regression coefficient

b = linear regression coefficient

The coefficients a and b were determined from the regression analyses presented in Section 5.1 through 5.3 and are shown in Table 5.1 and Table 5.2 for granular and cohesive soils, respectively.

The error between the measured pile deflection and the best-fit regression line is estimated from the residuals, r_R, of the regression analysis. The model uncertainty is estimated from the probability density function for the residuals, which are shown in Figure 5.9 through Figure 5.14.

Table 5.1. Linear regression coefficients for granular soils

Coefficient	LPile	DFSAP	MFAD
a	0.8159	0.8965	0.8509
b	-0.2362	-0.08130	-0.08800

Table 5.2. Linear regression coefficients for cohesive soils

Coefficient	LPile	DFSAP	MFAD
a	0.519	1.288	1.100
b	-0.3282	0.08510	0.2349

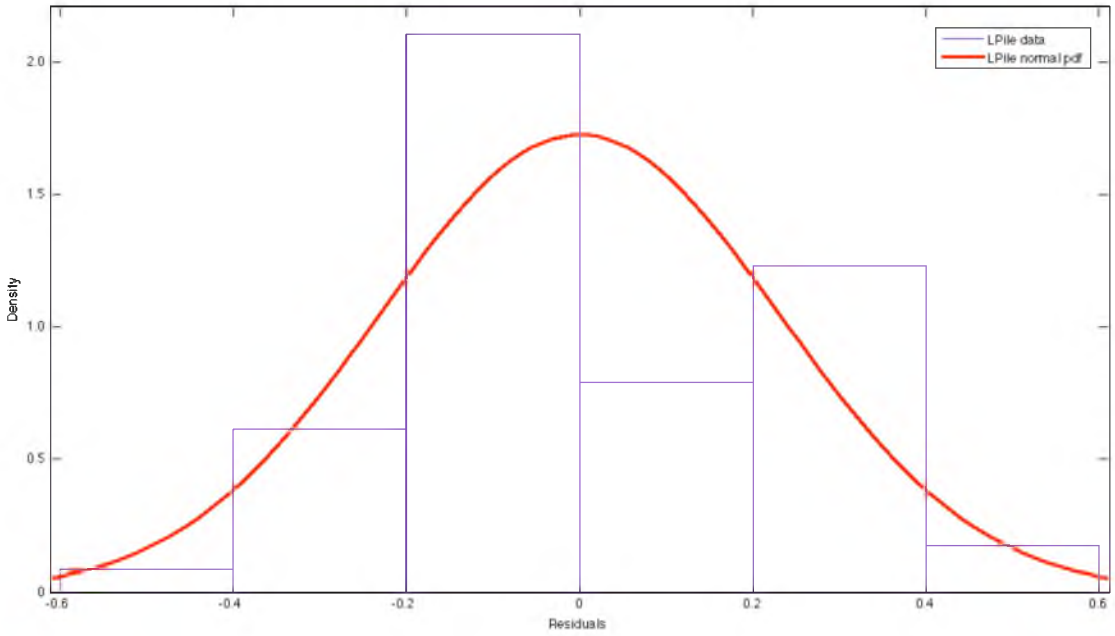

Figure 5.9. Probability density function for LPile results in granular soil

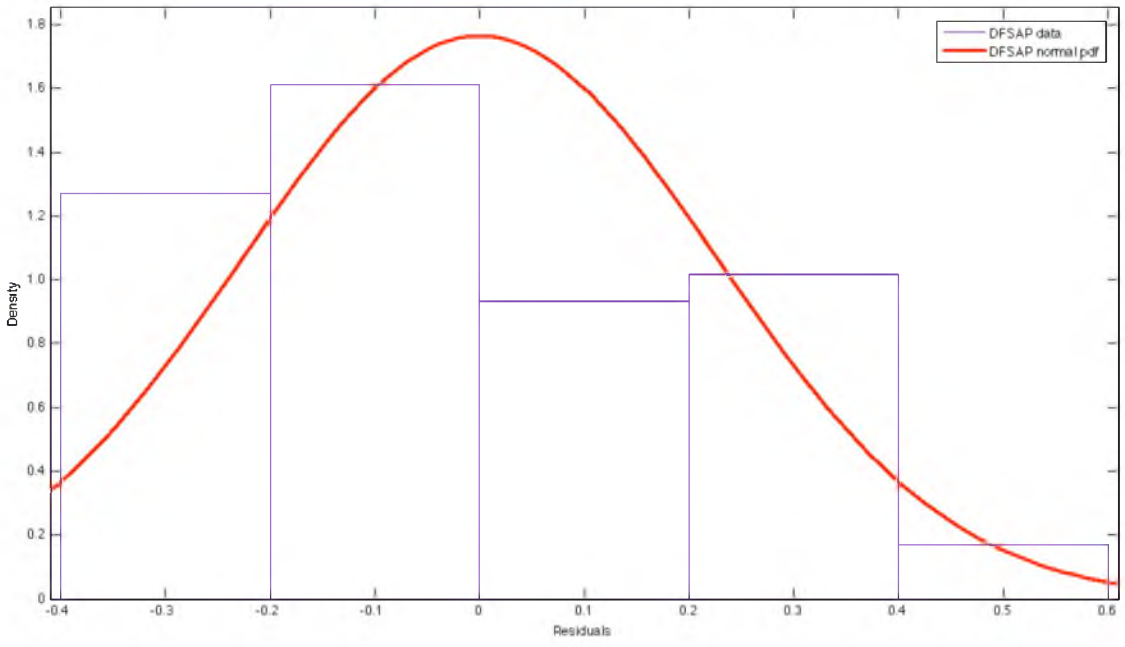

Figure 5.10. Probability density function for DFSAP results in granular soil

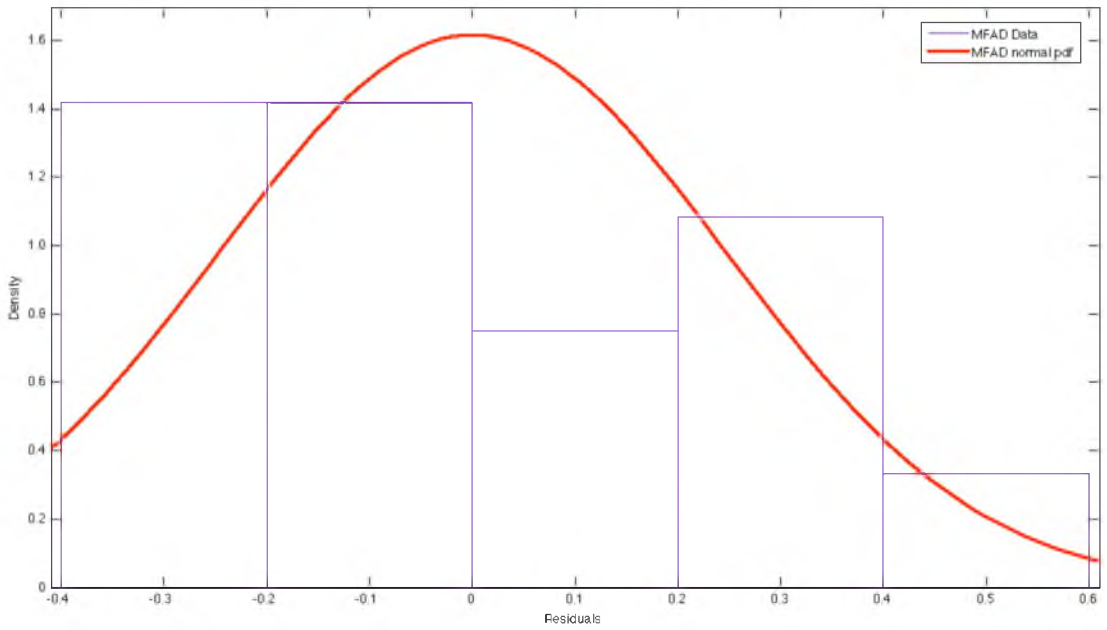

Figure 5.11. Probability density function for MFAD results in granular soil

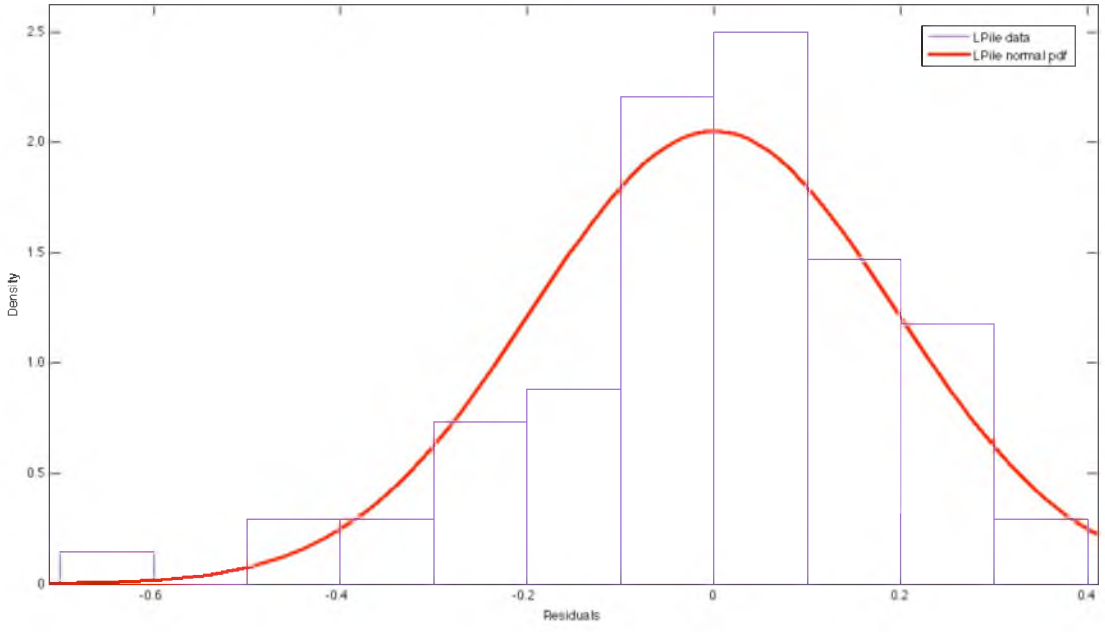

Figure 5.12. Probability density function for LPile results in cohesive soil

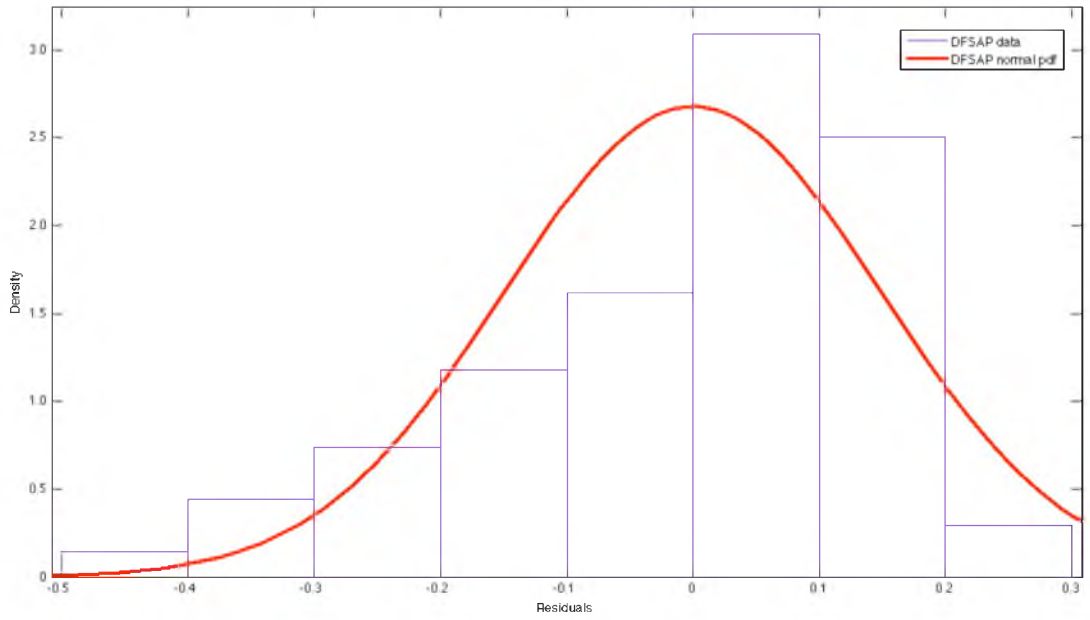

Figure 5.13. Probability density function for DFSAP results in cohesive soil

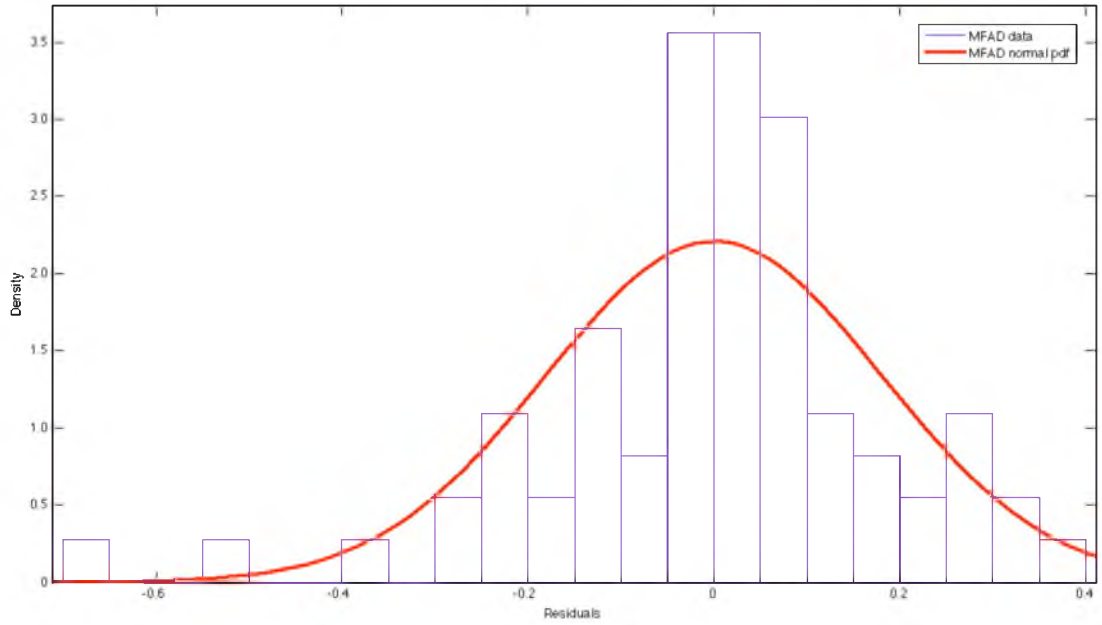

Figure 5.14. Probability density function for MFAD results in cohesive soil

The equation for the predicted deflection from a particular analysis method for a chosen level of reliability is

$$\log(\delta_{predicted}) \leq \frac{\log(\delta_{probable}) - r_R - b}{a} \quad \textbf{(5.2)}$$

where:

$\delta_{predicted}$ = pile deflection predicted by analysis method

$\delta_{probable}$ = probable deflection of pile

r_R = residual for reliability R

a = linear regression coefficient

b = linear regression coefficient

The value of r_R is determined from the probability density functions shown in Figure 5.9 through Figure 5.14.

Recall from probability theory that the probability of some residual value less than r_R is the area under the curve of the probability density function for reliability less than r_R. The inverse probability density function is used to solve for r_R from a chosen value of R, and Equation (5.2) is then solved for $\delta_{predicted}$ to obtain the required value of predicted deflection for chosen value of design deflection (shown in Equation (5.2) as $\delta_{probable}$ to emphasize that the deflection is really a probabilistic deflection). Values of rR for R were obtained using the inverse probability density function in MATLAB for a normal distribution, and these values are plotted in Table 5.3.

The results of the regression analysis for the combined results from each analysis method are shown in Figure 5.15 through Figure 5.20 along with the lines representing reliability of 5% and 95%. Certainly a reliability of 5% would never be used in design;

Table 5.3. Select values of rR as a function of R for granular and cohesive soils for LPile, DFSAP, and MFAD analysis

R	rR (granular soil)			rR (cohesive soil)		
	LPile	DFSAP	MFAD	LPile	DFSAP	MFAD
0.40	-0.0586	-0.0573	-0.0625	-0.0493	-0.0378	-0.0466
0.42	-0.0467	-0.0457	-0.0498	-0.0393	-0.0301	-0.0372
0.44	-0.0349	-0.0342	-0.0373	-0.0294	-0.0225	-0.0278
0.46	-0.0232	-0.0228	-0.0248	-0.0196	-0.0150	-0.0185
0.48	-0.0116	-0.0114	-0.0124	-0.0098	-0.0075	-0.0092
0.50	0.0000	-0.0001	0.0000	0.0000	0.0000	0.0000
0.52	0.0116	0.0113	0.0124	0.0097	0.0075	0.0093
0.54	0.0233	0.0227	0.0248	0.0195	0.0150	0.0185
0.56	0.0350	0.0341	0.0373	0.0294	0.0225	0.0278
0.58	0.0467	0.0456	0.0498	0.0393	0.0301	0.0372
0.60	0.0586	0.0572	0.0625	0.0493	0.0378	0.0467
0.62	0.0707	0.0690	0.0754	0.0594	0.0455	0.0563
0.64	0.0830	0.0810	0.0884	0.0697	0.0534	0.0660
0.66	0.0955	0.0932	0.101	0.0802	0.0615	0.0760
0.68	0.108	0.105	0.115	0.0910	0.0697	0.0861
0.70	0.121	0.118	0.129	0.102	0.0781	0.0966
0.72	0.134	0.131	0.143	0.113	0.0869	0.107
0.74	0.148	0.145	0.158	0.125	0.0959	0.118
0.76	0.163	0.159	0.174	0.137	0.105	0.130
0.78	0.178	0.174	0.190	0.150	0.115	0.142
0.80	0.194	0.190	0.207	0.163	0.125	0.155
0.82	0.211	0.206	0.225	0.178	0.136	0.168
0.84	0.230	0.224	0.245	0.193	0.148	0.183
0.86	0.249	0.244	0.266	0.210	0.161	0.198
0.88	0.271	0.265	0.289	0.228	0.175	0.216
0.90	0.296	0.289	0.316	0.249	0.191	0.236
0.92	0.325	0.317	0.346	0.273	0.209	0.258
0.94	0.359	0.351	0.383	0.302	0.231	0.286
0.96	0.405	0.395	0.431	0.340	0.260	0.322
0.98	0.475	0.464	0.506	0.399	0.306	0.378

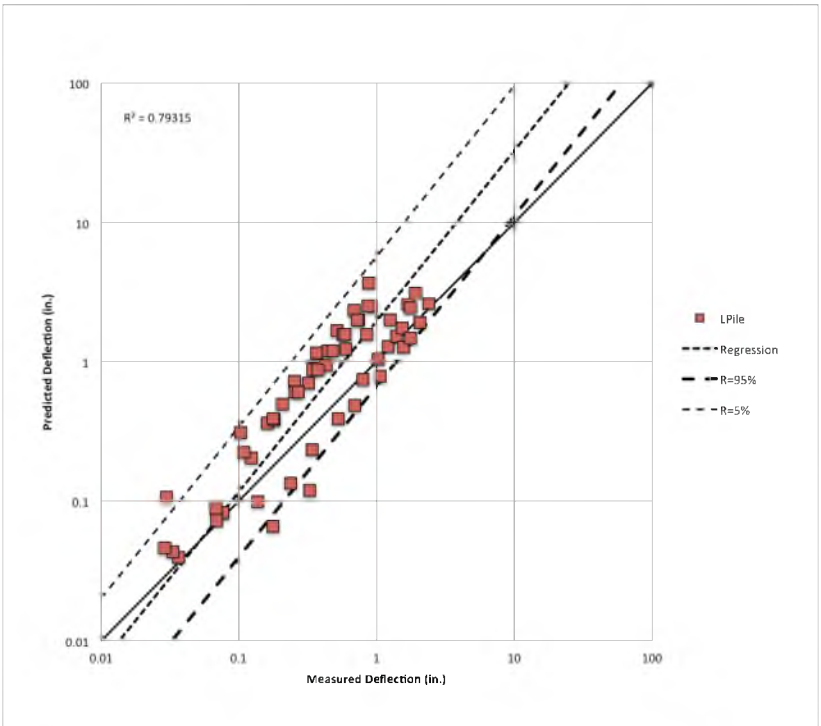

Figure 5.15. Regression analysis for combined LPile results in granular soils with R=5% and 95%

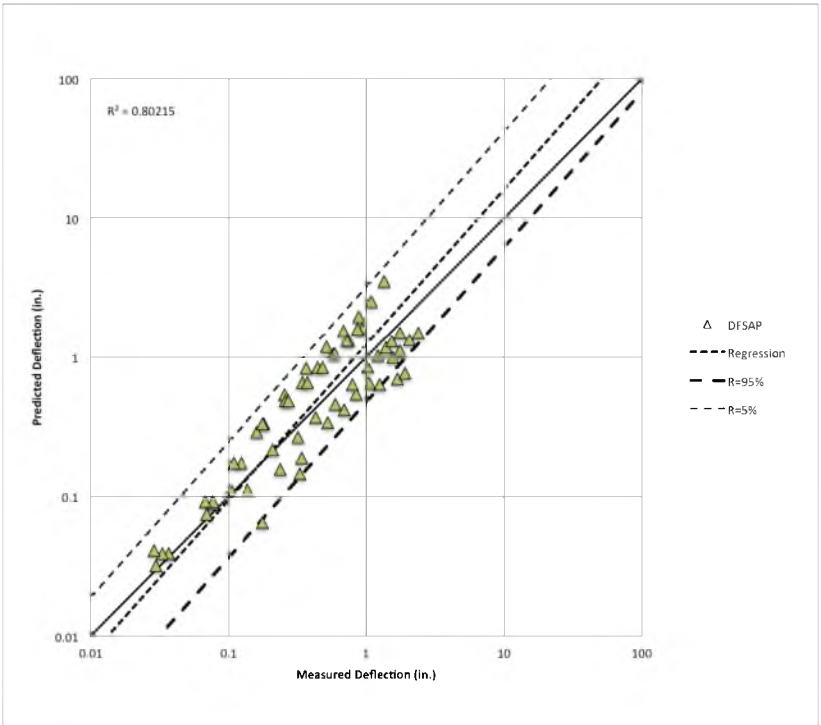

Figure 5.16. Regression analysis for combined DFSAP results in granular soils with R=5% and 95%

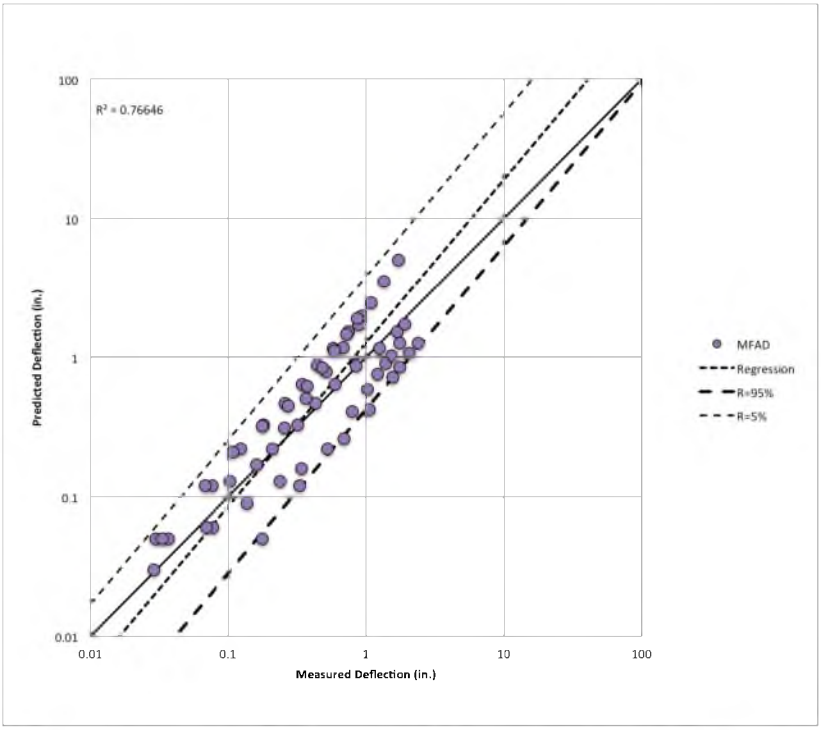

Figure 5.17. Regression analysis for combined MFAD results in granular soils with R=5% and 95%

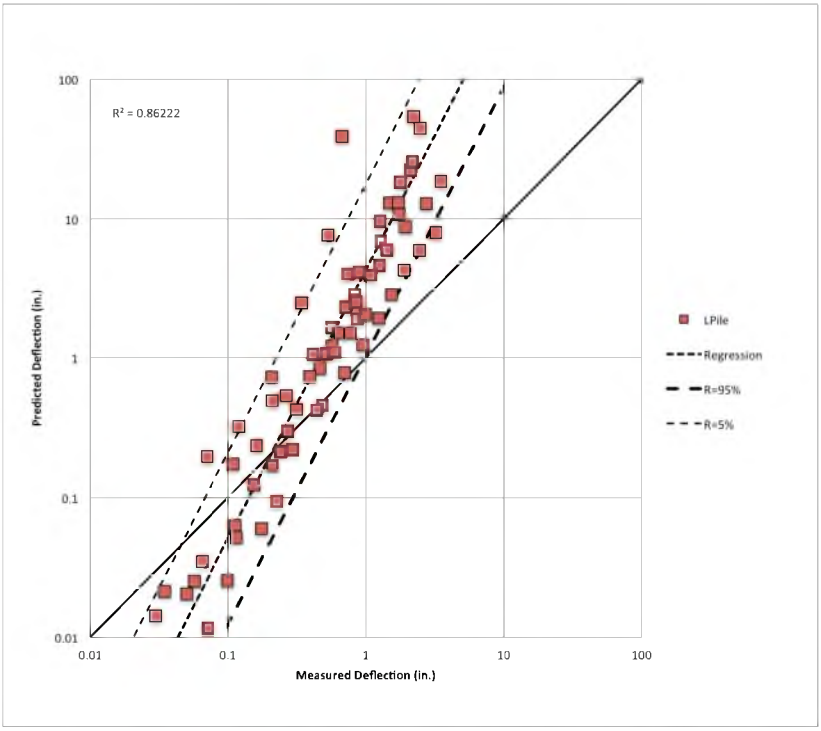

Figure 5.18. Regression analysis for combined LPile results in cohesive soils with R=5% and 95%

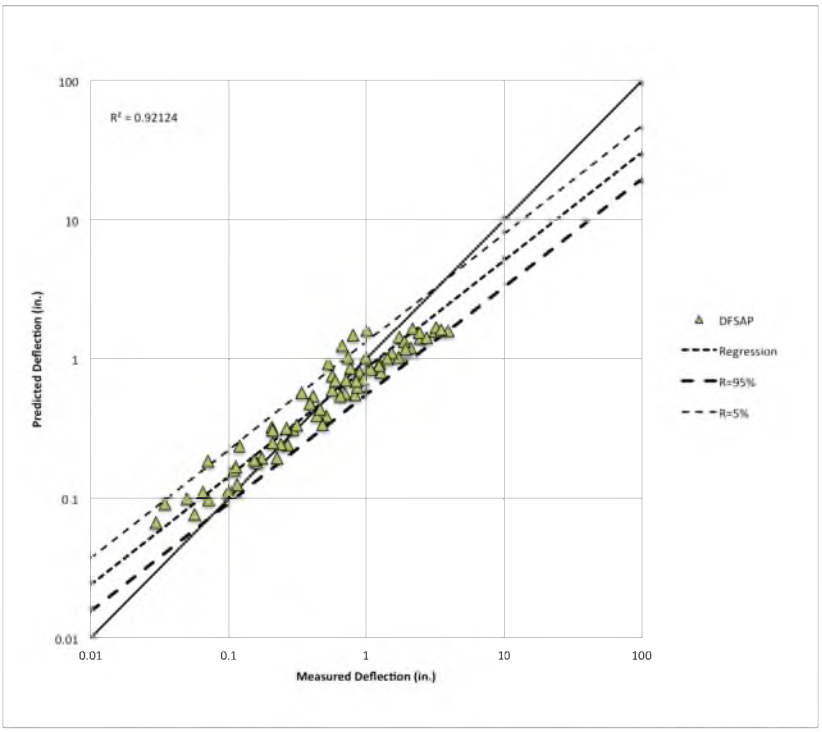

Figure 5.19. Regression analysis for combined DFSAP results in cohesive soils with R=5% and 95%

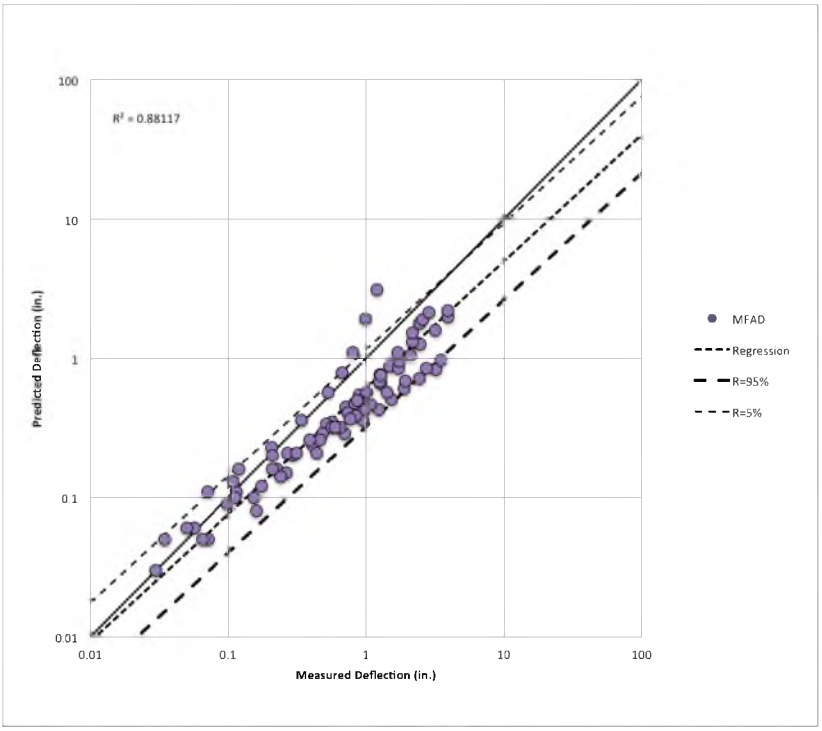

Figure 5.20. Regression analysis for combined MFAD results in cohesive soils with R=5% and 95%

however, this is shown to illustrate that the bounds are symmetric about the bet-fit line, which is expected for an unbiased regression fit, i.e., one with R = 50%. For values of predicted deflection using the R = 95% line, it can be said that there is a 95% chance the actual pile deflection will not exceed the acceptable or design value of pile deflection. The data from most of the analysis methods are bounded by the 5% and 95% lines, so it is clear from the experimentally-observed results that this is a valid statement. Of course, the designer is ultimately responsible for choosing an appropriate level of reliability for an acceptable level of risk for the foundation design.

6 CONCLUSIONS AND RECOMMENDATIONS

6.1 Drilled Shaft Analysis in Granular Soils

The results and subsequent analysis of the large-scale load tests presented in this investigation showed that all three analysis methods (*LPile*, *DFSAP* and *MFAD*) provided reasonably accurate predictions for pile deflection. Furthermore, the results showed that the estimated design values for soil properties were reasonably accurate, and inaccuracy of the soil properties on the disparity between observed and predicted deflection was likely minimal. Some notable exceptions include moderate overprediction of pile head deflection by *LPile* for DS 11-1 and general inconsistency in behavior between *DFSAP* results and experimentally-observed results for DS 11-1. It is recommended that drilled shafts in granular soils be analyzed using *MFAD* or *DFSAP* with *MFAD* being preferred for drilled shafts subjected to large overturning moments. Recall that *MFAD* should only be used for $2 < D/B < 10$. *MFAD* tended to be the most sensitive to soil input properties, while *DFSAP* tended to be the least sensitive to soil input properties. Therefore, in situations where data are limited or correlations are being used to establish soil properties, *DFSAP* may be the preferred analysis method. The sensitivity of all three analysis methods increases exponentially as ϕ decreases. In general, ϕ should always be estimated from in-situ or laboratory tests – particularly at shallow depths – for drilled shaft design. Sensitivity analyses should be performed in a real design scenario to assess the sensitivity of the design to the input parameters. If large variations in pile head

deflection occur with minor variation of soil properties, a more rigorous field exploration or laboratory testing program should be implemented. It should be noted that *LPile* also yielded reasonable results for granular soils, and these results tended to be slightly conservative even for upper bound values of ϕ. For this reason, *LPile* can also be used to analyze drilled shafts in granular soils with minimal concern for overestimating pile deflection if somewhat unconservative soil input properties are used.

It is also recommended that the drilled shaft analysis be conduced using the results of the regression analysis shown in Section 5.5. Using this method, the designer selects an acceptable level of reliability and solves Equation (5.2) for the deflection that should be predicted by the chosen analysis method. This method is advantageous because it directly accounts for the error in the analysis method and allows the designer to choose an acceptable level of reliability. The disadvantage of this method is that the data available for granular soils are limited, and the results are dependent upon the input properties for the tests included in the database.

6.2 Drilled Shaft Analysis in Cohesive Soils

The results and subsequent analysis of the large scale load tests performed in cohesive soils showed much more variable results than the results for the load tests performed in granular soils. In general, the results of the analyses from all three analysis methods suggest that *DFSAP* yields the most accurate results while *LPile* yields the least accurate results. All three analysis methods exhibited increasing sensitivity with increasing magnitude of applied load with *LPile* exhibiting considerable dependency on load magnitude, *MFAD* exhibiting moderate to considerable dependency on load magnitude, and *DFSAP* exhibiting minor dependency on load magnitude.

The sensitivity of all three analysis methods increases exponentially as s_u decreases. Additionally, the sensitivity of *MFAD* increases exponentially as E_p decreases, while *DFSAP* and *LPile* were much less sensitive to changes in ε_{50}. The results showed that *LPile* and *DFSAP* were most sensitive to changes in s_u, while *MFAD* was most sensitive to changes in E_p. In general, s_u and E_p should always be estimated from in-situ or laboratory tests – particularly at shallow depths – for drilled shaft design. Sensitivity analyses should be performed in a real design scenario to assess the sensitivity of the design to the input parameters. If large variations in pile head deflection occur with minor variation of soil properties, a more rigorous field exploration or laboratory testing program should be implemented.

It is recommended that drilled shafts in cohesive soils be analyzed using *DFSAP* to establish the most likely value of actual groundline deflection, while *MFAD* and *LPile* can be used to estimate upper and lower bound estimates. The results of the *MFAD* and *DFSAP* analyses show that *MFAD* consistently predicts less deflection than *DFSAP*; however, the disparity between the results was generally small. Although the difference between *DFSAP* and *MFAD* results were generally small, *DFSAP* did under predict settlement for some load tests presented in this investigation, and it should not automatically be assumed that the actual groundline deflection will be bounded by *DFSAP* and *MFAD*. If it is unclear whether *DFSAP* is conservative or unconservative, it is recommended that *LPile* be used to estimate the upper bound of actual deflection. In this case, the design values for s_u or ε_{50} should not be conservative as the *LPile* estimates of deflection are likely to be much higher than the estimates of *DFSAP* or *MFAD*.

It is also recommended that the drilled shaft analysis be conduced using the results of the regression analysis shown in Section 5.5. Using this method, the designer

selects an acceptable level of reliability and solves Equation (5.2) for the deflection that should be predicted by the chosen analysis method. This method is advantageous because it directly accounts for the error in the analysis method and allows the designer to choose an acceptable level of reliability. The disadvantage of this method is that the data available for cohesive soils are limited.

6.3 Recommendations for Future Research

The unit weight was held as a fixed variable during the parametric evaluation of each analysis method. Further parametric studies should be conducted wherein the effect of the unit weight is evaluated.

The effects of large diameter and rigidity of a drilled shaft foundation, as measured by the *D/B* ratio in this investigation, are difficult to evaluate because large-scale load test data for drilled shafts with varying *D/B* ratios at the same site are extremely limited. As such, an evaluation of these effects could be undertaken using numerical techniques. One approach would be to create a numerical model using well-developed data from a large-scale load test of a slender drilled shaft and then to calibrate the model such that the observed and predicted results are in good agreement. Model simulations could then be performed on foundations with varying length, diameter, and resulting *D/B* ratios to obtain "synthetic" large-scale load test results, which can be compared to the results of the analysis methods used in this investigation.

The soil types considered in this investigation were limited to clay and sand. Additional research should be performed to assess the accuracy of these models for other types of soil. In the author's experience, *LPile* is used to model drilled shaft foundations in many different types of granular soils; however, there is no canned *p-y* curve for these

other types of granular soils, and as such, the sand *p-y* curve is typically used because it is the most similar. The uncertainty of the results for these types of analyses is completely unknown.

The regression analysis of the results in this investigation are based on limited data from a limited number of test sites. The robustness of the regression analysis increases as the number of load tests increases. As such, the analyses used in this investigation should be performed as future load test data becomes available, and these results should be included in the data set. The regression analysis of the data should be performed include new data, and the recommendations presented in this thesis should be updated accordingly.

The loads applied to the drilled shafts in this investigation were applied to the top of the foundation or to the top of the structure on top of the foundation. Although this type of loading is most common, many instances occur in civil engineering where kinematic lateral loading is applied to the foundation. Examples include surface fault rupture where the trace of the fault passes through the foundation, liquefaction-induced lateral spreading, and slopes reinforced with deep foundations. Limited research has been performed to assess the accuracy of any of the analysis methods presented in this thesis for situations where kinematic lateral loading is the primary loading mechanism, and additional research should be performed to investigate the accuracy of these methods for this type of load mechanism.

REFERENCES

ACI 318-11. (2011). *Building Code Requirements for Structural Concrete and Commentary.* Farmington Hills: American Concrete Institute.

Adams, J., & Radhakrishna, H. (1973). The Lateral Capacity of Deep Augered Footings. *Proceedings, 8th International Conference on Soil Mechanics and Foundation Engineering*, *2*, 1-8. Moscow.

Alizadeh, M., & Davisson, M. T. (1970). Lateral Load Tests on Piles - Arkansas River Project. *Proceedings of the American Society of Civil Engineers , 96* (SM5), 1583-1604.

Amann, P., Wollenhaupt, H., & Bahn, R. (1988). Experiences with Pile Foundations in Lake-Clay. *Proceedings, 1st International Geotechnical Seminar on Deep Foundation on Bored and Auger Piles*, 261-267. Ghent.

Anderson, J. B., & Townsend, F. C. (1999). Validation of p-y Curves from Pressuremeter Tests at Pascaguola Mississippi. *Proceedings, XI Pan American Conf on Soil Mechanics and Geotechnical Engineering*, 1643-1. Foz do Iguassu.

Anderson, J. B., Townsend, F. C., & Grajales, B. (2003). Case History Evaluation of Laterally Loaded Piles. *Journal of Geotechnical and Geoenvironmental Engineering*, 187-196.

API. (1993). *Recommended Practice for Planning, Designing, and Constructing Fixed Offshore Platforms - Working Stress Design.* Washington, D.C.: American Petrolium Institute.

Ashour, M., & Norris, G. (2000). Modeling Lateral Soil-Pile Response Baed on Soil-Pile Interaction. *Journal of Geotechnical and Geoenvironmental Engineering , 126* (5), 420-428.

Ashour, M., Norris, G. M., Bowman, S., Beeston, H., Billing, P., & Shamsabadi, A. (2001). Modeling Pile Lateral Response in Weathered Rock. *Proceedings, 36th Engineering Geology and Geotechnical Engineering Symposium, 28-30*. Las Vegas.

Ashour, M., Norris, G., & Piling, P. (2002). Strain Wedge Model Capability of Analyzing Behavior of Laterally Loaded Isolated Piles, Drilled Shafts, and Pile Groups. *Journal of Bridge Engineering , 7* (4), 245-254.

Ashour, M., Norris, G., & Pilling, P. (1998). Lateral Loading of a Pile in Layered Soil Using the Strain Wedge Model. *Journal of Geotechnical and Geoenvironmental Engineering , 124* (4), 303-315.

Baguelin, F., Goulet, G., & Jezequel, J. (1972). Experimental Study of the Behavior of a Laterally Loaded Pile. *Proceedings, 5th European Conference on Soil Mechanics and Foundation Engineering, 1*, 317-324. Madrid.

Beer, F. P., Johnston, J. E., & DeWolf, J. T. (2006). *Mechanics of Materials* (4th ed.). New York: McGraw-Hill.

Behn, F. E. (1960). Tests of Tilting Moment Resistance of Cylindrical Reinforced Concrete Foundations for Overhead Sign Supports. *Highway Research Board Bulletin 247*, 14-33. Washington, D.C.: FHWA.

Bhushan, K., & Askari, S. (1984). Lateral-Load Tests on Drilled Pier Foundations for Solar Plant Heliostats. In J. A. Langer, & C. D. E. T. Mosley, *Laterally Loaded Deep Foundations: Analysis and Performance, ASTM STP 835*, 140-156. American Society for Testing and Materials.

Bhushan, K., & Scheyhing, C. (2002). Lateral Load Tests on Drilled Piers in San Diego Area Residual and Formational Soils. *Proceedings of the DFI 27th Annual conference on Deep Foundations.* San Diego: DFI.

Bhushan, K., Haley, S. C., & Fong, P. T. (1979). Lateral Load Tests on Drilled Piers. *Journal of the Geotechnical Engineering Division , 105* (GT8), 969-985.

Bhushan, K., Lee, L. J., & Grime, D. B. (1981). Lateral Load Tests on Drilled Piers in Sand. *Proceedings, Drilled Piers and Caissons*, 114-131. St. Louis:ASCE

Bierschwale, M. W., Coyle, H. M., & Bartoskewitz, R. E. (1981). Lateral Load Tests on Drilled Shafts Founded In Clay. *Drilled Piers and Caissons* , 98-113.

Biot, M. A. (1937). Bending of Infinite Beams on an Elastic Foundation. *Journal of Applied Mechanics , 59*, A1-7.

Botea, E., Manoliu, I., & Abramescu, T. (1973). Large Diameter Piles under Axial and Lateral Loads. *Proceedings, 8th International Conference on Soil Mechanics and Foundation Engineering, 2*, 27-32. Moscow.

Bowman, E. R. (1958). *Investigation of the Lateral Resistance to Movement of a Plate in Cohesionless Soil.* Austin: The University of Texas.

Briaud, J.-L., Smith, T., & Meyer, B. (1984). Laterally Loaded Piles and the Pressuremeter: Comparison of Existing Methods. *Laterally Loaded Deep Foundations*, 97-111.

Briaud, J.-L., Smith, T., & Meyer, B. (1983). Pressuremeter Gives Elementary Model for Laterally Loaded Piles. *International Symposium on In-Situ Testing of Soil and Rock, 2*, 217-221. Paris.

Briaud, J.-L., Smith, T., & Tucker, L. (1985). A Pressuremeter Method for Laterally Loaded PIles. *International Conference on Soil Mechanics and Foundation Engineering.* San Francisco.

Broms, B. (1964a). Lateral Resistance of Piles in Cohesionless Soils. *Journal of Soil Mechanics and Foundations Division , 90* (SM3), 123-156.

Broms, B. (1964b). Lateral Resistance of Piles in Cohesive Soils. *Journal of Soil Mechanics and Foundations Division , 90* (SM2), 27-63.

Brown, D. A., Hidden, S. A., & Zhang, S. (1994). Determination of p-y Curves Using Inclinometer Data. *Geotechnical Testing Journal , 17* (2), 150-158.

Brown, D. A., Morrison, C., & Reese, L. C. (1988). Lateral load behavior of pile group in sand. *Journal of Geotechnical Engineering , 114* (11), 1261-1276.

Callanan, J. F., & Kulhawy, F. H. (1980). *Evaluation of Procedures for Predicting Foundation Uplift Movements.* Palo Alto: Electric Power Research Institute.

Chai, Y., & Hutchinson, T. (1999). *Flexural Strength and Ductility of Reinforced Concrete Bridge Piles.* Report UCD-STR-99-2. University of California, Davis.

Chang, M. F., & Goh, A. (1988). Laterally Loaded Bored Piles in Residual Soils and Weathered Rocks. *Proceedings, 2nd International Conference on Geomechanics in Tropical Soils, 1*, 303-310. Singapore.

Charles, W. W., Zhang, L., & Dora, C. N. (2001). Response of Laterally Loaded Large-Diameter Bored Pile Groups. *Journal of Geotechnical and Geoenvironmental Engineering , 127* (8), 658-669.

Chen, Y.-J., & Kulhawy, F. H. (1994). *Case History Evaluation of the Behavior of Drilled Shafts Under Axial and Lateral Loading.* Report TR-104601. Palo Alto: EPRI.

Chiou, J.-S., Ko, Y.-Y., Hsu, S.-Y., & Tsai, Y.-C. (2012). Testing and Analysis of a Laterally Loaded Bridge Caisson Foundation in Gravel. *Soils and Foundations , 52* (3), 562-573.

Cho, K. H., Clark, S. C., Keaney, B. D., Gabr, M. A., & Borden, R. H. (2001). Laterally Loaded Drilled Shafts Embedded in Soft Rock. *Transportation Research Record. 1772*, 3-11. Washington, D.C.: Transportation Research Board.

Clark, J. I., McKeown, S., Lester, W. B., & Eibner, L. J. (1985). The Lateral Load Capacity of Large Diameter Concrete Piles. *Proceedings of the 38th Canadian Geotechnical Conference.* Edmonton: Canadian Geotechnical Society.

Cox, W. R., Reese, L. C., & Grubbs, B. R. (1974). Field Testing of Laterally Loaded Piles in Sand. *Sixth Annual Offshore Technology Conference.* Houston.

Coyle, H. M., & Reese, L. C. (1966). Load Transfer for Axially Loaded Piles in Clay. *Journal of the Soil Mechanics and Foundations Division , 92* (2), 1-26.

Davidson, H. L., & Donovan, T. D. (1977). *Design Approach for Laterally Loaded Drilled Piers.* Pennsylvania Power and Light Company.

Davidson, H. L., Cass, P. G., Khilji, K. H., & McQuade, P. V. (1982). *Laterally Loaded Drilled Pier Research Volume 1: Design Methodology.* Report EL 2197-1. Palo Alto: Electric Power Research Institute.

Davidson, H. L., Cass, P. G., Khilji, K. H., & McQuade, P. V. (1982). *Laterally Loaded Drilled Pier Research Volume 2: Research Documentation.* Report EL-2197-2. Palo Alto: Electric Power Research Institute.

Diagnostic Engineering Consultants, Ltd. (1997). *Load Test Report for Taiwan Rail BridgeFoundation in Chiayi.* Taiwan.

Diagnostic Engineering Consultants, Ltd. (1994). *Report on Lateral Load Test of Bored Piles for Bei-Tou Incinerator.* Taiwan.

Diagnostic Engineering Consultants, Ltd. (1998). *Report on Lateral Load Test of Bored Piles for Neihu Sewage Treatment Plant.* Taiwan.

Diagnostic Engineering Consultants, Ltd. (1994). *Report on Lateral Load Test of Bored Piles for Taipei MRT Tamshui Line.* Taiwan.

Dunnavant, T. W., & O'Neill, M. W. (1985). *Performance, Analysis, and Interpretation of a Lateral Load Test of a 72-inch-diameter Bored Pile in Overconsolidated Clay.* University of Houston, Department of Civil Engineering.

EPRI. (2014). *User Guide for MFAD 5.1 (Moment Foundation Analysis & Design).* Palo Alto: EPRI and DiGioia, Gray & Associates, LLC.

Feda, J. (1972). Test of Laterally Loaded Piles. *Proceedings: 5th European Conference on Soil Mechanics and Foundation Engineering, 1*, 357-364. Madrid.

Fenelli, G. B., & Galateri, C. (1981). soil Modulus for Laterally Loaded Piles in Pozzolana. *Proceedings, 10th International Conference on Soil Mechanics and Foundation Engineering, 2*, 703-708. Stockholm.

Franke, E. (1973). Principles for Test Loading of Large Bored Piles by Horizontal Loads. *Proceedings, 8th International Conference on Soil Mechanics and Foundation Engineering, 2*, 97-104. Moscow.

Frizzi, R. P., & Meyer, M. E. (2000). Augercast Piles - South Florida Experience. In N. D. Dennis Jr., R. Castelli, & M. W. O'Neill (Eds.), *New Technological and Design Developments in Deep Foundations, GSP 100*, 382-396. ASCE.

Fukuoka, M. (1988). Large Cast-in-place Piles in Japan. *Proceedings, 1st International Geotechnical Seminar on Deep Foundation on Bored and Auger Piles*, 95-106. Ghent:

Gabr, M. A., Lunne, T., & Powell, J. J. (1994). P-y Analysis of Laterally Loaded Piles in Clay Using DMT. *Journal of Geotechnical Engineering , 120* (5), 816-837.

Garassino, A., Jamiolkowski, M., & Pasqualini, E. (1976). Soil Modulus for Laterally Loaded Piles in Sands and N.C. Clays. *Proceedings, 6th European Conference on Soil Mechanics and Foundation Engineering, 1*, 429-434. Vienna.

GECL Engineering Consultants, Ltd. (1997). *Report on Lateral Load Test of Bored Piles for Xinbeitou Station.* Taiwan.

Geokon, I. (2012). *About Us and Our Technology*. Retrieved May 15, 2012, from Geokon, Inc.: http://www.geokon.com/company/profile.php

Geokon, Inc. (2012). *Inclinometers*. Retrieved June 4, 2012, from Geokon, Inc.: http://www.geokon.com/inclinometers/

Georgiadis, M. C., Anagnostopoulos, C., & Naskos, N. (1997). Effect of Pile-Head Enlargement on Lateral and Axial Response of a Bored Pile. *Proceedings, 14th International Conference on Soil Mechanics and Foundation Engineering*, 809-812. Hamburg.

Goh, A., & Lam, T. (1988). Lateral Load Tests on Some Bored Piles in Singapore. *Proceedings, 5th Australia-New Zealand Cponference on Geomechanics*, 509-513. Sydney.

Guedes de Mello, F. A., & Esteves Ferreira, M. (1989). Horizontal Load TEst on Free Head Pile. *Proceedings, 12th International Conference on Soil Mechanics and Foundation Engineering*, 1159-1160. Rio de Janeiro.

Habibagahi, K., & Langer, J. A. (1984). Horizontal Subgrade Modulus of Granular Soils. *ASTM STP 835* , 21-34.

Hansen, J. (1961). *Ultimate Resistance of Rigid Piles Against Transversal Forces.* Danish Geotechnical Institute. Copenhagen: Bulletin 12.

Harris, M. C., Papanicolas, D., & Rogers, W. G. (1985). Behavior of Test Piles Subjected to Lateral Loading. *Proceedings of the 38th Canadian Geotechnical Conference*, 399-406. Edmonton: Canadian Geotechnical Society.

Hatzigogos, T. N., Pitilakis, K. D., & Tsotsos, S. S. (1991). Axial and Lateral Response of Large Diameter Bored Piles. *Proceedings, 10th European Conference on Soil Mechanics and Geotechnical Engineering*, 437-440. Florence.

Hetenyi, M. (1946). *Beams on Elastic Foundation.* Ann Arbor, MI: The University of Michigan Press.

Hirany, A., & Kulhawy, F. H. (1988). *Conduct and Interpretation of Load Tests on Drilled Shaft Foundations - Volume 1: Detailed Guidelines.* Report EL-5915(1). Palo Alto: EPRI.

Hoit, M., Hays, C., & McVay, M. (1997). The Florida Pier Analysis Program: Methods and Models for Pier Analysis and Design. *Transportation Research Record: Journal of the Transportation Research Board , 1569*, 1-7.

Holtz, W. G., & Gibbs, H. J. (1979). Discussion of SPT and Relative Density in Coarse Sand. *Journal of the Geotechnical Engineering Division , 105* (GT3), 439-441.

Honjo, Y., Zaika, Y., & Pokharel, G. (2005). Estimation of Subgrade Reaction Coefficient for Horizontally Loaded Piles by Statistical Analyses. *Soils and Foundations, 45* (3), 51-70.

Huang, A.-B., Hsueh, C.-K., O'Neill, M. W., Chern, S., & Chen, C. (2001). Effects of construction on Laterally Loaded Pile Groups. *Journal of Geotechnical and Geoenvironmental Engineering , 127* (5), 385-397.

Isenhower, W. M., & Wang, S.-T. (2010). *Technical Manula for LPile, Version 6.* Ensoft, Inc.

Ismael, N. F. (1990). Behavior of Laterally Loaded Bored Piles in Cemented Sands. *Journal of Geotechnical Engineering , 116* (11), 1678-1699.

Ismael, N. F. (2010). Behavior of Step Tapered Bored Piles in Sand under Static Lateral Loading. *Journal of Geotechnical and Geoenvironmental Engineering , 136* (5), 669-676.

Ismael, N. F., & Klym, T. W. (1978). Behavior of Rigid Piers in Layered Cohesive Soils. *Journal of the Geotechnical Engineering Division , 104* (GT8), 1061-1074.

Ismael, N. F., & Klym, T. W. (1981). Lateral Capacity of Augered Tower Foundations in Sand. *IEEE Transactions on Power Apparatus and Systems. PAS-100*, 2963-2968. Atlanta: IEEE Power Engineering Society.

Janoyan, K. D., & Whelan, M. J. (2004). Interface Stresses Between Soil and Large Diameter Drilled Shaft Under Lateral Loading. *ASCE Special Publication, 124*, 816-825.

Janoyan, K. D., Stewart, J. P., & Wallace, J. W. (2001). Analysis of p-y Curves from Lateral Load Test of Large Diameter Drilled Shaft in Stiff Clay. *Proceedings from the Caltrans 6th Seismic Design Workshop, Paper 5-105.* Sacramento.

Janoyan, K. D., Wallace, J. W., & Stewart, J. P. (2006). Full-Scale Cyclic Lateral Load Test of Reinforced Concrete Pier-Column. *ACI Structural Journal , 103* (2), 178-187.

Jeon, K. S., Kim, J. H., Kim, S. H., & Kim, M. M. (2000). Analysis of Lateral Head Movements of CIP Piles. In N. D. Dennis Jr., R. Castelli, & M. W. O'Neill (Eds.), *New Technological and Design Developments in Deep Foundations, GSP 100*, 254-268. ASCE.

Juirnarongrit, T., & Ashford, S. (2001). Effect of Pile Diameter on p-y Curves, Paper No. 05-103. *The 6th Caltrans Seismic Research Workshop.* Sacramento.

Kanai, S., & Yabuuchi, S. (1988). Loading Tests of Bored Piles Inserted Nodular and Cylindrical Piles. *Proceedings, 1st International Geotechnical Seminar on Deep Foundation on Bored and Auger Piles*, 429-434. Ghent.

Kasch, V. R., Coyle, H. M., Bartoskewitz, R. E., & Sarver, W. G. (1977). *Lateral Load Test of a Drilled Shaft in Clay.* Texas Transportation Institute. College Station: Texas A&M University.

Kulhawy, F. H., & Chen, Y. -J. (1995). A Thirty Year Perspective of Broms' Lateral Loading Models, As Applied to Drilled Shafts. *Proceedings, Bengt B. Broms Symposium on Geotechnical Engineering,* 225-240. Singapore.

Kulhawy, F. H., & Mayne, P. W. (1990). *Manual on Estimating Soil Properties for Foundation Design.* Report EL-6800. Palo Alto:EPRI.

Kulhawy, F. H., Trautmann, C. H., Beech, J. F., O'Rourke, T. D., McGuire, W., Wood, W. A., et al. (1983). *Transmission Line Structure Foundations for Uplift-Compression Loading.* Report EL-2870. Palo Alto: EPRI.

Lin, S.-S., & Liao, J.-C. (2006). Lateral Response Evaluation of Single Piles Using Inclinometer Data. *Journal of Geotechnical and Geoenvironmental Engineering , 132* (12), 1566-1573.

Little, R. L., & Briaud, J. L. (1988). *Full Scale Cyclic Lateral Load Tests on Six Single Piles in Sand.* Geotechnical Division, Civil Engineering Department. College Station: Texas A&M University.

Long, J. H., & Reese, L. C. (1984). Testing and Analysis of Two Offshore Piles Subjected to Lateral Loads. (J. A. Langer, E. Mosely, & C. Thompson, Eds.) *Laterally Loaded Deep Foundations: Analysis and Performance, ASTM STP 835* , 214-228.

Lu, S. S., Xie, J. W., & Zhan, S. T. (1987). Laterally Loading Test of Large Diameter Bored Piles. *Proceedings, 8th Asian Conference on Soil Mechanics and Foundation Engineering, 1*, 393-396. Kyoto.

Lutenegger, A. J., & Miller, G. A. (1993). Behavior of Laterally Loaded Drilled Shafts in Stiff Soil. *Proceedings: Third International Conference on Case Histories in Geotechnical Engineering*, 147-151. St. Louis.

Lyndon, A., Price, G., Wardle, I. F., & Varey, L. S. (1989). The Effect of Vertical Pile Loading on Subsequent Lateral Behavior. *Proceedings, 3rd International Conference on Piling and Deep Foundations*, 377-382. London: ASCE.

Macklin, P., & Chou, N. (1989). A Lateral Load Test on Seven Foot Diameter Caissons. In F. H. Kulhawy (Ed.), *Foundation Engineering: Current Principles and Practices, Proceedings of the Congress*, 1122-1131. Evanston: ASCE.

Matlock, H. (1970). Correlations for Design of Laterally Loaded Piles in Soft Clay. *Proceedings, 2nd Annual Offshore Technology Conference*, 577-607. Houston.

Matlock, H. (1958). Discussion of "Soil Modulus for Laterally Loaded Piles" by B. McClelland and J.A. Focht, Jr. *Transactions , 123* (Paper 2954), 1077-1081.

Mayne, P. W. (2004). Lateral Drilled Shaft Response from Dilatometer Tests. In J. P. Turner, & P. W. Mayne (Eds.), *GeoSupport 2004: Drilled Shafts, Micropiling, Deep Mixing, Remedial Methods, and Specialty Foundation Systems, GSP 124,* 415-428. Orlando: ASCE.

McClelland, B., & Focht, J. A. (1956). Soil Modulus for Laterally Loaded Piles. *Journal of the Soil Mechanics and Foundations Division , 82* (SM4), 1-22.

McClelland, B., & Focht, J. (1958). Soil Modulus for Laterally Loaded Piles. *Transactions of the ASCE , 123* (Paper 2954), 1049-1086.

Meyerhof, G. G. (1956). Penetration Tests and Bearing Capacity of Cohesionless Soils. *Journal of the Soil Mechanics and Foundations Division , 82* (SM1), 1-19.

Meyerhof, G. G. (1951). The Ultimate Bearing Capacity of Foundations. *Géotechnique, 2* (4), 301-332.

Naramore, S. A., & Feng, F. Y. (1990). *Field Tests of Large Diameter Drilled Shafts, Part 1-Lateral Loads.* Report No. FHWA/CA/SD-88/02. Sacramento: California Department of Transportation.

Newman, F. B., Salver, H. A., & Turka, R. J. (1981). 1000-Ton Drilled Pier Load Test at Sammis Plant. *Drilled Piers and Caissons*, 34-52. New York: ASCE.

Norris, G. M. (1986). *Proceedings, Third International Conference on Numerical Methods in Offshore Piling,* 361-386. Paris.

Nunes, A. J., Costa, R. J., & Rausa, E. P. (1977). High Capacity Load Tests on Large Diameter Piles. *Proceedings, 9th International Conference on Soil Mechanics and Foundation Engineering, 1*, 675-678. Tokyo.

Ohya, S., Imai, T., & Matsubara, M. (1982). Relationships Between N Value by SPT and LLT Pressuremeter Results. *Proceedings, 2nd European Symposium on Penetration Testing, 1*, 125-130. Amsterdam.

O'Neill, M. W., & Murchison, J. M. (1983). *An Evaluation of p-y Relationships in Sands.* University of Houston, Dept. of Civil Engineering. Houston: University of Houston.

O'Neill, M. W., Vipulanandan, C., & Hassan, K. (2000). Modeling of Laterally Loaded ACIP Piles in Overconsolidated Clay. *Proceedings, New Technological and Design Developments in Deep Foundations*, 471-485. Denver.

Parsons Brinckerhoff - Hirota Associates. (1991). *Drilled Shaft Test Program.* Report FAIP I-H3-1(67). Honolulu: Deptartment of Transportation.

Peck, R. B., Hanson, W. E., & Thornburn, T. H. (1974). *Foundation Engineering* (2nd ed.). New York: John Wiley and Sons.

Phoon, K.-K., & Kulhawy, F. H. (2005). Characterisation of Model Uncertainties for Laterally Loaded Rigid Drilled Shafts. *Géotechnique, 55* (1), 45-54.

Poepsel, P., & Sheahan, J. (1988). Lateral Load Testing and Foundation Design Methodology. *Soil Properties Evaluation from Centrifugal Models and Field Performance*, 118-133.

Portugal, J. C., & Pinto, P. S. (1993). Analysis and Design of Piles under Lateral Loads. In W. F. Van Impe (Ed.), *Proceedings, 2nd International Geotechnical Seminar on Deep Foundations on Bored and Auger Piles - BAP II*, 309-312. Ghent.

Poulos, H. G. (1971a). Behavior of laterally loaded piles. I: Single piles. *Journal of the Soil Mechanics and Foundations Division , 97* (5), 711-731.

Poulos, H. G. (1971b). Behavior of laterally loaded piles. II: Pile groups. *Journal of the Soil Mechanics and Foundations Division , 97* (5), 733-751.

Poulos, H. G., & Davis, E. H. (1980). *Pile Foundation Analysis and Design.* New York, NY: John Wiley and Sons.

Price, G., & Wardle, I. F. (1987). *Vertical and Lateral Load Tests on Driven Cast-in-place Piles at Yarmouth.* Contractor Report No. 47. Crowthorne: Transport and Road Research Laboratory.

Reese, L. C. (1997). Analysis of Piles in Weak Rock. *Journal of the Geotechnical and Geoenvironmental Engineering Division* , 1010-1017.

Reese, L. C. (1958). Discussion of "Soil Modulus for Laterally Loaded Piles" by B. McClelland and J.A. Focht, Jr. *Transactions , 123* (Paper 2954), 1071-1074.

Reese, L. C. (1958). Soil Modulus for Laterally Loaded Piles. *Transactions , 123*, 1071-1074.

Reese, L. C. (1962). Ultimate Resistance Against a Rigid Cylinder Moving Laterally in a Cohesionless Soil. *Journal of the Society of Petroleum Engineers , 2* (4), 355-359.

Reese, L. C., & Nyman, K. J. (1978). *Field Load Test of Instrumented Drilled Shafts at Islamorada, Florida.* Clearwater: Report to Girdler foundation and Exploration Corporation, Clearwater, Florida (Unpublished).

Reese, L. C., & Welch, R. C. (1975). Lateral Loading of Deep Foundations in Stiff Clay. *J. Geotech. Eng. Div. , 101* (GT7), 633-649.

Reese, L. C., Cox, W. R., & Koop, F. D. (1975). Field Testing and Analysis of Laterally Loaded Piles in Stiff Clay. *Proceedings, 7th Offshore Technology Conference,* 672-690.

Reese, L. C., Wang, S. T., Isenhower, W. M., & Arrellaga, J. A. (2004). *LPILE Plus 5.0 for Windows - Technical Manual.* Ensoft, Inc.

Reese, L., Cox, W., & Koop, F. (1974). Analysis of Laterally Loaded Piles in Sand. *Proceedings, 6th Annual Offshore Technology Conference*, 473 - 485. Houston: Offshore Technology Conference.

Ripperger, E. A. (1958). Discussion of "Soil Modulus for Laterally Loaded Piles" by B. McClelland and J.A. Focht, Jr. *Transactions , 123* (Paper 2954), 1074-1077.

Robertson, P. K., & Campanella, R. G. (1983). Interpretation of Cone Penetration Tests. Part I: Sand. *Canadian Geotechnical Journal , 20* (4), 718-733.

Robertson, P. K., Davies, M. P., & Campanella, R. G. (1989). Design of Laterally Loaded Drivel Piles Using the Flat Dilatometer. *Geotechnical Testing Journal , 12* (1), 30-38.

Robertson, P. K., Hughes, J. M., Campanella, R. G., Brown, P., & McKeown, S. (1986). Design of Laterally Loaded Piles Using the Pressuremeter. *The Pressuremeter and its Marine Applications: Second International Symposium.* ASTM STP 950.

Robertson, P. K., Hughes, M. J., Campanella, R. G., & Sy, A. (1983). Design of Laterally Loaded Displacement Piles using Driven Pressuremeter. *Design & Performance of Laterally Loaded Piles and PIle Groups.* Kansas City.

Rollins, K. M., Hales, L. J., & Ashford, S. A. (2005). p-y Curves for Large Diameter Shafts in Liquefied Sands from Blast Liquefaction Tests. *Seismic Performance and Simulation of Pile Foundations in Liquefied and Laterally Spreading Ground* , 11-23.

Salgado, R. (2008). *The Engineering of Foundations* (1st ed.). New York: McGraw-Hill.

Sarhan, H. A., O'Neill, M. W., & Hassan, K. M. (2002). Flexural Performance of Drilled Shafts with Minor Flaws in Stiff Clay. *Journal of Geotechnical and Geoenvironmental Engineering , 128* (12), 974-985.

Schmertmann, J. H. (1975). Measurement of In-Situ Shear Strength. *Proceedings, Specialty Conference on In-Situ Measurement of Soil Properties, 2*, 57-138 (closure: 175-179). Raleigh: ASCE.

Schmertmann, J. H. (1970). Static Cone to Compute Static Settlement Over Sand. *Journal of the Soil Mechanics and Foundations Division , 96* (No. SM3), 1011-1043.

Seychuck, J. L. (1970). Load Tests on Bedrock. *Canadian Geotechnical Journal , 7* (4), 464-470.

Shilts, W. L., Graves, L. D., & Driscoll, G. G. (1948). A Report of Field and Laboratory Tests on the Stability of Posts against Lateral Loads. *Proceedings of the Second International Conference on Soil Mechanics and Foundation Engineering*, 107-122. Rotterdam.

Skempton, A. W. (1951). The Bearing Capacity of Clays. *Proceedings, Building Research Congress, Division 1*, 180-189. London.

Skempton, A. W. (1954). The pore pressure coefficients A and B. *Geotechnique, 4* (4), 148.

Smith, T., & Slyh, R. (1986). Side Friction Mobilization Rates for Laterally Loaded Piles from the Pressuremeter. *The Pressuremeter and Its Marine Applications: Second International Symposium*, 478-491. ASTM STP 950.

Teng, W. C., & Manuel, F. S. (1976). Caisson Foundations Subjected to Lateral Forces. *IEEE Transactions on Power Apparatus and Systems , PAS-95* (4), 1435 - 1442.

Terzaghi, K. (1955). Evaluation of the Coefficients of Subgrade Reaction. *Géotechnique , 5* (4), 297-326.

Terzaghi, K., Peck, R. B., & Mesri, G. (1996). *Soil Mechanics in Engineering Practice* (3rd ed.). New York: John Wiley & Sons, Inc.

Tomlinson, M. J. (1957). The Adhesion of Piles Driven in Clay Soils. *Proceedings, Fourth International Conference on Soil Mechanics and Foundation Engineering. 2*, 66-71. London.

Vesic, A. (1961). Bending of Beams Resting on Isotropic Elastic Solid. *Journal of Engineering Mechanics Division , 87* (EM2), 35-53.

Welch, R. C., & Reese, L. C. (1972). *Lateral Load Behavior of Drilled Shafts.* Center for Highway Research. The University of Texas at Austin.

Winkler, E. (1867). *Die Lehre von der Elasticitaet und Festigkeit (On Elasticity and Fixity)* (1st ed.). Prague: H. Dominicus.

Wood, J. H., & Phillips, M. H. (1991). *Lateral Stiffnes of Bridge Pile Foundations: Load Tests on Charwell River Bridge.* Report ST 90/2. Lower Hutt: Philips & Wood Consulting Engineers.

Wood, J. H., & Phillips, M. H. (1989). *Lateral Stiffness of Bridge Pile Foundations: Load Tests on Maitai River Bridge.* ST Report 88/1. Lower Hutt: Phillips & Wood Consulting Engineers.

Wood, J. H., & Phillips, M. H. (1987). *Lateral Stiffness of Bridge Pile Foundations: Load Tests on Newmans Bridge.* Report ST 87/2. Lower Hutt: Phillips and Wood Consulting Engineers.

Yang, K. (2006). *Analysis of Laterally Loaded Drilled Shafts in Rock.* PhD Dissertation. Akron: The University of Akron.

Yang, K., & Liang, R. (2006). Methods for Deriving p-y Curves from Instrumented Lateral Load Tests. *Geotechnical Testing Journal , 30* (1), 8.

Yang, K., Liang, R., & Liu, S. (2005). Analysis and Test of Rock-Socketed Drilled Shafts Under Lateral Loads. *The 40th U.S. Symposium on Rock Mechanics: Rock Mechanics for Energy, Mineral, and Infrastructure Development in the Northern Regions.* Anchorage.

Zhang, F., Kimura, M., Nakai, T., & Hoshikawa, T. (2000). Mechanical Behavior of Pile Foundations Subjected to Cyclic Lateral Loading up to the Ultimate State. *Soils and Foundations , 40* (5), 1-17.